11-18-2010

Role of Voltage-Dependent Calcium Channels in Subarachnoid Hemorrhage-Induced Constriction of Intracerebral Arterioles

Matthew Nystoriak
University of Vermont

ROLE OF VOLTAGE-DEPENDENT CALCIUM CHANNELS IN SUBARACHNOID HEMORRHAGE-INDUCED CONSTRICTION OF INTRACEREBRAL ARTERIOLES

A Dissertation Presented

by

Matthew A. Nystoriak

to

The Faculty of the Graduate College

of

The University of Vermont

In Partial Fulfillment of the Requirements
for the Degree of Doctor of Philosophy
Specializing in Pharmacology

October, 2010

Accepted by the Faculty of the Graduate College, The University of Vermont, in partial fulfillment of the requirements for the degree of Doctor of Philosophy, specializing in Pharmacology.

Dissertation Examination Committee:

George C. Wellman, Ph.D. **Advisor**

Joseph E. Brayden, Ph.D.

Victor May, Ph.D.

Mark T. Nelson, Ph.D.

Margaret A. Vizzard, Ph.D. **Chairperson**

Domenico Grasso, Ph.D. **Dean, Graduate College**

Date: August 30, 2010

ABSTRACT

Subarachnoid hemorrhage (SAH) following cerebral aneurysm rupture is associated with substantial morbidity and mortality. The ability of SAH to induce vasospasm in large diameter pial arteries has been extensively studied, although the contribution of this phenomenon to patient outcome is unclear. Conversely, little is known regarding the impact of SAH on intracerebral (parenchymal) arterioles, which are critical for regulation of cerebral blood flow. To assess the function of parenchymal arterioles following SAH, measurements of diameter, intracellular Ca^{2+} ($[Ca^{2+}]_i$) and membrane potential were performed in intact arterioles from unoperated (control), sham-operated and SAH model rats. At physiological intravascular pressure, parenchymal arterioles from SAH animals exhibited significantly elevated $[Ca^{2+}]_i$ and enhanced constriction compared with arterioles from control and sham-operated animals. Elevated $[Ca^{2+}]_i$ and enhanced tone following SAH were observed in the absence of vascular endothelium and were abolished by the L-type voltage-dependent Ca^{2+} channel (VDCC) inhibitor nimodipine. Molecular assessment of the L-type VDCC $Ca_V1.2$ indicated unchanged mRNA and protein expression in arterioles from SAH animals. Increased $Ca_V1.2$ activity following SAH may also reflect enhanced pressure-induced membrane potential depolarization of arteriolar smooth muscle. Membrane potential measurements in arteriolar myocytes using intracellular microelectrodes revealed approximately 7 mV depolarization at 40 mmHg in myocytes from SAH animals. Further, when membrane potential was adjusted to similar values, arteriolar $[Ca^{2+}]_i$ and tone were similar between groups. These results demonstrate that greater pressure-dependent membrane potential depolarization results in increased activity of $Ca_V1.2$ channels, elevated $[Ca^{2+}]_i$ and enhanced constriction of parenchymal arterioles from SAH animals. Thus, impaired regulation of parenchymal arteriolar $[Ca^{2+}]_i$ and diameter may restrict cerebral blood flow in SAH patients.

Although nimodipine is used clinically to prevent delayed neurological deficits in SAH patients, the use of this drug has been limited by hypotension and treatment options remain inadequate. Therefore, our next objective was to explore strategies to selectively suppress $Ca_V1.2$ channels in the cerebral vasculature. To do so, we examined the physiological role of smooth muscle $Ca_V1.2$ splice variants containing the alternatively-spliced exon 9* in cerebral artery constriction. Using antisense oligonucleotides, we demonstrate that suppression of exon 9*-containing $Ca_V1.2$ splice variants results in substantially reduced cerebral artery constriction to elevated extracellular $[K^+]$. In addition, no further reduction in constriction was observed following suppression of all $Ca_v1.2$ splice variants, suggesting that exon 9* splice variants are functionally dominant in cerebral artery constriction. In summary, results shown in this dissertation demonstrate that increased $Ca_V1.2$ activity following SAH results in enhanced constriction of parenchymal arterioles. Furthermore, evidence is provided supporting the concept that $Ca_V1.2$ splice variants with exon 9* are critical for cerebral artery constriction and may provide a novel target for the prevention of delayed ischemic deficits in SAH patients.

CITATIONS

Material from this dissertation has been published in the following form:

Nystoriak, M.A., Murakami, K., Penar, P.L., Wellman, G.C.. (2009) $Ca_v1.2$ splice variant with exon 9* is critical for regulation of cerebral artery diameter. *American Journal of Physiology, Heart and Circulatory Physiology*, 297(5):H1820-8.

Material from this dissertation has been accepted for publication in the following form:

Koide, M., Nystoriak, M.A., Brayden, J.E., Wellman, G.C.. (December, 2009) Impact of subarachnoid hemorrhage on local and global calcium signaling in cerebral artery myocytes. *Early Brain Injury or Cerebral Vasospasm, Vol. 1: Pathophysiology*, Springer Press, Inc.

Nystoriak, M.A., Koide, M., Wellman, G.C.. (February, 2010) Assessment of intracellular calcium in cerebral artery myocytes. *Animal Models of Acute Neurological Injuries II: Injury and Mechanistic Assessments*, Springer Press, Inc.

Koide, M., Nystoriak, M.A., Krishnamoorthy, G., O'Connor, K.P., Bonev, A.D., Nelson, M.T., Wellman, G.C.. (July, 2010) Reduced Ca^{2+} spark activity following subarachnoid hemorrhage disables BK channel control of cerebral artery tone. *Journal of Cerebral Blood Flow and Metabolism*.

Material from this dissertation has been submitted for publication to American Journal of Physiology, Heart and Circulatory Physiology on August 2, 2010 in the following form:

Nystoriak, M.A., Sonkusare, S.K., Brayden, J.E., Nelson, M.T., Wellman, G.C.. Fundamental increase in pressure-dependent constriction of brain parenchymal arterioles from subarachnoid hemorrhage model rats due to membrane depolarization. *American Journal of Physiology, Heart and Circulatory Physiology*.

ACKNOWLEDGEMENTS

I believe that the success of one in pursuit of a doctoral degree is determined not only by the effort put forth by the student, but also that put forth by the mentor. With that said, I am extremely fortunate to have worked with my advisor, Dr. George Wellman. From day one, George has been a truly great mentor and the experience that I have had working with him has been invaluable. I would like to thank George for everything, including help with wrting manuscripts and proposals, advice with designing and performing experiments, as well as encouraging me to attend scientific meetings and work on my golf swing. In addition, this dissertation is physical proof that a Yankees fan can peacefully and productively coexist with a Red Sox fan.

I also feel very fortunate to have had a dissertation committee consisting of faculty members who are internationally recognized as experts in their respective fields. For their time and effort in helping to guide my work, I would like to thank: Drs. Joseph Brayden, Victor May, Mark Nelson, and Margaret Vizzard. I believe that the willingness of these outstanding scientists to share their expertise is very much reflected in my research.

I must thank everyone working in the Wellman laboratory for all of their help: Drs. Masayo Koide and Kentaro Murakami, Mr. Micah Been-Miller, Mr. Colby Cantu,

Ms. Jaqueline Hubbard, Mr. Kevin O'Connor, Ms. Ashley Ross, and Ms. Sheila Russell. Working alongside you every day in the lab has been a very enjoyable experience. I would also like to express gratitude toward Dr. Natalia Gokina for taking time to share expertise regarding the use of fura-2 to measure intracellular calcium in intact arteries. Members of the Center of Biomedical Research Excellence Program, particularly Thomm Buttolph and Edward Zelazny, were also instrumental in my training and understanding of several techniques.

As an undergraduate at the Unversity of Vermont, I spent time as a work-study student in the department of Phamacology in Dr. Deborah Damon's laboratory. Initially, most time was spent washing dishes, but later I began to perform various molecular biology and cell culture techniques. It was during this time that I first became excited by research. I would like to thank Dr. Damon for allowing me to work in her laboratory, as I would not have chosen this career path otherwise.

This dissertation is dedicated to my parents, Barbara and David Nystoriak. From a very early age, my parents taught me the importance of working hard and receiving a high-quality education. Without their constant encouragement, I never would have dreamed of pursuing a career in science. I would also like to thank my friends and family in New York for their love and support.

Finally, I am deeply indepted to my wife and best friend Jessica. On days when experiments failed, she would see my frustration and remind me to bear in mind how good the good days feel. I couldn't have done this without all of her unwavering love and support.

"The secret to creativity is knowing how to hide your sources" ~Albert Einstein

TABLE OF CONTENTS

LIST OF TABLES

LIST OF FIGURES

CHAPTER 1: LITERATURE REVIEW

CHAPTER 2: JOURNAL ARTICLE

CHAPTER 3: JOURNAL ARTICLE

CHAPTER 4: CONCLUSIONS AND FUTURE DIRECTIONS

APPENDIX A: BOOK CHAPTER

APPENDIX B: BOOK CHAPTER

APPENDIX C: JOURNAL ARTICLE

CHAPTER 1: LITERATURE REVIEW

Introduction

Maintenance of adequate blood flow to the brain is essential for human life. Insufficient delivery of oxygen and glucose to metabolically active regions of the brain quickly results in neuronal necrosis, neurological impairment and death. Therefore, the function of small diameter cerebral arteries and arterioles, which control blood flow, is highly regulated. Following intracranial aneurysm rupture and subarachnoid hemorrhage (SAH), mechanisms mediating cerebral artery diameter may become compromised, leading to enhanced vasoconstriction and reduced blood flow. Consequently, ischemia leads to further morbidity and mortality in a large number of patients surviving the initial intracranial bleed (Kassell et al., 1985). The complex mechanisms involved in arterial narrowing and reduced blood flow associated with SAH are not well understood, but may involve enhanced contraction of vascular smooth muscle.

The contractile state of smooth muscle is dictated by the concentration of global cytosolic free Ca^{2+} ($[Ca^{2+}]_i$), representing averaged Ca^{2+} throughout the cell. In the vasculature, smooth muscle $[Ca^{2+}]_i$ is largely determined by membrane potential and the degree of Ca^{2+} influx via plasmalemmal L-type voltage-dependent Ca^{2+} channels (VDCCs). The L-type VDCC α1 pore-forming subunit in vascular smooth muscle is a splice variant of the gene $Ca_V1.2$, which also encodes cardiac muscle and neuronal VDCCs. Although the molecular identity of L-type VDCCs involved in cerebral artery constriction is not known, evidence suggests that these channels may be more active following SAH, leading to elevation of smooth muscle $[Ca^{2+}]_i$ and enhanced vasoconstriction (Faraci and Heistad, 1998; Wellman, 2006). Given their relevance in

cerebrovascular physiology, understanding the function of L-type VDCCs in cerebral artery myocytes is critical for improvement of therapeutic strategies preventing reduced cerebral blood flow following SAH.

This literature review will provide an overview of the regulation of cerebrovascular tone in both normal conditions and in pathological conditions following SAH. Part one will discuss mechanisms involved in vascular smooth muscle contraction, with a focus on the role of intracellular Ca^{2+} and L-type VDCCs. Part two will discuss prominent pathways involved in enhanced arterial constriction following SAH. In addition, this section will also review emerging evidence in support of SAH-induced dysfunction of the cerebral microcirculation.

Part 1: Cerebrovascular physiology

General anatomy of the cerebral arterial blood supply

Blood is supplied to the human brain by two vertebral arteries and two internal carotid arteries. The vertebral arteries enter the skull through the foramen magnum and converge to form the basilar artery on the ventral brain stem. The internal carotid arteries enter through the base of the skull and join the basilar artery to form an arterial circle on the base of the brain called the Circle of Willis (Figure 1). The unique anatomic structure of the Circle of Willis functions to provide collateral blood supply to the entire brain in the event of occlusion of any of the arteries contributing to the circle.

Three major pairs of arteries supply blood to the cerebral hemispheres. The anterior cerebral arteries (ACA) arise from the internal carotid arteries at the Circle of Willis and supply the most medial portions of the frontal and parietal lobes. The major branches supplying the majority of the lateral hemispheres are the middle cerebral arteries (MCA). The posterior cerebral arteries extend from the intersection of the posterior communicating and basilar arteries and supply the inferior and medial regions of the temporal and occipital lobes. Each major cerebral artery divides to form a highly interconnected grid of surface or "pial" arteries and arterioles. It has been shown that occlusion of a pial cerebral artery leads to only modest decreases in downstream blood flow due to the reversal of flow in downstream communicating arterioles (Schaffer et al., 2006). Therefore, redundant connections among pial arteries and arterioles may also provide a source of collateral blood flow following arterial occlusion.

Penetrating arterioles arise from pial arteries and arterioles and enter the brain parenchyma. The penetrating arterioles are surrounded by an invagination of the pia mater, called the Virchow-Robin space, which is continuous with the subarachnoid space (Figure 2). Downstream of penetrating arterioles and the Virchow-Robin space are intracerebral or parenchymal arterioles. Whereas an interconnected arterial network exists in pial arteries on the surface of the brain, limited collateral flow exists between penetrating and parenchymal arterioles (Nishimura et al., 2007). Hence, thrombosis in penetrating arterioles results in greatly diminished downstream flow (Nishimura et al., 2007) suggesting that ischemia may be most severe following enhanced constriction or occlusion of these vessels.

Also distinguishing the parenchymal arterioles from pial vessels is a lack extrinsic perivascular innervation (Cipolla et al., 2004; Handa et al., 1990). Consistent with this, parenchymal arterioles do not respond to the neurotransmitters norepinephrine or serotonin, which are potent vasoconstrictors in pial vessels (Cipolla et al., 2004). In addition, parenchymal arterioles are almost completely encased by astrocytic endfeet and are essential for coupling neuronal activity to local blood flow ("functional hyperemia") (Filosa et al., 2006; Iadecola and Nedergaard, 2007). Thus, parenchymal arterioles operate in a unique environment and are functionally distinct from pial vessels on the brain surface.

Control of cerebral blood flow: cerebrovascular resistance

Blood moves through the circulatory system from regions of high pressure (i.e. aorta) to regions of low pressure (i.e. capillaries) (Silverthorn, 2004). As this pressure gradient (ΔP) increases, blood flow also increases. On the other hand, blood flow is opposed by vascular resistance. Hence, blood flow is directly proportional to ΔP, and inversely proportional to vascular resistance (R):

$$\text{Flow} \propto \Delta P/R$$

Resistance is a function of length (L) and radius (r) of the vessel as well as the viscosity (η) of the fluid moving through the vessel. Accordingly, resistance can be expressed by the following equation, known as Poiseuille's Law:

$$R=8L\eta/\pi r^4$$

Because the length of the circulatory system and blood viscosity are essentially constant, this equation may also be expressed as:

$$R \propto 1/r^4$$

This equation states that vascular resistance is inversely proportional to radius to the fourth power. In an example, a 20 percent decrease in arterial diameter will cause greater than 50 percent reduction in blood flow. Thus, arterial diameter is a major determinant of vascular resistance and small changes in diameter can have profound effects on blood flow and organ perfusion.

Cerebral autoregulation and Ca^{2+}-dependence of vascular tone

To maintain a constant level of blood flow to the brain during fluctuations in blood pressure, the cerebral resistance vasculature constricts when intravascular pressure increases and dilates when pressure is reduced. The phenomenon of arterial constriction in response to increases in intravascular pressure, or "myogenic tone" was first described by Bayliss in 1902 (Bayliss, 1902). Constrictions to increases in intravascular pressure were found to be independent of neurogenic, humoral or endothelial influences (Falcone et al., 1991; Knot and Nelson, 1995; McCarron et al., 1989). Thus, myogenic tone is an intrinsic characteristic of vascular smooth muscle within the arterial wall. It is now established that increasing intravascular pressure in the physiological range leads to membrane potential depolarization of vascular smooth muscle, activation of voltage-dependent Ca^{2+} channels (VDCCs), a rise in $[Ca^{2+}]_i$ and contraction of vascular smooth muscle (Brayden and Wellman, 1989; Harder, 1984; Knot and Nelson, 1998). In the

cerebral circulation, the degree of pressure-dependent constriction varies with diameter and is more prominent in small diameter arteries and arterioles (Thorin-Trescases et al., 1997). In addition, this physiological response to pressure is thought to maintain vessels in a partially constricted state in vivo (Meininger and Davis, 1992), allowing various vasoactive factors to increase or decrease arterial diameter and blood flow depending on the metabolic demands of the brain.

Initiation of Smooth muscle contraction: Vascular smooth muscle contraction is a Ca^{2+}-dependent process. The first step in excitation-contraction coupling in arterial myocytes is a rise in $[Ca^{2+}]_i$ and activation of the ubiquitous Ca^{2+}-binding protein calmodulin (CaM) (Figure 3). Upon binding Ca^{2+} at two EF hand motifs on the N- and C-termini (Gifford et al., 2007), CaM undergoes a conformational change that allows it to interact with numerous proteins, including myosin light chain kinase (Walsh, 1981). CaM-dependent activation of myosin light chain kinase leads to a subsequent increase in phosphorylation at serine-19 on the 20 kDa regulatory myosin light chain protein (Kamisoyama et al., 1994). This phosphorylation event induces a conformational change in the myosin molecule which enhances myosin ATPase activity, actin binding and cross-bridge cycling (Chacko et al., 1977). Shortening of the contractile filaments results in force generation or increased muscle tension (Hai and Murphy, 1989). An increase in crossbridge cycling and contraction may also result from an increase in the sensitivity of the contractile machinery to intracellular Ca^{2+}. For example, the regulatory proteins caldesmon and calponin tonically inhibit myosin ATPase activity in smooth muscle

(Horowitz et al., 1996). This inhibition is relieved by phosphorylation and leads to increased smooth muscle contraction and vascular tone independent of increases in $[Ca^{2+}]_i$ (Horowitz et al., 1996; Mino et al., 1995).

Relaxation of smooth muscle is triggered by a decrease in $[Ca^{2+}]_i$ and dephosphorylation of myosin light chain at serine-19 by myosin light chain phosphatase (Murphy, 1982). Ca^{2+} ions are extruded from the cytoplasm by the plasmalemmal Ca^{2+} ATPase (PMCA) and Na^+/Ca^{2+} exchanger, and sequestered into the SR by the sarco-/endoplasmic reticulum Ca^{2+}-ATPase (SERCA) (Floyd and Wray, 2007). PMCA and SERCA both use energy from the hydrolysis of ATP to transport Ca^{2+} ions against a chemical gradient. On the other hand, the Na^+/Ca^{2+} exchanger uses the electrochemical gradient for Na^+, which is established by the Na^+/K^+ ATPase, to transport a single Ca^{2+} ion out of the cell in exchange for three Na^+ ions into the cell (Blaustein and Lederer, 1999). Therefore, arterial myocytes expend energy in the form of ATP hydrolysis in order to maintain cytosolic Ca^{2+} at low concentrations relative to extracellular levels. Previous work using the ratiometric Ca^{2+}-sensitive fluorescent dye fura-2 estimates that smooth muscle $[Ca^{2+}]_i$ of fully dilated middle cerebral arteries is ~50-100 nM (Knot and Nelson, 1998). Further, the Ca^{2+} sensitivity of arterial diameter was found to be 1 μm/ nM $[Ca^{2+}]_i$ with the entire range of arterial diameters associated with a change in arterial wall Ca^{2+} of approximately 250 nM (Knot and Nelson, 1998). Thus, $[Ca^{2+}]_i$ in vascular smooth muscle is tightly regulated and small changes in the cytosolic concentration of this ionic species can have a major impact on arterial diameter and blood flow.

Regulation of vascular smooth muscle $[Ca^{2+}]_i$: L-type voltage-dependent Ca^{2+} channels

Calcium ions enter the cytosol of vascular smooth muscle predominantly via voltage-dependent calcium channels (VDCCs) in the plasma membrane and Ca^{2+} release channels in the sarcoplasmic reticulum. Thus, $[Ca^{2+}]_i$ in cerebral artery myocytes is determined by the steady-state balance between Ca^{2+} influx from the extracellular fluid or intracellular stores and Ca^{2+} extrusion from the cytoplasm or SR sequestration. In cerebrovascular smooth muscle, Ca^{2+} influx via VDCCs is the major pathway by which $[Ca^{2+}]_i$ increases for initiation of contraction (Brayden and Wellman, 1989; Knot and Nelson, 1998; Nelson et al., 1990; Nelson et al., 1988). Blocking VDCCs with the selective L-type VDCC antagonist nisoldipine reduces $[Ca^{2+}]_i$ to resting levels and abolishes pressure-induced constrictions (Figure 3), essentially uncoupling the relationship between membrane potential and arterial diameter (Knot and Nelson, 1998). Thus, in cerebral artery myocytes, $[Ca^{2+}]_i$ is largely determined by the activity of dihydropyridine-sensitive L-type VDCCs. Further, many vasoactive factors exert their effects on arterial diameter and cerebral blood flow by directly altering VDCC gating or by changing membrane potential (Nelson et al., 1988; Worley et al., 1991). This section will review the basic structural, electrophysiological and pharmacological properties of VDCCs with a focus on L-type VDCCs encoded by $Ca_v1.2$.

Structure: In 1984, Curtis and Catterall first purified voltage-dependent Ca^{2+} channels from skeletal muscle transverse tubule membranes (Curtis and Catterall, 1984). It was

found that these channels were heterooligomeric complexes comprised of a pore-forming α_1 subunit in association with accessory β, α_2-δ, and γ subunits (Catterall, 2000; Curtis and Catterall, 1984). It is now known that the α1 subunit confers most functional properties of the channel including voltage sensitivity, Ca^{2+} permeability, sensitivity to pharmacological activators and inhibitors, and Ca^{2+}-dependent inactivation (Catterall, 2000). Ten distinct α_1 subunits have been described: $Ca_V1.1$-1.4 ("L-type"), $Ca_V2.1$-2.2 ("P- or Q-type"), $Ca_V2.3$ ("R-type"), and $Ca_V3.1$-3.3 ("T-type"). The α_1 proteins (~2000 amino acids; ~190-240 kDa) consist of four repeat domains (I-IV), each containing six transmembrane segments (S1-S6) (Tanabe et al., 1987). The S4 transmembrane segments each contain positively charged arginine and lysine residues and confer voltage sensitivity to the channel. These segments rotate and move outward in response to membrane depolarization, inducing a conformational change which opens the pore (Tanabe et al., 1987; Yamaguchi et al., 1999). In addition to cytoplasmic N- and C-termini, domains I-IV are connected in tandem by intracellular linker regions. The C-terminus, which contains sites of interaction for cAMP-dependent protein kinase (PKA) and A-kinase anchoring protein (AKAP15), is proteolytically cleaved in vivo (De Jongh et al., 1996; Hulme et al., 2003). Although the functional importance of this post-translational modification is currently unclear, one report suggests that the cleaved C-terminal portion may remain associated with the remainder of the α1 subunit to regulate channel function by formation of an autoinhibitory complex (Hulme et al., 2006).

Although α_1 subunit expression is sufficient to produce functional VDCCs, abnormal expression, kinetics and voltage-dependence of Ca^{2+} currents are observed in

the absence of auxiliary subunits. Non-covalent association between the α_1 and cytosolic β subunit appears to be most important in the modulation of VDCC expression and function. The four known β subunits (β_{1-4}) belong to the membrane-associated guanylate kinase (MAGUK) family of scaffolding proteins and consist of two conserved central alpha helix domains flanked by subtype-specific N- and C- termini (Cohen et al., 2005). The guanylate kinase (GK) region of the β interactive domain (BID) is required for high affinity interaction with the alpha interactive domain (Maeda et al.) within the I-II intracellular linker of the α_1 subunit (Pragnell et al., 1994). Coexpression of α_1 and β subunits leads to significantly increased transmembrane currents and causes channel activation and inactivation at more negative membrane potentials (Kamp et al., 1996). It is thought that this modulation of channel function may reflect both increased insertion of the α_1 subunit in the plasma membrane as well as a conformational change in the α_1 subunit upon binding the β subunit (Chien et al., 1995; Kamp et al., 1996). Protein for both β_2 and β_3 has been reported in the vasculature (Hullin et al., 1992; Murakami et al., 2003). Aortic myocytes from mice lacking the β_3 subunit exhibited significantly reduced Ca^{2+} currents (Murakami et al., 2003). It was proposed that residual Ca^{2+} currents after β_3 gene ablation may represent a redundant role for the β_2 subunit in channel trafficking and gating. Altered channel function by β subunits may represent an important means of integration of intracellular signals to alter Ca^{2+} influx. For example, β subunits contain conserved sites for PKA-mediated phosphorylation (Puri et al., 1997). In cardiac muscle, beta-adrenergic receptor activation and PKA-mediated stimulation of L-type Ca^{2+}

currents may be partially due to phorphorylation of the β_{2a} subunit at serine 478 and serine 479 (Bunemann et al., 1999).

While the expression profile and functional role of VDCC γ subunits in vascular smooth muscle remain unclear (Sonkusare et al., 2006), the importance of the $\alpha_2\delta$ subunit has recently been evaluated. Four genes encoding $\alpha_2\delta$ subunits have been cloned ($\alpha_2\delta$1-4) (Davies et al., 2007). Each $\alpha_2\delta$ protein (~170 kDa) is the product of a single gene which undergoes proteolytic cleavage and reassociates via a disulfide bond as an extracellular α_2 and transmembrane δ (Takahashi et al., 1987). One recent study found that suppression of membrane bound $\alpha_2\delta$-1 subunits in myocytes from resistance-sized cerebral arteries inhibits membrane insertion of α_1 subunits, decreases $Ca_V1.2$ currents and causes prolonged vasodilation (Bannister et al., 2009). Interestingly, it was discovered that a class of drugs used to treat neuropathic pain, the gabapentenoids (i.e. pregabalin), exert their effects through binding VDCC $\alpha_2\delta$-1 and $\alpha_2\delta$-2 subunits (Bian et al., 2006). Hence, $\alpha_2\delta$ subunits may also play an important role in the functionality of neuronal L-type VDCCs in addition to smooth muscle channels.

Physiological and Pharmacological Properties: VDCCs switch between open conducting states to closed nonconducting states. As membrane potential becomes more positive, the amount of time spent in the open state, or open-state probability (P_{open}), increases. In vivo membrane potential of resistance artery myocytes (-55 to -40 mV) (Neild and Keef, 1985) is within the range in which the opening of L-type VDCCs is steeply voltage-dependent (Nelson et al., 1988). For example, at membrane potentials negative to -40

mV, VDCC activation is an exponential function of membrane potential with an approximately e-fold increase in P_{open} per 8.5 mV depolarization (Figure 5) (Nelson et al., 1990). At membrane potentials positive to -40 mV, increases in P_{open} are opposed by long-term channel inactivation, which is both voltage- and Ca^{2+}-dependent. Thus, P_{open} can be expressed by (Nelson et al., 1990):

$$P_{open}=(P_{act})(1-P_{inact})(P_{funct})$$

where P_{act} is P_{open} in the absence of inactivation, $1-P_{inact}$ is the probability of the channel not being in the inactivated state and P_{funct} is the probability that the channel is functional. It has been estimated that each cerebral artery myocyte has approximately 5000 functional channels (Rubart et al., 1996). Each channel has a measured conductance of 3 to 5 pS and can produce currents of 0.1 to 0.3 pA at 2 mM Ca^{2+} and physiological membrane potentials (Gollasch et al., 1992; Rubart et al., 1996). It has been shown that a depolarization from -40 mV to -20 mV causes approximately four-fold increase in steady-state Ca^{2+} current, which is capable of raising $[Ca^{2+}]_i$ 1.3 μM/second in the absence of Ca^{2+} buffering and sequestration (Rubart et al., 1996). Thus, altering membrane potential can lead to substantial changes in the rate of Ca^{2+} influx in arterial smooth muscle.

Since Ca^{2+} currents were first recorded in cardiac myocytes (Reuter, 1979), multiple types of Ca^{2+} channels have been categorized by physiological as well as pharmacological characteristics (Catterall, 2000). In addition to their high voltage-dependent activation and slow voltage-dependent inactivation, L-type VDCCs can be defined pharmacologically by sensitivity to selective Ca^{2+} channel antagonists including

dihydropyridines, phenylalkylamines, and benzothiazepines (Catterall, 2000; Reuter, 1983). Inhibition by dihydropyridine compounds is state-dependent and VDCCs become more sensitive to these compounds as membrane potential is more depolarized (Sanguinetti and Kass, 1984). The binding sites for L-type VDCC antagonists are located on the α_1 subunit and binding locks the channel in the inactive or closed state (Williams and Tremble, 1982). Given the critical role of L-type VDCCs in cardiovascular function, L-type VDCC antagonists are an important therapeutic option in the treatment of a variety of disorders including several types of arrhythmia, hypertension, and angina pectoris.

Several other VDCC subtypes have been reported in the vasculature including a low-voltage activated (T-type; Ca_V3) (Nikitina et al., 2007), ω-agatoxin IVA-sensitive (P/Q; $Ca_V2.1$) (Hansen et al., 2000), and a nifedipine-resistant high-voltage activated Ca^{2+} channel (Itonaga et al., 2002; Morita et al., 1999). However, as dihydropyridine compounds completely abolish pressure-induced as well as agonist-induced cerebral artery constriction (Gokina et al., 1999; Knot and Nelson, 1998), L-type VDCCs are widely accepted as the major route of Ca^{2+} influx in arterial smooth muscle.

Alternative splicing of mRNA encoding $Ca_V1.2$: In addition to vascular smooth muscle contraction, $Ca_V1.2$ channels play a critical role in numerous physiological processes such as cardiac muscle contraction, neurotransmitter release, gene expression and hormone secretion. Transcript scanning of the human $Ca_V1.2$ gene indicated that 19 of the 55 exons comprising the channel are subject to alternative splicing, suggesting that

structural diversity among tissue-selective splice variants may account for functional distinctions between cell types (Tang et al., 2004). The 40 identified splice variations at 12 splice loci of $Ca_V1.2$ are shown in Figure 6 (Liao et al., 2005).

The essential role of L-type VDCCs in cardiovascular function has been demonstrated by embryonic fatality in homozygous knockout mice lacking $Ca_V1.2$ (Seisenberger et al., 2000) and severe hypotension and death in mice following conditional smooth muscle-specific ablation of $Ca_V1.2$ (Moosmang et al., 2003). The cardiac muscle form of $Ca_V1.2$ was proposed to consist of exons 1a/8a/31 while the predominant smooth muscle form consists of exons 1c/8/32 with the addition of a 75 nucleotide cassette exon between exons 9 and 10 (termed exon 9*). These tissue-specific combinatorial splicing patterns may underlie electrophysiological and pharmacological distinctions between cardiac and smooth muscle channels. For example, dihydropyridine calcium channel antagonists are potent vasodilators and are routinely used to treat hypertension and angina pectoris. Although these agents bind with high affinity to constitutively expressed residues at IIIS5, IIIS6, and IVS6, selective expression of exon 8 within IS6 of smooth muscle channels determines dihydropyridine sensitivity (Welling et al., 1997). In addition, smooth muscle channels may be functionally specialized in order to allow activation at physiological membrane potentials. An early study aiming to determine the role of exon 9* in smooth muscle $Ca_V1.2$ found that 9* inclusion resulted in a hyperpolarized shift in voltage-dependent activation when expressed in HEK293 cells (Liao et al., 2004). The authors of this study proposed that functional specialization of VDCCs allowing activation at more hyperpolarized membrane potentials may be

required for Ca^{2+} influx and smooth muscle tension to modest membrane potential depolarization. Further studies have also shown that expression of the N-terminal exon 1c can produce a similar shift in voltage-dependent activation, but this effect is not additive to the effect of exon 9* expression (Cheng et al., 2009). Although exon 1c and exon 9* are within close proximity to the site of interaction between α1 and β subunits (see Figure 6), whether these effects are dependent on β subtype is currently unknown. Regardless, these studies together suggest that alternative splicing may be responsible for generating significant functional diversity among cardiac and smooth muscle L-type VDCCs. Further, alternative splicing patterns may become altered in pathophysiological conditions as a shift in alternative exon expression has been observed in atheroschlerosis, Timothy syndrome and hypertension (Tang et al., 2008a; Tiwari et al., 2006; Yarotskyy et al., 2009). For example, cardiomyocytes of hypertrophic hearts from spontaneously hypertensive rats were found to express channels with significantly altered combinations of mutually exclusive exons 21/22 and 31/32 compared with cardiomyocytes isolated from normotensive rats (Tang et al., 2008b). Although splice variants expressed in hearts of hypertensive rats display distinct electrophysiological characteristics when expressed in HEK293 cells, the functional importance of $Ca_v1.2$ molecular remodeling in cardiovascular disease is currently unclear.

Regulation of smooth muscle membrane potential

Smooth muscle Potassium channels

As described above, VDCC P_{open} and smooth muscle $[Ca^{2+}]_i$ is determined by membrane potential. Due to the relatively high permeability of the plasma membrane to K^+ ions and the chemical gradient for K^+, the resting membrane potential is largely determined by the intracellular and extracellular K^+ concentrations. Given that the intracellular concentration of K^+ ($[K^+]_i \approx 140$ mM) is considerably greater than extracellular K^+ ($[K^+]_o \approx 3$ mM), the direction of the chemical driving force for K^+ ions is toward the extracellular fluid. However, efflux of K^+ ions loss of positive charge increases the electrical driving force, which is toward the intracellular fluid. The membrane potential at which the inward and outward driving forces are zero and there is no net movement of K^+ ions is termed the K^+ equilibrium potential (E_K). In arterial smooth muscle, membrane potential is always positive to E_K (Hulme et al.). Thus, increasing the permeability of the plasma membrane to K^+ will result in efflux of K^+ such that membrane potential will hyperpolarize towards E_K. Vascular smooth muscle is equipped with various K^+-selective channels to regulate membrane potential. This section briefly reviews properties of K^+ channels expressed by cerebral artery myocytes: voltage-dependent (K_V), large conductance Ca^{2+}-activated (BK), ATP-sensitive (K_{ATP}), and inwardly-rectifying (K_{IR}) K^+ channels.

Voltage-dependent K^+ channels: Voltage-dependent K^+ (K_v) channel subtypes expressed in cerebral artery myocytes include $K_V1.2$, $K_V1.3$, $K_V1.5$, $K_V2.1$ (Xu et al., 1999). Studies have also suggested expression of $K_V2.2$ in canine cerebral artery myocytes

(Jahromi et al., 2008a). However, heteromeric channels composed of $K_V1.2$ and $K_V1.5$ subunits have been shown to play a predominant role in the regulation of arterial diameter (Albarwani et al., 2003; Plane et al., 2005). K_V channels open in response to membrane depolarization, resulting in K^+ efflux and hyperpolarization. In addition to increasing the open probability of K_V channels, depolarization also increases the electrical driving force for K^+ efflux. Steady-state K_V activity represents a balance between voltage-dependent activation and inactivation, and currents are observed in cerebral artery myocytes at physiological membrane potentials (Nelson and Quayle, 1995). Studies have suggested that tonic K_V channel activity in cerebral artery myocytes may represent an important feedback mechanism in response to pressure-induced depolarization. Consistent with this, application of the non-selective K_V blocker 4-aminopyridine causes robust constriction of pressurized cerebral arteries (Robertson and Nelson, 1994). In addition, a number of vasodilators may function via activation of K_V channels. Endogenous factors resulting in activation of the cyclic adenosine monophosphate→PKA, or cyclic guanosine monophosphate→PKG pathways (see below) may relax vascular smooth muscle at least partially via increased activity of K_V channels (Aiello et al., 1995; Keef et al., 2001).

Large-conductance Ca^{2+}-activated K^+ channels: Activation of large-conductance Ca^{2+}-activated K^+ (BK_{Ca}) channels occurs in response to micromolar increases in Ca^{2+} as well as membrane potential depolarization (Ledoux et al., 2006). Similar to blocking K_V channels, inhibition of BK_{Ca} channels with paxilline or iberiotoxin causes profound

constriction of pressurized cerebral arteries (Knot et al., 1998), suggesting an important feedback role for these channels in the regulation of cerebral artery tone. In smooth muscle, the majority of BK_{Ca} activity occurs in response to transient localized increases in Ca^{2+} release events from clusters of ryanodine receptors (RyR) in the sarcoplasmic reticulum, or "Ca^{2+} sparks" (Wellman et al., 2002). Each spark can elevate local Ca^{2+} to 10-100 μM and activates ~20-100 plasmalemmal BK_{Ca} channels (Perez et al., 2001). Thus, the frequency of transient outward currents via activation of BK_{Ca} channels is directly proportional to Ca^{2+} spark frequency (Benham and Bolton, 1986; Nelson et al., 1995). Studies in toad stomach smooth muscle have shown that Ca^{2+} spark frequency can be modulated by the concentration of SR Ca^{2+} (ZhuGe et al., 1999), which reflects changes in cytosolic Ca^{2+}. Thus, Ca^{2+} sparks, activation of BK_{Ca} channels and subsequent hyperpolarization may also represent a feedback mechanism for a rise in cytosolic Ca^{2+} following depolarization and activation of VDCCs. Furthermore, mechanisms which result in increased uptake of Ca^{2+} by the SR (i.e. PKA stimulated phosphorylation of the SERCA regulatory protein phospholamban) (Wellman et al., 2001) may cause relaxation of smooth muscle through increased Ca^{2+} spark frequency and BK_{Ca} activity.

Inwardly Rectifying K^+ channels: Inwardly rectifying K^+ channels pass K^+ ions inward more readily than outward. When membrane potential is negative to E_K, inward conductance of K^+ ions via K_{IR} channels occurs. However, membrane potential of cerebral artery myocytes in vivo (-50 mV to -35 mV) is positive to E_K (approximately -85

mV), yet currents through K_{IR} channels at positive potentials is less than expected. This inward rectification is caused by voltage-dependent intracellular block of the channel by polyamines and Mg^{2+} ions (Nichols and Lopatin, 1997). K_{IR} channels display voltage-dependent block by relatively low external concentrations ($K_i \approx 5$ μM) of Ba^{2+} ions. Cerebral artery myocytes express mRNA transcripts for $K_{IR}2.1$, and K_{IR} currents are absent in cerebral artery myocytes from genetically altered mice lacking this gene (Zaritsky et al., 2000). Patch-clamp electrophysiology experiments have demonstrated K_{IR} currents in cerebral artery myocytes suggesting that these channels function to regulate arterial tone in the cerebral circulation.

Inhibition of K_{IR} channels by positively charged ions and proteins is relieved by modest elevation in extracellular K+ ions (5-20 mM) (Nichols and Lopatin, 1997). Given that membrane potential of cerebral artery myocytes is positive to E_K at physiological intravascular pressures, activation of K_{IR} channels by external K^+ results in K^+ efflux and hyperpolarization toward E_K. These K^+-induced dilations are inhibited by Ba^{2+} (Knot et al., 1996) and are absent in knockout mice lacking $K_{IR}2.1$ (Sobey and Faraci, 2000; Zaritsky et al., 2000). This mechanism is thought to be important for coupling cerebral blood flow to metabolic demands of the brain (Filosa et al., 2006; Paulson and Newman, 1987). For example, increases in neuronal activity can dilate local parenchymal arterioles via activation of astrocytic BK_{Ca} channels, release of K^+ ions and activation of vascular smooth muscle K_{IR} channels to induce hyperpolarization and relaxation (Filosa et al., 2006). In addition, activation of K_{IR} channels may result following release of K^+ from neurons and glial cells during hypoxia, ischemia and hypoglycemia (Sieber et al., 1993;

Somjen, 1979). Thus, when oxygen and glucose delivery to metabolically active neurons is compromised, K^+-induced dilations via activation of K_{IR} channels may represent an important mechanism to increase cerebral blood flow to maintain neuronal viability.

ATP-sensitive K^+ channels: Adenosine 5'-triphosphate-sensitive K^+ channels (K_{ATP}) are also expressed in cerebral artery myocytes and are thought to couple metabolic signals to blood flow. These channels open in response to reduced $[ATP]_i$, Po_2, or pH, and increased Pco_2 and prostacyclin, causing hyperpolarization and vasodilation (Faraci and Heistad, 1998; Ko et al., 2008). K_{ATP} channels are heteromultimers comprised of pore-forming subunits (typically K_{IR} subunits) and sulfonylurea receptor subunits (Babenko et al., 1998). K_{ATP} channels are selectively inhibited by sulfonylureas such as glibenclamide (de Weille et al., 1988) and activated by synthetic compounds such as cromakalim and pinacidil (Grover, 1997; Standen et al., 1989). Intraparenchymal injection of cromakalim produces an increase in local cerebral blood flow that is blocked by glibenclamide (Reid et al., 1995), suggesting that K_{ATP} channels are present and functional in cerebral vessels. However, application of glibenclamide does not alter myogenic tone in basilar artery (Faraci and Heistad, 1993) or cerebral arterioles (Armstead, 1996) suggesting that tonic K_{ATP} channel activity does not oppose pressure-dependent constriction. However, K_{ATP} channels are reported to play an important role in vasodilation produced by a number of endogenous compounds including calcitonin gene-related peptide (CGRP) (Kitazono et al., 1993b), prostacyclin (Fredricks et al., 1994),

adenosine (Armstead, 1997), norepinephrine (Kitazono et al., 1993a), and vasoactive intestinal peptide (Faraci and Heistad, 1998; Standen et al., 1989).

Mechanosensitive ion channels:

Chloride channels: Considering intracellular [Cl^-] of 40-70 mM and extracellular [Cl^-] of 140 mM, the equilibrium potential for Cl^- ions is in the range of -30 to -20 mV. Therefore, it was postulated that activation of outward Cl^- currents may represent a mechanism for depolarization of smooth muscle in response to increased intravascular pressure. Consistent with this hypothesis, Ca^{2+}-activated Cl^- channels and volume-regulated Cl^- channels have been reported in vascular smooth muscle and increasing intravascular pressure results in Cl^- efflux (Doughty and Langton, 2001). Further, shifting E_{Cl} from -25 mV to -2 mV augments the myogenic tone response at physiological intravascular pressures (Nelson et al., 1997). Inhibition of Cl^- channels with indanyloxyacetic acid (IAA-94) and 4,4'-diisothiocyanatostilbene-2,2'-disulfonic acid (DIDS) hyperpolarizes and dilates pressurized (80 mmHg) cerebral arteries (Nelson et al., 1997). It was also shown that the potent inhibitor of Ca^{2+}-activated Cl^- channels niflumic acid had no effect on arterial tone suggesting that pressure-induced depolarization of cerebral artery myocytes may be mediated by volume-regulated Cl^- channels. However, later isolation of a current induced by cell swelling was found to shift with the equilibrium potential for Na^+, rather than E_{Cl} (Welsh et al., 2000). Further, these swelling-activated currents and pressure-induced depolarizations were blocked by Gd^{3+} ions, a non-selective cation channel blocker. These findings argued against a role

for Cl^- conductance and instead indicated a direct role for non-selective cation channels in pressure-induced depolarization of cerebral artery myocytes.

Non-selective cation channels: The mammalian TRP superfamily of cation channels are grouped into the following major subfamilies: TRPC (canonical), TRPM (melastatin), TRPV (vanilloid), TRPP (polycystin), TRPML (mucolipin) and TRPA (ankyrin) (Clapham, 2003). With a few exceptions, TRP channels permeate both monovalent and divalent cations. Vascular smooth muscle has been reported to express TRPC1, TRPC3, TRPC4, TRPC6, TRPM4, TRPV2 and TRPV4 (Facemire et al., 2004; Inoue et al., 2006). The finding that Gd^{3+} ions blocked swelling-induced currents in vascular smooth muscle led to the hypothesis that mechanosensitive TRP channels may play a major role in depolarization of cerebral artery myocytes to increasing intravascular pressure. Welsh and colleagues were the first to demonstrate that downregulation of TRPC6 channels, which are mechanosensitive and highly expressed in vascular smooth muscle, greatly attenuates cation currents in response to swelling as well as pressure-induced depolarization and constriction in rat cerebral arteries (Welsh et al., 2002).

Recent studies also indicate an important role for TRPM4 channels in pressure-induced depolarization of cerebral artery myocytes. TRPM4 channels permeate monovalent cations and are activated by intracellular Ca^{2+} and membrane stretch (Morita et al., 2007; Owsianik et al., 2006). Cerebral artery myocyte depolarizations in response to increased intravascular pressure are attenuated when TRPM4 channels are suppressed in vitro (Earley et al., 2004). Furthermore, infusion of antisense oligonucleotides into the

cerebral spinal fluid to suppress TRPM4 channels in vivo caused significantly increased cerebral blood flow over a range of mean arterial pressures (Reading and Brayden, 2007) suggesting disruption of autoregulatory function. Considering that suppression of either TRPC6 or TRPM4 channels results in a similar reduction in pressure-induced depolarization suggests that these channels may function in series rather than in parallel. Hence, a current model of pressure-induced depolarization of cerebral artery myocytes proposes that mechanical forces in response to increased pressure leads to Ca^{2+} entry via TRPC6 channels (Brayden et al., 2008). The resulting increase in local Ca^{2+} thereby activates TRPM4 channels leading to Na^{+} influx, depolarization, activation of VDCCs and smooth muscle contraction.

Second messenger pathways involved in smooth muscle contraction

Cerebrovascular tone can also be modulated by the activity of several second messengers. One particularly important signal transduction system in the control of vascular smooth muscle contraction involves the generation of inositol 1,4,5 trisphosphate (IP_3) and diacylglycerol (DAG) following G_q-dependent activation of phopholipase C. Activators of this pathway include intravascular pressure, vasoconstrictors circulating in the blood (i.e. angiotensin II) as well as neurotransmitters (i.e. serotonin) (Gokina et al., 1999; Mattiazzi, 1997; Parsons et al., 1996). Pharmacological inhibitors of PLC and PKC reduce pressure-induced constrictions in cerebral artery segments (Osol et al., 1991). Following activation of PLC, an increase in IP_3 signals a release of Ca^{2+} from intracellular stores via IP_3 receptors on the SR (Johns et al., 1987). On the other hand,

diacylglycerol is a potent endogenous activator of protein kinase C (PKC). PKC-mediated contraction of vascular smooth muscle can occur via direct phosphorylation of myosin light chain kinase (Nishikawa et al., 1985), phosphorylation of actin binding proteins (i.e. caldesmon, calponin) (Horowitz et al., 1996; Mino et al., 1995) and decreased myosin light chain phosphatase activity (Masuo et al., 1994). All of these effects increase the sensitivity of the smooth muscle contractile apparatus to Ca^{2+}, a process referred to as "Ca^{2+} sensitization". Thus, an increase in smooth muscle PKC activity results in a greater level of arterial constriction for a given level of cytosolic Ca^{2+}. However, it has been shown that cerebral artery constriction in response to the synthetic PKC activator indolactam V is blocked by nisoldipine suggesting that constriction following PKC stimulation requires VDCC-mediated Ca^{2+} influx (Gokina et al., 1999). In addition, PKC activation can also have widespread effects on the activity of smooth muscle ion channels to promote membrane potential depolarization and increased VDCC activity. A number of endogenous vasoconstrictors have been suggested to stimulate smooth muscle VDCC activity via a PKC-dependent mechanism (Gollasch and Nelson, 1997; Keef et al., 2001). For example, PKC activation can directly decrease the activity of both K_{ATP} and K_V channels (Aiello et al., 1996; Quayle et al., 1997) and indirectly decrease BK channel activity via a reduction in Ca^{2+} spark frequency (Bonev et al., 1997). In addition, constriction of cerebral arteries in response to PKC-stimulation is attenuated following suppression of TRPM4 channels (Earley et al., 2007), suggesting that mechanosensitive cation channels may also be a target of PKC. Furthermore, agonist-induced (i.e. phenylephrine, UTP) vasoconstriction may involve activation of

TRPC channels by diacylglycerol in a PKC-independent manner (Inoue et al., 2001; Reading et al., 2005). These effects of PLC/DAG/PKC activation would presumably lead to enhanced depolarization and increased activity of VDCCs. Thus, agonists of G_q-coupled receptors lead to enhanced smooth muscle contraction via elevation of cytosolic Ca^{2+} as well as increased Ca^{2+} sensitivity of the contractile machinery.

The small GTPase Rho can also regulate the function of vascular smooth muscle through its downstream effector Rho-kinase. Rho-kinase activation leads to inhibition of myosin light chain phosphatase via phosphorylation at the myosin binding subunit (Kimura et al., 1996). A subsequent increase in myosin light chain phosphorylation levels then enhances smooth muscle contraction and vasoconstriction. Thus, activation of the Rho-kinase pathway reduces the calcium requirement for prolonged contraction. Agonists of G protein coupled receptors such as serotonin, endothelin-1 and angiotensin II may promote Ca^{2+}-independent contraction via activation of Rho-kinase (Kawano et al., 2002). Rho and Rho-kinase have now been implicated in several cardiovascular disorders and are attracting interest as potential targets for future therapeutics (Hu and Lee, 2003).

Cyclic nucleotides also play an important role in the regulation of cerebral blood flow. A rise in the cytoplasmic concentration of cyclic guanosine 3',5' monophosphate (cGMP) activates cGMP-dependent protein kinase (PKG) and triggers smooth muscle relaxation and vasodilation by several mechanisms. PKG-mediated phosphorylation at specific sites within the VDCC complex may inhibit the channel and reduce Ca^{2+} influx (Jiang et al., 2000). Other potential mechanisms of PKG-induced relaxation of arterial

smooth muscle involve direct activation of BK_{Ca} channels by PKG (Robertson et al., 1993) as well as enhanced uptake of Ca^{2+} into the SR, resulting in increased Ca^{2+} spark frequency and increased BK_{Ca} channel activity (Porter et al., 1998). Evidence suggests that this vasodilatory pathway may also contribute to relaxation in response to G_s stimulation, increased production of cyclic adenosine 3',5' monophosphate (cAMP) and activation of cAMP-dependent protein kinase (PKA). Consistent with this, inhibitors of Ca^{2+} sparks such as ryanodine, abolish both PKA and PKG-mediated increases in transient BK_{Ca} channel activity (Porter et al., 1998). Studies have demonstrated that PKA phosphorylates the SERCA regulatory protein phospholamban, leading to increased SR Ca^{2+} uptake and Ca^{2+} spark frequency in myocytes of pressurized cerebral arteries (Wellman et al., 2001). In addition to the effect on BK channel activity, the cAMP-PKA pathway can also increase the activity of K_{ATP} and K_V channels (Aiello et al., 1995; Quayle et al., 1994), leading to membrane potential hyperpolarization and decreased VDCC P_{open}.

Endothelial influences

For over one hundred years after their discovery in brain capillaries in 1845, endothelial cells were regarded as the inactive lining of blood vessels and capillary walls. However, the modulation of vascular tone by the release of vasoactive factors from endothelial cells has been under intense investigation. Following is a brief overview of major mechanisms in endothelial modulation of vascular smooth muscle contraction, focusing on major

vasoacitve substances released by endothelial cells: Nitric oxide (NO), endothelium-dependent hyperpolarizing factor (EDHF), eicosanoids, and endothelin-1 (ET-1).

Nitric oxide: In 1978, Furchgott observed that acetylcholine, acting on muscarinic receptors, stimulates the release of diffusible substances from the endothelium that cause relaxation of vascular smooth muscle, or "endothelial-derived relaxing factor" (Furchgott and Zawadzki, 1980). Later, Furchgott and Ignarro demonstrated that endothelium-derived relaxing factor was in fact nitric oxide (Furchgott, 1999). In independent studies at the same time, Murad and colleagues found that the potent vasodilator nitroglycerin exerts it effects by releasing nitric oxide, which relaxes vascular smooth muscle and increases blood flow.

Nitric oxide is produced in the conversion of L-arginine to L-citrulline by nitric oxide synthase (NOS) (Fleming and Busse, 1999). Three NOS isoforms have been identified: neuronal (nNOS), endothelial (eNOS) and inducible (iNOS). Under normal conditions, vascular endothelial cells express only eNOS. Increased endothelial Ca^{2+} causes eNOS activation and NO production by Ca^{2+}/calmodulin-dependent displacement of the eNOS protein from the inhibitory scaffolding protein caveolin-1 (Michel et al., 1997). eNOS can also be directly activated by the regulatory heat shock protein (HSP90) (Khurana et al., 2000). Studies suggest this mechanism may be important for basal NO production as well as acetylcholine-mediated dilation (Xu et al., 2002a).

Diffusion of NO to smooth muscle results in activation of soluble guanylate cyclase and increased production of cGMP (Murad, 2004). PKG activation causes increased activity of K^+ channels, smooth muscle hyperpolarization, and decreased VDCC activity (Faraci and Sobey, 1999). For example, PKG can increase BK_{Ca} channel activity directly (Robertson et al., 1993), or indirectly by suppressing synthesis of the BK_{Ca} inhibitor 20-HETE and increasing Ca^{2+} spark frequency (Alonso-Galicia et al., 1997). A recent report also suggests that NO-mediated relaxation may occur via reducing the sensitivity of contractile apparatus to Ca^{2+} (Lehen'kyi et al., 2005).

Release of NO by the endothelium represents an important vasodilator pathway that contributes to modulation of vascular tone both in vitro and in vivo. Inhibition of eNOS with L-NNA results in reduced cerebral blood flow in normal mice, but not in mice lacking the gene for eNOS (Ayata et al., 1996; Ma et al., 1996). These findings suggest that tonic release of NO from the endothelium is a major contributor to cerebrovascular tone and cerebral blood flow.

EDHF: Following the discovery of nitric oxide as an endothelium-derived relaxing factor, another endothelium-dependent vasodilatory mechanism was found which was independent of NOS or cyclooxygenase (COX) (Hoeffner et al., 1989; Vanhoutte, 2004). For example, substances such as UTP and ATP can maximally dilate cerebral arteries following inhibition of NOS and COX (You et al., 1997; You et al., 1999). This vasodilatory process, which may or may not be a diffusible factor, is referred to as endothelium-derived hyperpolarizing factor (EDHF) and is characterized by

endothelium-dependence, hyperpolarization of vascular smooth muscle and activation of endothelial Ca^{2+}-activated K^+ channels (Golding et al., 2002). EDHF-mediated dilation requires an increase in endothelial Ca^{2+} and endothelial hyperpolarization. This hyperpolarization is blocked by application of TRAM-34, an inhibitor of intermediate conductance Ca^{2+}-activated K^+ channels (Marrelli, 2001; Marrelli et al., 2003). In addition, studies also suggest that activity of apamin-sensitive endothelial small conductance Ca^{2+}-activated K^+ (SK_{Ca}) channels may also contribute to endothelial hyperpolarization involved in EDHF (Burnham et al., 2002; Eichler et al., 2003). Although it is not clear how hyperpolarization of endothelial cells leads to smooth muscle hyperpolarization, this may depend on myoendothelial gap junctions (Griffith et al., 2004; Xu et al., 2002b) or SK_{Ca}/IKCa-mediated K^+ release leading to activation of smooth muscle K_{IR} channels (McNeish et al., 2005).

Whereas NO is important in large diameter vessels, EDHF may play a more prominent role as arterial diameter decreases (You et al., 1999). Dilations in response to ATP in middle cerebral arteries are blocked by the NOS inhibitor nitro-L-arginine methyl ester. However, these dilations in penetrating arterioles are resistant to NOS and COX inhibition, but are completely abolished by the endothelial IK_{Ca} inhibitor charybdotoxin (Xu et al., 2001). Heterogeneity in EDHF-mediated control of vascular tone may be important for controlling blood flow to metabolically diverse brain regions.

Prostacyclin and other eicosanoids: The term eicosanoid collectively refers to metabolites of arachidonic acid, which is liberated from the phopholipid membrane by

the enzyme phospholipase A2. Arachidonic acid is metabolized by cyclooxygenase (COX), lipoxygenase, epoxygenase, or Ω hydroxylase (Bogatcheva et al., 2005). The COX pathway was the first arachidonic acid metabolism pathway to be discovered. In the cerebrovascular endothelium, COX produces vasodilator products including prostaglandin I2 (prostacyclin), prostaglandin E2 (Moore et al., 1988), and prostaglandin D2 (Smith et al., 1996), and vasoconstrictor products including prostaglandin F2 and thromboxane A2. The effects of the endothelial vasodilatory compound prostacyclin are well established. Upon prostacyclin binding to G-protein coupled receptors, G_S stimulates activation of adenylyl cyclase and increased cAMP (Bogatcheva et al., 2005). A subsequent increase in PKA activity then enhances K^+ channel activity, resulting in smooth muscle hyperpolarization (Parkington et al., 2004). Vasoconstrictor eicosanoids are thought to be elevated in brain injury (Dewitt et al., 1988; Shohami et al., 1987; Yergey and Heyes, 1990) and may contribute to constriction following ischemia and reperfusion (Cole et al., 1993).

Endothelial epoxygenase catalyzes the metabolism of arachidonic acid to epoxyeicosatrienoic acids (EETs). EETs compounds relax vascular smooth muscle and have been proposed to be one form of EDHF (Fleming and Busse, 2006). One recent study has demonstrated that endothelial-derived 11,12 EET increases the frequency of Ca^{2+} sparks and spontaneous BK_{Ca} currents in cerebral artery myocytes (Earley et al., 2005). This effect was prevented by suppression of TRPV4 channels using antisense oligonucleotides. Thus, 11,12 EETs activate TRPV4 channels and the resulting Ca^{2+}

influx induces Ca^{2+} release events from the SR. This increase in Ca^{2+} spark frequency enhances activity in nearby BK_{Ca} channels and relaxes vascular smooth muscle.

Endothelin-1: The potent endothelium-derived vasoconstrictor endothelin-1 (ET-1) was first characterized in 1988 by Yanagisawa and colleagues (Yanagisawa et al., 1988). Under normal conditions, endothelin release does not significantly contribute to cerebral blood flow (Koedel et al., 1998). However, ET-1 is increased and may contribute to vascular dysfunction in several pathophysiological states including ischemia and reperfusion (Matsuo et al., 2001; Petrov and Rafols, 2001), hyperoxia (Armstead, 1999), and diabetes (Dumont et al., 2003).

ET_A and ET_B receptors are expressed in vascular smooth muscle and endothelial cells, respectively (Arai et al., 1990; Sakurai et al., 1990). Binding of ET-1 to smooth muscle ET_A receptors causes vasoconstriction by several mechanisms (Faraci, 1989; Patel et al., 1996; Pierre and Davenport, 1999; Sagher et al., 1994; Zhou et al., 2004). ET_A activation initially elevates $[Ca^{2+}]_i$ via a mechanisms involving IP_3-mediated Ca^{2+} release from intracellular stores (Zubkov et al., 2004). On the other hand, a sustained Ca^{2+} increase that follows the initial phase is dependent on extracellular Ca^{2+} influx (Miyauchi and Masaki, 1999; Zubkov et al., 2004). In addition, it has been shown that ET-1 can activate the Rho/Rho-kinase pathway in rabbit basilar arteries, which may lead to decreased activity of myosin light chain phosphatase (Zubkov et al., 2004). Depolarization and increased VDCC-mediated Ca^{2+} may also result from ET-1 release via activation of Cl^- channels (Dai and Zhang, 2004). In contrast to activation of ET_A

receptors on smooth muscle, exposure of cerebral arteries to low concentrations of ET-1 causes vasodilation due to endothelial ET_B receptor activation and NO release (Szok et al., 2001).

Part 2: Cerebrovascular pathophysiology associated with subarachnoid hemorrhage.

Introduction

Subarachnoid hemorrhage (SAH) is defined as the extravasation of blood in the subarachnoid space, or the area between the arachnoid membrane and pia mater (see figure 2). Spontaneous SAH most commonly results from the rupture of an aneurysm, or congenital weakness in arterial tunica media, in a cerebral artery on the brain surface. Although the prevalence of unruptured intracranial aneurysms is controversial, reports estimate rates as high as 6 % of the general population are harboring these vascular abnormalities (McCormick and Nofzinger, 1965; Nakagawa and Hashi, 1994). Intracranial aneurysm rupture occurs in approximately 30,000 individuals in the United States each year (Kassell et al., 1985). Major risk factors for SAH include smoking, hypertension, and alcohol consumption (Teunissen et al., 1996).

The consequences of aneurysm rupture and SAH are devastating, with 30 day mortality rates as high as 50% (Kassell et al., 1985; Teunissen et al., 1996; Weir, 1995). Immediately following rupture, the rapid discharge of blood into the subarachnoid space is followed by an acute rise in intracranial pressure. Increased intracranial pressure above the level of intravascular pressure in the cerebral circulation may result in cessation of blood flow, global cerebral ischemia and death. Of the patients surviving the initial hemorrhage, a significant portion develop delayed cognitive deficits that may lead to further morbidity and mortality (Kassell et al., 1985). For decades, it has been widely

accepted that a blood-induced delayed and sustained constriction of conduit arteries on the brain surface ("cerebral vasospasm") is the major contributor to death and disability in patients surviving the initial hemorrhage. However, recent evidence suggests that phenomena other than large artery vasospasm contribute to the development of neurological deficits following SAH, including global transient ischemia, blood-brain barrier disruption, activation of inflammatory pathways and vascular remodeling, and dysfunction of the cerebral microcirculation (Ohkuma et al., 2000; Pluta et al., 2009). In addition, pathological events independent of the cerebral vasculature may also contribute to neurological impairment in SAH patients including early brain injury and cortical spreading depression (Pluta et al., 2009). This section will review major concepts regarding mechanisms of enhanced cerebral artery constriction following SAH, focusing on the role of elevated $[Ca^{2+}]_i$ and enhanced smooth muscle contractility. In addition, emerging evidence supporting a role for small diameter cerebral arteries and arterioles in cerebral ischemia following SAH will also be discussed.

Experimental models of SAH

Experimental models of SAH aim to reproduce the human pathological condition. However, this objective is compromised by the goal to achieve reproducibility and avoid high mortality rates in animals. In addition, certain aspects of human SAH (i.e. spontaneous aneurysm rupture, etc.) are lacking in animal models, which use controlled surgical procedures. Thus, although vasospasm has been reproducibly observed in a variety of animal models, the issue of the most appropriate model for studying the impact

of SAH on the cerebral vasculature has not been completely resolved. Primate and canine SAH models are generally thought to most closely resemble pathology observed in human SAH (Megyesi et al., 2000). However, rodent SAH models are far less expensive and also display many of the pathophysiological properties observed in humans (Lee et al., 2008).

In 1965, Echlin demonstrated that application of clotted autologous blood into the subarachnoid space produces marked spasm of primate basilar and vertebral arteries (Echlin, 1965). Weir et al. reported chronic vasospasm and neurological deficits in these animals over a similar time course to that seen in humans (Weir et al., 1970). In contrast, Simeone and colleagues used small needles to puncture the intracranial internal carotid artery in primates to mimic the rupture of an aneurysm and SAH (Simeone et al., 1968). This method also caused prolonged angiographic vasospasm lasting up to four days. Today, experimental animal models routinely employed to mimic the rupture of an intracranial aneurysm and SAH are: 1) fresh non-clotted autologous blood injected into the subarachnoid space (injection model) or 2) the internal carotid artery or basilar artery is punctured using an endovascular filament (perforation model) (Kozniewska et al., 2006). The perforation model has been limited by much higher mortality rates than the injection model and results vary depending on the size of the blood clot and location of the perforated vessel (Kozniewska et al., 2006; Lee et al., 2009). On the other hand, procedures using a single intracisternal blood injection are associated with low mortality, yet this model fails to reproducibly exhibit significant changes in the vasculature (Clower et al., 1986; Megyesi et al., 2000). To overcome this, the injection model was first

modified in dogs by Varsos et al. by performing a two successive injections of blood 48 hours apart ("double hemorrhage" model) to increase the severity and reproducibility of vasospasm (Varsos et al., 1983). In a variety of species, the double hemorrhage model has been found to exhibit many of the features of SAH found in humans including vasospasm, behavioral deficits and reduced cortical blood flow (Lee et al., 2009; Vatter et al., 2006). Thus, the double injection SAH model has become widely used to study mechanisms of delayed cerebral vasospasm.

Mechanisms of enhanced smooth muscle contraction following SAH

Blood components: Whole blood consists of erythrocytes, leukocytes, platelets, soluble proteins, glucose, hormones and gases. In the 1970's, evidence was obtained supporting the hypothesis that the occurrence of vasospasm was correlated with erythrocyte lysis and levels of the blood component oxyhemoglobin in the cerebral spinal fluid (CSF). Purified oxyhemoglobin alone is capable of producing sustained cerebral artery constriction in vitro (Tanishima, 1980; Wellum et al., 1980). Oxyhemoglobin concentrations measured in the CSF of SAH patients are sufficient to produce significant constriction of arteries in vitro and are correlated with development of vasospasm (Kajikawa et al., 1979). Following erythrocyte lysis, oxyhemoglobin is oxidized to methemoglobin and superoxide radical. Superoxide radical combines with water to form hydrogen peroxide, which can react with ferrous iron of methemoglobin to form hydroxyl radical. Subsequent hydroxyl radical-induced lipid peroxidation can lead to functional and morphological changes and has been proposed as an important mechanism in the

pathogenesis of vasospasm (Sakaki et al., 1986). In a primate SAH model, the inhibitor of iron-dependent lipid peroxidation U74006F was shown to greatly attenuate vasospasm (Steinke et al., 1989). However, clinical trials using this agent as well as the antioxidants superoxide dismutase and catalase have failed to significantly benefit SAH patients (Wellum et al., 1982; Zhang et al., 2010). As will be discussed, oxyhemoglobin may also lead to enhanced cerebral artery constriction by interfering with the NO-cGMP signaling pathway as well as inhibition of smooth muscle K^+ channel activity.

In addition to erythrocyte lysis products, activated leukocytes and platelets have also been implicated in inflammatory processes contributing to vascular dysfunction following SAH. Activation of leukocytes and platelets following SAH may occur due to the upregulated expression of specific adhesion molecules by endothelial cells or disruption of the endothelial monolayer, exposing leukocytes and platelets to collagen, elastin and basement membrane (Davies and Hagen, 1993; Vane et al., 1990). Studies have shown the presence of platelet microthrombi surrounding vasospastic arteries as well as polymorphonuclear leukocytes in the intima of cerebral arteries following SAH (Minami et al., 1991; Suzuki et al., 1990). Activated platelets and leukocytes are capable of releasing numerous vasoactive substances including thromboxane A_2, endothelin-1, 5-HT and ATP (Siminiak et al., 1995). Thus, activation of these blood components following SAH is likely to contribute to enhanced cerebral artery constriction.

Role of $[Ca^{2+}]_i$

Although vascular smooth muscle contractility is largely determined by the concentration of intracellular Ca^{2+}, the role of elevated $[Ca^{2+}]_i$ in cerebral artery myocytes leading to enhanced constriction following SAH is controversial. In 1976, Peterson and Leblanc first proposed that vasospasm following subarachnoid hemorrhage was dependent on increased vascular smooth muscle $[Ca^{2+}]_i$ caused by spasmogens in blood (Peterson and Leblanc, 1976). The authors additionally proposed that increasing the intracellular concentration of cAMP may be effective for reversing vasospasm due to increased uptake of Ca^{2+} into the SR. Later, the development of Ca^{2+} sensitive fluorescent dyes made it possible to directly measure intracellular Ca^{2+} in vascular smooth muscle in spastic arteries isolated from experimental SAH animals. Bulter et al. used the photoprotein aequorin from the luminescent jellyfish *Aequorea victoria* to measure intracellular Ca^{2+} in vasospastic anterior spinal arteries isolated from a canine double-hemorrhage SAH model (Bulter et al., 1996). It was found that $[Ca^{2+}]_i$ in vasospastic cerebral arteries was significantly elevated (by ~140 nM) compared to normal arteries. This elevation in $[Ca^{2+}]_i$ was correlated with a marked increase in myosin light chain phosphorylation. Another study using the ratiometric Ca^{2+}-sensitive fluorescent dye fura-2 also suggested that impaired regulation of smooth muscle $[Ca^{2+}]_i$ may contribute to vasospasm following SAH (Kim et al., 1996b). Conversely, reports have also suggested contribution of Ca^{2+}-independent contractile pathways (i.e. Rho-kinase mediated inhibition of myosin light chain phosphatase) to the development of vasospasm following SAH (Laher and Zhang,

2001; Nishizawa and Laher, 2005). Thus, the role of increased $[Ca^{2+}]_i$ in the pathogenesis of cerebral vasospasm remains unclear.

Role of voltage-dependent Ca^{2+} channels

Inhibitors of VDCCs are used clinically and provide a modest beneficial effect in SAH patients (Treggiari-Venzi et al., 2001). Following SAH, elevated vascular smooth muscle $[Ca^{2+}]_i$ may result from increased density of VDCCs, a direct alteration of VDCC gating, or indirect increase in channel activity via membrane potential depolarization. Aihara et al. found no change in mRNA expression of $Ca_V1.2$ in basilar arteries from a canine SAH model (Aihara et al., 2004). However, whether expression of $Ca_V1.2$ is altered in resistance sized cerebral arteries and arterioles following SAH is not known. In addition, no studies to date have measured expression of auxiliary VDCC β subunits, which are critical for membrane insertion of α_1 subunits (Chien et al., 1995), in cerebral arteries from SAH animals. A study by Ishiguro et al. used patch clamp electrophysiology to measure whole cell VDCC currents in cerebral artery myocytes from SAH rabbits (Ishiguro et al., 2005). These experiments found that VDCC currents in cerebral artery myocytes from SAH animals were increased by ~40% and were partially resistant to L-type VDCC inhbitiors. The selective R-type VDCC blocker SNX-482 abolished nifedipine-insensitive VDCC currents in myocytes from SAH animals. Consistent with this, small diameter cerebral arteries from SAH animals were found to express mRNA and protein for both $Ca_v1.2$ (L-type) and $Ca_V2.3$ (R-type), whereas arteries from control animals expressed only $Ca_V1.2$. Upregulated expression and function of R-type VDCCs

in cerebral arteries was also demonstrated following incubation for 5 days with the blood component oxyhemoglobin (Link et al., 2008). Thus, although oxyhemoglobin does not appear to directly increase VDCC activity (Kim et al., 1996a), this spasmogen may lead to enhanced membrane Ca^{2+} currents via upregulation of R-type channels following SAH. Further, vasoactive blood components released into the CSF following SAH, such as norephinephrine, serotonin, and 20-hydroxyeicostetraenoic acid (20-HETE), are reported to increase the VDCC activity in vascular smooth muscle and have been implicated in the development of cerebral vasospasm (Gebremedhin et al., 1998; Nelson et al., 1988; Svendgaard et al., 1977; Takeuchi et al., 2006; Worley et al., 1991). Thus, substantial evidence supports the hypothesis that elevated smooth muscle $[Ca^{2+}]_i$ following SAH may result from increased VDCC activity.

Role of K^+ channels

Smooth muscle membrane potential depolarization may lead to increased Ca^{2+} influx in cerebral artery myocytes via increased VDCC P_{open}. Harder and colleagues were the first to propose that membrane potential depolarization of vascular smooth muscle following SAH may result from decreased K^+ conductance (Harder et al., 1987). In this study, it was shown that vasospasm could be reversed by hyperpolarization induced by application of the K^+ channel opener nicorandil. Since then, others have also reported that vasospastic cerebral artery myocytes from SAH model animals are more depolarized compared with controls (Harder et al., 1987; Waters and Harder, 1985; Zuccarello et al., 1996a) and that dilations in response to synthetic K^+ channel activators are enhanced in

arteries from SAH animals (Sobey et al., 1997; Zuccarello et al., 1996b). It is becoming increasingly clear that components of blood can constrict cerebral arteries via suppression of smooth muscle K^+ channel activity.

K_V channels: Quan and Sobey first provided evidence that voltage-dependent K^+ channels were suppressed following SAH with the finding that constrictions to the non-selective K_V channel blocker 4-aminopyridine were reduced in basilar arteries from SAH rats compared with controls (Quan and Sobey, 2000). Molecular assessment of K_v channel expression has revealed that mRNA for $K_V2.1$ and $K_V2.2$ are downregulated in canine basilar arteries following SAH (Aihara et al., 2004) and is correlated with ~50% decrease in K_V2 currents (Jahromi et al., 2008a). Additionally, studies in our laboratory have also demonstrated that $K_V1.5$ channels are suppressed in cerebral artery myocytes following SAH by a mechanism involving oxyhemoglobin-induced activation of the tyrosine kinase EGF receptor and channel endocytosis (Ishiguro et al., 2006; Koide et al., 2007). Thus, suppression of K_V channel activity is likely to contribute to membrane potential depolarization and enhanced arterial constriction following SAH.

BK_{Ca} channels: BK channels act as an important feedback mechanism to limit membrane potential depolarization and elevated $[Ca^{2+}]_i$ in cerebral artery myocytes. Studies have shown that mRNA and protein for BK α and β_1 subunits are unchanged following SAH (Aihara et al., 2004). A later study found no significant differences between normal and vasospastic myocytes in BK current density, kinetics, Ca^{2+}- or voltage-sensitivity, or

single channel conductance (Jahromi et al., 2008b). However, BK channel activity may be suppressed in vivo following SAH due to increased levels of the endogenous BK channel inhbitor 20-HETE in the CSF (Poloyac et al., 2005; Roman et al., 2006). Further, studies in our laboratory have discovered decreased spontaneous transient BK_{Ca} currents and Ca^{2+} spark frequency in cerebral artery myocytes from SAH model rabbits (Koide, 2009). This decrease in Ca^{2+} spark frequency may be caused by reduced expression of ryanodine receptor type 2 (RyR2) and increased expression of the RyR2 stabilizing protein FKBP12.6 in cerebral arteries from SAH animals (see Appendix C). In addition, incubation of cerebral arteries in purified oxyhemoglobin also reduces the frequency of Ca^{2+} sparks, leading to decreased outward BK_{Ca} currents, depolarization and enhanced constriction (Jewell et al., 2004). Therefore, although BK_{Ca} channel density and functional properties may be unchanged following SAH, factors regulating the activation of these channels may be altered causing decreased activity of this vasodilator pathway.

K_{IR} channels: Few studies have directly examined the expression and function of smooth muscle K_{IR} channels in the cerebral vasculature following SAH. However, Aihara et al. found a ~350% increase in $K_{IR}2.1$ protein in vasospastic canine basilar arteries compared with normal arteries (Aihara et al., 2004). Consistent with this, a subsequent study by Weyer et al. found that depolarization and constriction in response to Ba^{2+} in the presence of 4-aminopyridine (K_V blocker) and paxilline (BK_{Ca} blocker) were greater in myocytes from vasospastic arteries from SAH animals compared with controls (Weyer et al., 2006).

Further, patch-clamp electrophysiology demonstrated significantly increased K_{IR} currents in canine basilar artery myocytes following SAH (Weyer et al., 2006). The authors of this report proposed that upregulation of K_{IR} channels following SAH may represent a potential compensatory mechanism to counteract sustained arterial constriction. However, unpublished observations from our laboratory found no significant effect of SAH on the magnitude of K_{IR} currents in myocytes from small diameter cerebral arteries arteries in rats and rabbits (Koide and Wellman, unpublished observations). Thus, the impact of SAH on the function and expression of K_{IR} channels in the cerebral vasculature may vary with vessel caliber or species.

K_{ATP} channels: Studies have shown that dilations induced by activators of K_{ATP} channels are enhanced following SAH (Sugai et al., 1999; Zuccarello et al., 1996b), suggesting that these channels remain functional in the cerebral vasculature. However, other reports have demonstrated a decrease in the levels of the endogenous activator of K_{ATP} channels calcitonin gene-related peptide (CGRP) following SAH (Edvinsson et al., 1991; Edvinsson et al., 1994) suggesting that decreased K_{ATP} activity may contribute to cerebral vasospasm in vivo. Implantation of CGRP tablets in the subarachnoid space of SAH model animals was shown to reverse vasospasm (Inoue et al., 1996). However, the use of CGRP in SAH patients did not improve patient outcome in a multi-center single-blind trial (1992). Hypotension was reported as a common limiting side effect in this study, most likely due to activation of K_{ATP} channels in the systemic circulation.

Role of Protein Kinase C

Activation of PKC leads to increased smooth muscle contractility by several Ca^{2+}-dependent and Ca^{2+}-independent mechanisms (see *"second messenger pathways involved in smooth muscle contraction"* above). Activation of the PLC/PKC pathway may also contribute to the pathophysiologic regulation of vascular tone following SAH (Matsui et al., 1991; Nishizawa et al., 1996; Nishizawa et al., 1995; Shiota et al., 1996). Levels of diacylglycerol, an endogenous activator of PKC, are elevated in basilar arteries following SAH on days 2, 4, and 7 but is reduced to normal levels on day 14 (Matsui et al., 1991). Several studies suggest significantly increased membrane bound activated PKCα and decreased cytosolic PKCα which is correlated with angiographic vasospasm on days 4 and 7 following SAH (Matsui et al., 1991; Matsui et al., 1993; Nishizawa et al., 1992; Takuwa et al., 1993).

The use of PKC inhibitors to relieve vasospasm has yielded inconsistent results. The PKC inhibitors staurosporine and H-7 reversed vasospasm on day 7 in a canine double hemorrhage SAH model (Matsui et al., 1991). However, application of the PKC inhibitor staurosporine failed to reverse vasospasm in rabbit basilar arteries whereas the K_{ATP} channel opener cromakalim completely relaxed these vessels (Zuccarello et al., 1996b). Thus, it is possible that the contribution of PKC activation leading to enhanced vasoconstriction following SAH varies between species and experimental SAH models.

Role of Rho/Rho kinase

Activation of the small GTPase RhoA and subsequent activation of Rho kinase leads to a decrease in myosin light chain phosphatase activity and sensitization of smooth muscle contractile filaments. Increased mRNA for RhoA and Rho kinase were demonstrated in arteries exhibiting vasospasm from a rat double hemorrhage SAH model (Miyagi et al., 2000). Increased Rho-kinase and myosin light chain phosphorylation were also demonstrated in canine basilar arteries following experimental SAH (Sato et al., 2000). Topical application of the Rho-kinase inhibitor Y-27632 caused a dose-dependent decrease in myosin light chain phosphorylation and dilation in spastic canine basilar arteries on day 7 following hemorrhage (Sato et al., 2000). The partially selective inhibitor of Rho-kinase fasudil is approved for use in SAH patients in Japan and provides slight improvement in clinical outcome (Nakashima et al., 1998; Tachibana et al., 1999).

Effect of SAH on the endothelium

NO: Tonic NO release is an important regulator of cerebrovascular tone. The bioavailability of this potent vasodilator may be reduced following SAH due to the high affinity binding of NO by hemoglobin following erythrocyte lysis (Edwards et al., 1992). Many reports suggest that SAH can also disrupt the NO→cGMP feedback process to cause enhanced cerebral artery constriction. In support of this hypothesis, mRNA encoding eNOS was significantly decreased in vasospastic cerebral arteries from a primate SAH model (Hino et al., 1996). However, the contribution of decreased NO release to enhanced cerebral artery constriction following SAH is controversial, as other

studies have demonstrated normal eNOS expression and activity in basilar arteries from SAH dogs (Kasuya et al., 1995; Kim et al., 1989; Naveri et al., 1994). Some, but not all studies have also indicated diminished vasodilator response to exogenous NO after SAH (Afshar et al., 1995; Nakao et al., 1996; Pluta et al., 2000). This may result from decreased expression or functionality of smooth muscle soluble guanylate cyclase or protein kinase G, or via increased phosphodiesterase activity in vascular smooth muscle, leading to reduced steady-state cGMP levels. In addition, normal basal NO release prior to SAH may also function to inhibit PKC activation (Nishizawa et al., 1996). Therefore, diminished release of NO or decreased cGMP levels may also lead to enhanced PKC-dependent vascular smooth muscle contraction following SAH.

Endothelin-1: In addition to decreased NO release following SAH, other observations suggest that increased endothelial release of the potent vasoconstrictor ET-1 may be a major contributor to vasospasm. Several studies have demonstrated increased ET-1 levels in basilar arteries and CSF following SAH (Hirose et al., 1995; Kobayashi et al., 1991; Kraus et al., 1991). In a study by Itoh et al., mRNA encoding ET_A receptors was not detected in basilar arteries from control animals but was markedly increased in vessels 3 days following SAH in dogs (Itoh et al., 1994). Activity of endothelin converting enzyme (ECE), which converts preproendothelin-1 to active ET-1, is also increased 3-fold in basilar arteries from SAH model animals (Roux et al., 1995). Further supporting a role for ET-1 in vasospasm, ET_A receptor antagonists, ECE inhibitors, and antisense oligonucleotides against preproendothelin-1 mRNA substantially attenuate

vasospasm and constriction in response to hemolysate application (Itoh et al., 1994; Matsumura et al., 1991; Onoda et al., 1996). In addition to increasing intracellular Ca^{2+}, increased levels of ET-1 following SAH may also lead to enhanced vascular smooth muscle contraction via activation of PKC (Murray et al., 1992).

Impact of SAH on the cerebral microcirculation

Following angiographic demonstration of SAH-induced arterial narrowing in 1951, extensive clinical research has aimed at preventing enhanced constriction of large diameter conduit cerebral arteries in SAH patients. Overall, clinical trials have been ineffective at reducing angiographic vasospasm. However, one recent trial using a selective ET_A receptor antagonist, clazosentan, demonstrated a significant dose-dependent reduction in moderate to severe angiographic vasospasm at day 9 following aneurysm rupture (Macdonald et al., 2008). Despite approximately 50% decrease in the occurrence of vasospasm, clazosentan did not significantly reduce the rate of poor clinical outcome based on the modified Rankin scale. On the other hand, clinical use of the VDCC blocker nimodipine produces a modest improvement in clinical outcome in SAH patients (Petruk et al., 1988). However, studies suggest that nimodipine does not significantly influence the incidence of moderate or severe angiographic vasospasm (Petruk et al., 1988). Thus, large artery vasospasm does not always correlate with the occurrence of ischemia-related neurological deficits in SAH patients.

Recently emerging evidence suggests that small diameter cerebral arteries and arterioles, which are critical for autoregulation of cerebral blood flow may be more

constricted following SAH. Takeuchi and colleagues made the observation that cerebral blood flow was significantly reduced at mean arterial blood pressures from 40 to 100 mmHg in SAH model primates (Takeuchi et al., 1991). This finding suggests that SAH may impair cerebral autoregulation such that physiological increases in intravascular pressure lead to greater constriction of resistance arteries and arterioles in the cerebral circulation, thus reducing cortical blood flow. Consistent with this hypothesis, Ishiguro et al. demonstrated enhanced pressure-dependent constriction of small diameter (100-200 μm diameter) cerebral arteries from a rabbit SAH model at physiological intravascular pressures in vitro (Figure 7) (Ishiguro et al., 2002). Decreased cerebral circulation time and regional cerebral blood flow measurements in humans 5 and 7 days after SAH (Ohkuma et al., 2000) also suggests decreased luminal caliber of intracerebral arterioles. Furthermore, Knuckey et al. observed decreased cerebral blood flow in SAH patients which was not secondary to increased intracranial pressure or angiographic vasospasm (Knuckey et al., 1985). Although various histological studies of parenchymal arterioles from SAH model animals have suggested enhanced constriction of these vessels following SAH (Ohkuma et al., 1997; Ohkuma and Suzuki, 1999), the function of isolated parenchymal arterioles following SAH has not been investigated.

Summary

The cerebral circulation is exquisitely regulated by numerous mechanisms to ensure adequate delivery of oxygen and nutrients to the brain. Under normal conditions, cerebral artery diameter is largely controlled by vascular smooth muscle membrane

potential and the activity of voltage-dependent Ca^{2+} channels, which represent a splice variant of the gene $Ca_V1.2$. Following SAH, factors released into the cerebrospinal fluid exert a profound influence over vascular smooth muscle leading to enhanced contraction and decreased blood flow. Although decades of research has focused on the impact of SAH on large diameter arteries on the brain surface, evidence suggests that small diameter arterioles within the brain parenchyma may be more constricted and reduce local cerebral blood flow.

Part 3: Hypotheses

1. Increased L-type VDCC activity causes enhanced pressure-dependent constriction of parenchymal arterioles following experimental SAH.

The overall objective in Chapter 2 of this dissertation was to examine the relationship between intravascular pressure, smooth muscle intracellular Ca^{2+} ($[Ca^{2+}]_i$), membrane potential and diameter of isolated parenchymal arterioles from unoperated, sham-operated and SAH model rats. A combination of techniques were used to test the hypothesis that increased activity of smooth muscle L-type VDCCs ($Ca_V1.2$) leads to elevated $[Ca^{2+}]_i$ and enhanced pressure-induced constriction of parenchymal arterioles from SAH animals. Therefore, it was also predicted that enhanced constriction of parenchymal arterioles following SAH was primarily the result of elevated $[Ca^{2+}]_i$, rather than Ca^{2+} sensitization of the smooth muscle contractile machinery (i.e. via increased PKC or Rho kinase activation). Examination of the relationship between $[Ca^{2+}]_i$ and

constriction revealed that enhanced arteriolar tone was due to increased Ca^{2+} influx via L-type channels and elevated $[Ca^{2+}]_i$. We also hypothesized that increased L-type VDCC activity following SAH may result from either increased VDCC expression or membrane potential depolarization. We provide evidence suggesting that L-type VDCC mRNA and protein expression is not altered in parenchymal arterioles from SAH animals. However, parenchymal arteriolar myocytes were significantly depolarized at physiological intravascular pressures. Our data support the hypothesis that membrane potential depolarization causes increased L-type VDCC-mediated Ca^{2+} influx and enhanced constriction following SAH. We propose enhanced constriction of parenchymal arterioles may contribute to reduced cerebral blood flow and neurological deficits in SAH patients.

2. The smooth muscle selective L-type VDCC splice variant containing exon 9* is dominant in cerebral artery constriction.

Oral administration of voltage-dependent Ca^{2+} channel antagonists is standard treatment in SAH patients and provides a modest beneficial effect (Treggiari-Venzi et al., 2001). However, these agents can also act on VDCCs in the systemic circulation leading to drastic reductions in vascular resistance and blood pressure. Thus, the use of VDCC antagonists in SAH patients has been greatly limited by hypotension. Therefore, the overall objective in Chapter 3 of this dissertation was to develop a strategy to suppress VDCC activity specifically in the cerebral vasculature. We hypothesized that targeting a population of $Ca_V1.2$ splice variants specifically expressed by smooth muscle with

antisense oligonucleotides may provide a means of cerebral artery dilation while avoiding suppression of neuronal channels. In addition, future administration of antisense into the cerebrospinal fluid of SAH model animals should limit effects to the cerebral vasculature.

Previous studies demonstrate that inclusion of the smooth muscle-selective alternatively-spliced exon 9* in $Ca_V1.2$ channels causes a shift in voltage-dependent activation towards more negative potentials (Liao et al., 2004). Therefore, inclusion of exon 9* may be important for development of tone at physiological membrane potentials in vascular smooth muscle. This finding led us to hypothesize that exon 9* $Ca_V1.2$ splice variants play a critical role in the regulation of cerebral artery diameter. Data presented in Chapter three of this dissertation suggest that suppression of $Ca_V1.2$ channels containing exon 9* results in markedly reduced cerebral artery constriction in response to K^+-induced membrane depolarization in vitro. Our results suggest that exon 9* containing $Ca_v1.2$ channels are functionally dominant in cerebral artery constriction and may provide a novel target for prevention of elevated $[Ca^{2+}]_i$ and enhanced constriction following SAH.

Figures

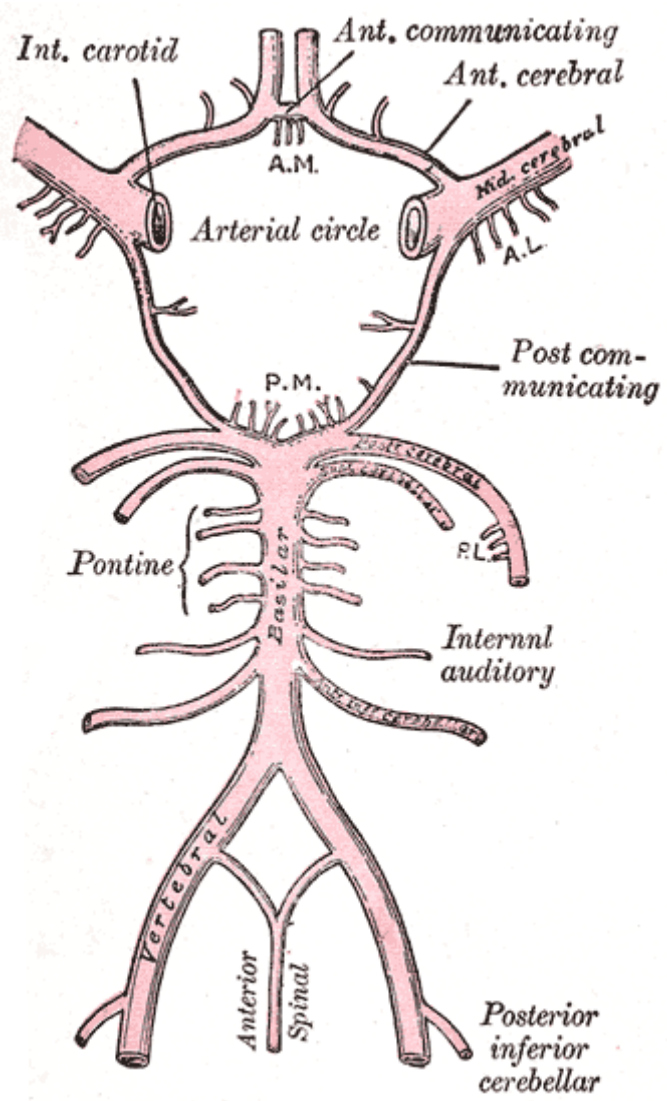

Figure 1: ***Cerebral blood supply.***

Illustration of major arteries on the base of the brain. The Circle of Willis receives blood from the basilar and internal carotid arteries. These arteries are connected by the anterior communicating and posterior communicating arteries. The major arteries supplying the cerebral hemispheres branch off of the Circle of Willis. Modified from Gray, *Anatomy of the Human Body: 20th Edition*. 2000 with permission.

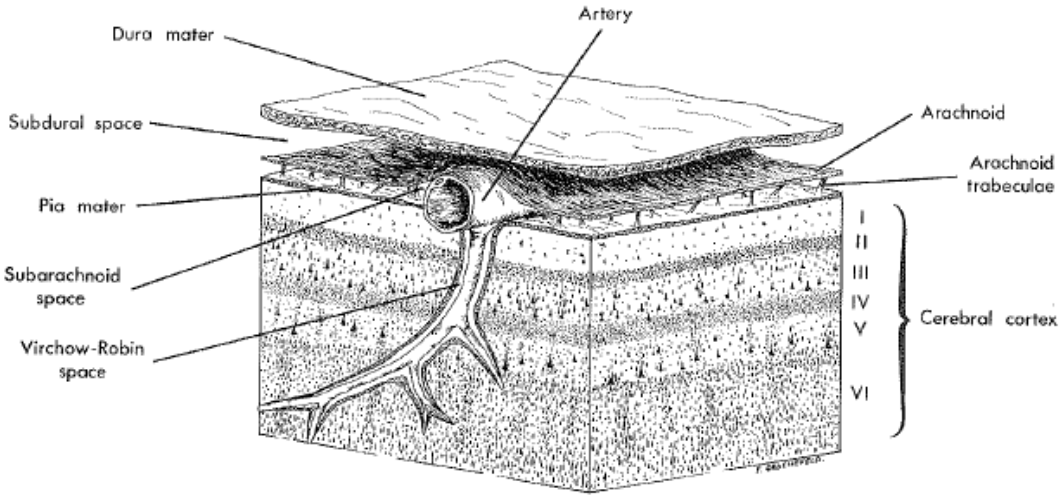

Figure 2: ***Organization of pial and parenchymal vasculature.***

Schematic representation showing pial cerebral arteries on the brain surface and penetrating and parenchymal arterioles within the cortex. Superficially, the Virchow-Robin space is continuous with the subarachnoid space. Distally, this space transitions into perivascular space separating astrocytic endofeet and vascular smooth muscle of parenchymal arterioles. Modified from Edvinsson and Krause, *Cerebral Blood Flow and Metabolism: Second Edition*. 2002 with permission from Wolters Kluwer.

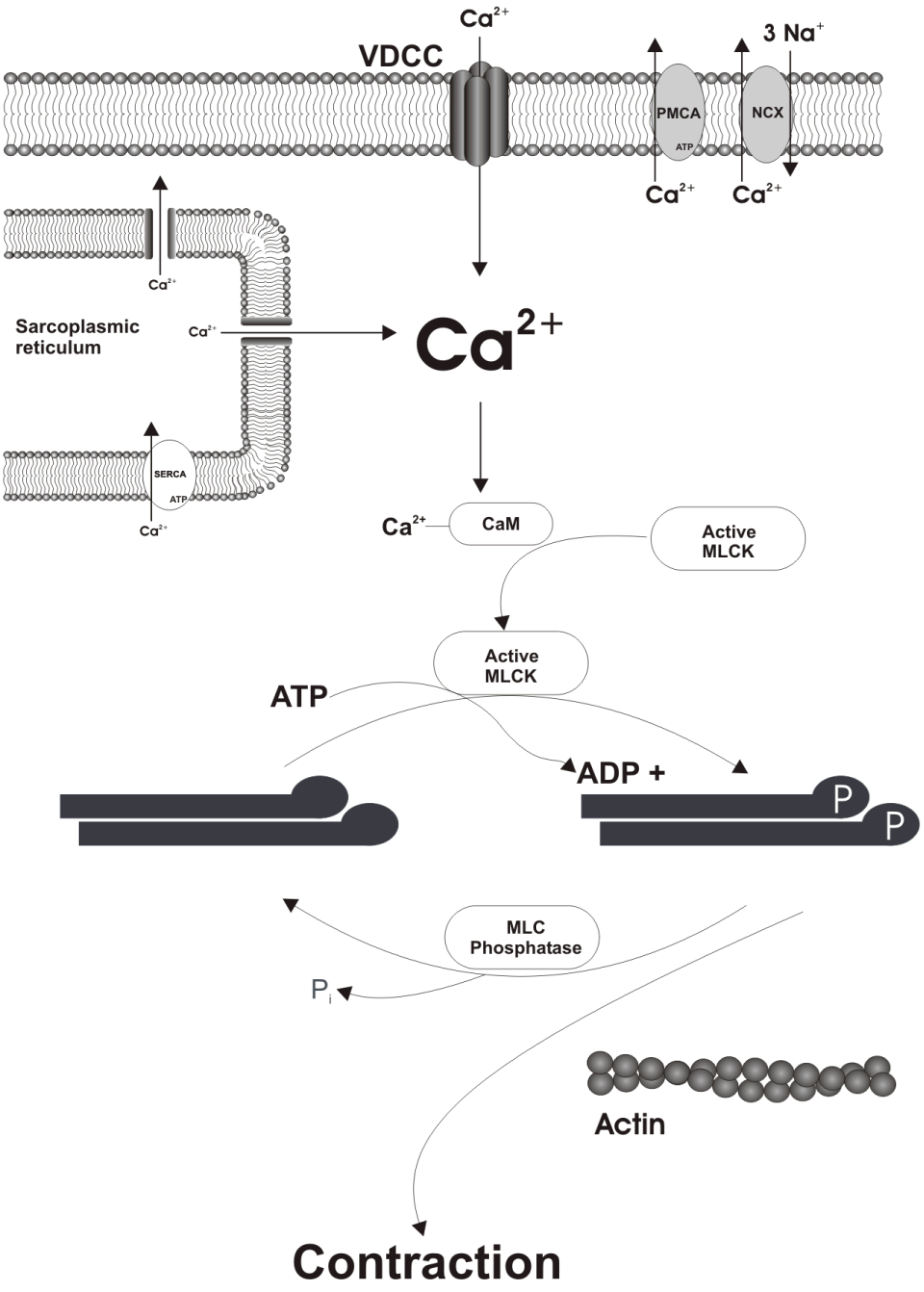

Figure 3: ***Regulation of intracellular Ca^{2+}.***

Major pathways for Ca^{2+} influx and extrusion are shown. SERCA: sarcoplasmic/endoplasmic reticulum Ca^{2+} ATPase; PMCA: plasma membrane Ca^{2+} ATPase; NCX: Na^{+}/Ca^{+} exchanger; CaM: calmodulin; MLC: myosin light chain; MLCK: myosin light chain kinase.

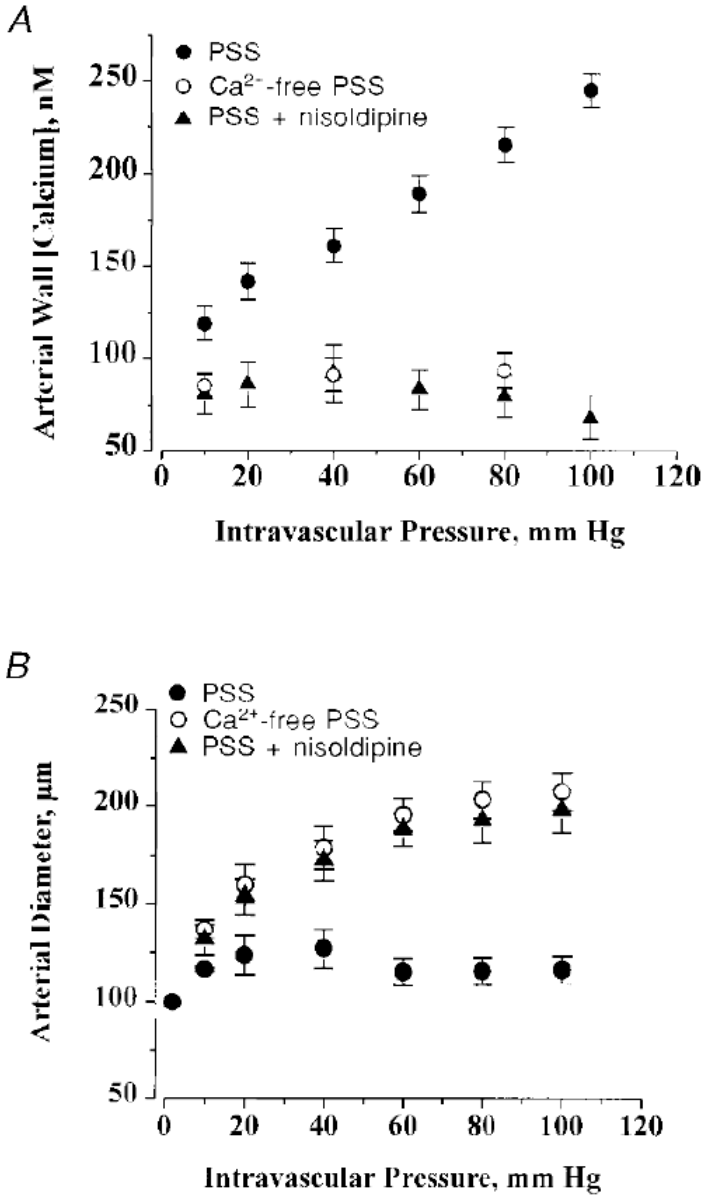

Figure 4: ***Role of VDCCs in pressure-induced constriction.***

Elevation of Intravascular pressure results in increased cytosolic Ca^{2+} and decreased diameter (constriction). This response to increased pressure is abolished by the dihydropyridine L-type VDCC inhibitor nisoldipine or removal of Ca^{2+} from the bath solution. Modified from Knot HJ and Nelson MT, Regulation of arterial diameter and wall $[Ca^{2+}]_i$ in cerebral arteries of rat by membrane potential and intravascular pressure. *J. Physiol*., 1998 with permission.

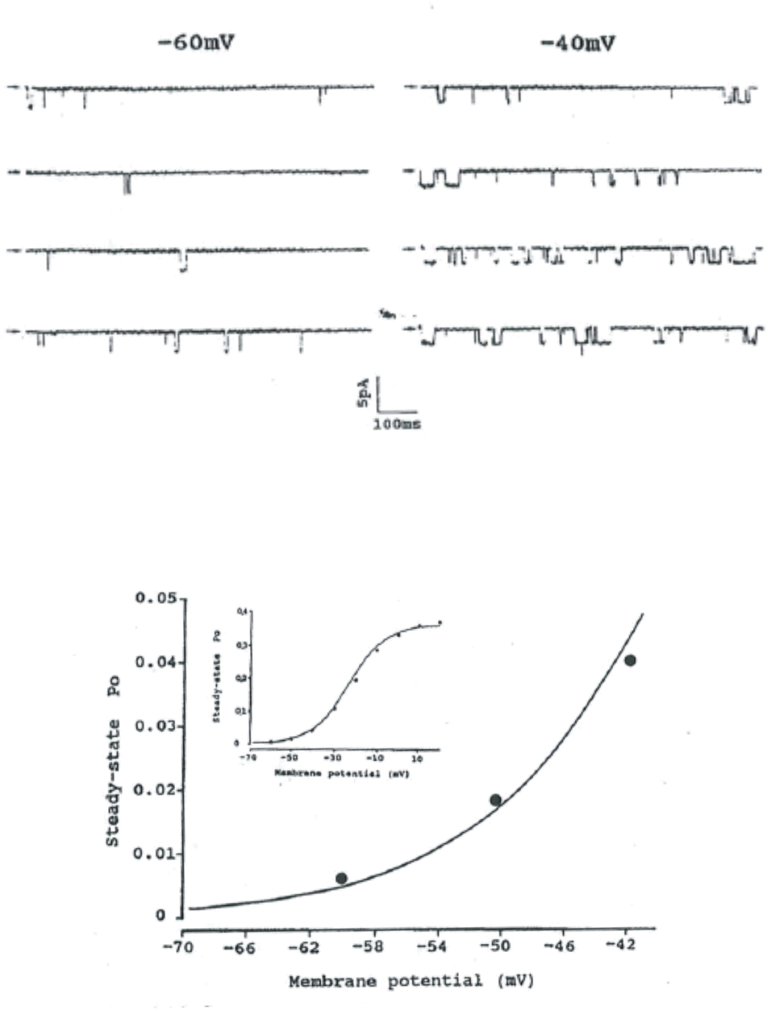

Figure 5: ***Voltage-dependence of VDCC open-state probability.***

Top- On-cell patch recording from rabbit mesenteric artery myocytes. Traces show single Ca^{2+} channel openings at -60 and -40 mV from holding potential of -95 mV, using Ba^{2+} as a charge carrier in the presence of the dihydropyridine L-type VDCC agonist Bay R 5417. *Bottom*- Steady state P_{open} (from single channel openings during 1 second voltage pulses) over physiological range of membrane potentials. Inset shows P_{open} over a wider range of voltages. Modified from Nelson MT et al., Calcium channels, potassium channels and voltage dependence of arterial smooth muscle tone. *Am J Physiol*., 1990 with permission from American Physiological Society.

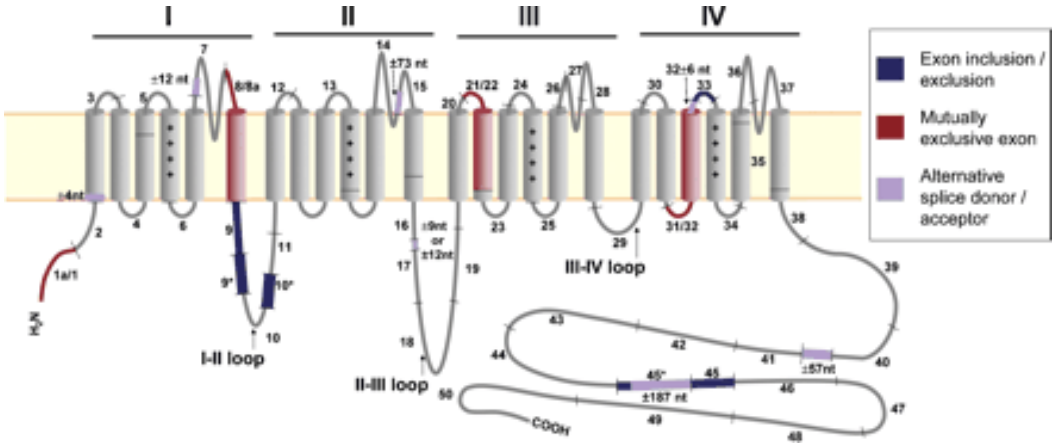

Figure 6: ***Alpha 1 pore-forming subunit of $Ca_V1.2$ VDCCs.***

The α_1 subunit consists of four homologous domains (I-IV). Each domain contains six transmembrane segments (S1-S6). The S4 segments of each domain confers voltage-sensitivity to the channel. Exons encoding the α_1 subunit are numbered. Boundaries between exons are denoted by perpendicular lines. Modified from Liao P. et al., Splicing for alternative structures of $Ca_V1.2$ calcium channels in cardiac and smooth muscles., *Cardiovasc Res*., 2005 with permission from Oxford University Press.

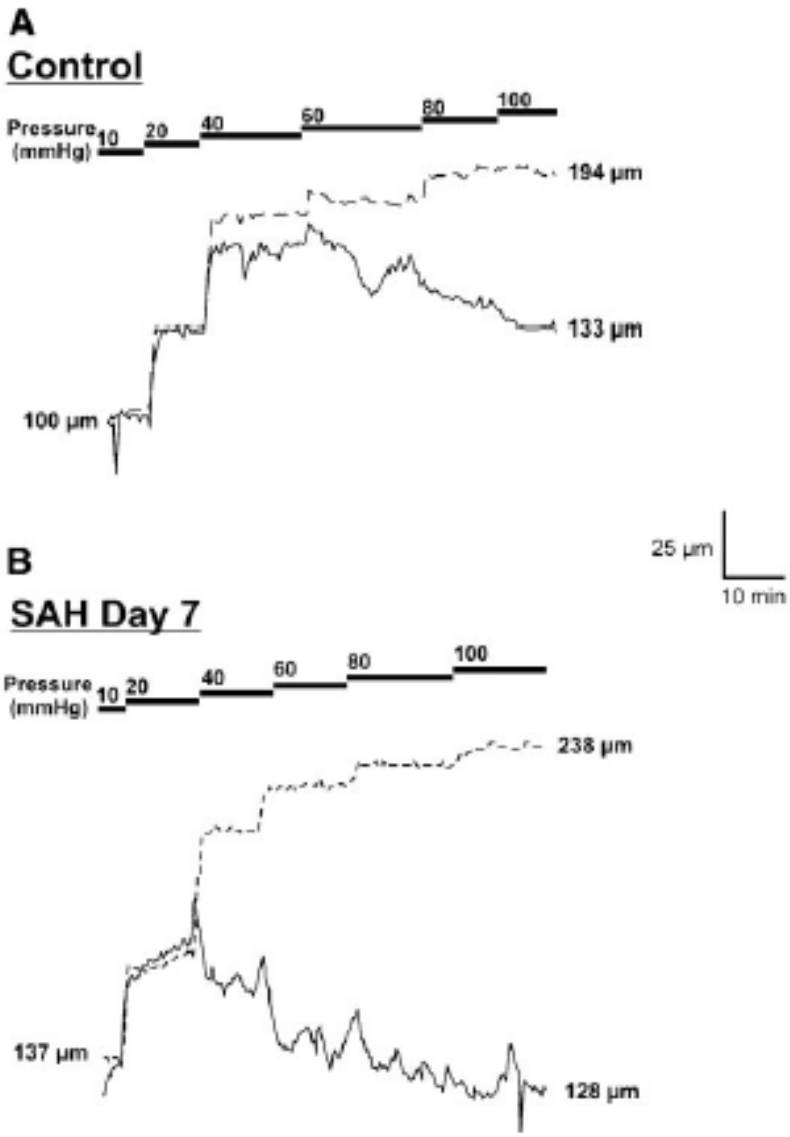

Figure 7: ***Impact of SAH on cerebral artery tone.***

Enhanced pressure-induced constriction of small diameter cerebral arteries from SAH model rabbits. Representative diameter traces from arteries isolated from control unoperated (Control, A) and SAH model animals (B). Solid lines represent active constrictions in response to elevated pressure. Dashed lines represent passive diameter obtained in Ca^{2+}-free physiological saline solution containing the L-type VDCC inhibitor diltiazem. Modified from Ishiguro M. et al., Enhanced myogenic tone in cerebral arteries from a rabbit model of subarachnoid hemorrhage, *Am J Physiol*., 2002 with permission from American Physiological Society.

CHAPTER 2: JOURNAL ARTICLE

Fundamental increase in pressure-dependent constriction of brain parenchymal arterioles from subarachnoid hemorrhage model rats due to membrane depolarization.

Matthew A. Nystoriak[1], Swapnil K. Sonkusare[1], Joseph E. Brayden[1], Mark T. Nelson[1], George C. Wellman[1,2].

Departments of Pharmacology[1] and Surgery, Division of Neurological Surgery[2], University of Vermont, College of Medicine, Burlington, Vermont.

Running Head: Enhanced parenchymal arteriolar constriction following SAH.

Contact Information: Address for reprint requests and other correspondence: G. C. Wellman, Univ. of Vermont, Dept. of Pharmacology, Given Bldg., 89 Beaumont Ave., Burlington, VT 05405-0068 (e-mail: george.wellman@uvm.edu)

Abstract

Intracerebral (parenchymal) arterioles are morphologically and physiologically unique in comparison to pial arteries and arterioles. The ability of subarachnoid hemorrhage (SAH) to induce vasospasm in large diameter pial arteries has been extensively studied, although the contribution of this phenomenon to patient outcome is controversial. Currently, little is known regarding the impact of SAH on parenchymal arterioles, which are critical for regulation of local and global cerebral blood flow. Here, diameter, smooth muscle intracellular Ca^{2+} ($[Ca^{2+}]_i$) and membrane potential measurements were used to assess the function of intact brain parenchymal arterioles isolated from unoperated (control), sham-operated and SAH model rats. At low intravascular pressure (5 mmHg), membrane potential and $[Ca^{2+}]_i$ were not different in arterioles from control, sham and SAH animals. However, raising intravascular pressure caused significantly greater membrane potential depolarization, elevation in $[Ca^{2+}]_i$ and constriction in SAH arterioles. This SAH-induced increase in $[Ca^{2+}]_i$ and tone occurred in the absence of the vascular endothelium and was abolished by the L-type voltage-dependent calcium channel (VDCC) inhibitor nimodipine. Arteriolar $[Ca^{2+}]_i$ and tone were not different between groups when smooth muscle membrane potential was adjusted to the same value. mRNA and protein levels of the L-type VDCC, $Ca_V1.2$, were similar in parenchymal arterioles isolated from control and SAH animals, suggesting SAH did not cause VDCC upregulation. We conclude that enhanced parenchymal arteriolar tone following SAH is driven by smooth muscle membrane potential depolarization, leading to increased L-type VDCC-mediated Ca^{2+} influx. We propose that inhibition of VDCCs

by calcium channel antagonists or hyperpolarizing vasodilators may be therapeutic strategies to enhance cortical blood flow in SAH patients.

Keywords: voltage-dependent calcium channels, vascular smooth muscle, cerebral blood flow, endothelium, ion channels

Introduction

Cerebral blood flow is regulated by the diameter of resistance arteries and arterioles both on the surface of the brain and within the brain parenchyma. Parenchymal arterioles, unlike pial arteries and arterioles, lack extrinsic innervation and are encased by astrocytic processes ("endfeet") (20, 28). The close association of this microvasculature with astrocytic endfeet is essential for functional hyperemia, whereby focal increases in neuronal activity are coupled to vasodilation of nearby arterioles and increased blood flow (7, 18, 28, 42). In addition to their role in neurovascular coupling, parenchymal arterioles also contribute significantly to autoregulation of global cerebral blood flow and account for approximately 40% of total cerebral vascular resistance (16). Thus, parenchymal arterioles are a unique vascular bed, central in the regulation of both local and global cerebral blood flow.

Pial arteries and arterioles constrict to physiological increases in intravascular pressure via a process involving vascular smooth muscle membrane potential depolarization, activation of voltage-dependent Ca^{2+} channels (VDCCs), and increased global intracellular Ca^{2+} ($[Ca^{2+}]_i$) (2, 17, 21, 33, 41). Recent work has established that pressure-dependent constriction, or myogenic tone, is significantly greater in isolated parenchymal arterioles than pial arteries (4). The cellular basis for enhanced pressure-dependent myogenic tone in the parenchymal vasculature is unclear. Further, the relationship between intravascular pressure, membrane potential, $[Ca^{2+}]_i$ and diameter of isolated parenchymal arterioles is not known.

Dysfunction of the cerebral microcirculation, including parenchymal arterioles, has been implicated in a number of brain pathologies, including vascular dementia, Alzheimer's disease and the development of delayed neurological deficits associated with cerebral aneurysm rupture and subarachnoid hemorrhage (SAH) (27, 58). A number of studies have suggested that SAH causes enhanced constriction of the microcirculation to limit parenchymal blood flow (35, 44, 51, 52, 58). However, the small size of parenchymal arterioles (maximum lumenal diameter: 30-60 μm) poses a significant technical challenge to directly examine their function (45, 53). Consequently, the impact of SAH on the regulation of parenchymal arteriolar diameter is unknown.

The objective of the present study was to elucidate the relationship between intravascular pressure, $[Ca^{2+}]_i$, membrane potential and diameter of isolated parenchymal arterioles from unoperated, sham-operated and SAH model rats. In unoperated animals, membrane potential depolarization and elevations in $[Ca^{2+}]_i$ are enhanced at lower intravascular pressures in parenchymal arterioles compared with pial arteries. Our results are consistent with the concept that intravascular pressure constricts parenchymal arterioles through smooth muscle depolarization, activation of VDCCs, and elevation of intracellular calcium. Furthermore, our data indicate that following SAH, intravascular pressure causes greater membrane depolarization, which leads to enhanced vasoconstriction.

Methods

Animals. Sprague Dawley rats (males, 300-350 g, 10-15 weeks; Charles River Laboratories, Saint Constant, Quebec, Canada) were used in this study. All experiments were conducted in accordance with the *Guidelines for the Care and Use of Laboratory Animals* (NIH Publication 85-23, Revised 1996) and followed protocols approved by the Institutional Animal Use and Care Committee of the University of Vermont.

Rat SAH model. Animals were initially anesthetized by isoflurane (5%) using an induction chamber, then maintained on isoflurane (2-2.5%) anesthesia with the aid of a nose cone. A small (0.5-1.5 cm), longitudinal, midline suboccipital incision was centered over the foramen magnum, and the neck muscles were dissected until dura was visualized. Autologous unheparinized blood (0.5 ml) drawn from the tail artery was injected into the cisterna magna (day 0) using a 25-guage butterfly needle (38). The animal was then positioned on an incline board at a 45° angle with the head down in neutral position for 30 min. Twenty four hours later, a second injection of blood was delivered by repeating the above procedure. Sham-operated animals were treated in a similar manner except: injection of 0.5 ml of saline was substituted for injection of 0.5 ml of unheparinized blood. Buprenorphine (0.01 mg/kg) was given every 12 h (for 36 h, then as needed) as an analgesic. On day 4, animals were euthanized under deep pentobarbital anesthesia by decapitation and parenchymal arterioles (30-60 μm in diameter) were dissected from the middle cerebral artery territory (8) in cold (4˚C) MOPS-buffered saline solution of the following composition (in mM): 145 NaCl, 5 KCl,

1 $MgSO_4$, 2.5 $CaCl_2$, 1 KH_2PO_4, 0.02 EDTA, 3 3-(N-morpholino)propanesulfonic acid, 2 pyruvate, 5 glucose, 1% bovine serum albumin (pH 7.4).

Measurement of intracellular Ca^{2+} concentration and diameter. Freshly isolated parenchymal arterioles were cannulated on glass micropipettes mounted in a 5 ml myograph chamber (University of Vermont Instrumentation and Model Facility) as described previously (8, 30). Vascular endothelium was removed from some arterioles by passing an air bubble through the lumen following cannulation of one end (55). Following cannulation, arterioles were loaded with the ratiometric Ca^{2+}-sensitive dye fura-2 (acetoxymethyl (AM) ester membrane-permeable form) by incubating in MOPS buffered saline solution containing fura-2 AM (5 μM) (Invitrogen, Carlsbad, CA) with pluronic acid (0.1%) (Invitrogen, Carlsbad, CA) at room temperature (~22˚C) for 45 minutes. Next, the myograph chamber was mounted on a Nikon TE2000-S inverted fluorescence microscope. To allow for equilibration and de-esterification of fura-2 AM, arterioles were pressurized to 5 mmHg and continuously superfused (37˚C, 30 min) with artificial cerebrospinal fluid (aCSF) of the following composition (in mM): 125 NaCl, 3 KCl, 18 $NaHCO_3$, 1.25 NaH_2PO_4, 1 $MgCl_2$, 2 $CaCl_2$, 5 glucose aerated with 5% CO_2, 20% O_2, 75% N_2. Bath pH was closely monitored and maintained at 7.30-7.35 (11).

Following the equilibration period, studies were performed in which intravascular pressure was increased to 10, 20, 40 and 60 mmHg or extracellular K^+ was increased from 3 mM to 60 mM using aCSF made by isosmotic replacement of NaCl with KCl. Fluorescence ratio was obtained from background corrected ratio of the 510 nm emission

from arterioles alternately excited at 340 and 380 nm with hardware and software developed by IonOptix (Milton, MA). $[Ca^{2+}]_i$ was estimated using the following equation (19): $[Ca^{2+}] = K_d \times \beta \times (R - R_{min})/(R_{max} - R)$. R_{min} and R_{max}, the ratios of emission signals under Ca^{2+}-free and Ca^{2+}-saturated conditions, respectively, were measured from a separate set of ionomycin-treated arterioles, and β was determined. Calibration values were not significantly different between arterioles obtained from either healthy or SAH animals (Table 1) and were pooled for calculations of $[Ca^{2+}]_i$, using an apparent dissociation constant (K_d) of 282 nM of fura-2 for Ca^{2+} (33). Total fluorescence counts (photomultiplier signal at $F_{340} + F_{380}$) measured immediately following the equilibration period were not significantly different between endothelium intact (539 ± 66 counts) and denuded arterioles (532 ± 40 counts), suggesting endothelial loading with fura-2 was negligible.

Luminal diameter of arterioles was simultaneously recorded with $[Ca^{2+}]_i$ using a CCD camera and the edge-detection function of IonOptix software. Constriction is presented as a decrease in arterial diameter relative to the maximum diameter at a given pressure obtained at the end of each experiment using Ca^{2+}-free aCSF containing nimodipine (300 nM) (30, 59).

Measurement of membrane potential: Arterioles were cannulated as described above and pressurized to either 5 or 40 mmHg. Smooth muscle membrane potential was measured by insertion of a sharp glass microelectrode (~100-MΩ resistance) filled with 0.5 M KCl into the vessel wall. The criteria for successful impalement was *1*) an abrupt

negative potential deflection upon entry, *2*) a stable membrane potential for ≥30 seconds, and *3*) an abrupt positive potential deflection upon removal (33, 46). Measurements were made using an electrometer (World Precision Instruments), and recorded via computer using Axotape and Dataq software.

RT-PCR: Total RNA was extracted using RNA STAT-60 total RNA/mRNA isolation reagent (Tel-test, Friendswood, TX) and reverse transcribed to cDNA using SuperScript First-Strand synthesis system (Invitrogen, Carlsbad, CA) (43). Polymerase chain reaction was performed using primers detecting $Ca_V1.2$ (Genbank accession No. X55763) [*forward* (5'-CAGCAGGTCCTATGTCAGCA-3'), *reverse* (5'-CCGACAGCAGTGAATGAAGA-3')], and 18S (Genbank accession No. M11188) [forward (5'-AGTCGCCGTGCCTACCAT-3'), reverse (5'-GCCTGCTGCCTTCCTTG-3')]. Amplification was performed with a taq core PCR kit (Qiagen, Valencia, CA) using a thermocycler (Techne, Burlington, NJ). Band intensity in the linear range of amplification ($Ca_V1.2$: 29 cycles; 18S rRNA: 30 cycles) was quantified using Quantity One 1-D Analysis software (Bio-Rad, Hercules, CA). Expression levels were normalized to band intensity values for 18S rRNA.

Western blot analysis: Parenchymal arterioles were pooled from two animals per sample (n). Whole parenchymal arteriole lysates were prepared by sonication (20 min, 4˚C) in a triton lysis buffer solution containing (in mM): 50 HEPES, 150 NaCl, 1 EGTA, 1.5 $MgCl_2$, 1% triton-X, 10% glycerol with protease inhibitors (10 μg/mL of leupeptin, aprotinin, antipain and 10 mM phenylmethylsulfonyl fluoride). Tissue debris and nuclear

fragments were removed by centrifugation at 7000 rpm (10 min, 4°C). The whole cell lysate was obtained as the supernatant and protein concentration was determined by Bradford assay. Molecular weight marker (Invitrogen, Carlsbad, CA) was loaded as a size standard and protein samples (~15 μg total protein) were separated under reducing conditions on a 7.5% polyacrylamide gel (Bio-Rad, Hercules, CA) by electrophoresis. Samples were run at 120 V for 1.5 hours on an 8x10-cm electrophoresis cell (BioRad, Hercules, CA) and electrophoretically transferred to a nitrocellulose membrane at 80 V for 2 hours (4˚C). The membranes were washed in tris-buffered saline with 0.1% Tween-20 (TBS-T), and blocked with 10% nonfat dried milk in TBS-T (1 hour, room temperature). Membranes were then incubated with the specific polyclonal antibodies against $Ca_V1.2$ (1:200, overnight, 4˚C, Alomone, Jerusalem), or monoclonal antibody against GAPDH (1:100,000, 30 min, room temperature, Sigma, St. Louis, MO), prepared in 5% nonfat dried milk in TBS-T. Membranes were then incubated (1 hour; room temperature) with horseradish peroxidase-labeled donkey anti-rabbit IgG ($Ca_V1.2$, 1:5000; GAPDH, 1:10,000, GE Healthcare, Waukesha, WI) in TBS-T containing 5% nonfat dried milk. Bands were identified by chemiluminescence and exposed to X-ray films. Densitometry for immunoreactive bands was performed using NIH software (ImageJ) and density was expressed as a percent of GAPDH density for each lane.

Statistical analysis. Values are presented as means ± SEM. One-way analysis of variance followed by Tukey multiple comparison test was used in the comparison of

multiple groups. Student's t-test was used in the comparison of two groups. Statistical significance was considered at the level of $p < 0.05$ (*) or $p < 0.01$ (**).

Results

Parenchymal arterioles isolated from SAH model animals exhibit elevated cytosolic Ca^{2+} and enhanced tone at physiological intravascular pressures.

To assess the role of cytosolic Ca^{2+} in pressure-induced parenchymal arteriolar constriction, simultaneous measurements of $[Ca^{2+}]_i$ and diameter were obtained from freshly isolated parenchymal arterioles loaded with the ratiometric Ca^{2+} indicator fura-2. In response to step-wise increases in intravascular pressure, arterioles from unoperated (control), sham-operated (sham) and SAH animals exhibited graded increases in cytosolic Ca^{2+} ($[Ca^{2+}]_i$) and active constriction. At low intravascular pressure (5-10 mmHg), similar levels of $[Ca^{2+}]_i$ and tone were observed in vessels isolated from all groups. However, as intravascular pressure was increased to physiological levels (i.e. 20 to 60 mmHg) (16, 23), arterioles from SAH animals exhibited markedly enhanced levels of $[Ca^{2+}]_i$ and constriction compared with arterioles from control and sham-operated animals (Fig. 1A-E). For example, at 40 mmHg, $[Ca^{2+}]_i$ was ~33% higher in arterioles from SAH animals (349 ± 11 nM, n = 5) compared with arterioles isolated from control animals (261 ± 8 nM, n = 6). Corresponding to this SAH-induced increase in $[Ca^{2+}]_i$, at 40 mmHg, vessels from SAH animals constricted 29 ± 2 μm (53 ± 4% decrease in diameter, n = 5), compared with a constriction of 14 ± 1 μm in arterioles from control animals (29 ± 2% decrease in diameter, n = 6). Although, $[Ca^{2+}]_i$ and tone at a given pressure were greater in arterioles from SAH model animals, the relationship between $[Ca^{2+}]_i$ and constriction were remarkably similar between arterioles isolated from control and SAH animals (Fig. 1F). These data suggest that elevated $[Ca^{2+}]_i$ is sufficient to account for

enhanced pressure-induced constriction of parenchymal arterioles from SAH model animals.

The role of L-type VDCCs in SAH-induced elevation of $[Ca^{2+}]_i$ and arteriolar tone was examined by applying the dihydropyridine L-type VDCC inhibitor nimodipine (300 nM) prior to increasing intravascular pressure. Pressure-induced increases in $[Ca^{2+}]_i$ and constriction were abolished by nimodipine in control and SAH groups (Fig. 1D,E) indicating that Ca^{2+} influx in parenchymal myocytes from both control and SAH animals is mediated by L-type VDCCs. These results indicate that elevation of intravascular pressure leads to greater L-type VDCC-mediated Ca^{2+} influx, increased $[Ca^{2+}]_i$ and enhanced constriction of parenchymal arterioles from SAH animals.

Increased L-type VDCC activity, rather than increased channel expression, mediates enhanced parenchymal arteriolar constriction following SAH.

SAH-induced Ca^{2+} influx via L-type VDCCs could reflect either an increase in the density of functional channels or a more depolarized membrane potential leading to an increase in the open-state probability (P_{open}) of existing channels. To explore whether upregulation of L-type VDCC expression occurs following SAH, RT-PCR was used to examine $Ca_V1.2$ mRNA, encoding the predominantly expressed L-type VDCC pore-forming α_1 subunit in vascular smooth muscle (3, 40). Expression of $Ca_V1.2$ mRNA, normalized to 18S rRNA levels, was similar in parenchymal arterioles isolated from control and SAH animals (Fig. 2A, B). In addition, protein levels of $Ca_V1.2$, determined

by Western blot, were not different between groups (Fig. 2C, D). These data suggest that upregulation of $Ca_V1.2$ does not contribute to elevated $[Ca^{2+}]_i$ following SAH.

Based on the above data, we hypothesized that greater smooth muscle membrane potential depolarization, rather than increased VDCC expression, underlie enhanced pressure-induced constriction of parenchymal arterioles following SAH. Thus, at a given membrane potential, similar $[Ca^{2+}]_i$ and constriction would be predicted for arterioles from control and SAH animals. To test this possibility, $[Ca^{2+}]_i$ and constriction were measured when extracellular K^+ concentration ($[K^+]_o$) was elevated from 3 mM to 60 mM by isosmotic replacement of NaCl with KCl in the bath solution. In pial arteries, membrane potential closely follows the K^+ equilibrium potential (E_K) at $[K^+]_o$ greater than 16 mM (25, 33). This also appears to be the case with parenchymal arterioles, as smooth muscle membrane potential in arterioles bathed in 60 mM $[K^+]_o$ was very close to theoretical E_K (Control: -22 ± 1 mV, n = 4; SAH –21 ± 1 mV, n = 4), predicted by the Nernst equation (-22 mV; assuming intracellular $[K^+]$ = 140 mM) (Fig. 3A). When smooth muscle membrane potential was "clamped" using 60 mM $[K^+]_o$, $[Ca^{2+}]_i$ was not different in parenchymal arterioles isolated from healthy (393 ± 18 nM, n = 7) and SAH animals (388 ± 14 nM, n = 5) (Fig. 3B). Constriction was also similar for control and SAH arterioles in the presence of 60 mM $[K^+]_o$ (Fig. 3C). Elevations in $[Ca^{2+}]_i$ and constrictions in response to 60 mM $[K^+]_o$ were abolished by nimodipine (300 nM) in arterioles from both groups (Fig. 3B,C). These findings suggest that enhanced pressure-induced constrictions following experimental SAH likely reflect differences in smooth muscle membrane potential, rather than increased VDCC expression.

Elevation of intravascular pressure leads to greater smooth muscle membrane potential depolarization following experimental subarachnoid hemorrhage.

To directly assess the impact of SAH on smooth muscle membrane potential, myocytes of intact parenchymal arterioles were impaled from the adventitial surface using intracellular microelectrodes. At low intravascular pressure (5 mmHg), membrane potential was similar in arterioles isolated from control (-58 ± 2 mV, n = 4) and SAH animals (-59 ± 2 mV, n = 4) (Fig. 4A). Raising intravascular pressure from 5 to 40 mmHg resulted in membrane potential depolarization in arterioles from both groups. However, parenchymal arteriolar myocytes from SAH animals were significantly more depolarized at 40 mmHg (-28 ± 1 mV; n = 4) compared with arterioles from control animals (-35 ± 1 mV; n = 5) (Fig. 4B,C). These data suggest that greater pressure-dependent membrane potential depolarization underlies enhanced parenchymal arteriolar tone following SAH.

Endothelial function promotes vasodilation in parenchymal arterioles following SAH.

Membrane potential of arteriolar myocytes can be modulated by the vascular endothelium (17). Previous work has indicated that endothelial SK_{Ca} and IK_{Ca} channel activity promotes smooth muscle membrane potential hyperpolarization and plays an important role in the regulation of parenchymal arteriolar tone and cortical blood flow (5, 14). Thus, to assess endothelial function in parenchymal arterioles following SAH, we examined the effect of NS309, an opener of endothelial small- (SK_{Ca}) and intermediate-

conductance (IK_{Ca}) Ca^{2+}-activated K^+ channels (26, 50), on arteriolar $[Ca^{2+}]_i$ and diameter. At 40 mmHg intravascular pressure, NS309 (1 μM) caused hyperpolarization in endothelium-intact arterioles from both control (–67 ± 2 mV, n = 5) and SAH animals (–67 ± 2 mV, n = 4) (Fig. 5A). Consistent with membrane potential hyperpolarization, NS309 also caused a significant decrease in $[Ca^{2+}]_i$ in arterioles from control (242 ± 7 nM to 141 ± 15 nM; n = 4) and SAH animals (330 ± 11 nM to 151 ± 14 nM; n = 4) and induced >90% vasodilation in both groups (Fig. 5B). These results demonstrate that activation of endothelial SK_{Ca} and IK_{Ca} channels causes a similar marked membrane potential hyperpolarization and vasodilation of arterioles from control and SAH animals.

To examine whether altered endothelial function contributes to elevated $[Ca^{2+}]_i$ and enhanced constriction of parenchymal arterioles from SAH animals, $[Ca^{2+}]_i$ and diameter were measured in endothelial-denuded vessels. The endothelium was removed from parenchymal arterioles by passing an air bubble through the vessel lumen during the cannulation procedure. Although endothelium-denuded arterioles displayed increased $[Ca^{2+}]_i$ and constriction compared to corresponding endothelium-intact vessels in both groups, these parameters remained significantly higher in parenchymal arterioles from SAH animals (Fig. 5C). Application of NS309 was used to confirm absence of endothelial function in denuded vessels. Consistent with expression of SK_{Ca} and IK_{Ca} channels in endothelial cells but not smooth muscle, NS309 had no effect on $[Ca^{2+}]_i$ or diameter in denuded arterioles from either control or SAH animals (Fig 5D). These results suggest that SAH-induced elevated $[Ca^{2+}]_i$ and enhanced arteriolar tone result

from a direct modulation of smooth muscle membrane potential, rather than decreased endothelial vasodilatory influence.

Discussion

Here, we report that cytosolic Ca^{2+} is elevated and pressure-dependent constriction is enhanced in parenchymal arterioles from experimental SAH animals. Our data demonstrate elevations in intravascular pressure cause greater membrane potential depolarization following SAH, leading to increased activity of L-type VDCCs and enhanced constriction. The following observations are consistent with these novel findings: *1)* Increasing intravascular pressure resulted in significantly greater elevation of $[Ca^{2+}]_i$ and enhanced myogenic tone in parenchymal arterioles isolated from SAH model animals. *2)* Pressure-induced elevations in $[Ca^{2+}]_i$ and myogenic tone were abolished by the L-type VDCC inhibitor nimodipine. *3)* Arteriolar $[Ca^{2+}]_i$ and constriction were similar in arterioles from control and SAH animals when membrane potential was clamped at E_K (≈ -22 mV) using 60 mM extracellular $[K^+]$. *4)* At 40 mmHg, smooth muscle membrane potential was approximately 7 mV more depolarized in arterioles isolated from SAH versus control animals. *5)* $Ca_V1.2$ mRNA and protein expression were not altered by SAH. *6)* Differences in $[Ca^{2+}]_i$ and tone at 40 mmHg were independent of vascular endothelium. In addition, endothelium-dependent hyperpolarization of smooth muscle using NS309 reduced $[Ca^{2+}]_i$ to basal levels and dilated parenchymal arterioles from control and SAH animals.

This work also provides novel information regarding the physiological function of arterioles within the brain parenchyma. Previous studies have found that parenchymal arterioles develop significantly greater pressure-induced myogenic tone compared with middle cerebral arteries (4, 5). To assess the contribution of membrane potential and

$[Ca^{2+}]_i$ to these differences, we compared our data presently obtained for isolated parenchymal arterioles from unoperated rats with data previously reported by Knot and Nelson (33) for rat middle cerebral arteries. At a given level of intravascular pressure, parenchymal arterioles display greater $[Ca^{2+}]_i$ compared with middle cerebral arteries (Fig. 6A) (i.e. 267 nM versus ~190 nM, respectively, at 60 mmHg intravascular pressure). However, the relationships between $[Ca^{2+}]_i$ and constriction are remarkably similar in these vascular beds (Fig. 6B), suggesting that in healthy animals, enhanced pressure-dependent constriction observed in parenchymal arterioles results from a greater elevation in $[Ca^{2+}]_i$. A comparison of the relationship between intravascular pressure and membrane potential indicates that at a given intravascular pressure, smooth muscle membrane potential is more depolarized in parenchymal arterioles. For example, membrane potential measured in parenchymal myocytes was approximately -35 mV at 40 mmHg; however, this level of membrane potential depolarization was not reached in middle cerebral arteries until intravascular pressure was increased to 80-100 mmHg (33). Thus, the relationship between intravascular pressure and membrane potential appears to be shifted towards lower pressures in parenchymal arterioles, thereby accounting for the similar leftward shift in the pressure versus $[Ca^{2+}]_i$ relationship (Fig. 6A). This functional distinction may be critical for development of parenchymal arteriolar tone at the lower physiological pressures they experience in vivo.

We also demonstrate that the relationship between intravascular pressure and $[Ca^{2+}]_i$ is further shifted to the left in parenchymal arterioles following SAH. This effect is correlated with enhanced pressure-induced depolarization at physiological

intravascular pressure in arterioles from SAH animals. Hence, increasing intravascular pressure within the physiological range leads to greater membrane potential depolarization, increased Ca^{2+} influx via L-type VDCCS, elevated $[Ca^{2+}]_i$ and enhanced constriction of parenchymal arterioles following experimental SAH. However, when membrane potential is equalized between SAH and control arterioles using 60 mM $[K^+]_o$ or NS309, L-type VDCC-mediated Ca^{2+} influx and arteriolar $[Ca^{2+}]_i$ is similar between groups. Thus, our data imply that increased Ca^{2+} influx following SAH reflects membrane potential depolarization, rather than increased VDCC density at the plasma membrane. The membrane potentials reported here for parenchymal arteriolar myocytes (± SAH) are within the range in which L-type VDCC current is steeply voltage-dependent (41). At voltages between -60 and -30 mV, VDCC open-state probability is an exponential function of membrane potential and it is estimated that depolarization of 7 mV (-35 mV to -28 mV, Fig. 4C) could more than double VDCC P_{open} from 0.016 to 0.035 (41). Therefore, the depolarization observed following SAH in this study is consistent with a substantial increase in VDCC activity, leading to a marked increase in Ca^{2+} entry in parenchymal arteriolar myocytes.

Vascular smooth muscle membrane potential can be modulated by vasoactive factors released by the endothelium. A number of studies suggest that nitric oxide-mediated vasodilation is impaired in large diameter cerebral arteries in experimental models of SAH (6, 17). Similar findings have been reported in basilar arteries of SAH patients (24). However, the contribution of endothelial dysfunction to cerebral artery constriction is controversial and others have reported that endothelium-dependent

relaxation is unchanged following SAH (10, 39). The relative contribution of endothelium-dependent vasodilators to vascular tone may depend on vessel size and the effects of SAH on endothelial function may differ between large and small diameter vessels. Whereas basal NO production seems to control tone in both cerebral arteries and arterioles, the contribution of endothelium-derived hyperpolarizing factor (EDHF) to blood flow regulation may be greater at the level of the microcirculation (57). Previous studies suggest that EDHF-mediated relaxation requires the activity of endothelial SK_{Ca} and IK_{Ca} (13, 60) and these channels are involved in modulating basal tone in parenchymal arterioles, but not in middle cerebral arteries (5). Here, we show that activation of endothelial SK_{Ca} and IK_{Ca} channels with NS309 caused a similar reduction of $[Ca^{2+}]_i$ to basal levels and profound dilation of parenchymal arterioles from both control and SAH animals. Further, endothelial removal did not ablate SAH-induced pressure-induced increases in $[Ca^{2+}]_i$ and myogenic tone. Therefore, reduced endothelial vasodilator influence cannot account for enhanced vasoconstriction of parenchymal arterioles following SAH. These findings are in agreement with previous data for small diameter brainstem arteries (32) and penetrating arterioles (53) and suggest that a direct alteration of smooth muscle membrane potential regulation contributes to dysfunction of cerebral microvessels from SAH animals.

Our results indicate that elevated parenchymal arteriolar $[Ca^{2+}]_i$ and tone following SAH depends on intravascular pressure. At this time, it is unclear how SAH causes enhanced pressure-dependent depolarization in parenchymal arterioles. Activation of mechanosensitive non-selective cation channels belonging to the transient

receptor potential family (i.e. TRPC6,TRPM4) is reported to contribute to membrane potential depolarization of cerebral artery myocytes to increased pressure (15, 56). Thus, increased expression or activity of these channels following SAH may lead to membrane depolarization and enhanced VDCC activity. On the other hand, SAH-induced depolarization may also result from suppressed hyperpolarizing influence. For example, significant voltage-dependent K^+ channel (K_V)-mediated current is observed at physiological membrane potentials (47) and activation of these channels represents an important feedback mechanism in response to pressure-induced depolarization. Consistent with this hypothesis, inhibition of K_V channels with 4-aminopyridine causes membrane potential depolarization and vasoconstriction (34, 49). Numerous studies have suggested that substances within blood may lead to membrane potential depolarization of cerebral artery myocytes via suppression of K^+ channel activity (17, 22, 48). For example, using pial arteries from a rabbit SAH model, our laboratory has shown that acute exposure of vascular smooth muscle to the blood component oxyhemoglobin can cause internalization of (K_V1.5) via a mechanism involving protein tyrosine kinase activation (29, 36). Others have additionally demonstrated that mRNA and protein levels of K_V2.2 channels were decreased in basilar arteries from a canine SAH model (31). Hence, further studies are required to determine whether K_V channel suppression contributes to enhanced pressure dependent depolarization of parenchymal arteriolar myocytes in SAH animals.

Enhanced constriction of cerebral arteries and arterioles associated with SAH requires Ca^{2+} influx via VDCCs in vascular smooth muscle (54). Currently, oral

administration of the L-type VDCC inhibitor nimodipine is regarded as standard therapy for patients with SAH and is associated with a modest improvement in clinical outcome (37). The mechanism of the beneficial effects of nimodipine in SAH patients is unclear, however this agent does not significantly reduce large artery, or "angiographic" vasospasm (1). Our results are consistent with speculation that nimodipine treatment may be effective for reversal of enhanced constriction of microvessels within the brain parenchyma, which are beyond the resolution limits of angiography (12). Although further studies are required to examine this possibility, such a mechanism would point to significant role for microcirculatory dysfunction in the development of delayed neurological deficits in SAH patients.

To summarize, we provide evidence that myocytes of parenchymal arterioles are more depolarized at physiological intravascular pressures leading to increased L-type VDCC activity, elevated $[Ca^{2+}]_i$ and enhanced constriction. Furthermore, we demonstrate that inhibitors of L-type VDCCs (i.e. nimodipine) as well as agents that cause hyperpolarization (i.e. NS309) are effective in reducing $[Ca^{2+}]_i$ and dilating parenchymal vessels from SAH animals. We propose that therapeutic strategies targeting this enhanced vasoconstriction of the cerebral microcirculation may be beneficial in reducing neurological deficits associated with SAH.

Grants

This work was supported by the Totman Medical Research Trust Fund, the Peter Martin Brain Aneurysm Endowment, National Institutes of Health Grants P20-RR-16435, R01-HL-078983, R01-HL-078983-0551, P01-HL-095488, R01-HL-44455, R01-HL-098243 and R01-HL-58231, and American Heart Association pre-doctoral fellowship award (0815736D).

Acknowledgements

The authors wish to thank Drs. Natalia Gokina and Masayo Koide, and Ms. Jacqueline Hubbard, Mr. Kevin O'Connor, and Ms. Sheila Russell for helpful comments and assistance with this study. We also acknowledge the University of Vermont Neuroscience COBRE Molecular Biology and Microscopy Imaging Center core facilities.

References

1. **Biondi A, Ricciardi GK, Puybasset L, Abdennour L, Longo M, Chiras J, and Van Effenterre R**. Intra-arterial nimodipine for the treatment of symptomatic cerebral vasospasm after aneurysmal subarachnoid hemorrhage: preliminary results. *AJNR Am J Neuroradiol* 25: 1067-1076, 2004.
2. **Brayden JE, and Wellman GC**. Endothelium-dependent dilation of feline cerebral arteries: role of membrane potential and cyclic nucleotides. *J Cereb Blood Flow Metab* 9: 256-263, 1989.
3. **Catterall WA**. Structure and regulation of voltage-gated Ca^{2+} channels. *Annu Rev Cell Dev Biol* 16: 521-555, 2000.
4. **Cipolla MJ, Li R, and Vitullo L**. Perivascular innervation of penetrating brain parenchymal arterioles. *J Cardiovasc Pharmacol* 44: 1-8, 2004.
5. **Cipolla MJ, Smith J, Kohlmeyer MM, and Godfrey JA**. SK_{Ca} and IK_{Ca} Channels, myogenic tone, and vasodilator responses in middle cerebral arteries and parenchymal arterioles: effect of ischemia and reperfusion. *Stroke* 40: 1451-1457, 2009.
6. **Cook DA**. Mechanisms of cerebral vasospasm in subarachnoid haemorrhage. *Pharmacol Ther* 66: 259-284, 1995.
7. **Cox SB, Woolsey TA, and Rovainen CM**. Localized dynamic changes in cortical blood flow with whisker stimulation corresponds to matched vascular and neuronal architecture of rat barrels. *J Cereb Blood Flow Metab* 13: 899-913, 1993.
8. **Dacey RG, Jr., and Duling BR**. A study of rat intracerebral arterioles: methods, morphology, and reactivity. *Am J Physiol* 243: H598-606, 1982.
9. **De Jongh KS, Murphy BJ, Colvin AA, Hell JW, Takahashi M, and Catterall WA**. Specific phosphorylation of a site in the full-length form of the alpha 1 subunit of the cardiac L-type calcium channel by adenosine 3',5'-cyclic monophosphate-dependent protein kinase. *Biochemistry* 35: 10392-10402, 1996.
10. **Debdi M, Seylaz J, and Sercombe R**. Early changes in rabbit cerebral artery reactivity after subarachnoid hemorrhage. *Stroke* 23: 1154-1162, 1992.
11. **Dietrich HH, and Dacey RG, Jr.** Effects of extravascular acidification and extravascular alkalinization on constriction and depolarization in rat cerebral arterioles in vitro. *J Neurosurg* 81: 437-442, 1994.
12. **Dietrich HH, and Dacey RG, Jr.** Molecular keys to the problems of cerebral vasospasm. *Neurosurgery* 46: 517-530, 2000.
13. **Dora KA, Gallagher NT, McNeish A, and Garland CJ**. Modulation of endothelial cell $K_{Ca}3.1$ channels during endothelium-derived hyperpolarizing factor signaling in mesenteric resistance arteries. *Circ Res* 102: 1247-1255, 2008.
14. **Dunn KM, Nelson, M.T.** Effect of small and intermediate conductance calcium activated potassium channel modulation on cortical cerebral blood flow in vivo. *The FASEB Journal* 23: 613.624, 2009.
15. **Earley S, Waldron BJ, and Brayden JE**. Critical role for transient receptor potential channel TRPM4 in myogenic constriction of cerebral arteries. *Circ Res* 95: 922-929, 2004.

16. **Faraci FM, and Heistad DD**. Regulation of large cerebral arteries and cerebral microvascular pressure. *Circ Res* 66: 8-17, 1990.
17. **Faraci FM, and Heistad DD**. Regulation of the cerebral circulation: role of endothelium and potassium channels. *Physiol Rev* 78: 53-97, 1998.
18. **Filosa JA, Bonev AD, Straub SV, Meredith AL, Wilkerson MK, Aldrich RW, and Nelson MT**. Local potassium signaling couples neuronal activity to vasodilation in the brain. *Nat Neurosci* 9: 1397-1403, 2006.
19. **Grynkiewicz G, Poenie M, and Tsien RY**. A new generation of Ca^{2+} indicators with greatly improved fluorescence properties. *J Biol Chem* 260: 3440-3450, 1985.
20. **Hamel E**. Perivascular nerves and the regulation of cerebrovascular tone. *J Appl Physiol* 100: 1059-1064, 2006.
21. **Harder DR**. Pressure-dependent membrane depolarization in cat middle cerebral artery. *Circ Res* 55: 197-202, 1984.
22. **Harder DR, Dernbach P, and Waters A**. Possible cellular mechanism for cerebral vasospasm after experimental subarachnoid hemorrhage in the dog. *J Clin Invest* 80: 875-880, 1987.
23. **Harper SL, Bohlen HG, and Rubin MJ**. Arterial and microvascular contributions to cerebral cortical autoregulation in rats. *Am J Physiol* 246: H17-24, 1984.
24. **Hatake K, Wakabayashi I, Kakishita E, and Hishida S**. Impairment of endothelium-dependent relaxation in human basilar artery after subarachnoid hemorrhage. *Stroke* 23: 1111-1116; discussion 1116-1117, 1992.
25. **Hirst GD, and van Helden DF**. Ionic basis of the resting potential of submucosal arterioles in the ileum of the guinea-pig. *J Physiol* 333: 53-67, 1982.
26. **Hougaard C, Eriksen BL, Jorgensen S, Johansen TH, Dyhring T, Madsen LS, Strobaek D, and Christophersen P**. Selective positive modulation of the SK3 and SK2 subtypes of small conductance Ca^{2+}-activated K^+ channels. *Br J Pharmacol* 151: 655-665, 2007.
27. **Iadecola C**. Neurovascular regulation in the normal brain and in Alzheimer's disease. *Nat Rev Neurosci* 5: 347-360, 2004.
28. **Iadecola C, and Nedergaard M**. Glial regulation of the cerebral microvasculature. *Nat Neurosci* 10: 1369-1376, 2007.
29. **Ishiguro M, Morielli AD, Zvarova K, Tranmer BI, Penar PL, and Wellman GC**. Oxyhemoglobin-induced suppression of voltage-dependent K^+ channels in cerebral arteries by enhanced tyrosine kinase activity. *Circ Res* 99: 1252-1260, 2006.
30. **Ishiguro M, Puryear CB, Bisson E, Saundry CM, Nathan DJ, Russell SR, Tranmer BI, and Wellman GC**. Enhanced myogenic tone in cerebral arteries from a rabbit model of subarachnoid hemorrhage. *Am J Physiol Heart Circ Physiol* 283: H2217-2225, 2002.
31. **Jahromi BS, Aihara Y, Ai J, Zhang ZD, Nikitina E, and Macdonald RL**. Voltage-gated K^+ channel dysfunction in myocytes from a dog model of subarachnoid hemorrhage. *J Cereb Blood Flow Metab* 28: 797-811, 2008.
32. **Katusic ZS, Milde JH, Cosentino F, and Mitrovic BS**. Subarachnoid hemorrhage and endothelial L-arginine pathway in small brain stem arteries in dogs. *Stroke* 24: 392-399, 1993.

33. **Knot HJ, and Nelson MT**. Regulation of arterial diameter and wall [Ca^{2+}] in cerebral arteries of rat by membrane potential and intravascular pressure. *J Physiol* 508 (Pt 1): 199-209, 1998.
34. **Knot HJ, and Nelson MT**. Regulation of membrane potential and diameter by voltage-dependent K^+ channels in rabbit myogenic cerebral arteries. *Am J Physiol* 269: H348-355, 1995.
35. **Knuckey NW, Fox RA, Surveyor I, and Stokes BA**. Early cerebral blood flow and computerized tomography in predicting ischemia after cerebral aneurysm rupture. *J Neurosurg* 62: 850-855, 1985.
36. **Koide M, Penar PL, Tranmer BI, and Wellman GC**. Heparin-binding EGF-like growth factor mediates oxyhemoglobin-induced suppression of voltage-dependent potassium channels in rabbit cerebral artery myocytes. *Am J Physiol Heart Circ Physiol* 293: H1750-1759, 2007.
37. **Langley MS, and Sorkin EM**. Nimodipine. A review of its pharmacodynamic and pharmacokinetic properties, and therapeutic potential in cerebrovascular disease. *Drugs* 37: 669-699, 1989.
38. **Lee JY, Huang DL, Keep R, and Sagher O**. Characterization of an improved double hemorrhage rat model for the study of delayed cerebral vasospasm. *J Neurosci Methods* 168: 358-366, 2008.
39. **Maeda Y, Hirano K, Kai Y, Hirano M, Suzuki SO, Sasaki T, and Kanaide H**. Up-regulation of proteinase-activated receptor 1 and increased contractile responses to thrombin after subarachnoid haemorrhage. *Br J Pharmacol* 152: 1131-1139, 2007.
40. **Moosmang S, Schulla V, Welling A, Feil R, Feil S, Wegener JW, Hofmann F, and Klugbauer N**. Dominant role of smooth muscle L-type calcium channel $Ca_v1.2$ for blood pressure regulation. *EMBO J* 22: 6027-6034, 2003.
41. **Nelson MT, Patlak JB, Worley JF, and Standen NB**. Calcium channels, potassium channels, and voltage dependence of arterial smooth muscle tone. *Am J Physiol* 259: C3-18, 1990.
42. **Ngai AC, Ko KR, Morii S, and Winn HR**. Effect of sciatic nerve stimulation on pial arterioles in rats. *Am J Physiol* 254: H133-139, 1988.
43. **Nystoriak MA, Murakami K, Penar PL, and Wellman GC**. $Ca_v1.2$ splice variant with exon 9* is critical for regulation of cerebral artery diameter. *Am J Physiol Heart Circ Physiol* 297: H1820-1828, 2009.
44. **Ohkuma H, Manabe H, Tanaka M, and Suzuki S**. Impact of cerebral microcirculatory changes on cerebral blood flow during cerebral vasospasm after aneurysmal subarachnoid hemorrhage. *Stroke* 31: 1621-1627, 2000.
45. **Park KW, Metais C, Dai HB, Comunale ME, and Sellke FW**. Microvascular endothelial dysfunction and its mechanism in a rat model of subarachnoid hemorrhage. *Anesth Analg* 92: 990-996, 2001.
46. **Reading SA, Earley S, Waldron BJ, Welsh DG, and Brayden JE**. TRPC3 mediates pyrimidine receptor-induced depolarization of cerebral arteries. *Am J Physiol Heart Circ Physiol* 288: H2055-2061, 2005.

47. **Robertson BE, and Nelson MT**. Aminopyridine inhibition and voltage dependence of K^+ currents in smooth muscle cells from cerebral arteries. *Am J Physiol* 267: C1589-1597, 1994.
48. **Sobey CG, and Faraci FM**. Subarachnoid haemorrhage: what happens to the cerebral arteries? *Clin Exp Pharmacol Physiol* 25: 867-876, 1998.
49. **Straub SV, Girouard H, Doetsch PE, Hannah RM, Wilkerson MK, and Nelson MT**. Regulation of intracerebral arteriolar tone by K_v channels: effects of glucose and PKC. *Am J Physiol Cell Physiol* 297: C788-796, 2009.
50. **Strobaek D, Teuber L, Jorgensen TD, Ahring PK, Kjaer K, Hansen RS, Olesen SP, Christophersen P, and Skaaning-Jensen B**. Activation of human IK and SK Ca^{2+} -activated K^+ channels by NS309 (6,7-dichloro-1H-indole-2,3-dione 3-oxime). *Biochim Biophys Acta* 1665: 1-5, 2004.
51. **Takeuchi H, Handa Y, Kobayashi H, Kawano H, and Hayashi M**. Impairment of cerebral autoregulation during the development of chronic cerebral vasospasm after subarachnoid hemorrhage in primates. *Neurosurgery* 28: 41-48, 1991.
52. **Vergouwen MD, Vermeulen M, Coert BA, Stroes ES, and Roos YB**. Microthrombosis after aneurysmal subarachnoid hemorrhage: an additional explanation for delayed cerebral ischemia. *J Cereb Blood Flow Metab* 28: 1761-1770, 2008.
53. **Vollmer DG, Takayasu M, and Dacey RG, Jr.** An in vitro comparative study of conducting vessels and penetrating arterioles after experimental subarachnoid hemorrhage in the rabbit. *J Neurosurg* 77: 113-119, 1992.
54. **Wellman GC**. Ion channels and calcium signaling in cerebral arteries following subarachnoid hemorrhage. *Neurol Res* 28: 690-702, 2006.
55. **Wellman GC, and Bevan JA**. Barium inhibits the endothelium-dependent component of flow but not acetylcholine-induced relaxation in isolated rabbit cerebral arteries. *J Pharmacol Exp Ther* 274: 47-53, 1995.
56. **Welsh DG, Morielli AD, Nelson MT, and Brayden JE**. Transient receptor potential channels regulate myogenic tone of resistance arteries. *Circ Res* 90: 248-250, 2002.
57. **You J, Johnson TD, Marrelli SP, and Bryan RM, Jr.** Functional heterogeneity of endothelial P2 purinoceptors in the cerebrovascular tree of the rat. *Am J Physiol* 277: H893-900, 1999.
58. **Yundt KD, Grubb RL, Jr., Diringer MN, and Powers WJ**. Autoregulatory vasodilation of parenchymal vessels is impaired during cerebral vasospasm. *J Cereb Blood Flow Metab* 18: 419-424, 1998.
59. **Zaritsky JJ, Eckman DM, Wellman GC, Nelson MT, and Schwarz TL**. Targeted disruption of $K_{ir}2.1$ and $K_{ir}2.2$ genes reveals the essential role of the inwardly rectifying K^+ current in K^+-mediated vasodilation. *Circ Res* 87: 160-166, 2000.
60. **Zygmunt PM, and Hogestatt ED**. Role of potassium channels in endothelium-dependent relaxation resistant to nitroarginine in the rat hepatic artery. *Br J Pharmacol* 117: 1600-1606, 1996.

Figure Legends

Figure 1: Elevated cytosolic Ca^{2+} and enhanced myogenic tone in parenchymal arterioles from SAH animals. A-C: Representative simultaneous $[Ca^{2+}]_i$ and diameter measurements obtained from intact arterioles isolated from unoperated (control; *A*), sham-operated (sham; *B*) and SAH (*C*) animals. Recordings were obtained during step-wise increases in intravascular pressure and subsequent nimodipine application (300 nM) at 60 mmHg. **D,E.** Summary of $[Ca^{2+}]_i$ (*D*) and constriction (*E*) obtained from unoperated (control; n = 6), sham-operated (sham; n = 6) and SAH (n = 5) animals in the absence and presence of 300 nM nimodipine. Myogenic tone is expressed as a percent decrease from the passive diameter (obtained in Ca^{2+}-free aCSF with 300 nM nimodipine) of arterioles at a given intravascular pressure. Passive diameters were not statistically different between groups at any intravascular pressure tested. *****P<0.05, **P<0.01 vs. control healthy and sham-operated. **F.** Relationship between $[Ca^{2+}]_i$ and constriction for arterioles isolated from control and SAH animals derived from summary data depicted in panel *D* and *E*. Numbers represent intravascular pressure (mmHg). The concentration of Ca^{2+} causing half-maximal arteriolar constriction, obtained from Boltzmann fit of data (using 60 mM $[K^+]_o$ as maximum; see figure 3), were similar between groups (Control: 226 ± 26 nM, n = 5-7; SAH: 240 ± 10 nM, n = 5).

Figure 2: $Ca_V1.2$ mRNA and protein expression is unchanged following SAH. RT-PCR and Western blotting were used to measure $Ca_V1.2$ mRNA and protein,

respectively. **A.** Representative PCR gel showing bands corresponding to $Ca_V1.2$ and 18S ribosomal RNA (rRNA). **B.** Summary of RT-PCR data obtained from quantitative analysis of band intensities for arterioles isolated from control (n = 6) and SAH (n = 6) animals. $Ca_V1.2$ mRNA is expressed as relative to 18S rRNA. NS: P>0.05 vs. control. **C.** Representative Western blot images for $Ca_V1.2$ and GAPDH using whole cell lysates of parenchymal arterioles (each lane represents pooled arterioles from two animals). $Ca_V1.2$ immunoreactivity (~200-240 kDa) was observed as a doublet representing the full length and truncated forms of $Ca_V1.2$ (9). GAPDH (~36 kDa) was used as an internal standard. **D.** Summary of Western blot data obtained by densitometry using ImageJ software (NIH). $Ca_V1.2$ protein levels were normalized to GAPDH and expressed as fold-change compared to corresponding control in each experiment (n = 4). NS: P>0.05 vs. control.

Figure 3: Elevated arteriolar Ca^{2+} and enhanced constriction following SAH depend on membrane potential depolarization. **A.** Summary membrane potential data obtained from isolated pressurized (5 mmHg) parenchymal arterioles bathed in 60 mM extracellular K^+ ($[K^+]_o$). Membrane potential closely matched the theoretical E_K of -22 mV in arterioles from both control (n = 4) and SAH animals (n = 4). **B,C.** Summary data showing $[Ca^{2+}]_i$ (*B*) and constriction (*C*; percent decrease in diameter) in control (n = 7) and SAH arterioles (n = 5) exposed to aCSF containing either 3 mM or 60 mM $[K^+]_o$. Nimodipine (300 nM) reduced $[Ca^{2+}]_i$ to basal levels and dilated arterioles. NS: P>0.05

Figure 4: Myocytes of pressurized parenchymal arterioles are depolarized following SAH. A-B. Representative smooth muscle membrane potential measurements in arterioles isolated from control and SAH animals at 5 mmHg (*A*) and 40 mmHg (*B*) intravascular pressure. Scale bars represent 10 seconds. **C.** Summary of membrane potential measurements obtained at 5 and 40 mmHg. At 40 mmHg, myocytes of arterioles isolated from SAH animals were significantly more depolarized (-28 ± 1 mV, n = 4) compared with myocytes of arterioles isolated from control animals (-35 ± 1 mV, n = 5) **P<0.01 vs. control.

Figure 5: Elevated $[Ca^{2+}]_i$ and enhanced myogenic tone following SAH is independent of endothelial function. A. Summary of membrane potential measurements obtained from pressurized (40 mmHg) endothelium-intact parenchymal arterioles in the presence of NS309 (1 μM). **B.** Summary of $[Ca^{2+}]_i$ and dilation resulting from NS309 (1 μM) application for endothelium-intact parenchymal arterioles from control (n = 4) and SAH animals (n = 4). **C.** Summary of $[Ca^{2+}]_i$ and myogenic tone (percent decrease in diameter) obtained from endothelium-denuded arterioles from control (n = 5) and SAH animals (n = 5). Endothelium was removed by passing an air bubble through the vessel lumen for ~30 seconds. **P<0.01 vs. control **D.** Summary of $[Ca^{2+}]_i$ and dilation resulting from NS309 (1 μM) application for endothelium-denuded parenchymal arterioles from control (n = 5) and SAH animals (n = 5). **P<0.01 vs. control.

Figure 6: The relationship between intravascular pressure, cytosolic Ca^{2+} and diameter of parenchymal arterioles vs. pial arteries from control animals. A. Relationship between intravascular pressure and $[Ca^{2+}]_i$ for parenchymal arterioles and middle cerebral arteries (MCA; obtained from results published in Knot et al., 1998) (33) **B.** Relationship between $[Ca^{2+}]_i$ and constriction for parenchymal arterioles and middle cerebral arteries (33). Constriction is expressed as a percentage of maximal constriction obtained in 60 mM $[K^+]_o$ (see figure 4).

Table 1: Fura-2 Calibration values. R_{min}, R_{max} and β was determined from a separate set of arterioles (see Methods). No differences were found among control (n = 4) and SAH (n = 4) arterioles. Pooled values (n = 8) shown in table were used for analysis of $[Ca^{2+}]_i$ measurements.

Figures

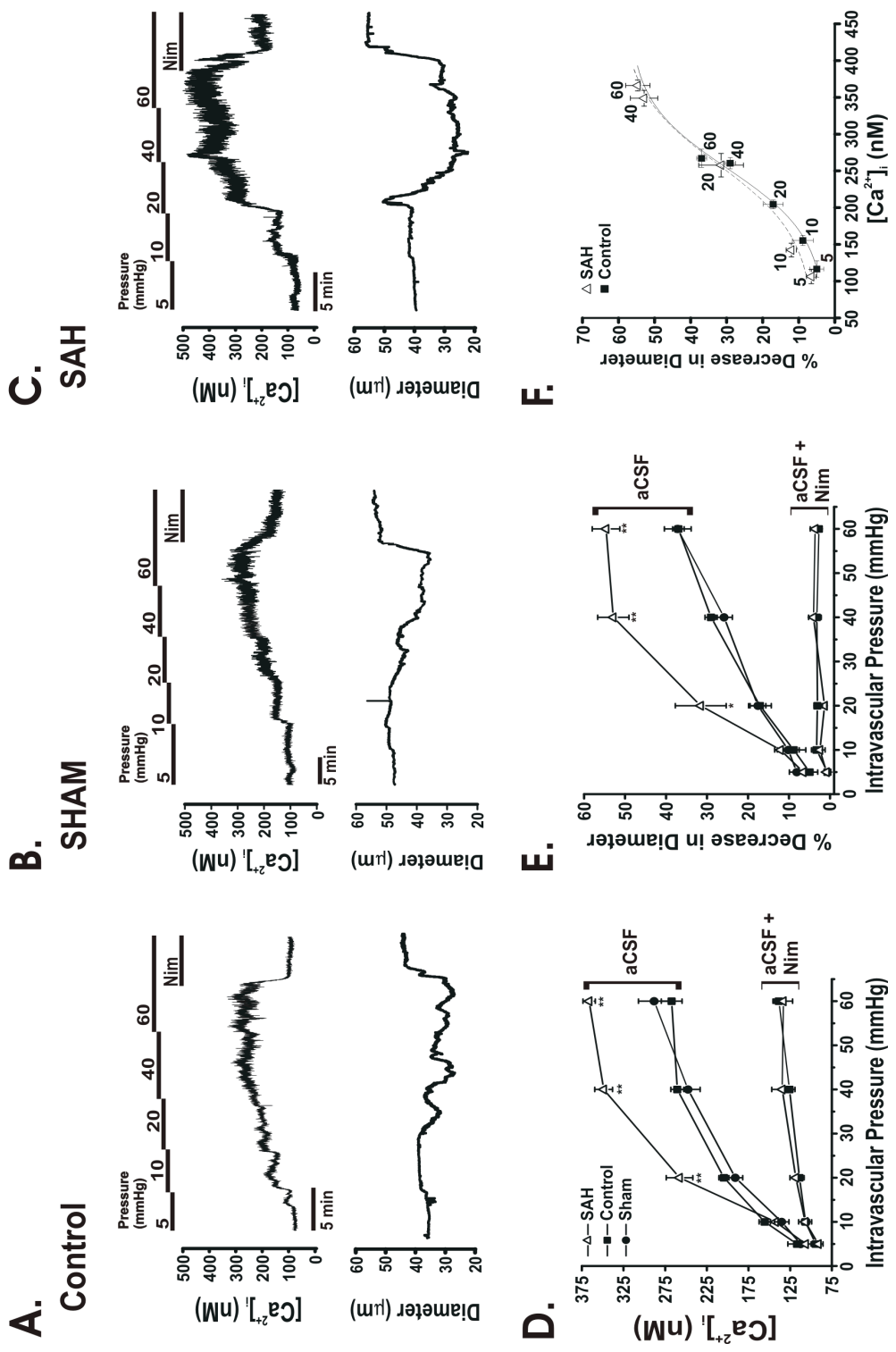

Figure 1: *Elevated Ca^{2+} and enhanced tone in parenchymal arterioles from SAH animals.*

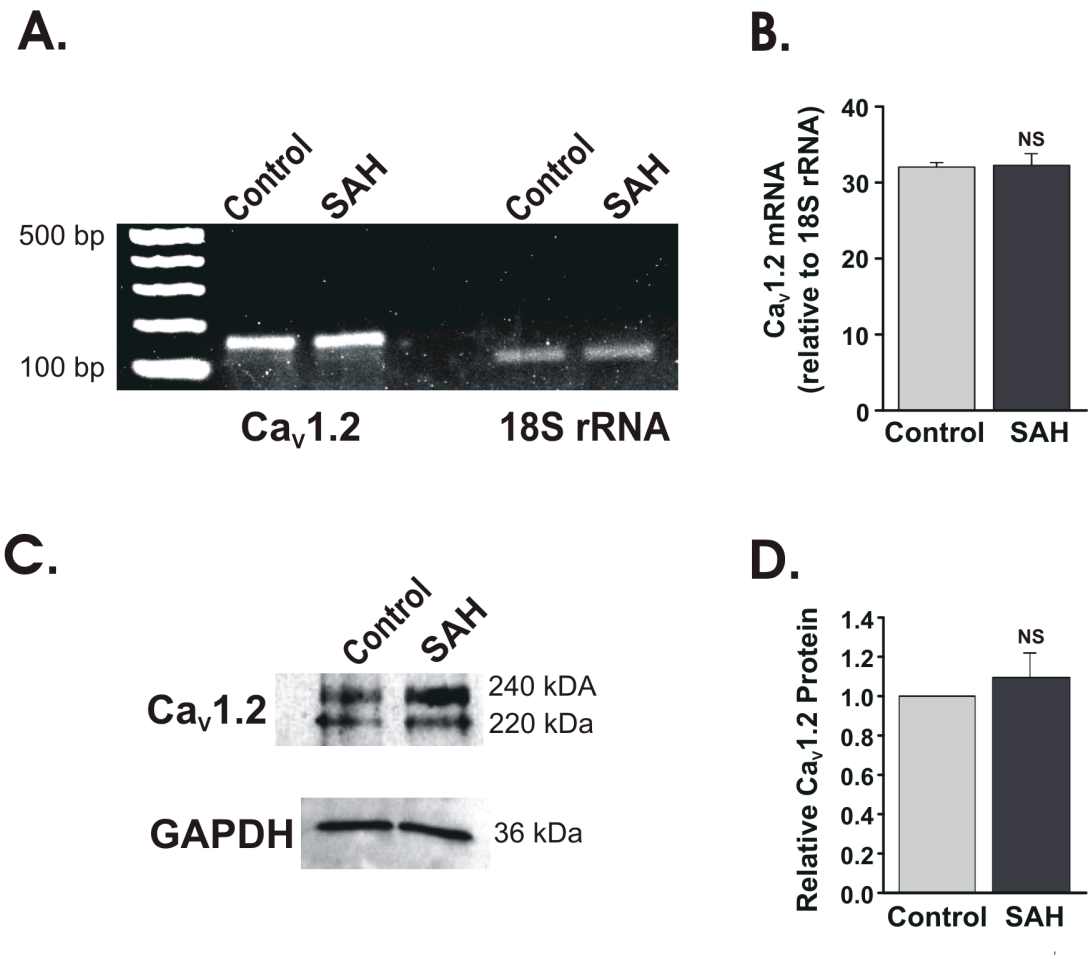

Figure 2: ***Ca_V1.2 mRNA and protein expression is unchanged following SAH.***

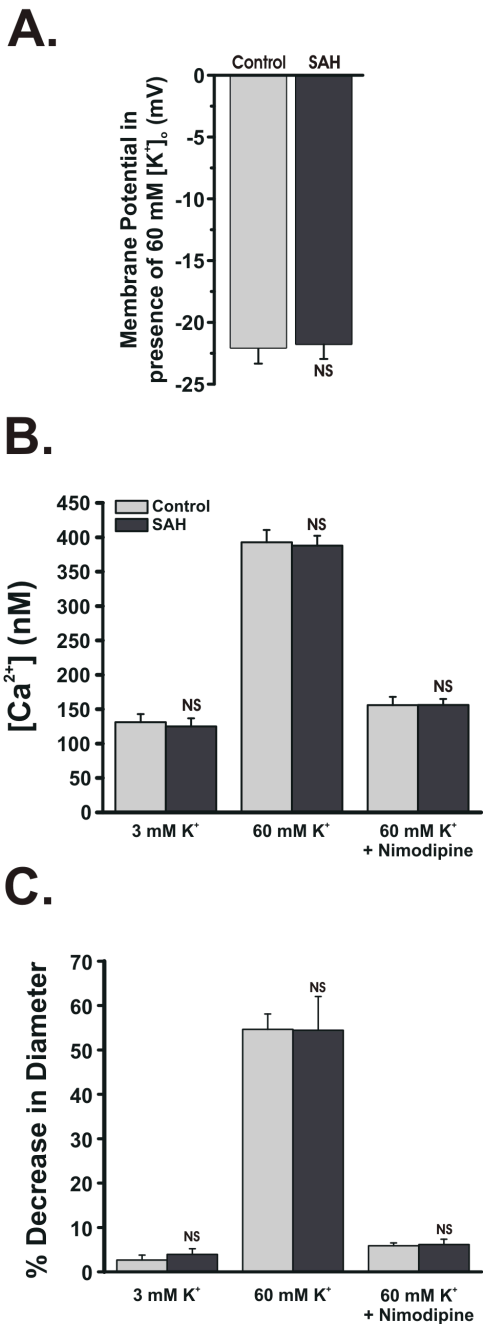

Figure 3: ***Elevated arteriolar Ca^{2+} and enhanced constriction following SAH depend on membrane potential depolarization.***

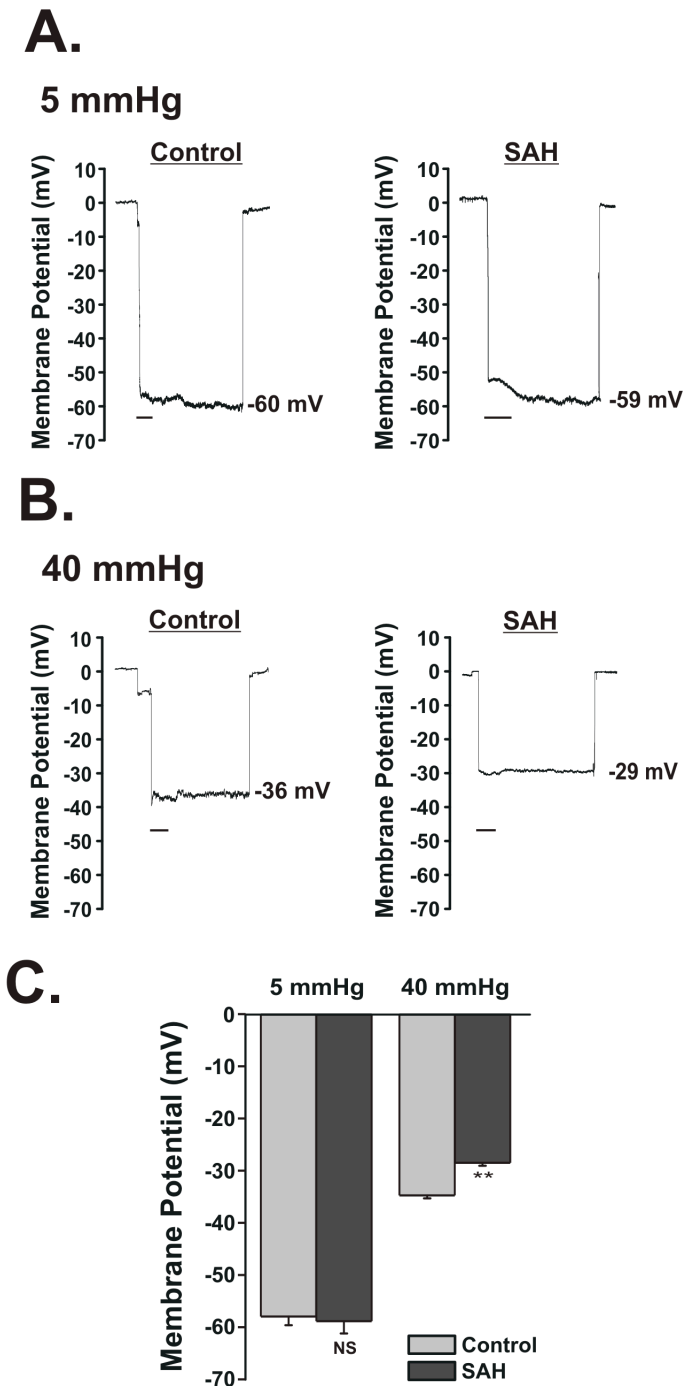

Figure 4: ***Myocytes of pressurized parenchymal arterioles are depolarized following SAH.***

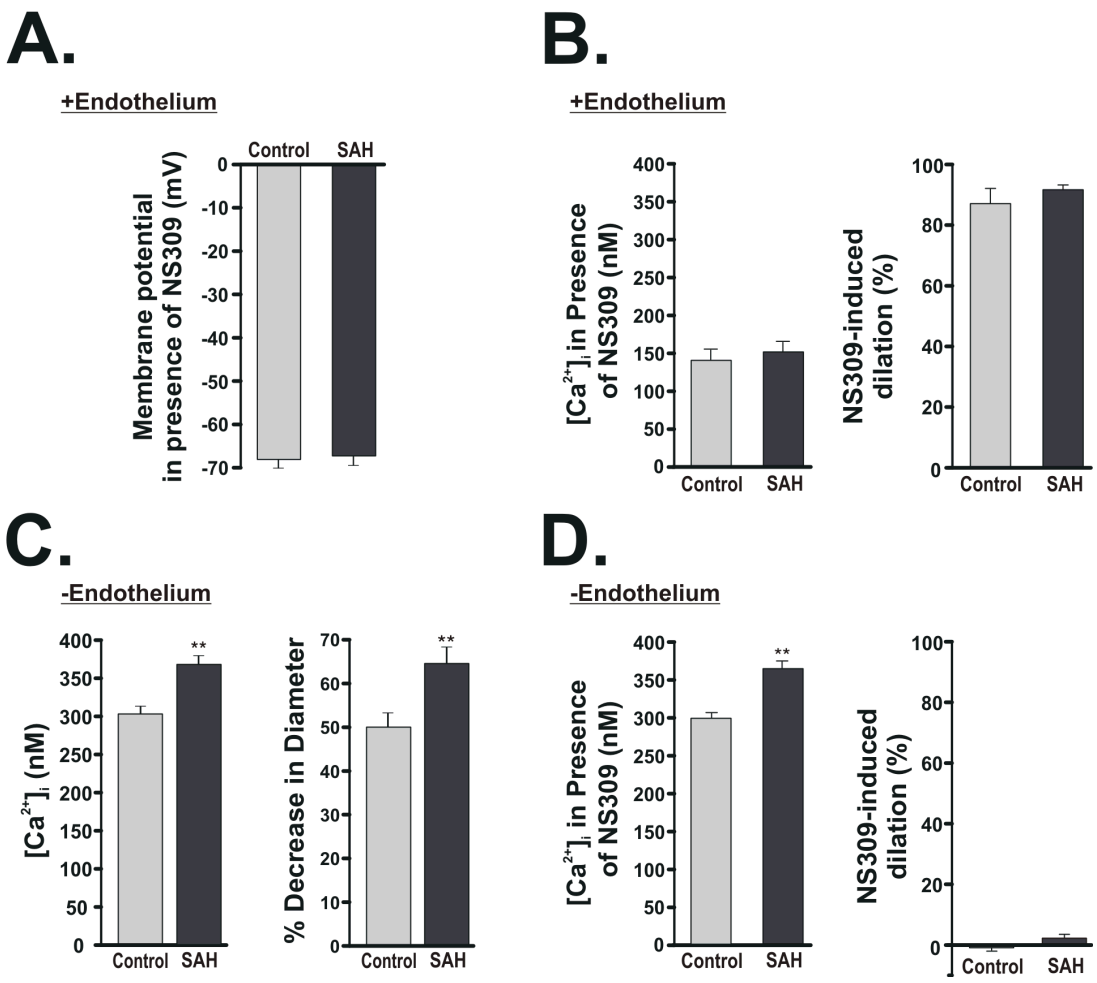

Figure 5: ***Elevated $[Ca^{2+}]_i$ and enhanced myogenic tone following SAH is independent of endothelial function.***

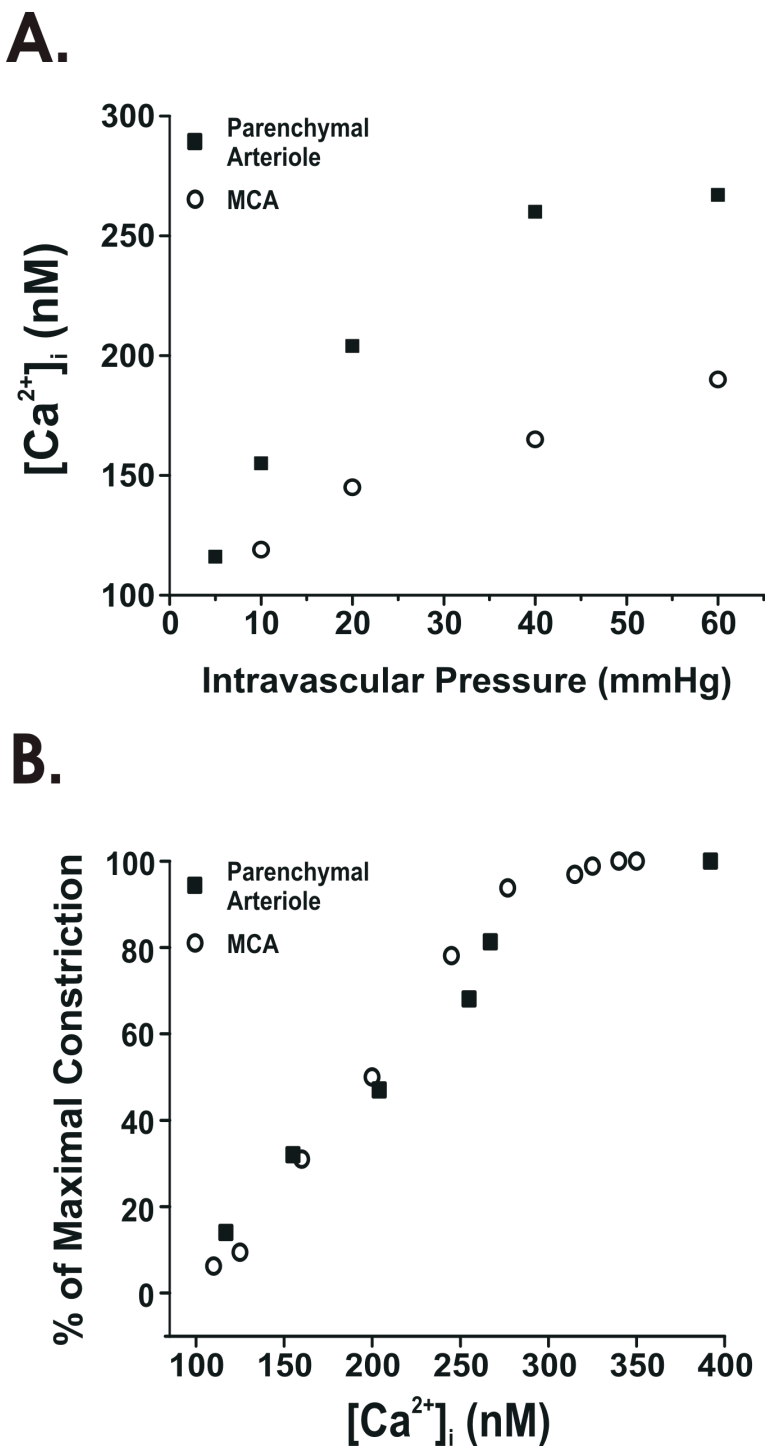

Figure 6: ***The relationship between intravascular pressure, cytosolic Ca^{2+} and diameter of parenchymal arterioles vs. pial arteries from control animals.***

Chapter 2 Table 1: ***Fura-2 Calibration Values.***

	Rmin	Rmax	β
Control (n = 4)	0.371± 0.008	9.969 ± 0.565	8.031 ± 0.895
SAH (n = 4)	0.378 ± 0.005	10.064 ± 0.795	7.764 ± .370
Pooled	0.374 ± 0.004	10.017 ± 0.483	7.898 ± 0.451

Values are means ± SEM.

CHAPTER 3: JOURNAL ARTICLE

$Ca_v1.2$ splice variant with exon 9* is critical for regulation of cerebral artery diameter.

Matthew A. Nystoriak[1], Kentaro Murakami[1], Paul L. Penar[2], and George C. Wellman[1,2] .

Departments of Pharmacology[1] and Surgery, Division of Neurological Surgery[2], University of Vermont, College of Medicine, Burlington, Vermont.

Running Head: Exon 9* $Ca_v1.2$ Regulates Cerebral Artery Constriction.

Contact Information: Address for reprint requests and other correspondence: G. C. Wellman, Univ. of Vermont, Dept. of Pharmacology, Given Bldg., 89 Beaumont Ave., Burlington, VT 05405-0068 (e-mail: george.wellman@uvm.edu)

Abstract

L-type voltage-dependent Ca^{2+} channels (VDCCs) are essential for numerous processes in the cardiovascular and nervous systems. Alternative splicing modulates proteomic composition of $Ca_v1.2$ to generate functional variation between channel isoforms. Here, we describe expression and function of $Ca_v1.2$ channels containing alternatively spliced exon 9* in cerebral artery myocytes. RT-PCR showed expression of $Ca_v1.2$ splice variants both containing ($\alpha1C_{9/9*/10}$) and lacking ($\alpha1C_{9/10}$) exon 9* in intact rabbit and human cerebral arteries. Using laser capture microdissection and RT-PCR, expression of mRNA for both $\alpha1C_{9/9*/10}$ and $\alpha1C_{9/10}$ was demonstrated in isolated cerebral artery myocytes. Quantitative real-time PCR revealed significantly greater $\alpha1C_{9/9*/10}$ expression relative to $\alpha1C_{9/10}$ in intact rabbit cerebral arteries compared with cardiac tissue and cerebral cortex. To demonstrate a functional role for $\alpha1C_{9/9*/10}$, smooth muscle of intact cerebral arteries was treated with antisense oligonucleotides targeting $\alpha1C_{9/9*/10}$ ($\alpha1C_{9/9*/10}$-AS) or exon 9 (α1C-AS), expressed in all $Ca_v1.2$ splice variants, by reversible permeabilization and organ cultured for 1-4 days. Treatment with $\alpha1C_{9/9*/10}$-AS reduced maximal constriction induced by elevated extracellular K^+ ($[K^+]_o$) by approximately 75% compared with $\alpha1C_{9/9*/10}$-sense treated arteries. Maximal constriction in response to the Ca^{2+} ionophore ionomycin and $[K^+]_o$ EC_{50} values were not altered by antisense treatment. Decreases in maximal $[K^+]_o$-induced constriction were similar between $\alpha1C_{9/9*/10}$-AS and α1C-AS groups (22.7 ± 9% and 25.6 ± 4% constriction, respectively). We conclude that although cerebral artery myocytes express both $\alpha1C_{9/9*/10}$ and $\alpha1C_{9/10}$ VDCC splice variants, $\alpha1C_{9/9*/10}$ is functionally dominant in the control of cerebral artery diameter.

Keywords: vascular smooth muscle, calcium channels, cerebral blood flow, splice variant.

Introduction

L-type voltage dependent calcium channels (VDCCs) play a crucial role in the physiological processes of numerous cell types. In the resistance circulation, arterial constriction is dependent on membrane potential depolarization and Ca^{2+} entry via $Ca_v1.2$ channels in vascular smooth muscle (15, 21). An increase in global cytosolic Ca^{2+} leads to Ca^{2+}/calmodulin-dependent activation of myosin light chain kinase, myosin light chain phosphorylation, increased actin-myosin interaction, smooth muscle contraction and decreased vessel diameter. This mechanism is essential for proper regulation of organ perfusion and systemic blood pressure.

VDCCs are multimeric protein complexes comprised of an α1 pore-forming subunit associated with β and $\alpha_2\delta$ auxiliary subunits (5, 8, 24). L-type VDCC currents are distinguished by high activation potentials, slow inactivation of barium currents, and selective inhibition by dihydropyridines (DHPs), phenylalkylamines, and benzothiazepines (5). The $Ca_v1.2$ gene, *CACNA1C* consists of 55 exons, 19 of which are subject to extensive alternative splicing with 40 splice variations found at 12 loci (34). cDNA library screening studies have allowed the identification of the cardiac and smooth muscle $Ca_v1.2$ isoforms, differing in composition at four alternative splice sites (2, 22, 28, 31). The purported smooth muscle splice combination consists of exons 1/8/+ 9*/32 while the cardiac form consists of exons 1a/8a/- 9*/31. Smooth muscle L-type channels are reported to activate at more hyperpolarized (~15 mV) membrane potentials (14, 30) and display greater DHP sensitivity than analogous channels in the heart (35). A previous study suggests that the presence of exon 8 rather than 8a to form transmembrane

segment 6 of domain I (IS6) in smooth muscle channels contributes to differences in DHP inhibition (36). Other work has shown that the inclusion of the 25 amino acid insertion exon 9* in the intracellular linker region between homologous domains I and II affects channel gating properties resulting in a hyperpolarizing shift in activation potential and current-voltage relationship (26). The electrophysiological alteration imposed by the addition of exon 9* to the channel protein structure suggests that expression of exon 9* may be a critically important mechanism for the fine-tuning of channel function such that smooth muscle VDCCs activate at physiologically relevant membrane potentials. Although such a role for $Ca_v1.2$ channels expressing exon 9* would be suitable for proper vascular function, the physiological significance of this splice variant in the regulation of blood vessel diameter has not been directly investigated.

Here, the objective was to determine the role of the exon 9* $Ca_v1.2$ splice variant in constriction of resistance size cerebral arteries. Consistent with previous findings by others (3, 13, 26), we provide evidence for exon 9* expression in cerebral arteries and further show a significantly higher ratio of exon 9* mRNA relative to total $Ca_v1.2$ mRNA in cerebral arteries compared with cerebral cortex and cardiac tissue. RT-PCR performed on cDNA obtained from myocytes isolated by laser-capture microdissection found expression of both splice variants in cerebral artery smooth muscle. Antisense oligodeoxynucleotides were used to selectively suppress $\alpha 1C_{9/9*/10}$ in cerebral artery smooth muscle to examine the functional role for this splice variant in cerebral artery constriction. Our findings indicate that despite heterogeneous mRNA expression of both

$\alpha 1C_{9/9*/10}$ and $\alpha 1C_{9/10}$ isoforms by cerebral artery myocytes, $\alpha 1C_{9/9*/10}$ channels play a dominant role in constriction of these vessels.

Methods

Animals. New Zealand White rabbits (males, 3.0-3.5 kg) were used in this study. All experiments were conducted in accordance with the G*uidelines for the Care and Use of Laboratory Animals* (NIH Publication 85-23, 1985) and followed protocols approved by the Institutional Animal Use and Care Committee of the University of Vermont. Animals were euthanized under deep pentobarbital anesthesia (150 mg/kg iv) by exsanguination and decapitation. Posterior cerebral and cerebellar arteries were dissected in ice cold physiological saline solution (PSS) of the following composition (in mM): 118.5 NaCl, 4.7 KCl, 24 $NaHCO_3$, 1.18 KH_2PO_4, 2.25 $CaCl_2$, 1.2 $MgCl_2$, 0.023 EDTA, and 11 glucose, aerated with 5% CO_2, 20% O_2, 75% N_2 (bath pH: 7.4). Cerebral artery myocytes (40-60 cells/sample) were collected from enzymatically dissociated freshly isolated posterior cerebral arteries (23, 37) using a P.A.L.M. Laser Capture Microdissection system (Zeiss, Bernried, Germany). Human cerebral arteries, removed as a necessary part of a required procedure, were obtained from two consenting surgical patients. Patients were not receiving calcium channel blockers or other antihypertensive agents at the time of surgery. The University of Vermont has an approved assurance of compliance on file with the Department of Health and Human Services covering this activity (Assurance identification number: FWA723; IRB identification number 0485).

RT-PCR. Total RNA was extracted using RNA STAT-60 total RNA/mRNA isolation reagent (Tel-test, Friendswood, TX) (4). Total RNA was reverse transcribed to cDNA

using SuperScript First-Strand synthesis system (Invitrogen, Carlsbad, CA). Semi-quantitative PCR was performed using primers detecting the region spanning exons 7-11 of $Ca_v1.2$ (Genbank accession No. X55763) (Fig. 1a) of the following sequences: *forward* (5'-TGCTTTCGCCATGTTGACG-3'), *reverse* (5'-GAATTTCGACTTGGAGATCCGG-3'). Amplification was performed with Taq PCR core kit (Qiagen) using the following protocol: 94˚ C 3 min, 35 cycles of 94˚ C 1 min, 55˚ C 1 min, 72˚ C 1 min, and final extension at 72˚ C for 10 min. PCR products were separated by electrophoresis using 2% agarose gel. Quantitative real-time PCR was performed using primers detecting exons 9*-10 [$\alpha 1C_{9/9*/10}$ *forward* (5'-CTTGCATGCCCAGAAGAAAG-3'), *reverse* (5'-TAGCGGCTGAATTTCGACTT-3')], exons 9-10 [$\alpha 1C_{9/9*/10}$ *forward* (5'-CCCGAAACATGAGCATGC-3'), *reverse* (5'-GCACTTTCTCCTGCAGAACC-3')] by using a sense primer specific for the boundary of exons 9/10 of $Ca_v1.2$ (Fig. 2A), and 18S [18S forward (5'-AGTCGCCGTGCCTACCAT-3'), reverse (5'-GCCTGCTGCCTTCCTTG-3')]. Amplification was performed with SYBR Green JumpStart Taq ReadyMix (Sigma, St. Louis, MO) using a real-time PCR system (Applied Biosystems, Carlsbad, CA). Quantification was performed using standard curves constructed by amplification of serially diluted plasmids containing target genes.

Cerebral artery myocytes samples were screened for cell-specific markers using the following primer sets: smooth muscle myosin heavy chain [*forward* (5'-CACCACACATCTACGCCATC-3'), *reverse* (5'-TGATGCTCGTGTCCTTCTTG-3')], endothelin 1 [*forward* (5'-AAAGGCAAAGACTGCTCCAA-3'), *reverse* (5'-

GCACTCCTTGGTCTCTCCTG-3')], fibroblast specific protein 1 [*forward* (5'-GGGGTGACAAGTTCAAGCTC-3'), *reverse* (5'-CTGGAAGTCCACCTCGTTGT-3')], and growth associated protein-43 [*forward* (5'-AGCCAAGGAGGAGCCTAAAC-3') *reverse* (5'-TCAGGCATGTTCTTGGTCAG-3')]. Nested PCR was performed using primers for exons 7-11 (above) of $Ca_v1.2$ for first round amplification (35 cycles) and using the following nested PCR primers for 35 cycles of amplification of 1:100 dilution of first round products: *forward* (5'-CGTGCTGTACTGGGTCAATG-3'), *reverse* (5'-CAGCCACGTTTTCAGTGTTG-3').

Immunostaining of isolated cerebral artery myocytes. Dissociated cell suspensions were fixed with 4% formalin and plated on Superfrost Plus microscope slides (Fisher Scientific, Waltham, MA) with a cytocentrifuge. Cells were dried for 10 min and blocked and permeabilized in 3% milk/0.1% Triton-X 100 phosphate-buffered saline (PBS) for 20 min. Cells were rinsed with PBS for 30 min and incubated (4˚C/overnight) in PBS containing mouse monoclonal antibody raised against rabbit smooth muscle myosin heavy chain 2 (SM-MHC) (1:125 dilution; Abcam, Cambridge, MA) or monoclonal antibody against α-smooth muscle actin conjugated to Cy3 (1:200; Sigma, St. Louis, MO). Cells were then rinsed in PBS, and slides treated with anti-SM-MHC were incubated in anti-mouse IgG conjugated to Cy3 (1:500; Jackson ImmunoResearch Laboratories, West Grove, PA). Images were taken (40x) using a Zeiss LSM 510 Meta confocal microscope.

Use of antisense oligonucleotides. For suppression of $\alpha 1C_{9/9*/10}$, antisense oligonucleotides (Operon Biotechnologies, Huntsville, AL) were designed to target a sequence specific to the coding region of exon 9* of $Ca_v1.2$ mRNA transcripts: $\alpha 1C_{9/9*/10}$-AS: 5'-A*A*G*C*CCGCTGGAGTGC*C*T*C*T-3'. To suppress the total population of $Ca_v1.2$ channels, antisense oligodeoxynucleotides were designed to target exon 9 which is not alternatively spliced and is expressed in all $Ca_v1.2$ transcripts: α1C-AS 5'-C*T*C*T*TCCAGCTGCTGCTTC*T*C*C*C-3'. Control sense oligonucleotides of the following sequences were designed: $\alpha 1C_{9/9*/10}$-sense: 5'-A*G*A*G*GCGCTCCAGCGG*G*C*T*T-3' and α1C-sense: 5'-G*G*G*A*GAAGCAGCAGCTGGA*A*G*A*G-3'. The first and last four bases of each oligonucleotide were phosphorothioated to prevent degradation by cellular nucleases (designated by "*"). All oligonucleotides were reconstituted with nuclease-free water at a concentration of 10 mM.

Reversible permeabilization and organ culture of cerebral arteries. The introduction of oligonucleotides into smooth muscle of intact cerebral arteries was achieved by a reversible permeabilization (RP) procedure (9, 25). Arterial segments were first incubated at 4˚C for 30 min in the following solution (in mM): 120 KCl, 2 $MgCl_2$, 10 EGTA, 5 NaATP, 20 N-tris-(hydroxymethyl)methyl-2-aminoethanesulfonic acid (pH 6.8). Arteries were then incubated in a similar solution containing oligonucleotide (10 μM) for 90 min at 4˚C and then in a solution containing elevated $MgCl_2$ (10 mM). Permeabilization of arteries was reversed by incubating arteries for 30 min at room

temperature in physiological solution containing the following (in mM): 140 NaCl, 5 KCl, 10 $MgCl_2$, 5.6 glucose, 2 3-(N-morpholino)propanesulfonic acid (pH 7.1). Next, [Ca^{2+}] was gradually increased in this solution from nominally Ca^{2+}-free to 0.01, 0.1, and 1.8 mM over a period of 45 min. Following reversible permeabilization, arterial segments were organ cultured by placing the arteries in serum-free DMEM-F12 culture media (Invitrogen, Carlsbad, CA) and incubating at 37˚C and 5% CO_2 for 1 to 4 days (18, 27).

Diameter measurements in isolated arteries. Freshly isolated and cultured cerebral artery segments were cannulated on glass micropipettes mounted in a 5 ml myograph chamber (University of Vermont Instrumentation and Model Facility) as described previously (18, 19, 27). Following cannulation, arteries were pressurized at 20 mmHg and continuously superfused with aerated PSS at 37˚ C and pH 7.4 for 30 min to allow equilibration. Arterial diameter was measured with video edge detection equipment and recorded using data acquisition software (Dataq Instruments Inc., Akron, OH). Arteries were exposed to PSS containing elevated [K^+], made by isoosmotic replacement of NaCl with KCl. Arterial constriction was expressed using the following equation: $\%\ Constriction = (1-(D - D_{min}/D_{max} - D_{min}))\ X\ 100$ where D_{max} is the maximum diameter obtained in Ca^{2+}-free PSS containing diltiazem (100 μM) and forskolin (1 μM) and D_{min} is the minimum diameter obtained with the Ca^{2+} ionophore ionomycin (10 μM) at the end of each experiment. Ionomycin-induced constrictions (table 1) are presented as a percentage of maximum diameter (D_{max}). Arteries not achieving >70 % constriction in

response to ionomycin were not used for analysis. Half-maximal effective concentration (EC_{50}) was determined from each $[K^+]_o$ concentration-response experiment.

Statistical analysis. Values are presented as means ± SEM. One-way analysis of variance followed by Tukey multiple comparison test was used in the comparison of multiple groups. Student's t-test was used in the comparison of two groups. Statistical significance was considered at the level of $p < 0.05$ (*) or $p < 0.01$ (**).

Results

Cerebral arteries demonstrate enhanced expression of $\alpha 1C_{9/9*/10}$ compared with brain and heart.

Previous work has shown selective expression of $\alpha 1C_{9/9*/10}$ splice variants by smooth muscle-containing tissues. However, mRNA expression of both α_{1c} splice variants including ($\alpha 1C_{9/9*/10}$) and excluding ($\alpha 1C_{9/10}$) exon 9* has been reported in aorta (3, 13, 26). Therefore, our first objective was to investigate whether small diameter (100-250 μm) cerebral arteries express mRNA for both $\alpha 1C_{9/9*/10}$ and $\alpha 1C_{9/10}$. To detect expression of $\alpha 1C_{9/9*/10}$, we designed PCR primers to generate products consisting of exons 7-11 of α_{1c} (Fig. 1A) such that a shift in product size would result if the 75 nucleotide (nt) insertion for exon 9* was expressed. RT-PCR analysis resulted in two distinct bands from rabbit cerebral arteries (Fig. 1B; n=7). Sequence analysis confirmed the lower band of 460 nt represents $\alpha 1C_{9/10}$ while the upper band of 535 nt represents $\alpha 1C_{9/9*/10}$. Human cerebral arteries were also analyzed and found to express both $\alpha 1C_{9/9*/10}$ and $\alpha 1C_{9/10}$ similar to arteries from rabbit (Fig. 1C). In contrast, cardiac tissue (left ventricle; n=8) and brain tissue (cerebral cortex; n=5) were found to express one dominant product corresponding to $\alpha 1C_{9/10}$ (Fig. 1B).

Quantitative real-time PCR was used to evaluate relative expression levels of $\alpha 1C_{9/9*/10}$ in these tissues. We hypothesized the fraction of mRNA for $Ca_v1.2$ expressing exon 9* is greater in cerebral arteries than cardiac and brain tissue. $\alpha 1C_{9/9*/10}$ and $\alpha 1C_{9/10}$ expression was measured separately by using either a PCR primer specific for exon 9* sequence ($\alpha 1C_{9/9*/10}$-specific) or a primer specific for the boundary of exons 9 and 10

($\alpha1C_{9/10}$-specific; Fig. 2A). $\alpha1C_{9/9*/10}$ and $\alpha1C_{9/10}$ expression was normalized to 18S ribosomal RNA levels. This approach allows quantification of the $\alpha1C_{9/9*/10}$:$\alpha1C_{9/10}$ mRNA ratio, which is representative of $\alpha1C_{9/9*/10}$ relative to overall $Ca_v1.2$ expression considering that $\alpha1C_{9/9*/10}$ and $\alpha1C_{9/10}$ are mutually exclusive splice variants. We found that cerebral arteries express significantly higher relative levels of $\alpha1C_{9/9*/10}$ compared with brain and heart tissues (Fig. 2B; ~fifty-two fold and ~six fold difference, respectively). Together, these results demonstrate mRNA for both $\alpha1C_{9/9*/10}$ and $\alpha1C_{9/10}$ splice variants in cerebral arteries and enhanced relative expression of $\alpha1C_{9/9*/10}$ in cerebral arteries compared with brain and heart.

Isolated cerebral artery myocytes express both $\alpha1C_{9/9*/10}$ and $\alpha1C_{9/10}$ splice variants.

We next chose to clarify whether cerebral artery myocytes express mRNA for both splice variants or if $\alpha1C_{9/10}$ detection was due to the presence of non-smooth muscle cell types within the vascular wall, such as fibroblasts or perivascular neurons, which are reported to express $Ca_v1.2$ (10, 13, 17, 32). Live freshly isolated cerebral artery myocytes (~40-60 cells) were collected by laser capture microdissection for RT-PCR analysis (Fig. 3B). These elongated spindle-shaped cells showed strong immunofluorescent staining for SM-MHC or SM-α-actin, markers commonly used to identify smooth muscle (1, 11) (Fig. 3A). RT-PCR was used to examine expression of specific cell markers: smooth muscle myosin heavy chain (SM-MHC; smooth muscle), endothelin-1 (ET-1; endothelium) (38), fibroblast specific protein-1 (FSP-1; fibroblast) (33) and growth associated protein-43 (GAP43; neuron) (39) in mRNA isolated from both intact arteries and isolated myocytes.

The above cell markers all amplified using intact cerebral artery mRNA (Fig. 3C), consistent with the presence of multiple cell types in intact vessels. However, only the smooth muscle marker SM-MHC was expressed in freshly isolated myocytes, confirming purity of our samples. Nested PCR for exons 7-11 of $Ca_v1.2$ demonstrated two bands corresponding to $\alpha1C_{9/9*/10}$ and $\alpha1C_{9/10}$ in isolated cerebral artery myocytes, similar to the intact tissue (Fig. 3D). These data demonstrate heterogeneous mRNA for both $\alpha1C_{9/9*/10}$ and $\alpha1C_{9/10}$ in isolated smooth muscle from cerebral arteries.

$\alpha1C_{9/9*/10}$ plays critical role in depolarization-induced constriction of cerebral arteries.

High expression levels of $\alpha1C_{9/9*/10}$ in cerebral artery myocytes suggest this splice variant may have an important role in vascular function. We therefore tested the hypothesis that $\alpha1C_{9/9*/10}$ splice variants are an important regulator of cerebral artery diameter. Two antisense oligonucleotide sequences were designed to examine the functional role of $\alpha1C_{9/9*/10}$. First, $\alpha1C_{9/9*/10}$-AS targeting a sequence specific for exon 9* was used for selective suppression of the $\alpha1C_{9/9*/10}$ variant. Second, α1C-AS targeting a sequence specific for exon 9, which is constitutively expressed in all L-type VDCC splice variants, was used for non-selective suppression of all $Ca_v1.2$ isoforms. Four days following treatment, standard RT-PCR and qPCR demonstrated a significant reduction (43 ± 6.9%) in $\alpha1C_{9/9*/10}$ expression following treatment with $\alpha1C_{9/9*/10}$-AS compared with $\alpha1C_{9/9*/10}$-sense treated arteries (Fig. 4A and B). However, suppression of $\alpha1C_{9/10}$ was not observed following treatment with $\alpha1C_{9/9*/10}$-AS. In contrast to the effect of $\alpha1C_{9/9*/10}$-AS, arteries

treated with α1C-AS exhibited a significant reduction in expression for both $\alpha1C_{9/9*/10}$ and $\alpha1C_{9/10}$ splice variants (Fig. 4A and B).

To examine the effect of suppressing $\alpha1C_{9/9*/10}$ on arterial constriction, luminal diameter measurements were performed while increasing external K^+ ($[K^+]_o$) in the bath solution over a range of concentrations from 6 to 120 mM following a period of 1 to 4 days in organ culture. The relationship between extracellular $[K^+]_o$ and membrane potential at $[K^+]_o > 16$ mM closely follows that which is predicted by the Nernst equation (16, 21).

Step-wise increases in $[K^+]_o$ caused graded arterial constriction of control freshly-isolated vessels (Fig. 5 and 6). $\alpha1C_{9/9*/10}$-AS, $\alpha1C_{9/9*/10}$-sense and RP only groups all responded similarly to freshly isolated vessels following one day in culture (Fig. 6). However, K^+-induced constrictions, expressed as a percentage of maximum constriction caused by ionomycin (see methods), was significantly reduced in $\alpha1C_{9/9*/10}$-AS arteries compared with control $\alpha1C_{9/9*/10}$-sense treated and RP arteries after two days. For example, $\alpha1C_{9/9*/10}$-AS treated vessels exhibited 52 ± 5.9% constriction in response to 60 mM K^+ on day 2 compared with 80 ± 2.1% and 75 ± 2.9% constriction in $\alpha1C_{9/9*/10}$-sense treated and RP vessels, respectively. Further reductions were observed in $\alpha1C_{9/9*/10}$-AS treated arteries on day 3 (e.g., 26 ± 4.1% in $[K^+]_o$ = 60 mM) and day 4 (e.g., 23 ± 4.9% in $[K^+]_o$ = 60 mM) of organ culture (Fig. 6). $\alpha1C_{9/9*/10}$-sense treated and RP arteries constricted to a similar degree as freshly isolated vessels at all time points tested (Fig. 5 and 6). Mean diameters of arteries exposed to these treatments are shown in Table 1. No significant differences in EC_{50} values for K^+ were observed between groups (Table 1).

Diameter values and maximal constriction to ionomycin were similar between groups at all time points tested (Table 1). Fully dilated arterial diameter, obtained in Ca^{2+}-free PSS containing diltiazem and forskolin, was not significantly different between groups ($\alpha1C_{9/9*/10}$-AS: 201 ± 13 μm, n=17; Sense: 214 ± 16 μm, n=17, RP: 199 ± 13 μm, n=16). Taken together, these data demonstrate an important role for $\alpha1C_{9/9*/10}$ in the regulation of cerebral artery constriction.

$\alpha1C_{9/9*/10}$ is the functionally dominant splice variant in cerebral arterial constriction.

Our data imply that although cerebral artery myocytes express both $\alpha1C_{9/9*/10}$ and $\alpha1C_{9/10}$, $\alpha1C_{9/9*/10}$ plays a major role in cerebral artery constriction. To examine the role of $\alpha1C_{9/10}$ in cerebral artery constriction, we compared the effect of suppressing $\alpha1C_{9/9*/10}$ to supressing all $Ca_v1.2$ splice variants (both $\alpha1C_{9/9*/10}$ and $\alpha1C_{9/10}$) using α1C-AS. Arteries treated with α1C-AS exhibited diminished constriction to 60 mM $[K^+]_o$ that was similar to that observed in arteries treated with $\alpha1C_{9/9*/10}$-AS (Fig. 7; $\alpha1C_{9/9*/10}$-AS: 23.5 ± 3.6%, n=6; α1C-AS: 25.6 ± 4.3%, n=5) suggesting that suppression of all $Ca_v1.2$ splice variants had no greater effect on constriction to 60 mM $[K^+]_o$ than selectively suppressing $\alpha1C_{9/9*/10}$. These data suggest that the isoform containing exon 9* is the functionally dominant $Ca_v1.2$ splice variant in cerebral artery constriction.

Discussion

Here we demonstrate that cerebral artery myocytes express $Ca_v1.2$ splice variants both containing ($\alpha1C_{9/9*/10}$) and lacking ($\alpha1C_{9/10}$) exon 9* and that $\alpha1C_{9/9*/10}$ plays a dominant role in cerebral artery constriction. The following observations are consistent with this novel finding: 1) cerebral arteries have a significantly higher ratio of $\alpha1C_{9/9*/10}$: $\alpha1C_{9/10}$ mRNA compared with cerebral cortex or cardiac tissue. 2) RT-PCR performed on cDNA from isolated cerebral artery myocytes confirmed expression of both $\alpha1C_{9/9*/10}$ and $\alpha1C_{9/10}$ in smooth muscle. 3) Selective suppression of the $\alpha1C_{9/9*/10}$ splice variant caused a marked reduction in K^+-induced arterial constriction. 4) Suppression of all $Ca_v1.2$ splice variants caused no further reduction in K^+-induced arterial constriction. In addition, we found a similar expression profile of $\alpha1C_{9/9*/10}$ and $\alpha1C_{9/10}$ splice variants in cerebral arteries from humans.

This work expands our understanding of the molecular composition of smooth muscle VDCCs responsible for the control of arterial diameter and blood flow. Unlike cardiac myocytes, vascular smooth muscle operates in a state of tonic contraction responding to modest changes in membrane potential caused, for example, by changes in intravascular pressure, neurotransmitter release, circulating catacholamines, and endothelial influences. Thus, L-type VDCCs expressed by vascular smooth muscle respond to small voltage changes at relatively negative membrane potentials compared to more depolarized membrane potentials reached during action potentials in cardiac myocytes or neurons. Recent studies using cell expression systems have found expression of the 25 amino acid insertion exon 9* causes a 9 mV hyperpolarizing shift in

L-type VDCC $V_{0.5,\ act}$ (6, 26). This hyperpolarizing shift in the activation of this splice variant would be well-suited to the range of vascular smooth membrane potential *in vivo* (-45 to -35 mV) (29). We now report that exon 9*-containing L-type VDCCs are the dominant $Ca_v1.2$ splice variant contributing to cerebral artery constriction. To our knowledge, this is the first study directly demonstrating a physiological role for a single $Ca_v1.2$ splice variant.

We have observed that whole arterial tissue containing smooth muscle, endothelial, fibroblast and perivascular neural cells expresses both $\alpha1C_{9/9*/10}$ and $\alpha1C_{9/10}$ splice variants. While endothelial cells are known to lack expression of VDCCs (13), $Ca_v1.2$ expression by fibroblasts and neurons is well documented (10, 17, 32). To further explore the composition of $Ca_v1.2$ splice variants in vascular smooth muscle, we performed PCR on mRNA obtained from freshly isolated vascular myocytes using laser capture microdissection. This approach demonstrated mRNA for both $\alpha1C_{9/9*/10}$ and $\alpha1C_{9/10}$ isoforms in a pure population native vascular smooth muscle. Compared to vascular tissue, we found a relatively low level of $\alpha1C_{9/9*/10}$ mRNA in heart and cerebral cortex tissue providing additional support that exon 9* is selectively expressed by smooth muscle. It is possible that apparent differences in the stoichiometry of $\alpha1C_{9/9*/10}$ and $\alpha1C_{9/10}$ splice variants may reflect discrepancies in total levels of $Ca_v1.2$ expressed between tissues. However, an earlier study by Graf et al. demonstrated that the ratio of +9*:-9* $Ca_v1.2$ is not well correlated with expression levels of total $Ca_v1.2$ (13). For example, it was shown that human cardiac ventricle and aorta express similar levels of total $Ca_v1.2$, although the +9*:-9* ratio is greater in aorta. Increased $\alpha1C_{9/9*/10}$: $\alpha1C_{9/10}$

mRNA ratio observed in vascular smooth muscle is therefore unlikely to be due to differential expression of total $Ca_v1.2$ levels compared with brain and heart.

The use of antisense oligonucleotides to specifically suppress 9*-containing $Ca_v1.2$ channels revealed a substantial decrease in K^+-induced constriction supporting a functional role for this splice variant in vascular physiology. In fact, antisense oligonucleotides targeting a region common to all $Ca_v1.2$ splice variants (exon 9) caused no greater decrease in contractility than suppression of only $\alpha1C_{9/9*/10}$. These data suggest exon 9*-containing $Ca_v1.2$ channels play a dominant role in regulating smooth muscle contraction. It should be noted that this conclusion is based on the assumptions that both antisense oligonucleotides used in this study suppress translation of their target with similar efficiency and that functional effects are not due to non-specific suppression of total $Ca_v1.2$ levels. Consistent with these assumptions, we observed a maximal response using both antisense oligonucleotides at day 4 with no greater suppression occurring after five days of treatment (data not shown). Further, the EC_{50} for $[K^+]_o$ was not altered by $\alpha1C_{9/9*/10}$-AS, consistent with a functional population of $Ca_v1.2$ channels with a uniform $V_{0.5,\ act}$. Considering the loss of endothelial function following prolonged organ culture of arteries (20), it is possible that compensatory changes in $Ca_v1.2$ splice variant expression may occur. However, we have found using RT-PCR that the ratio of $\alpha1C_{9/9*/10}$:$\alpha1C_{9/10}$ does not change following up to four days in culture (data not shown). Future studies are needed to address whether $\alpha1C_{9/9*/10}$ also plays a dominant role in vasoconstriction to endogenous compounds and physiological increases in intravascular pressure.

The unique location of exon 9* within the structure of the α_1 subunit may also play a role in post-translational regulation of VDCCs in vascular smooth muscle. Interestingly, the site of α_1/β subunit interaction, known as the alpha interaction domain is found 18 amino acids upstream of exon 9* within the I-II intracellular linker region of the α_{1c} protein. It has previously been shown that functional interaction between the α_1 and β subunit is required for correct targeting of the channel to the plasma membrane (12). It remains possible that α_1 subunits expressing exon 9* may differentially bind specific $Ca_v\beta$ isoforms compared to α_1 subunits lacking the insertion, leading to favored trafficking of $\alpha 1C_{9/9*/10}$ to the membrane and a dominant functional role for this splice variant. Further research is needed to elucidate whether the presence of exon 9* alters the binding of β subunit subtypes or splice isoforms. It should be noted that smooth muscle-selective alternatively spliced exons other than exon 9* could be preferentially expressed in 9*-containing channels and may also contribute to functional distinction of vascular smooth muscle VDCCs. For example, it has recently been shown that inclusion of exon 1c in full length cloned $Ca_v1.2$ channels can lead to a hyperpolarizing shift in $V_{0.5,act}$ in HEK293 cells, similar to inclusion of exon 9*(7).

In summary, this study suggests that the exon 9*-containing $Ca_v1.2$ splice variant controls cerebral artery myocyte Ca^{2+} influx, arterial diameter and cerebral blood flow. We propose that $\alpha 1C_{9/9*/10}$ may represent a novel target for therapeutics against vascular pathologies associated with increased Ca^{2+} influx in vascular smooth muscle leading to enhanced arterial constriction. Future genetic or pharmacological strategies targeting smooth muscle-selective $Ca_v1.2$ splice variants could provide a valuable means of

modulating vascular tone while avoiding widespread effects on VDCC isoforms in cardiac or nervous systems.

Grants

This work was supported by the Totman Medical Research Trust Fund, the Peter Martin Brain Aneurysm Endowment, National Institutes of Health Grants P20-RR-16435 and R01-HL-078983 and American Heart Association pre-doctoral fellowship award (0815736D).

Acknowledgements

We thank Drs. Joseph Brayden, Masayo Koide, Ping Liao, Victor May, Mark Nelson, Tuck Wah Soong, and Margaret Vizzard, and Ms. Kristin Schutz, Marilyn Wadsworth Theresa Wellman, and Mr. Thomm Buttolph, Colby Cantu and Edward Zelazny for helpful comments and assistance on this study. The authors also would like to acknowledge the University of Vermont Neuroscience COBRE molecular biology and Microscopy Imaging Center core facilities.

References

1. **Barillot W, Treguer K, Faucheux C, Fedou S, Theze N, and Thiebaud P.** Induction and modulation of smooth muscle differentiation in Xenopus embryonic cells. *Dev Dyn* 237: 3373-3386, 2008.
2. **Biel M, Ruth P, Bosse E, Hullin R, Stuhmer W, Flockerzi V, and Hofmann F.** Primary structure and functional expression of a high voltage activated calcium channel from rabbit lung. *FEBS Lett* 269: 409-412, 1990.
3. **Bielefeldt K.** Molecular diversity of voltage-sensitive calcium channels in smooth muscle cells. *J Lab Clin Med* 133: 469-477, 1999.
4. **Braas KM and May V.** Pituitary adenylate cyclase-activating polypeptides directly stimulate sympathetic neuron neuropeptide Y release through PAC(1) receptor isoform activation of specific intracellular signaling pathways. *The Journal of biological chemistry* 274: 27702-27710, 1999.
5. **Catterall WA.** Structure and regulation of voltage-gated Ca^{2+} channels. *Annu Rev Cell Dev Biol* 16: 521-555, 2000.
6. **Cheng X, Liu J, Asuncion-Chin M, Blaskova E, Bannister JP, Dopico AM, and Jaggar JH.** A novel Ca(V)1.2 N terminus expressed in smooth muscle cells of resistance size arteries modifies channel regulation by auxiliary subunits. *The Journal of biological chemistry* 282: 29211-29221, 2007.
7. **Cheng X, Pachuau J, Blaskova E, Asuncion-Chin M, Liu J, Dopico AM, and Jaggar JH.** Alternative splicing of $Ca_V1.2$ channel exons in smooth muscle cells of resistance-size arteries generates currents with unique electrophysiological properties. *American journal of physiology*, 2009.
8. **Dolphin AC.** Beta subunits of voltage-gated calcium channels. *J Bioenerg Biomembr* 35: 599-620, 2003.
9. **Earley S, Straub SV, and Brayden JE.** Protein kinase C regulates vascular myogenic tone through activation of TRPM4. *American journal of physiology* 292: H2613-2622, 2007.
10. **Ertel EA, Campbell KP, Harpold MM, Hofmann F, Mori Y, Perez-Reyes E, Schwartz A, Snutch TP, Tanabe T, Birnbaumer L, Tsien RW, and Catterall WA.** Nomenclature of voltage-gated calcium channels. *Neuron* 25: 533-535, 2000.
11. **Gan Q, Yoshida T, Li J, and Owens GK.** Smooth muscle cells and myofibroblasts use distinct transcriptional mechanisms for smooth muscle alpha-actin expression. *Circulation research* 101: 883-892, 2007.
12. **Gao T, Chien AJ, and Hosey MM.** Complexes of the alpha1C and beta subunits generate the necessary signal for membrane targeting of class C L-type calcium channels. *The Journal of biological chemistry* 274: 2137-2144, 1999.
13. **Graf EM, Bock M, Heubach JF, Zahanich I, Boxberger S, Richter W, Schultz JH, and Ravens U.** Tissue distribution of a human Ca_v 1.2 alpha1 subunit splice variant with a 75 bp insertion. *Cell Calcium* 38: 11-21, 2005.

14. **Hadley RW and Lederer WJ.** Properties of L-type calcium channel gating current in isolated guinea pig ventricular myocytes. *J Gen Physiol* 98: 265-285, 1991.
15. **Harder DR.** Pressure-dependent membrane depolarization in cat middle cerebral artery. *Circulation research* 55: 197-202, 1984.
16. **Hirst GD and van Helden DF.** Ionic basis of the resting potential of submucosal arterioles in the ileum of the guinea-pig. *The Journal of physiology* 333: 53-67, 1982.
17. **Hofmann F, Biel M, and Flockerzi V.** Molecular basis for Ca^{2+} channel diversity. *Annu Rev Neurosci* 17: 399-418, 1994.
18. **Ishiguro M, Puryear CB, Bisson E, Saundry CM, Nathan DJ, Russell SR, Tranmer BI, and Wellman GC.** Enhanced myogenic tone in cerebral arteries from a rabbit model of subarachnoid hemorrhage. *American journal of physiology* 283: H2217-2225, 2002.
19. **Ishiguro M, Wellman TL, Honda A, Russell SR, Tranmer BI, and Wellman GC.** Emergence of a R-type Ca^{2+} channel (Ca_V 2.3) contributes to cerebral artery constriction after subarachnoid hemorrhage. *Circulation research* 96: 419-426, 2005.
20. **Kleppisch T, Winter B, and Nelson MT.** ATP-sensitive potassium channels in cultured arterial segments. *The American journal of physiology* 271: H2462-2468, 1996.
21. **Knot HJ and Nelson MT.** Regulation of arterial diameter and wall [Ca^{2+}] in cerebral arteries of rat by membrane potential and intravascular pressure. *The Journal of physiology* 508 (Pt 1): 199-209, 1998.
22. **Koch WJ, Ellinor PT, and Schwartz A.** cDNA cloning of a dihydropyridine-sensitive calcium channel from rat aorta. Evidence for the existence of alternatively spliced forms. *The Journal of biological chemistry* 265: 17786-17791, 1990.
23. **Koide M, Penar PL, Tranmer BI, and Wellman GC.** Heparin-binding EGF-like growth factor mediates oxyhemoglobin-induced suppression of voltage-dependent potassium channels in rabbit cerebral artery myocytes. *American journal of physiology* 293: H1750-1759, 2007.
24. **Lacerda AE, Kim HS, Ruth P, Perez-Reyes E, Flockerzi V, Hofmann F, Birnbaumer L, and Brown AM.** Normalization of current kinetics by interaction between the alpha 1 and beta subunits of the skeletal muscle dihydropyridine-sensitive Ca^{2+} channel. *Nature* 352: 527-530, 1991.
25. **Lesh RE, Somlyo AP, Owens GK, and Somlyo AV.** Reversible permeabilization. A novel technique for the intracellular introduction of antisense oligodeoxynucleotides into intact smooth muscle. *Circulation research* 77: 220-230, 1995.
26. **Liao P, Yu D, Lu S, Tang Z, Liang MC, Zeng S, Lin W, and Soong TW.** Smooth muscle-selective alternatively spliced exon generates functional variation in $Ca_v1.2$ calcium channels. *The Journal of biological chemistry* 279: 50329-50335, 2004.
27. **Link TE, Murakami K, Beem-Miller M, Tranmer BI, and Wellman GC.** Oxyhemoglobin-induced expression of R-type Ca^{2+} channels in cerebral arteries. *Stroke; a journal of cerebral circulation* 39: 2122-2128, 2008.

28. **Mikami A, Imoto K, Tanabe T, Niidome T, Mori Y, Takeshima H, Narumiya S, and Numa S.** Primary structure and functional expression of the cardiac dihydropyridine-sensitive calcium channel. *Nature* 340: 230-233, 1989.
29. **Neild TO and Keef K.** Measurements of the membrane potential of arterial smooth muscle in anesthetized animals and its relationship to changes in artery diameter. *Microvasc Res* 30: 19-28, 1985.
30. **Nelson MT, Standen NB, Brayden JE, and Worley JF, 3rd.** Noradrenaline contracts arteries by activating voltage-dependent calcium channels. *Nature* 336: 382-385, 1988.
31. **Rhee SW, Stimers JR, Wang W, and Pang L.** Vascular smooth muscle-specific knockdown of the noncardiac form of the L-type calcium channel by microRNA-based short hairpin RNA as a potential antihypertensive therapy. *J Pharmacol Exp Ther* 329: 775-782, 2009.
32. **Soldatov NM.** Molecular diversity of L-type Ca^{2+} channel transcripts in human fibroblasts. *Proc Natl Acad Sci U S A* 89: 4628-4632, 1992.
33. **Strutz F, Okada H, Lo CW, Danoff T, Carone RL, Tomaszewski JE, and Neilson EG.** Identification and characterization of a fibroblast marker: FSP1. *The Journal of cell biology* 130: 393-405, 1995.
34. **Tang ZZ, Liang MC, Lu S, Yu D, Yu CY, Yue DT, and Soong TW.** Transcript scanning reveals novel and extensive splice variations in human l-type voltage-gated calcium channel, $Ca_v1.2$ alpha1 subunit. *The Journal of biological chemistry* 279: 44335-44343, 2004.
35. **Triggle DJ.** Calcium-channel drugs: structure-function relationships and selectivity of action. *J Cardiovasc Pharmacol* 18 Suppl 10: S1-6, 1991.
36. **Welling A, Ludwig A, Zimmer S, Klugbauer N, Flockerzi V, and Hofmann F.** Alternatively spliced IS6 segments of the alpha 1C gene determine the tissue-specific dihydropyridine sensitivity of cardiac and vascular smooth muscle L-type Ca^{2+} channels. *Circulation research* 81: 526-532, 1997.
37. **Wellman GC, Nathan DJ, Saundry CM, Perez G, Bonev AD, Penar PL, Tranmer BI, and Nelson MT.** Ca^{2+} sparks and their function in human cerebral arteries. *Stroke; a journal of cerebral circulation* 33: 802-808, 2002.
38. **Wu BN, Luykenaar KD, Brayden JE, Giles WR, Corteling RL, Wiehler WB, and Welsh DG.** Hyposmotic challenge inhibits inward rectifying K^+ channels in cerebral arterial smooth muscle cells. *American journal of physiology* 292: H1085-1094, 2007.
39. **Zuber MX, Goodman DW, Karns LR, and Fishman MC.** The neuronal growth-associated protein GAP-43 induces filopodia in non-neuronal cells. *Science (New York, NY* 244: 1193-1195, 1989.

Figure Legends

Figure 1: Cerebral arteries express $\alpha 1C_{9/9*/10}$. ***A***: PCR primer design for the detection of $\alpha 1C_{9/9*/10}$ and $\alpha 1C_{9/10}$. Amplification of transcripts containing exon 9* results in 535 nt product while amplification of transcripts excluding exon 9* results in 460 nt product. ***B***: Representative gel demonstrating two bands corresponding to both $\alpha 1C_{9/9*/10}$ and $\alpha 1C_{9/10}$ present in whole cerebral arteries (n=7) while $\alpha 1C_{9/10}$ band is most prominent in brain (n=5) and heart tissue (n=8). ***C***: Resulting RT-PCR gel using cDNA obtained from whole cerebral arteries from human (n=2) demonstrates presence of two bands corresponding to $\alpha 1C_{9/9*/10}$ and $\alpha 1C_{9/10}$.

Figure 2: Quantitative real-time PCR (qPCR) shows high expression of $\alpha 1C_{9/9*/10}$ in cerebral arteries. ***A***: PCR primer sets for the specific detection of $\alpha 1C_{9/9*/10}$ and $\alpha 1C_{9/10}$. $\alpha 1C_{9/9*/10}$ specific (left) forward primer recognizes sequence specific to exon 9*. $\alpha 1C_{9/10}$ (right) forward primer recognizes sequence of boundary between exons 9 and 10. Sequence analysis of PCR products confirmed specificity of primers for target sequences. ***B***: Summary qPCR data for cerebral arteries, brain (cortex) and heart (left ventricle). The ratio of $\alpha 1C_{9/9*/10}$:$\alpha 1C_{9/10}$ mRNA was significantly greater in cerebral arteries relative to brain and heart (0.289 ± 0.024; n=7 compared to 0.006 ± 0.001; n=4 and 0.050 ± 0.006; n=8, respectively). $^{**}p<0.01$ vs. brain and heart.

Figure 3: Cerebral artery myocytes express both $\alpha 1C_{9/9*/10}$ and $\alpha 1C_{9/10}$ splice variants. ***A***: Immunostaining of isolated cerebral artery myocytes. Red: SM-MHC; Green: SM-α-actin (color changed from red to green to distinguish from SM-MHC); Blue: DAPI nuclear stain. Scale bars represent 10 μm. A lack of staining was observed for SM-MHC or SM-α-actin by cells incubated without primary antibody (right panel). ***B***: Microdissection of isolated cerebral artery myocytes. Live myocytes plated on P.A.L.M. Duplex dish (Ziess) were identified by cell morphology and the surrounding dish membrane was cut (i.). Myocytes were then catapulted (ii.) onto P.A.L.M. Adhesivecap collection tubes (Ziess) for mRNA extraction. Scale bars represent 25 μm. ***C***: Representative gel showing the presence of cell markers: smooth muscle myosin heavy chain (SM-MHC; smooth muscle), endothelin-1 (ET-1; endothelium), fibroblast specific protein-1 (FSP-1; fibroblast) and growth associated protein-43 (GAP43; neuronal). All markers are amplified using cDNA from whole cerebral arteries. cDNA from cerebral artery myocytes samples collected by laser capture microdissection demonstrate amplification of SM-MHC while other markers were not detected. ***D***: Results of nested PCR performed on cDNA from isolated cerebral artery myocytes. First round of amplification (35 cycles) was performed using primers for exons 7-11 of $Ca_v1.2$ (see Fig. 1A). Second round of amplification (35 cycles) was done using nested primers (see methods) and 1:100 dilution of first-round PCR products. Final products represent expression of $\alpha 1C_{9/9*/10}$ (upper band) and $\alpha 1C_{9/10}$ (lower band) (n=5).

Figure 4: Selective suppression of $Ca_v1.2$ splice variants following antisense treatment and organ culture for four days. ***A***: RT-PCR was performed on cDNA from arteries treated with $\alpha1C_{9/9*/10}$-AS, α1C-AS, and corresponding sense oligonucleotides. Band intensity corresponding to $\alpha1C_{9/9*/10}$ was reduced in $\alpha1C_{9/9*/10}$-AS treated artery samples following four days in organ culture compared with sense treated arteries (left, n=4). Lower band, corresponding to $\alpha1C_{9/10}$, was similar between two groups. RT-PCR gel demonstrating reduction in both $\alpha1C_{9/9*/10}$ and $\alpha1C_{9/10}$ band intensity following treatment with α1C-AS and organ culture for 4 days (right, n=4). Total RNA used was similar as shown by endogenous control 18S ribosomal RNA. ***B***: Quantification of changes in mRNA levels using qPCR in antisense-treated arteries compared with sense treated arteries from same animal. *$p<0.05$ ($\alpha1C_{9/9*/10}$-AS/S: n=4; α1C-AS/S: n=4).

Figure 5: Representative arterial diameter traces demonstrating important functional role for $\alpha1C_{9/9*/10}$ in arterial constriction. All arteries were cannulated, pressurized to 20 mmHg and perfused with PSS for 30 minutes prior to stepwise increases in $[K^+]_o$. Control freshly isolated and sense treated (day 4) arteries responded to increases in $[K^+]_o$ by graded constriction. $\alpha1C_{9/9*/10}$-AS treated (day 4) arteries exhibited a marked reduction in $[K^+]_o$-induced constriction. Ionomycin (10 μM) was applied at the end of each experiment.

Figure 6: Time course for $\alpha1C_{9/9*/10}$-AS effect. ***Day 1***: $\alpha1C_{9/9*/10}$-AS, $\alpha1C_{9/9*/10}$-sense treated ($\alpha1C_{9/9*/10}$-S), and RP arteries exhibit constriction similar to freshly isolated

cerebral arteries (day 0). ***Day 2-4***: $\alpha 1C_{9/9*/10}$-AS arteries exhibit significantly reduced arterial constriction in response to increased $[K^+]_o$ with constrictions nearly abolished following four days in organ culture compared with $\alpha 1C_{9/9*/10}$-sense and RP arteries organ cultured for the same period of time. *p<.05, **p<.01. No significant differences were observed in arterial constriction between $\alpha 1C_{9/9*/10}$-sense treated artery groups (days 1-4, n=4-5) and freshly isolated arteries (day 0, n=5). * p<0.05; **p<0.01.

Figure 7: $\alpha 1C_{9/9*/10}$ plays a dominant role in cerebral artery constriction. ***A***: Representative diameter traces showing response to 60 mM $[K^+]_o$ followed by application of 10 μM ionomycin. ***B***: Summary of 60 mM $[K^+]_o$ for antisense-treated arteries. All constrictions were normalized to minimum diameter obtained in ionomycinand maximum diameter obtained in Ca^{2+}-free PSS with diltiazem (100 μM) and forskolin (1 μM). After four days in organ culture following oligonucleotide treatment, arteries treated with α1C-AS exhibited similar response to 60 mM $[K^+]_o$ as arteries treated with $\alpha 1C_{9/9*/10}$-AS. $\alpha 1C_{9/9*/10}$-AS and α1C-AS groups were significantly decreased compared with corresponding sense-treated groups. No significant difference was observed between $\alpha 1C_{9/9*/10}$-AS and α1C-AS groups (*p<0.05; $\alpha 1C_{9/9*/10}$-sense, n=4; $\alpha 1C_{9/9*/10}$-AS, n=6; α1C-sense, n=5; α1C-AS, n=5).

Table 1: Diameter values are shown for $\alpha 1C_{9/9*/10}$-AS, $\alpha 1C_{9/9*/10}$-S, and RP arteries in PSS (6 mM $[K^+]_o$), 80 mM $[K^+]_o$, and 120 mM $[K^+]_o$ containing 10 μM ionomycin (ionomycin group) for all time points tested. Also shown is ionomycin constriction,

expressed as % decrease from maximum diameter and EC_{50} values calculated from $[K^+]_o$ concentration-response curves. *p<0.05, **p<0.05 vs. $\alpha 1C_{9/9*/10}$-sense and RP groups.

Figures

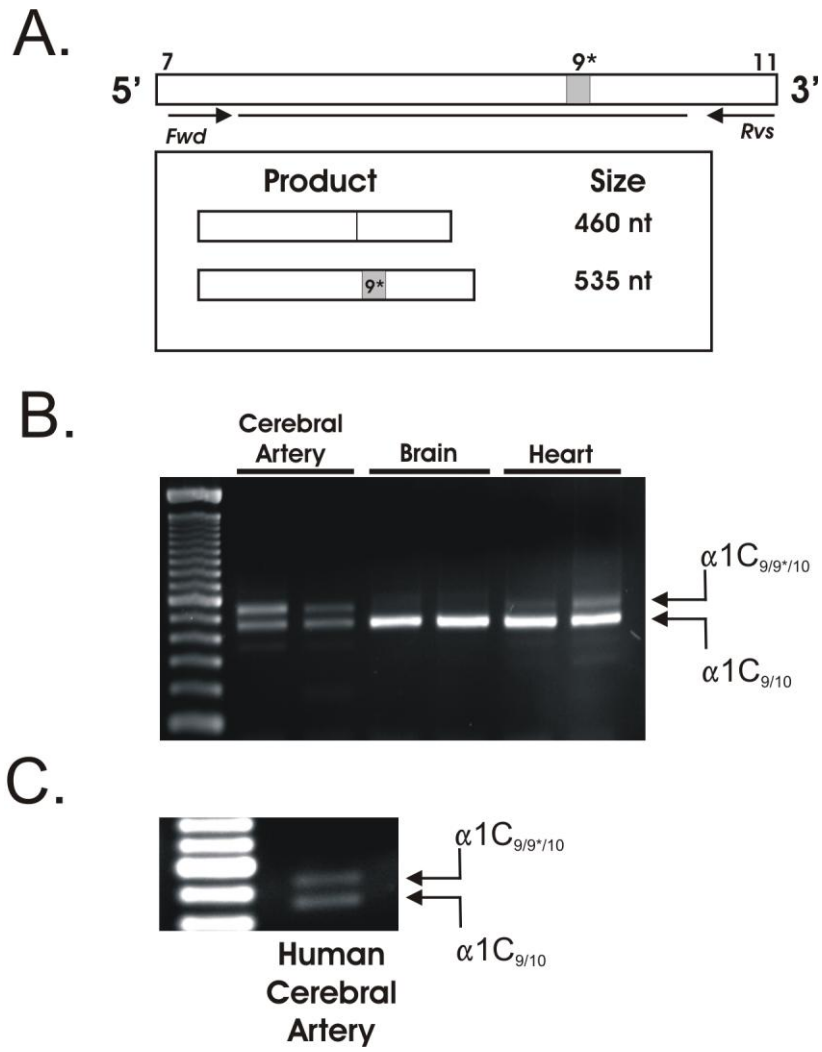

Figure 1: ***Cerebral arteries express exon 9*.***

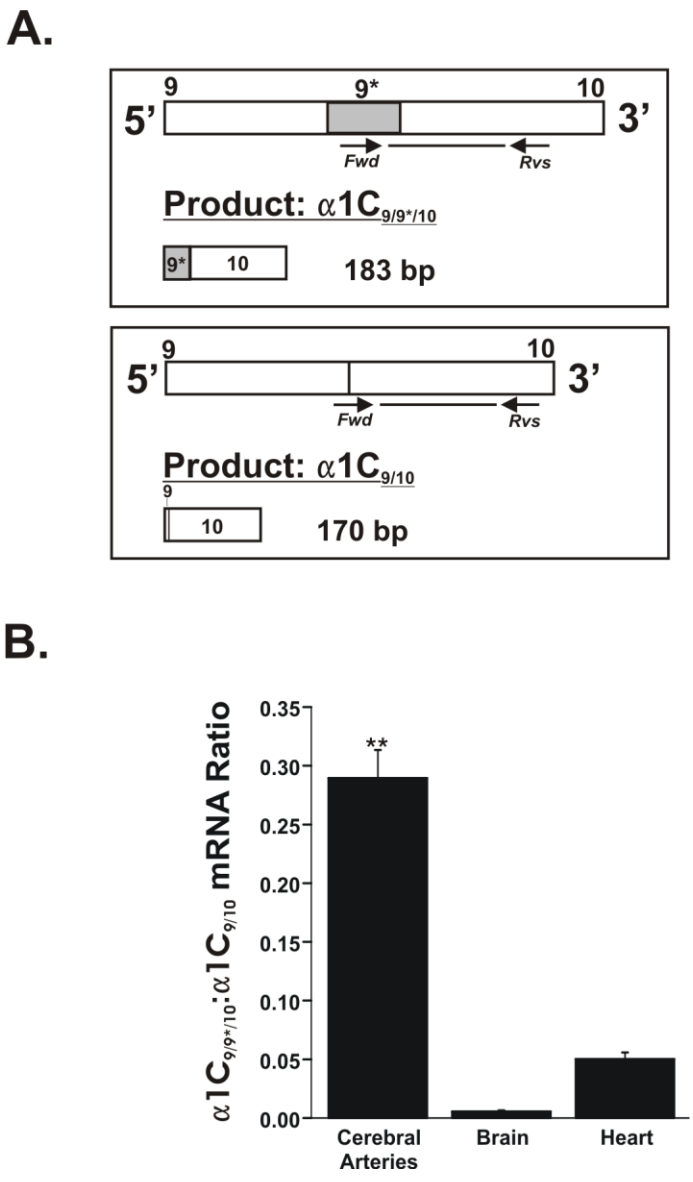

Figure 2: ***Selective expression of exon 9* in cerebral arteries.***

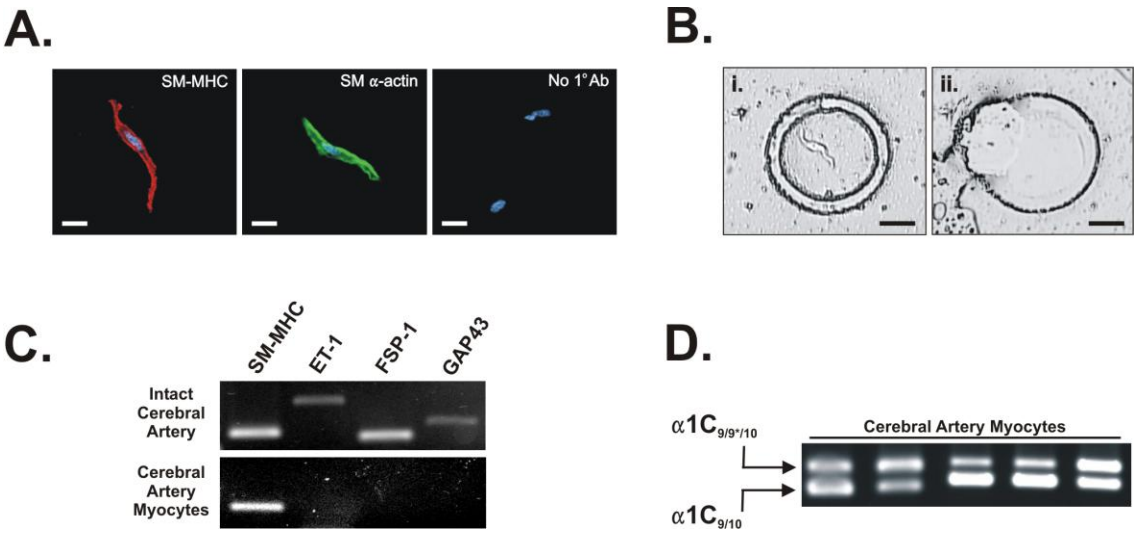

Figure 3: ***Cerebral artery myocytes express mixed population of $Ca_V1.2$ splice variants.***

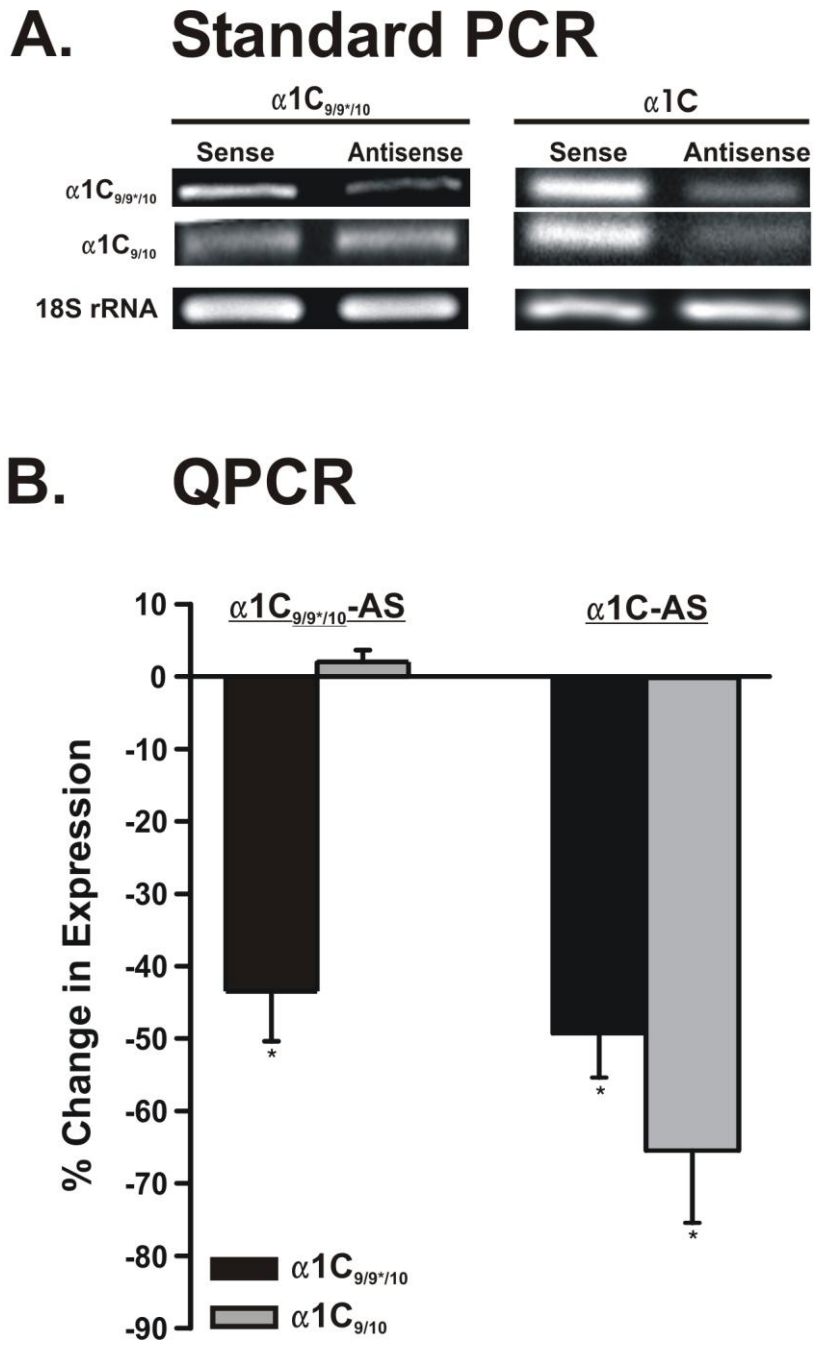

Figure 4: ***Selective suppression of $Ca_V1.2$ splice variants.***

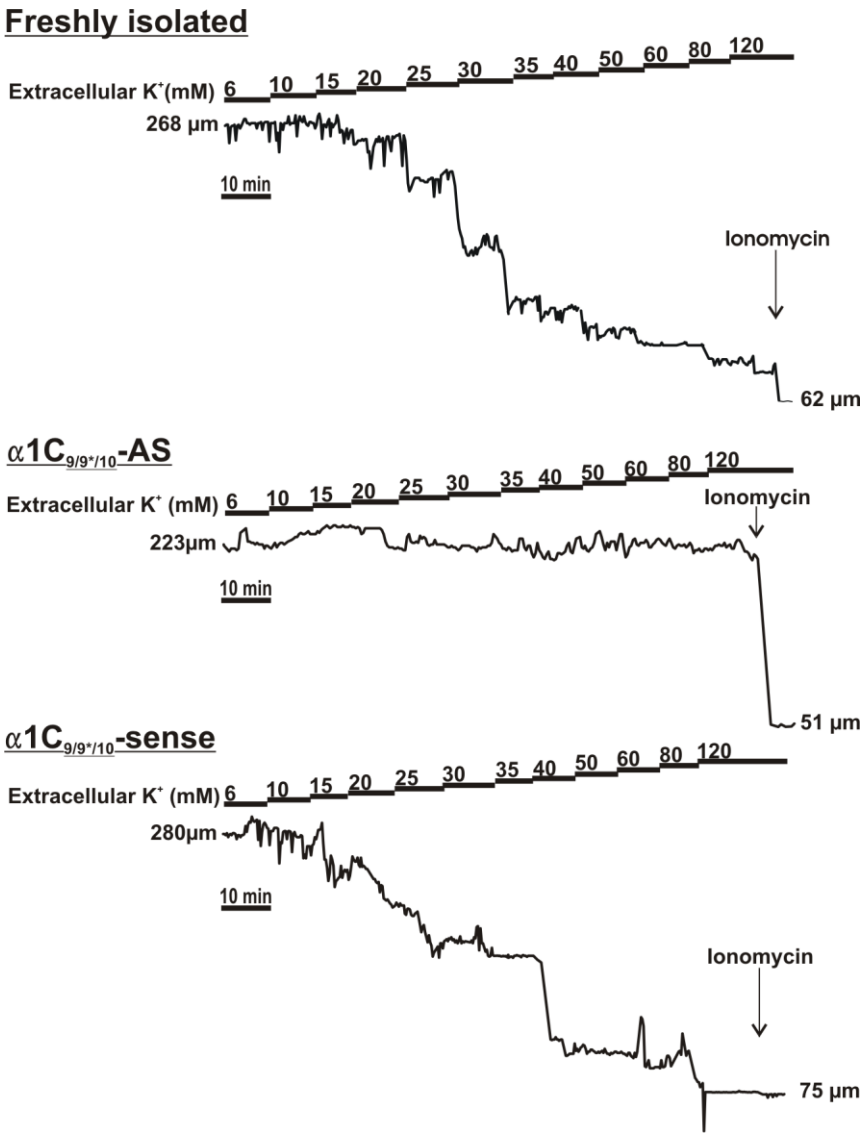

Figure 5: ***Representative constriction in response to increasing extracellular K^+.***

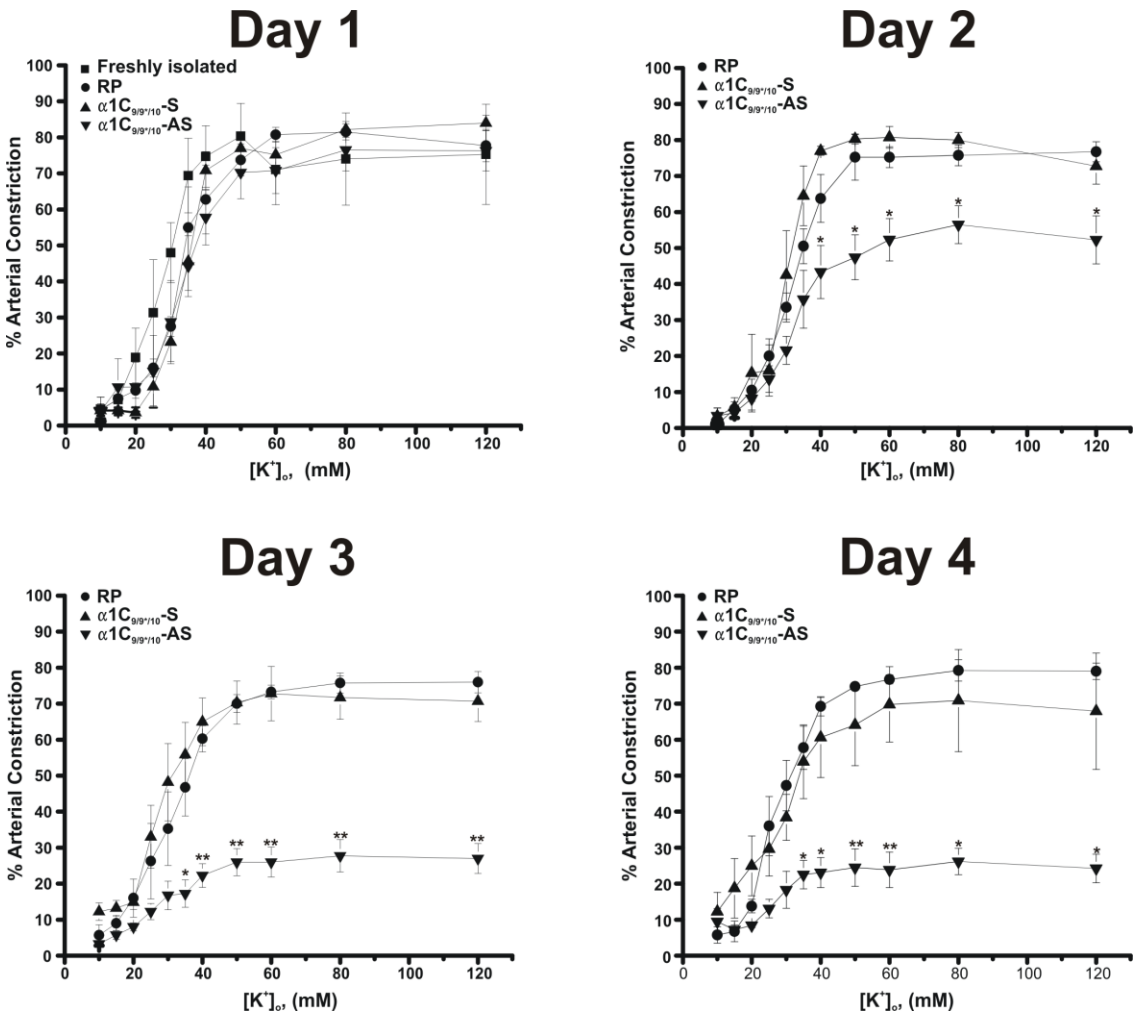

Figure 6: ***Time course for exon 9*-antisense effect.***

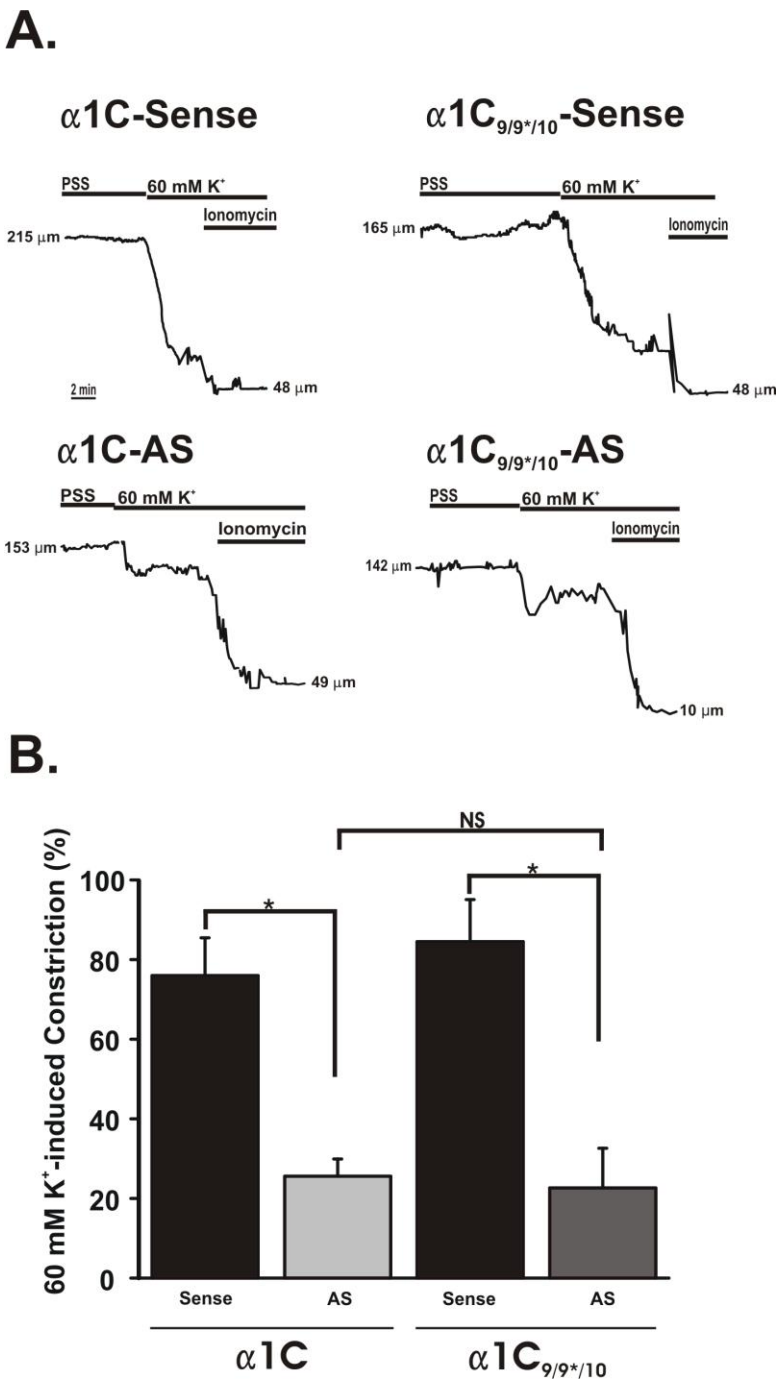

Figure 7: ***Exon 9* plays a dominant role in cerebral artery constriction.***

Table 1: ***Diameter values for K^+ concentration-response experiments.***

	RP	α1C$_{9/9*/10}$-Sense	α1C$_{9/9*/10}$-AS
Day 1			
Diameter (μm)			
6 mM $[K^+]_o$	170 ± 27.8	186 ± 18.7	182 ± 21.8
80 mM $[K^+]_o$	62 ± 16.1	66 ± 9.2	63 ± 7.6
Ionomycin	37 ± 13.1	37 ± 7.5	29 ± 2.6
Ionomycin-induced Constriction (% of maximum diameter)	81 ± 4.	80 ± 3.1	85 ± 2.7
$[K^+]_o$ EC_{50}	35 ± 3.5	4 ± 1.2	34 ± 2.3
Day 2			
Diameter			
6 mM $[K^+]_o$	194 ± 28.2	217 ± 34.7	165 ± 25.5
80 mM $[K^+]_o$	85 ± 11.7	87 ± 23.0	87 ± 12.5
Ionomycin	53 ± 9.7	49 ± 16.4	31 ± 5.6
Ionomycin-induced Constriction (% of maximum diameter)	72 ± 5.2	80 ± 3.7	83 ± 2.7
$[K^+]_o$ EC_{50}	32 ± 7.4	31 ± 1.3	33 ± 2.0
Day 3			
Diameter			
6 mM $[K^+]_o$	201 ± 20.4	216 ± 50.7	194 ± 13.0
80 mM $[K^+]_o$	81 ± 10.3	89 ± 14.3	149 ± 13.0**
Ionomycin	42 ± 11.4	51 ± 15.5	45 ± 8.9
Ionomycin-induced Constriction (% of maximum diameter)	80 ± 4.1	86 ± 3.4	81 ± 3.4
$[K^+]_o$ EC_{50}	31 ± 3.0	30 ± 2.1	32 ± 3.0
Day 4			
Diameter			
6 mM $[K^+]_o$	230 ± 25.5	205 ± 42.0	188 ± 4.6
80 mM $[K^+]_o$	78 ± 12.1	89 ± 14.3	155 ± 20.3**
Ionomycin	37 ± 12.7	51 ± 15.5	50 ± 15.3
Ionomycin-induced Constriction (% of maximum diameter)	85 ± 4.9	75 ± 6.9	73 ± 3.0
$[K^+]_o$ EC_{50}	33 ± 2.3	31 ± 2.3	30 ± 2.8

** $p < 0.05$ vs. sense and RP groups.

CHAPTER 4: CONCLUSIONS AND FUTURE DIRECTIONS

In Chapter one of this dissertation, it is demonstrated that constriction of parenchymal arterioles are markedly enhanced following SAH at physiological intravascular pressures. Evidence is provided suggesting that enhanced constriction results from greater pressure-dependent depolarization of parenchymal arteriolar myocytes, increased activity of L-type VDCCs and elevated $[Ca^{2+}]_i$. One major aim of future work will address the mechanisms by which SAH causes membrane potential depolarization of parenchymal arteriolar myocytes. As discussed in Chapter 2, this may result from increased activity of ion channels involved in pressure-dependent depolarization (i.e. transient receptor potential channels) or decreased activity of negative feedback pathways controlling vascular tone (i.e. K^+ efflux). Importantly, whether altered parenchymal arteriolar function results from exposure to spasmogens within blood, or vasoactive substances released from the brain parenchyma following SAH should also be addressed. For example, studies have demonstrated that intracisternally injected biotinylated oxyhemoglobin is capable of penetrating to deeper layers of the cortex of the rat (Turner et al., 1998) suggesting that parenchymal arterioles may be exposed to this spasmogen following erythrocyte lysis in SAH patients. Oxyhemoglobin has been shown to cause membrane potential depolarization of cerebral artery myocytes via reduction of Ca^{2+} spark frequency (Jewell et al., 2004; Koide, 2009) and suppression of K_V channel currents (Ishiguro et al., 2006; Koide et al., 2007). In addition, purified oxyhemoglobin was shown to induce expression of R-type VDCCs ($Ca_V2.3$) in rabbit pial cerebral artery myocytes (Link et al., 2008). Although we did not test whether $Ca_V2.3$ is expressed in parenchymal arteriolar myocytes following SAH, our data demonstrating similar $[Ca^{2+}]_i$

and tone in the presence of the L-type VDCC inhibitor nimodipine argue against a significant contribution of R-type channels in parenchymal vessels from SAH animals. These differing results may reflect variation between species or vascular beds with respect to environment and functional regulation.

Previous studies suggest that parenchymal arterioles contribute significantly to cerebrovascular resistance and autoregulation of cerebral blood flow (Faraci and Heistad, 1990; Harper et al., 1984). The relative contributions of large diameter vasospasm and enhanced constriction of parenchymal vessels to ischemia-related deficits in SAH patients remains unclear. It is plausible that in the absence of microcirculatory dysfunction, constriction of large diameter surface vessels following SAH may cause little reduction in regional perfusion due to compensatory redistribution of blood flow in downstream vessels (Schaffer et al., 2006). Conversely, a significant reduction in cortical blood flow and focal neuronal infarction may follow SAH-induced constriction of parenchymal arterioles, which display little communication with parallel arterioles and represent a bottleneck in blood supply to the cortex (Nishimura et al., 2007). Hence, enhanced pressure-dependent constriction of parenchymal arterioles may severely limit downstream blood flow and lead to significant neuronal damage after SAH.

In addition to their function in regulating global cerebral blood flow, parenchymal arterioles are also an essential component of the neurovascular unit which functions to couple blood flow with local neuronal activity and metabolic demands. Under normal physiological conditions, an increase in local neuronal activity signals release of vasodilatory substances from the astrocytic endfeet to cause vasodilation and increased

local blood flow (Iadecola and Nedergaard, 2007). This process is critical for sufficient delivery of oxygen and nutrients to active regions of the brain. Given the impact of blood on the function of arterioles deep within the cortex of SAH model animals shown in this study, future work should address the impact of SAH on neurovascular coupling mechanisms. Brain slice experiments have suggested that the magnitude and polarity of diameter change to increases in neuronal activity are dependent on the level of vascular tone (Blanco et al., 2008). For example, arterioles displaying greater myogenic tone exhibit more pronounced dilations in response to electrical field stimulation (neuronal activation). Thus, enhanced arteriolar tone following SAH may be localized to less active brain regions in vivo if functional hyperemic phenomena remain unaltered. However, studies in our laboratory have found a fundamental change in the neurovascular response in brain slices from SAH model rats. Whereas electrical field stimulation activates neurons and evokes parenchymal arteriolar dilation in brain slices from control animals, similar stimulation causes constriction in brain slices from SAH animals (Koide and Wellman, unpublished observations). These findings indicate that SAH causes a remarkable shift in the polarity of vascular response from dilation to constriction following increased neuronal activity. Therefore, impairment of mechanisms coupling neuronal activity with localized increases in blood flow may act in concert with enhanced pressure-dependent constriction to severely limit local cerebral blood flow following SAH. These findings suggest that neuronal infarction may be more severe in active brain regions in SAH patients.

Enhanced parenchymal arteriolar constriction following SAH requires extracellular Ca^{2+} entry via smooth muscle L-type VDCCs. Antagonists of L-type VDCCs are standard therapy for prevention of cerebral vasospasm and neurological deficits in SAH patients. Although nimodipine treatment has been indicated to reduce the severity of ischemic deficits (Tomassoni et al., 2008; Treggiari-Venzi et al., 2001), these positive effects do not depend on reversal or prevention of angiographic vasospasm (Petruk et al., 1988). Alternatively, consistent with our data is the hypothesis that nimodipine may increase blood flow to ischemic brain regions by preferential dilation of small diameter resistance arteries and arterioles. However, systemic nimodipine administration also inhibits smooth muscle VDCCs in the peripheral vasculature and use of this agent in SAH patients has been limited by hypotension (Treggiari-Venzi et al., 2001). Therefore, it is clear that future efforts should focus on improving strategies to suppress L-type VDCC activity in both pial and parenchymal myocytes, while avoiding effects on systemic targets.

L-type channels in the vasculature represent a mixed population of splice variations of the gene $Ca_V1.2$ (Cheng et al., 2009). In Chapter three of this dissertation, data is shown supporting an essential role for $Ca_V1.2$ containing the alternatively-spliced, smooth muscle-selective exon 9* ($\alpha1C_{9/9*/10}$) in cerebral artery constriction. In this study, antisense oligonucleotides and organ culture were used to specifically reduce the expression of exon 9* channels in myocytes of small diameter pial arteries. Following suppression of this splice variant, we observed dramatically reduced cerebral artery constriction to K^+-induced depolarization in vitro. We conclude that $\alpha1C_{9/9*/10}$ is the

major route of Ca^{2+} entry required for cerebral artery constriction resulting from membrane depolarization. Future experiments will aim to transfer this strategy of suppressing cerebrovascular VDCCs into the live animal. Information gained from this work will not only test the feasibility of reducing VDCC expression in vivo, but may also lead to new information regarding the function of VDCC splice variants in the control of cerebral blood flow. Preliminary RT-PCR experiments have revealed similar expression profile of $\alpha 1C_{9/9*/10}$ and $\alpha 1C_{9/10}$ splice variants in rat pial and parenchymal arterioles (Figure 1). Therefore, we hypothesize that suppression of $\alpha 1C_{9/9*/10}$ channels in the cerebral vasculature will lead to significantly increased cerebral blood flow.

In summary, it is clear that long-term exposure of tissues within the central nervous system to whole blood causes a myriad of changes in multiple cell types. While some of these effects may be beneficial, most are detrimental to neuronal viability. As whole blood is a complex mixture of vasoactive substances, delayed neurological deficits in patients surviving aneurysm rupture caused by enhanced cerebral artery constriction are likely to result from a complex combination of factors. In this dissertation, data is presented in support of increased Ca^{2+} influx via L-type VDCCs as a major cause of enhanced constriction of parenchymal arterioles following SAH. In addition, smooth muscle-selective L-type VDCC splice variants may represent a novel target for the prevention of delayed neurological deficits in SAH patients.

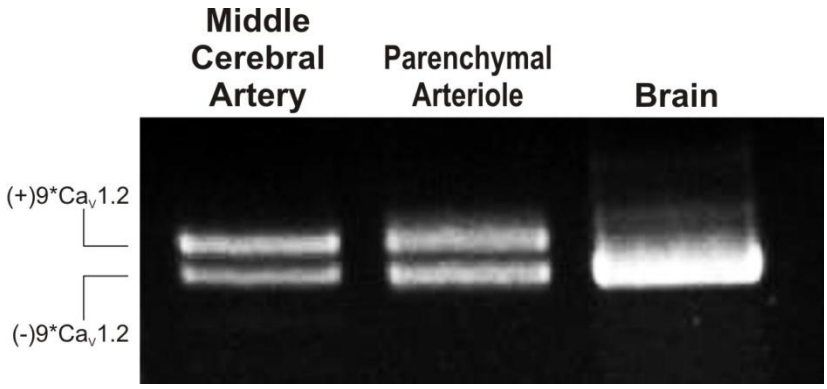

Figure 1: ***Similar expression of Ca_V1.2 splice variants in pial and parenchymal vasculature.***

RT-PCR gel demonstrating expression of Ca_V1.2 splice variants containing and lacking exon 9* ((+)9*Ca_V1.2 and (-)9*Ca_V1.2, respectively). Similar expression of both splice variants was observed in both pial and parenchymal arterioles from rat. Conversely, rat brain expressed only (-) 9*Ca_V1.2 splice variants.

COMPREHENSIVE BIBLIOGRAPHY

(1992). Effect of calcitonin-gene-related peptide in patients with delayed postoperative cerebral ischaemia after aneurysmal subarachnoid haemorrhage. European CGRP in Subarachnoid Haemorrhage Study Group. Lancet *339*, 831-834.

Afshar, J.K., Pluta, R.M., Boock, R.J., Thompson, B.G., and Oldfield, E.H. (1995). Effect of intracarotid nitric oxide on primate cerebral vasospasm after subarachnoid hemorrhage. J Neurosurg *83*, 118-122.

Aiello, E.A., Clement-Chomienne, O., Sontag, D.P., Walsh, M.P., and Cole, W.C. (1996). Protein kinase C inhibits delayed rectifier K^+ current in rabbit vascular smooth muscle cells. Am J Physiol *271*, H109-119.

Aiello, E.A., Walsh, M.P., and Cole, W.C. (1995). Phosphorylation by protein kinase A enhances delayed rectifier K^+ current in rabbit vascular smooth muscle cells. Am J Physiol *268*, H926-934.

Aihara, Y., Jahromi, B.S., Yassari, R., Nikitina, E., Agbaje-Williams, M., and Macdonald, R.L. (2004). Molecular profile of vascular ion channels after experimental subarachnoid hemorrhage. J Cereb Blood Flow Metab *24*, 75-83.

Albarwani, S., Nemetz, L.T., Madden, J.A., Tobin, A.A., England, S.K., Pratt, P.F., and Rusch, N.J. (2003). Voltage-gated K^+ channels in rat small cerebral arteries: molecular identity of the functional channels. J Physiol *551*, 751-763.

Alonso-Galicia, M., Drummond, H.A., Reddy, K.K., Falck, J.R., and Roman, R.J. (1997). Inhibition of 20-HETE production contributes to the vascular responses to nitric oxide. Hypertension *29*, 320-325.

Amberg, G.C., and Santana, L.F. (2003). Downregulation of the BK channel beta1 subunit in genetic hypertension. Circ Res *93*, 965-971.

Arai, H., Hori, S., Aramori, I., Ohkubo, H., and Nakanishi, S. (1990). Cloning and expression of a cDNA encoding an endothelin receptor. Nature *348*, 730-732.

Armstead, W.M. (1996). Role of ATP-sensitive K^+ channels in cGMP-mediated pial artery vasodilation. Am J Physiol *270*, H423-426.

Armstead, W.M. (1997). Role of nitric oxide, cyclic nucleotides, and the activation of ATP-sensitive K^+ channels in the contribution of adenosine to hypoxia-induced pial artery dilation. J Cereb Blood Flow Metab *17*, 100-108.

Armstead, W.M. (1999). Endothelin-1 contributes to normocapnic hyperoxic pial artery vasoconstriction. Brain Res *842*, 252-255.

Ayata, C., Ma, J., Meng, W., Huang, P., and Moskowitz, M.A. (1996). L-NA-sensitive rCBF augmentation during vibrissal stimulation in type III nitric oxide synthase mutant mice. J Cereb Blood Flow Metab *16*, 539-541.

Babenko, A.P., Aguilar-Bryan, L., and Bryan, J. (1998). A view of sur/K_{IR}6.X, K_{ATP} channels. Annu Rev Physiol *60*, 667-687.

Bannister, J.P., Adebiyi, A., Zhao, G., Narayanan, D., Thomas, C.M., Feng, J.Y., and Jaggar, J.H. (2009). Smooth muscle cell alpha2delta-1 subunits are essential for vasoregulation by $Ca_V1.2$ channels. Circ Res *105*, 948-955.

Barillot, W., Treguer, K., Faucheux, C., Fedou, S., Theze, N., and Thiebaud, P. (2008). Induction and modulation of smooth muscle differentiation in Xenopus embryonic cells. Dev Dyn *237*, 3373-3386.

Bayliss, W.M. (1902). On the local reactions of the arterial wall to changes of internal pressure. J Physiol *28*, 220-231.

Bederson, J.B., Connolly, E.S., Jr., Batjer, H.H., Dacey, R.G., Dion, J.E., Diringer, M.N., Duldner, J.E., Jr., Harbaugh, R.E., Patel, A.B., and Rosenwasser, R.H. (2009). Guidelines for the management of aneurysmal subarachnoid hemorrhage: a statement for healthcare professionals from a special writing group of the Stroke Council, American Heart Association. Stroke *40*, 994-1025.

Benham, C.D., and Bolton, T.B. (1986). Spontaneous transient outward currents in single visceral and vascular smooth muscle cells of the rabbit. J Physiol *381*, 385-406.

Berra-Romani, R., Mazzocco-Spezzia, A., Pulina, M.V., and Golovina, V.A. (2008). Ca^{2+} handling is altered when arterial myocytes progress from a contractile to a proliferative phenotype in culture. Am J Physiol Cell Physiol *295*, C779-790.

Bian, F., Li, Z., Offord, J., Davis, M.D., McCormick, J., Taylor, C.P., and Walker, L.C. (2006). Calcium channel alpha2-delta type 1 subunit is the major binding protein for pregabalin in neocortex, hippocampus, amygdala, and spinal cord: an ex vivo autoradiographic study in alpha2-delta type 1 genetically modified mice. Brain Res *1075*, 68-80.

Biel, M., Ruth, P., Bosse, E., Hullin, R., Stuhmer, W., Flockerzi, V., and Hofmann, F. (1990). Primary structure and functional expression of a high voltage activated calcium channel from rabbit lung. FEBS Lett *269*, 409-412.

Bielefeldt, K. (1999). Molecular diversity of voltage-sensitive calcium channels in smooth muscle cells. J Lab Clin Med *133*, 469-477.

Biondi, A., Ricciardi, G.K., Puybasset, L., Abdennour, L., Longo, M., Chiras, J., and Van Effenterre, R. (2004). Intra-arterial nimodipine for the treatment of symptomatic cerebral vasospasm after aneurysmal subarachnoid hemorrhage: preliminary results. AJNR Am J Neuroradiol *25*, 1067-1076.

Blanco, V.M., Stern, J.E., and Filosa, J.A. (2008). Tone-dependent vascular responses to astrocyte-derived signals. Am J Physiol Heart Circ Physiol *294*, H2855-2863.

Blaustein, M.P., and Lederer, W.J. (1999). Sodium/calcium exchange: its physiological implications. Physiol Rev *79*, 763-854.

Bogatcheva, N.V., Sergeeva, M.G., Dudek, S.M., and Verin, A.D. (2005). Arachidonic acid cascade in endothelial pathobiology. Microvasc Res *69*, 107-127.

Bonev, A.D., Jaggar, J.H., Rubart, M., and Nelson, M.T. (1997). Activators of protein kinase C decrease Ca^{2+} spark frequency in smooth muscle cells from cerebral arteries. Am J Physiol *273*, C2090-2095.

Braas, K.M., and May, V. (1999). Pituitary adenylate cyclase-activating polypeptides directly stimulate sympathetic neuron neuropeptide Y release through PAC(1) receptor isoform activation of specific intracellular signaling pathways. The Journal of biological chemistry *274*, 27702-27710.

Brayden, J.E., Earley, S., Nelson, M.T., and Reading, S. (2008). Transient receptor potential (TRP) channels, vascular tone and autoregulation of cerebral blood flow. Clin Exp Pharmacol Physiol *35*, 1116-1120.

Brayden, J.E., and Wellman, G.C. (1989). Endothelium-dependent dilation of feline cerebral arteries: role of membrane potential and cyclic nucleotides. J Cereb Blood Flow Metab *9*, 256-263.

Brenner, R., Perez, G.J., Bonev, A.D., Eckman, D.M., Kosek, J.C., Wiler, S.W., Patterson, A.J., Nelson, M.T., and Aldrich, R.W. (2000). Vasoregulation by the beta1 subunit of the calcium-activated potassium channel. Nature *407*, 870-876.

Bulter, W.E., Peterson, J.W., Zervas, N.T., and Morgan, K.G. (1996). Intracellular calcium, myosin light chain phosphorylation, and contractile force in experimental cerebral vasospasm. Neurosurgery *38*, 781-787; discussion 787-788.

Bunemann, M., Gerhardstein, B.L., Gao, T., and Hosey, M.M. (1999). Functional regulation of L-type calcium channels via protein kinase A-mediated phosphorylation of the beta2 subunit. J Biol Chem *274*, 33851-33854.

Burnham, M.P., Bychkov, R., Feletou, M., Richards, G.R., Vanhoutte, P.M., Weston, A.H., and Edwards, G. (2002). Characterization of an apamin-sensitive small-conductance Ca^{2+}-activated K^{+} channel in porcine coronary artery endothelium: relevance to EDHF. Br J Pharmacol *135*, 1133-1143.

Catterall, W.A. (2000). Structure and regulation of voltage-gated Ca^{2+} channels. Annu Rev Cell Dev Biol *16*, 521-555.

Chacko, S., Conti, M.A., and Adelstein, R.S. (1977). Effect of phosphorylation of smooth muscle myosin on actin activation and Ca^{2+} regulation. Proc Natl Acad Sci U S A *74*, 129-133.

Cheng, H., and Lederer, W.J. (2008). Calcium sparks. Physiol Rev *88*, 1491-1545.

Cheng, H., Lederer, W.J., and Cannell, M.B. (1993). Calcium sparks: elementary events underlying excitation-contraction coupling in heart muscle. Science *262*, 740-744.

Cheng, X., Liu, J., Asuncion-Chin, M., Blaskova, E., Bannister, J.P., Dopico, A.M., and Jaggar, J.H. (2007). A novel $Ca_V1.2$ N terminus expressed in smooth muscle cells of resistance size arteries modifies channel regulation by auxiliary subunits. The Journal of biological chemistry *282*, 29211-29221.

Cheng, X., Pachuau, J., Blaskova, E., Asuncion-Chin, M., Liu, J., Dopico, A.M., and Jaggar, J.H. (2009a). Alternative splicing of $Ca_V1.2$ channel exons in smooth muscle cells of resistance-size arteries generates currents with unique electrophysiological properties. American journal of physiology.

Cheng, X., Pachuau, J., Blaskova, E., Asuncion-Chin, M., Liu, J., Dopico, A.M., and Jaggar, J.H. (2009b). Alternative splicing of $Ca_v1.2$ channel exons in smooth muscle cells of resistance-size arteries generates currents with unique electrophysiological properties. Am J Physiol Heart Circ Physiol *297*, H680-688.

Chien, A.J., Zhao, X., Shirokov, R.E., Puri, T.S., Chang, C.F., Sun, D., Rios, E., and Hosey, M.M. (1995). Roles of a membrane-localized beta subunit in the formation and targeting of functional L-type Ca^{2+} channels. J Biol Chem *270*, 30036-30044.

Cipolla, M.J., Li, R., and Vitullo, L. (2004). Perivascular innervation of penetrating brain parenchymal arterioles. J Cardiovasc Pharmacol *44*, 1-8.

Cipolla, M.J., Smith, J., Kohlmeyer, M.M., and Godfrey, J.A. (2009). SK_{Ca} and IK_{Ca} Channels, myogenic tone, and vasodilator responses in middle cerebral arteries and parenchymal arterioles: effect of ischemia and reperfusion. Stroke *40*, 1451-1457.

Clapham, D.E. (2003). TRP channels as cellular sensors. Nature *426*, 517-524.

Clapham, D.E. (2007). Calcium signaling. Cell *131*, 1047-1058.

Clower, B.R., Kapp, J.P., Moore, N.A., Smith, R.R., and Haining, J.L. (1986). Intracisternal blood injections fail to produce cerebral angiopathy in cats. Exp Neurol *94*, 292-305.

Cohen, R.M., Foell, J.D., Balijepalli, R.C., Shah, V., Hell, J.W., and Kamp, T.J. (2005). Unique modulation of L-type Ca^{2+} channels by short auxiliary beta1d subunit present in cardiac muscle. Am J Physiol Heart Circ Physiol *288*, H2363-2374.

Cole, D.J., Patel, P.M., Schell, R.M., Drummond, J.C., and Osborne, T.N. (1993). Brain eicosanoid levels during temporary focal cerebral ischemia in rats: a microdialysis study. J Neurosurg Anesthesiol *5*, 41-47.

Cook, D.A. (1995). Mechanisms of cerebral vasospasm in subarachnoid haemorrhage. Pharmacol Ther *66*, 259-284.

Cox, D.H., Cui, J., and Aldrich, R.W. (1997). Allosteric gating of a large conductance Ca-activated K^+ channel. J Gen Physiol *110*, 257-281.

Cox, S.B., Woolsey, T.A., and Rovainen, C.M. (1993). Localized dynamic changes in cortical blood flow with whisker stimulation corresponds to matched vascular and neuronal architecture of rat barrels. J Cereb Blood Flow Metab *13*, 899-913.

Curtis, B.M., and Catterall, W.A. (1984). Purification of the calcium antagonist receptor of the voltage-sensitive calcium channel from skeletal muscle transverse tubules. Biochemistry *23*, 2113-2118.

Dacey, R.G., Jr., and Duling, B.R. (1982). A study of rat intracerebral arterioles: methods, morphology, and reactivity. Am J Physiol *243*, H598-606.

Dai, Y., and Zhang, J. (2004). Chloride efflux is involved in ET-1 and 5-HT-induced contraction in rabbit basilar artery. J Cardiovasc Pharmacol *44 Suppl 1*, S125-128.

Dalsgaard, T., Kroigaard, C., Bek, T., and Simonsen, U. (2009). Role of calcium-activated potassium channels with small conductance in bradykinin-induced vasodilation of porcine retinal arterioles. Invest Ophthalmol Vis Sci *50*, 3819-3825.

Davies, A., Hendrich, J., Van Minh, A.T., Wratten, J., Douglas, L., and Dolphin, A.C. (2007). Functional biology of the alpha$_2$delta subunits of voltage-gated calcium channels. Trends Pharmacol Sci *28*, 220-228.

Davies, M.G., and Hagen, P.O. (1993). The vascular endothelium. A new horizon. Ann Surg *218*, 593-609.

De Jongh, K.S., Murphy, B.J., Colvin, A.A., Hell, J.W., Takahashi, M., and Catterall, W.A. (1996). Specific phosphorylation of a site in the full-length form of the alpha 1 subunit of the cardiac L-type calcium channel by adenosine 3',5'-cyclic monophosphate-dependent protein kinase. Biochemistry *35*, 10392-10402.

de Weille, J., Schmid-Antomarchi, H., Fosset, M., and Lazdunski, M. (1988). ATP-sensitive K^+ channels that are blocked by hypoglycemia-inducing sulfonylureas in insulin-secreting cells are activated by galanin, a hyperglycemia-inducing hormone. Proc Natl Acad Sci U S A *85*, 1312-1316.

Debdi, M., Seylaz, J., and Sercombe, R. (1992). Early changes in rabbit cerebral artery reactivity after subarachnoid hemorrhage. Stroke *23*, 1154-1162.

Dewitt, D.S., Kong, D.L., Lyeth, B.G., Jenkins, L.W., Hayes, R.L., Wooten, E.D., and Prough, D.S. (1988). Experimental traumatic brain injury elevates brain prostaglandin E2 and thromboxane B2 levels in rats. J Neurotrauma *5*, 303-313.

Dietrich, H.H., and Dacey, R.G., Jr. (1994). Effects of extravascular acidification and extravascular alkalinization on constriction and depolarization in rat cerebral arterioles in vitro. J Neurosurg *81*, 437-442.

Dietrich, H.H., and Dacey, R.G., Jr. (2000). Molecular keys to the problems of cerebral vasospasm. Neurosurgery *46*, 517-530.

Dolphin, A.C. (2003). Beta subunits of voltage-gated calcium channels. J Bioenerg Biomembr *35*, 599-620.

Dong, L., Zheng, Y.M., Van Riper, D., Rathore, R., Liu, Q.H., Singer, H.A., and Wang, Y.X. (2008). Functional and molecular evidence for impairment of calcium-activated potassium channels in type-1 diabetic cerebral artery smooth muscle cells. J Cereb Blood Flow Metab *28*, 377-386.

Dora, K.A., Gallagher, N.T., McNeish, A., and Garland, C.J. (2008). Modulation of endothelial cell $K_{Ca}3.1$ channels during endothelium-derived hyperpolarizing factor signaling in mesenteric resistance arteries. Circ Res *102*, 1247-1255.

Doughty, J.M., and Langton, P.D. (2001). Measurement of chloride flux associated with the myogenic response in rat cerebral arteries. J Physiol *534*, 753-761.

Dumont, A.S., Dumont, R.J., McNeill, J.H., Kassell, N.F., Sutherland, G.R., and Verma, S. (2003). Chronic endothelin antagonism restores cerebrovascular function in diabetes. Neurosurgery *52*, 653-660; discussion 659-660.

Dunn, K.M., Nelson, M.T. (2009). Effect of small and intermediate conductance calcium activated potassium channel modulation on cortical cerebral blood flow in vivo. The FASEB Journal *23*, 613.624.

Earley, S., Heppner, T.J., Nelson, M.T., Brayden, J.E. (2005). TRPV4 forms a novel Ca^{2+} signaling complex with ryanodine receptors and BK_{Ca} channels. Circ Res 97, 1270-1279.

Earley, S., Straub, S.V., and Brayden, J.E. (2007). Protein kinase C regulates vascular myogenic tone through activation of TRPM4. Am J Physiol Heart Circ Physiol *292*, H2613-2622.

Earley, S., Waldron, B.J., and Brayden, J.E. (2004). Critical role for transient receptor potential channel TRPM4 in myogenic constriction of cerebral arteries. Circ Res *95*, 922-929.

Echlin, F.A. (1965). Spasm of basilar and vertebral arteries caused by experimental subarachnoid hemorrhage. J Neurosurg *23*, 1-11.

Edvinsson, L., Ekman, R., Jansen, I., McCulloch, J., Mortensen, A., and Uddman, R. (1991). Reduced levels of calcitonin gene-related peptide-like immunoreactivity in human brain vessels after subarachnoid haemorrhage. Neurosci Lett *121*, 151-154.

Edvinsson, L., Juul, R., and Jansen, I. (1994). Perivascular neuropeptides (NPY, VIP, CGRP and SP) in human brain vessels after subarachnoid haemorrhage. Acta Neurol Scand *90*, 324-330.

Edwards, D.H., Byrne, J.V., and Griffith, T.M. (1992). The effect of chronic subarachnoid hemorrhage on basal endothelium-derived relaxing factor activity in intrathecal cerebral arteries. J Neurosurg *76*, 830-837.

Eichler, I., Wibawa, J., Grgic, I., Knorr, A., Brakemeier, S., Pries, A.R., Hoyer, J., and Kohler, R. (2003). Selective blockade of endothelial Ca^{2+}-activated small- and intermediate-conductance K^{+}-channels suppresses EDHF-mediated vasodilation. Br J Pharmacol *138*, 594-601.

Ertel, E.A., Campbell, K.P., Harpold, M.M., Hofmann, F., Mori, Y., Perez-Reyes, E., Schwartz, A., Snutch, T.P., Tanabe, T., Birnbaumer, L., *et al.* (2000). Nomenclature of voltage-gated calcium channels. Neuron *25*, 533-535.

Facemire, C.S., Mohler, P.J., and Arendshorst, W.J. (2004). Expression and relative abundance of short transient receptor potential channels in the rat renal microcirculation. Am J Physiol Renal Physiol *286*, F546-551.

Falcone, J.C., Davis, M.J., and Meininger, G.A. (1991). Endothelial independence of myogenic response in isolated skeletal muscle arterioles. Am J Physiol *260*, H130-135.

Faraci, F.M. (1989). Effects of endothelin and vasopressin on cerebral blood vessels. Am J Physiol *257*, H799-803.

Faraci, F.M., and Heistad, D.D. (1990). Regulation of large cerebral arteries and cerebral microvascular pressure. Circ Res *66*, 8-17.

Faraci, F.M., and Heistad, D.D. (1993). Role of ATP-sensitive potassium channels in the basilar artery. Am J Physiol *264*, H8-13.

Faraci, F.M., and Heistad, D.D. (1998). Regulation of the cerebral circulation: role of endothelium and potassium channels. Physiol Rev *78*, 53-97.

Faraci, F.M., and Sobey, C.G. (1999). Role of soluble guanylate cyclase in dilator responses of the cerebral microcirculation. Brain Res *821*, 368-373.

Filosa, J.A., Bonev, A.D., Straub, S.V., Meredith, A.L., Wilkerson, M.K., Aldrich, R.W., and Nelson, M.T. (2006). Local potassium signaling couples neuronal activity to vasodilation in the brain. Nat Neurosci *9*, 1397-1403.

Fleming, I., and Busse, R. (1999). NO: the primary EDRF. J Mol Cell Cardiol *31*, 5-14.

Fleming, I., and Busse, R. (2006). Endothelium-derived epoxyeicosatrienoic acids and vascular function. Hypertension 47(4), 629-33

Floyd, R., and Wray, S. (2007). Calcium transporters and signalling in smooth muscles. Cell Calcium *42*, 467-476.

Fredricks, K.T., Liu, Y., Rusch, N.J., and Lombard, J.H. (1994). Role of endothelium and arterial K^+ channels in mediating hypoxic dilation of middle cerebral arteries. Am J Physiol *267*, H580-586.

Furchgott, R.F. (1999). Endothelium-derived relaxing factor: discovery, early studies, and identification as nitric oxide. Biosci Rep *19*, 235-251.

Furchgott, R.F., and Zawadzki, J.V. (1980). The obligatory role of endothelial cells in the relaxation of arterial smooth muscle by acetylcholine. Nature *288*, 373-376.

Gan, Q., Yoshida, T., Li, J., and Owens, G.K. (2007). Smooth muscle cells and myofibroblasts use distinct transcriptional mechanisms for smooth muscle alpha-actin expression. Circulation research *101*, 883-892.

Gao, T., Chien, A.J., and Hosey, M.M. (1999). Complexes of the alpha1C and beta subunits generate the necessary signal for membrane targeting of class C L-type calcium channels. The Journal of biological chemistry *274*, 2137-2144.

Gebremedhin, D., Lange, A.R., Narayanan, J., Aebly, M.R., Jacobs, E.R., and Harder, D.R. (1998). Cat cerebral arterial smooth muscle cells express cytochrome P450 4A2 enzyme and produce the vasoconstrictor 20-HETE which enhances L-type Ca^{2+} current. J Physiol *507 (Pt 3)*, 771-781.

Gee, K.R., Brown, K.A., Chen, W.N., Bishop-Stewart, J., Gray, D., and Johnson, I. (2000). Chemical and physiological characterization of fluo-4 Ca^{2+}-indicator dyes. Cell Calcium *27*, 97-106.

Gellen, B., Fernandez-Velasco, M., Briec, F., Vinet, L., LeQuang, K., Rouet-Benzineb, P., Benitah, J.P., Pezet, M., Palais, G., Pellegrin, N., *et al.* (2008). Conditional FKBP12.6 overexpression in mouse cardiac myocytes prevents triggered ventricular tachycardia through specific alterations in excitation-contraction coupling. Circulation *117*, 1778-1786.

Gifford, J.L., Walsh, M.P., and Vogel, H.J. (2007). Structures and metal-ion-binding properties of the Ca^{2+}-binding helix-loop-helix EF-hand motifs. Biochem J *405*, 199-221.

Go, L.O., Moschella, M.C., Watras, J., Handa, K.K., Fyfe, B.S., and Marks, A.R. (1995). Differential regulation of two types of intracellular calcium release channels during end-stage heart failure. J Clin Invest *95*, 888-894.

Gokina, N.I., Knot, H.J., Nelson, M.T., and Osol, G. (1999). Increased Ca^{2+} sensitivity as a key mechanism of PKC-induced constriction in pressurized cerebral arteries. Am J Physiol *277*, H1178-1188.

Golding, E.M., Marrelli, S.P., You, J., and Bryan, R.M., Jr. (2002). Endothelium-derived hyperpolarizing factor in the brain: a new regulator of cerebral blood flow? Stroke *33*, 661-663.

Gollasch, M., Hescheler, J., Quayle, J.M., Patlak, J.B., and Nelson, M.T. (1992). Single calcium channel currents of arterial smooth muscle at physiological calcium concentrations. Am J Physiol *263*, C948-952.

Gollasch, M., and Nelson, M.T. (1997). Voltage-dependent Ca^{2+} channels in arterial smooth muscle cells. Kidney Blood Press Res *20*, 355-371.

Gollasch, M., Wellman, G.C., Knot, H.J., Jaggar, J.H., Damon, D.H., Bonev, A.D., and Nelson, M.T. (1998). Ontogeny of local sarcoplasmic reticulum Ca^{2+} signals in cerebral arteries: Ca^{2+} sparks as elementary physiological events. Circ Res *83*, 1104-1114.

Graf, E.M., Bock, M., Heubach, J.F., Zahanich, I., Boxberger, S., Richter, W., Schultz, J.H., and Ravens, U. (2005). Tissue distribution of a human $Ca_v1.2$ alpha1 subunit splice variant with a 75 bp insertion. Cell Calcium *38*, 11-21.

Gray, H. (1918). Anatomy of the Human Body: 39 edn (Philadelphia, PA, Churchill Livingstone).

Griffith, T.M., Chaytor, A.T., Edwards, D.H., Daverio, F., and McGuigan, C. (2004). Enhanced inhibition of the EDHF phenomenon by a phenyl methoxyalaninyl phosphoramidate derivative of dideoxyadenosine. Br J Pharmacol *142*, 27-30.

Grover, G.J. (1997). Pharmacology of ATP-sensitive potassium channel (K_{ATP}) openers in models of myocardial ischemia and reperfusion. Can J Physiol Pharmacol *75*, 309-315.

Grynkiewicz, G., Poenie, M., and Tsien, R.Y. (1985). A new generation of Ca^{2+} indicators with greatly improved fluorescence properties. J Biol Chem *260*, 3440-3450.

Hadley, R.W., and Lederer, W.J. (1991). Properties of L-type calcium channel gating current in isolated guinea pig ventricular myocytes. J Gen Physiol *98*, 265-285.

Hai, C.M., and Murphy, R.A. (1989). Ca^{2+}, crossbridge phosphorylation, and contraction. Annu Rev Physiol *51*, 285-298.

Hamel, E. (2006). Perivascular nerves and the regulation of cerebrovascular tone. J Appl Physiol *100*, 1059-1064.

Handa, Y., Caner, H., Hayashi, M., Tamamaki, N., and Nojyo, Y. (1990). The distribution pattern of the sympathetic nerve fibers to the cerebral arterial system in rat as revealed by anterograde labeling with WGA-HRP. Exp Brain Res *82*, 493-498.

Hansen, P.B., Jensen, B.L., Andreasen, D., Friis, U.G., and Skott, O. (2000). Vascular smooth muscle cells express the alpha(1A) subunit of a P-/Q-type voltage-dependent

Ca^{2+} Channel, and It is functionally important in renal afferent arterioles. Circ Res *87*, 896-902.

Hansen-Schwartz, J., Vajkoczy, P., Macdonald, R.L., Pluta, R.M., and Zhang, J.H. (2007). Cerebral vasospasm: looking beyond vasoconstriction. Trends Pharmacol Sci *28*, 252-256.

Harder, D.R. (1984). Pressure-dependent membrane depolarization in cat middle cerebral artery. Circ Res *55*, 197-202.

Harder, D.R., Dernbach, P., and Waters, A. (1987). Possible cellular mechanism for cerebral vasospasm after experimental subarachnoid hemorrhage in the dog. J Clin Invest *80*, 875-880.

Harper, S.L., Bohlen, H.G., and Rubin, M.J. (1984). Arterial and microvascular contributions to cerebral cortical autoregulation in rats. Am J Physiol *246*, H17-24.

Hatake, K., Wakabayashi, I., Kakishita, E., and Hishida, S. (1992). Impairment of endothelium-dependent relaxation in human basilar artery after subarachnoid hemorrhage. Stroke *23*, 1111-1116; discussion 1116-1117.

Hattingen, E., Blasel, S., Dettmann, E., Vatter, H., Pilatus, U., Seifert, V., Zanella, F.E., and Weidauer, S. (2008). Perfusion-weighted MRI to evaluate cerebral autoregulation in aneurysmal subarachnoid haemorrhage. Neuroradiology *50*, 929-938.

Hino, A., Tokuyama, Y., Weir, B., Takeda, J., Yano, H., Bell, G.I., and Macdonald, R.L. (1996). Changes in endothelial nitric oxide synthase mRNA during vasospasm after subarachnoid hemorrhage in monkeys. Neurosurgery *39*, 562-567; discussion 567-568.

Hirose, H., Ide, K., Sasaki, T., Takahashi, R., Kobayashi, M., Ikemoto, F., Yano, M., and Nishikibe, M. (1995). The role of endothelin and nitric oxide in modulation of normal and spastic cerebral vascular tone in the dog. Eur J Pharmacol *277*, 77-87.

Hirst, G.D., and van Helden, D.F. (1982). Ionic basis of the resting potential of submucosal arterioles in the ileum of the guinea-pig. The Journal of physiology *333*, 53-67.

Hoeffner, U., Feletou, M., Flavahan, N.A., and Vanhoutte, P.M. (1989). Canine arteries release two different endothelium-derived relaxing factors. Am J Physiol *257*, H330-333.

Hofmann, F., Biel, M., and Flockerzi, V. (1994). Molecular basis for Ca^{2+} channel diversity. Annu Rev Neurosci *17*, 399-418.

Hop, J.W., Rinkel, G.J., Algra, A., and van Gijn, J. (1997). Case-fatality rates and functional outcome after subarachnoid hemorrhage: a systematic review. Stroke *28*, 660-664.

Horowitz, A., Menice, C.B., Laporte, R., and Morgan, K.G. (1996). Mechanisms of smooth muscle contraction. Physiol Rev *76*, 967-1003.

Hougaard, C., Eriksen, B.L., Jorgensen, S., Johansen, T.H., Dyhring, T., Madsen, L.S., Strobaek, D., and Christophersen, P. (2007). Selective positive modulation of the SK3 and SK2 subtypes of small conductance Ca^{2+}-activated K^{+} channels. Br J Pharmacol *151*, 655-665.

Hu, E., and Lee, D. (2003). Rho kinase inhibitors as potential therapeutic agents for cardiovascular diseases. Curr Opin Investig Drugs *4*, 1065-1075.

Hullin, R., Singer-Lahat, D., Freichel, M., Biel, M., Dascal, N., Hofmann, F., and Flockerzi, V. (1992). Calcium channel beta subunit heterogeneity: functional expression of cloned cDNA from heart, aorta and brain. EMBO J *11*, 885-890.

Hulme, J.T., Lin, T.W., Westenbroek, R.E., Scheuer, T., and Catterall, W.A. (2003). Beta-adrenergic regulation requires direct anchoring of PKA to cardiac $Ca_V1.2$ channels via a leucine zipper interaction with A kinase-anchoring protein 15. Proc Natl Acad Sci U S A *100*, 13093-13098.

Hulme, J.T., Yarov-Yarovoy, V., Lin, T.W., Scheuer, T., and Catterall, W.A. (2006). Autoinhibitory control of the $Ca_V1.2$ channel by its proteolytically processed distal C-terminal domain. J Physiol *576*, 87-102.

Iadecola, C. (2004). Neurovascular regulation in the normal brain and in Alzheimer's disease. Nat Rev Neurosci *5*, 347-360.

Iadecola, C., and Nedergaard, M. (2007). Glial regulation of the cerebral microvasculature. Nat Neurosci *10*, 1369-1376.

Inoue, R., Jensen, L.J., Shi, J., Morita, H., Nishida, M., Honda, A., and Ito, Y. (2006). Transient receptor potential channels in cardiovascular function and disease. Circ Res *99*, 119-131.

Inoue, R., Okada, T., Onoue, H., Hara, Y., Shimizu, S., Naitoh, S., Ito, Y., and Mori, Y. (2001). The transient receptor potential protein homologue TRP6 is the essential component of vascular $alpha_1$-adrenoceptor-activated Ca^{2+}-permeable cation channel. Circ Res *88*, 325-332.

Inoue, T., Shimizu, H., Kaminuma, T., Tajima, M., Watabe, K., and Yoshimoto, T. (1996). Prevention of cerebral vasospasm by calcitonin gene-related peptide slow-release tablet after subarachnoid hemorrhage in monkeys. Neurosurgery *39*, 984-990.

Ishiguro, M., Morielli, A.D., Zvarova, K., Tranmer, B.I., Penar, P.L., and Wellman, G.C. (2006). Oxyhemoglobin-induced suppression of voltage-dependent K^+ channels in cerebral arteries by enhanced tyrosine kinase activity. Circ Res *99*, 1252-1260.

Ishiguro, M., Puryear, C.B., Bisson, E., Saundry, C.M., Nathan, D.J., Russell, S.R., Tranmer, B.I., and Wellman, G.C. (2002). Enhanced myogenic tone in cerebral arteries from a rabbit model of subarachnoid hemorrhage. American journal of physiology *283*, H2217-2225.

Ishiguro, M., Wellman, T.L., Honda, A., Russell, S.R., Tranmer, B.I., and Wellman, G.C. (2005). Emergence of a R-type Ca^{2+} channel (Ca_V 2.3) contributes to cerebral artery constriction after subarachnoid hemorrhage. Circulation research *96*, 419-426.

Itoh, S., Sasaki, T., Asai, A., and Kuchino, Y. (1994). Prevention of delayed vasospasm by an endothelin ETA receptor antagonist, BQ-123: change of ETA receptor mRNA expression in a canine subarachnoid hemorrhage model. J Neurosurg *81*, 759-764.

Itonaga, Y., Nakajima, T., Morita, H., Hanano, T., Miyauchi, Y., Ito, Y., and Inoue, R. (2002). Contribution of nifedipine-insensitive voltage-dependent Ca^{2+} channel to diameter regulation in rabbit mesenteric artery. Life Sci *72*, 487-500.

Jahromi, B.S., Aihara, Y., Ai, J., Zhang, Z.D., Nikitina, E., and Macdonald, R.L. (2008a). Voltage-gated K^+ channel dysfunction in myocytes from a dog model of subarachnoid hemorrhage. J Cereb Blood Flow Metab *28*, 797-811.

Jahromi, B.S., Aihara, Y., Ai, J., Zhang, Z.D., Weyer, G., Nikitina, E., Yassari, R., Houamed, K.M., and Macdonald, R.L. (2008b). Preserved BK channel function in vasospastic myocytes from a dog model of subarachnoid hemorrhage. J Vasc Res *45*, 402-415.

Janiak, R., Wilson, S.M., Montague, S., and Hume, J.R. (2001). Heterogeneity of calcium stores and elementary release events in canine pulmonary arterial smooth muscle cells. Am J Physiol Cell Physiol *280*, C22-33.

Jewell, R.P., Saundry, C.M., Bonev, A.D., Tranmer, B.I., and Wellman, G.C. (2004). Inhibition of Ca^{++} sparks by oxyhemoglobin in rabbit cerebral arteries. J Neurosurg *100*, 295-302.

Ji, G., Feldman, M.E., Greene, K.S., Sorrentino, V., Xin, H.B., and Kotlikoff, M.I. (2004). RYR2 proteins contribute to the formation of Ca^{2+} sparks in smooth muscle. J Gen Physiol *123*, 377-386.

Jiang, L.H., Gawler, D.J., Hodson, N., Milligan, C.J., Pearson, H.A., Porter, V., and Wray, D. (2000). Regulation of cloned cardiac L-type calcium channels by cGMP-dependent protein kinase. J Biol Chem *275*, 6135-6143.

Johns, A., Leijten, P., Yamamoto, H., Hwang, K., and van Breemen, C. (1987). Calcium regulation in vascular smooth muscle contractility. Am J Cardiol *59*, 18A-23A.

Kajikawa, H., Ohta, T., Yoshikawa, Y., Funatsu, N., Yamamoto, M., and Someda, K. (1979). Cerebral vasospasm and hemoglobins--clinical and experimental studies. Neurol Med Chir (Tokyo) *19*, 61-71.

Kamisoyama, H., Araki, Y., and Ikebe, M. (1994). Mutagenesis of the phosphorylation site (serine 19) of smooth muscle myosin regulatory light chain and its effects on the properties of myosin. Biochemistry *33*, 840-847.

Kamp, T.J., Perez-Garcia, M.T., and Marban, E. (1996). Enhancement of ionic current and charge movement by coexpression of calcium channel beta 1A subunit with alpha 1C subunit in a human embryonic kidney cell line. J Physiol *492 (Pt 1)*, 89-96.

Kao, J.P. (1994). Practical aspects of measuring [Ca^{2+}] with fluorescent indicators. Methods Cell Biol *40*, 155-181.

Kassell, N.F., Sasaki, T., Colohan, A.R., and Nazar, G. (1985). Cerebral vasospasm following aneurysmal subarachnoid hemorrhage. Stroke *16*, 562-572.

Kasuya, H., Weir, B.K., Nakane, M., Pollock, J.S., Johns, L., Marton, L.S., and Stefansson, K. (1995). Nitric oxide synthase and guanylate cyclase levels in canine basilar artery after subarachnoid hemorrhage. J Neurosurg *82*, 250-255.

Katusic, Z.S., Milde, J.H., Cosentino, F., and Mitrovic, B.S. (1993). Subarachnoid hemorrhage and endothelial L-arginine pathway in small brain stem arteries in dogs. Stroke *24*, 392-399.

Kawano, Y., Yoshimura, T., and Kaibuchi, K. (2002). Smooth muscle contraction by small GTPase Rho. Nagoya J Med Sci *65*, 1-8.

Keef, K.D., Hume, J.R., and Zhong, J. (2001). Regulation of cardiac and smooth muscle Ca^{2+} channels ($Ca_V1.2a,b$) by protein kinases. Am J Physiol Cell Physiol *281*, C1743-1756.

Kelley-Hedgepeth, A., Peter, I., Montefusco, M.C., Levy, D., Benjamin, E.J., Vasan, R.S., Mendelsohn, M.E., Housman, D., Huggins, G.S., and Mitchell, G.F. (2009). The KCNMB1 E65K variant is associated with reduced central pulse pressure in the community-based Framingham Offspring Cohort. J Hypertens *27*, 55-60.

Khurana, V.G., Feterik, K., Springett, M.J., Eguchi, D., Shah, V., and Katusic, Z.S. (2000). Functional interdependence and colocalization of endothelial nitric oxide synthase and heat shock protein 90 in cerebral arteries. J Cereb Blood Flow Metab *20*, 1563-1570.

Kim, C.J., Weir, B., Macdonald, R.L., Marton, L.S., and Zhang, H. (1996a). Hemolysate inhibits L-type Ca^{2+} channels in rat basilar smooth muscle cells. J Vasc Res *33*, 258-264.

Kim, P., Lorenz, R.R., Sundt, T.M., Jr., and Vanhoutte, P.M. (1989). Release of endothelium-derived relaxing factor after subarachnoid hemorrhage. J Neurosurg *70*, 108-114.

Kim, P., Yoshimoto, Y., Iino, M., Tomio, S., Kirino, T., and Nonomura, Y. (1996b). Impaired calcium regulation of smooth muscle during chronic vasospasm following subarachnoid hemorrhage. J Cereb Blood Flow Metab *16*, 334-341.

Kimura, K., Ito, M., Amano, M., Chihara, K., Fukata, Y., Nakafuku, M., Yamamori, B., Feng, J., Nakano, T., Okawa, K., *et al.* (1996). Regulation of myosin phosphatase by Rho and Rho-associated kinase (Rho-kinase). Science *273*, 245-248.

Kitazono, T., Faraci, F.M., and Heistad, D.D. (1993a). Effect of norepinephrine on rat basilar artery in vivo. Am J Physiol *264*, H178-182.

Kitazono, T., Heistad, D.D., and Faraci, F.M. (1993b). Role of ATP-sensitive K^+ channels in CGRP-induced dilatation of basilar artery in vivo. Am J Physiol *265*, H581-585.

Kleppisch, T., and Nelson, M.T. (1995). ATP-sensitive K^+ currents in cerebral arterial smooth muscle: pharmacological and hormonal modulation. Am J Physiol *269*, H1634-1640.

Kleppisch, T., Winter, B., and Nelson, M.T. (1996). ATP-sensitive potassium channels in cultured arterial segments. The American journal of physiology *271*, H2462-2468.

Knot, H.J., and Nelson, M.T. (1995). Regulation of membrane potential and diameter by voltage-dependent K^+ channels in rabbit myogenic cerebral arteries. Am J Physiol *269*, H348-355.

Knot, H.J., and Nelson, M.T. (1998). Regulation of arterial diameter and wall [Ca^{2+}] in cerebral arteries of rat by membrane potential and intravascular pressure. J Physiol *508 (Pt 1)*, 199-209.

Knot, H.J., Standen, N.B., and Nelson, M.T. (1998). Ryanodine receptors regulate arterial diameter and wall [Ca^{2+}] in cerebral arteries of rat via Ca^{2+}-dependent K^+ channels. J Physiol *508 (Pt 1)*, 211-221.

Knot, H.J., Zimmermann, P.A., and Nelson, M.T. (1996). Extracellular K^+-induced hyperpolarizations and dilatations of rat coronary and cerebral arteries involve inward rectifier K^+ channels. J Physiol *492 (Pt 2)*, 419-430.

Knuckey, N.W., Fox, R.A., Surveyor, I., and Stokes, B.A. (1985). Early cerebral blood flow and computerized tomography in predicting ischemia after cerebral aneurysm rupture. J Neurosurg *62*, 850-855.

Ko, E.A., Han, J., Jung, I.D., and Park, W.S. (2008). Physiological roles of K^+ channels in vascular smooth muscle cells. J Smooth Muscle Res *44*, 65-81.

Kobayashi, H., Hayashi, M., Kobayashi, S., Kabuto, M., Handa, Y., Kawano, H., and Ide, H. (1991). Cerebral vasospasm and vasoconstriction caused by endothelin. Neurosurgery *28*, 673-678; discussion 678-679.

Koch, W.J., Ellinor, P.T., and Schwartz, A. (1990). cDNA cloning of a dihydropyridine-sensitive calcium channel from rat aorta. Evidence for the existence of alternatively spliced forms. The Journal of biological chemistry *265*, 17786-17791.

Koedel, U., Lorenzl, S., Gorriz, C., Arendt, R.M., and Pfister, H.W. (1998). Endothelin B receptor-mediated increase of cerebral blood flow in experimental pneumococcal meningitis. J Cereb Blood Flow Metab *18*, 67-74.

Koide, M., Krishnamoorthy, G., O'Connor, K.P., Nystoriak, M.A., Nelson, M.T., Wellman, G.C. (2009a). Decreases of Ca^{2+} spark frequency and ryanodine receptor-2 expression in cerebral artery myocytes after subarachnoid hemorrhage. Biophys J *96*, 278a-279a.

Koide, M., Krishnamoorthy, G., O'Connor, K.P., Nystoriak, M.A., Nelson, M.T., Wellman, G.C., (2009b). Decreases of Ca^{2+} spark frequency and ryanodine receptor-2 expression in cerebral artery myocytes after subarachnoid hemorrhage. Biophys J *96*, 278a-279a.

Koide, M., Nystoriak, M.A., Wellman, G.C. (2010). Impact of subarachnoid hemorrhage on local and global calcium signaling in cerebral artery myocytes. Acta Neurochir Suppl.

Koide, M., Penar, P.L., Tranmer, B.I., and Wellman, G.C. (2007). Heparin-binding EGF-like growth factor mediates oxyhemoglobin-induced suppression of voltage-dependent potassium channels in rabbit cerebral artery myocytes. American journal of physiology *293*, H1750-1759.

Kong, H., Jones, P.P., Koop, A., Zhang, L., Duff, H.J., and Chen, S.R. (2008). Caffeine induces Ca^{2+} release by reducing the threshold for luminal Ca^{2+} activation of the ryanodine receptor. Biochem J *414*, 441-452.

Kozniewska, E., Michalik, R., Rafalowska, J., Gadamski, R., Walski, M., Frontczak-Baniewicz, M., Piotrowski, P., and Czernicki, Z. (2006). Mechanisms of vascular dysfunction after subarachnoid hemorrhage. J Physiol Pharmacol *57 Suppl 11*, 145-160.

Kraus, G.E., Bucholz, R.D., Yoon, K.W., Knuepfer, M.M., and Smith, K.R., Jr. (1991). Cerebrospinal fluid endothelin-1 and endothelin-3 levels in normal and neurosurgical patients: a clinical study and literature review. Surg Neurol *35*, 20-29.

Lacerda, A.E., Kim, H.S., Ruth, P., Perez-Reyes, E., Flockerzi, V., Hofmann, F., Birnbaumer, L., and Brown, A.M. (1991). Normalization of current kinetics by interaction between the alpha 1 and beta subunits of the skeletal muscle dihydropyridine-sensitive Ca^{2+} channel. Nature *352*, 527-530.

Laher, I., and Zhang, J.H. (2001). Protein kinase C and cerebral vasospasm. J Cereb Blood Flow Metab *21*, 887-906.

Langley, M.S., and Sorkin, E.M. (1989). Nimodipine. A review of its pharmacodynamic and pharmacokinetic properties, and therapeutic potential in cerebrovascular disease. Drugs *37*, 669-699.

Ledoux, J., Werner, M.E., Brayden, J.E., and Nelson, M.T. (2006). Calcium-activated potassium channels and the regulation of vascular tone. Physiology (Bethesda) *21*, 69-78.

Lee, J.Y., Huang, D.L., Keep, R., and Sagher, O. (2008). Characterization of an improved double hemorrhage rat model for the study of delayed cerebral vasospasm. J Neurosci Methods *168*, 358-366.

Lee, J.Y., Sagher, O., Keep, R., Hua, Y., and Xi, G. (2009). Comparison of experimental rat models of early brain injury after subarachnoid hemorrhage. Neurosurgery *65*, 331-343; discussion 343.

Lee, K.R., Hoff, J.T. (1996). Intracranial Pressure. Neurological Surgery *W.B. Saunders Co., Philadelphia*.

Lehen'kyi, V.V., Zelensky, S.N., and Stefanov, A.V. (2005). Ca^{2+}-sensitivity and cGMP-independent effects of NO in vascular smooth muscle. Nitric Oxide *12*, 105-113.

Lesh, R.E., Somlyo, A.P., Owens, G.K., and Somlyo, A.V. (1995). Reversible permeabilization. A novel technique for the intracellular introduction of antisense oligodeoxynucleotides into intact smooth muscle. Circulation research *77*, 220-230.

Liao, P., Yong, T.F., Liang, M.C., Yue, D.T., and Soong, T.W. (2005). Splicing for alternative structures of $Ca_v1.2$ Ca^{2+} channels in cardiac and smooth muscles. Cardiovasc Res *68*, 197-203.

Liao, P., Yu, D., Lu, S., Tang, Z., Liang, M.C., Zeng, S., Lin, W., and Soong, T.W. (2004). Smooth muscle-selective alternatively spliced exon generates functional variation in $Ca_v1.2$ calcium channels. The Journal of biological chemistry *279*, 50329-50335.

Link, T.E., Murakami, K., Beem-Miller, M., Tranmer, B.I., and Wellman, G.C. (2008). Oxyhemoglobin-induced expression of R-type Ca^{2+} channels in cerebral arteries. Stroke *39*, 2122-2128.

Ma, J., Meng, W., Ayata, C., Huang, P.L., Fishman, M.C., and Moskowitz, M.A. (1996). L-NNA-sensitive regional cerebral blood flow augmentation during hypercapnia in type III NOS mutant mice. Am J Physiol *271*, H1717-1719.

Macdonald, R.L., Kassell, N.F., Mayer, S., Ruefenacht, D., Schmiedek, P., Weidauer, S., Frey, A., Roux, S., and Pasqualin, A. (2008). Clazosentan to overcome neurological ischemia and infarction occurring after subarachnoid hemorrhage (CONSCIOUS-1): randomized, double-blind, placebo-controlled phase 2 dose-finding trial. Stroke *39*, 3015-3021.

Macdonald, R.L., Pluta, R.M., and Zhang, J.H. (2007). Cerebral vasospasm after subarachnoid hemorrhage: the emerging revolution. Nat Clin Pract Neurol *3*, 256-263.

Maeda, Y., Hirano, K., Kai, Y., Hirano, M., Suzuki, S.O., Sasaki, T., and Kanaide, H. (2007). Up-regulation of proteinase-activated receptor 1 and increased contractile responses to thrombin after subarachnoid haemorrhage. Br J Pharmacol *152*, 1131-1139.

Mandala, M., Heppner, T.J., Bonev, A.D., and Nelson, M.T. (2007). Effect of endogenous and exogenous nitric oxide on calcium sparks as targets for vasodilation in rat cerebral artery. Nitric Oxide *16*, 104-109.

Marrelli, S.P. (2000). Selective measurement of endothelial or smooth muscle $[Ca^{2+}]_i$ in pressurized/perfused cerebral arteries with fura-2. J Neurosci Methods *97*, 145-155.

Marrelli, S.P. (2001). Mechanisms of endothelial P2Y1- and P2Y2-mediated vasodilatation involve differential $[Ca^{2+}]_i$ responses. Am J Physiol Heart Circ Physiol *281*, H1759-1766.

Marrelli, S.P., Eckmann, M.S., and Hunte, M.S. (2003). Role of endothelial intermediate conductance K_{Ca} channels in cerebral EDHF-mediated dilations. Am J Physiol Heart Circ Physiol *285*, H1590-1599.

Masuo, M., Reardon, S., Ikebe, M., and Kitazawa, T. (1994). A novel mechanism for the Ca^{2+}-sensitizing effect of protein kinase C on vascular smooth muscle: inhibition of myosin light chain phosphatase. J Gen Physiol *104*, 265-286.

Matsui, T., Takuwa, Y., Johshita, H., Yamashita, K., and Asano, T. (1991). Possible role of protein kinase C-dependent smooth muscle contraction in the pathogenesis of chronic cerebral vasospasm. J Cereb Blood Flow Metab *11*, 143-149.

Matsui, T., Takuwa, Y., Kaizu, H., and Asano, T. (1993). Possible involvement of C-kinase in occurrence of chronic cerebral vasospasm after subarachnoid hemorrhage. Adv Exp Med Biol *331*, 177-182.

Matsumura, Y., Ikegawa, R., Suzuki, Y., Takaoka, M., Uchida, T., Kido, H., Shinyama, H., Hayashi, K., Watanabe, M., and Morimoto, S. (1991). Phosphoramidon prevents cerebral vasospasm following subarachnoid hemorrhage in dogs: the relationship to endothelin-1 levels in the cerebrospinal fluid. Life Sci *49*, 841-848.

Matsuo, Y., Mihara, S., Ninomiya, M., and Fujimoto, M. (2001). Protective effect of endothelin type A receptor antagonist on brain edema and injury after transient middle cerebral artery occlusion in rats. Stroke *32*, 2143-2148.

Mattiazzi, A. (1997). Positive inotropic effect of angiotensin II. Increases in intracellular Ca^{2+} or changes in myofilament Ca^{2+} responsiveness? J Pharmacol Toxicol Methods *37*, 205-214.

McCarron, J.G., Osol, G., and Halpern, W. (1989). Myogenic responses are independent of the endothelium in rat pressurized posterior cerebral arteries. Blood Vessels *26*, 315-319.

McCormick, W.F., and Nofzinger, J.D. (1965). Saccular Intracranial Aneurysms: An Autopsy Study. J Neurosurg *22*, 155-159.

McNeish, A.J., Dora, K.A., and Garland, C.J. (2005). Possible role for K^+ in endothelium-derived hyperpolarizing factor-linked dilatation in rat middle cerebral artery. Stroke *36*, 1526-1532.

Megyesi, J.F., Vollrath, B., Cook, D.A., and Findlay, J.M. (2000). In vivo animal models of cerebral vasospasm: a review. Neurosurgery *46*, 448-460; discussion 460-441.

Meininger, G.A., and Davis, M.J. (1992). Cellular mechanisms involved in the vascular myogenic response. Am J Physiol *263*, H647-659.

Michel, J.B., Feron, O., Sacks, D., and Michel, T. (1997). Reciprocal regulation of endothelial nitric-oxide synthase by Ca^{2+}-calmodulin and caveolin. J Biol Chem *272*, 15583-15586.

Mikami, A., Imoto, K., Tanabe, T., Niidome, T., Mori, Y., Takeshima, H., Narumiya, S., and Numa, S. (1989). Primary structure and functional expression of the cardiac dihydropyridine-sensitive calcium channel. Nature *340*, 230-233.

Minami, N., Tani, E., Yokota, M., Maeda, Y., and Yamaura, I. (1991). Immunohistochemistry of leukotriene C4 in experimental cerebral vasospasm. Acta Neuropathol *81*, 401-407.

Mino, T., Yuasa, U., Naka, M., and Tanaka, T. (1995). Phosphorylation of calponin mediated by protein kinase C in association with contraction in porcine coronary artery. Biochem Biophys Res Commun *208*, 397-404.

Miyagi, Y., Carpenter, R.C., Meguro, T., Parent, A.D., and Zhang, J.H. (2000). Upregulation of rho A and rho kinase messenger RNAs in the basilar artery of a rat model of subarachnoid hemorrhage. J Neurosurg *93*, 471-476.

Miyauchi, T., and Masaki, T. (1999). Pathophysiology of endothelin in the cardiovascular system. Annu Rev Physiol *61*, 391-415.

Moore, S.A., Spector, A.A., and Hart, M.N. (1988). Eicosanoid metabolism in cerebromicrovascular endothelium. Am J Physiol *254*, C37-44.

Moosmang, S., Schulla, V., Welling, A., Feil, R., Feil, S., Wegener, J.W., Hofmann, F., and Klugbauer, N. (2003). Dominant role of smooth muscle L-type calcium channel $Ca_v1.2$ for blood pressure regulation. EMBO J *22*, 6027-6034.

Morita, H., Cousins, H., Onoue, H., Ito, Y., and Inoue, R. (1999). Predominant distribution of nifedipine-insensitive, high voltage-activated Ca^{2+} channels in the terminal mesenteric artery of guinea pig. Circ Res *85*, 596-605.

Morita, H., Honda, A., Inoue, R., Ito, Y., Abe, K., Nelson, M.T., and Brayden, J.E. (2007). Membrane stretch-induced activation of a TRPM4-like nonselective cation channel in cerebral artery myocytes. J Pharmacol Sci *103*, 417-426.

Murad, F. (2004). Discovery of some of the biological effects of nitric oxide and its role in cell signaling. Biosci Rep *24*, 452-474.

Murakami, M., Yamamura, H., Suzuki, T., Kang, M.G., Ohya, S., Murakami, A., Miyoshi, I., Sasano, H., Muraki, K., Hano, T., *et al.* (2003). Modified cardiovascular L-type channels in mice lacking the voltage-dependent Ca^{2+} channel beta3 subunit. J Biol Chem *278*, 43261-43267.

Murphy, R.A. (1982). Myosin phosphorylation and crossbridge regulation in arterial smooth muscle. State-or-the-art review. Hypertension *4*, 3-7.

Murray, M.A., Faraci, F.M., and Heistad, D.D. (1992). Effect of protein kinase C inhibitors on endothelin- and vasopressin-induced constriction of the rat basilar artery. Am J Physiol *263*, H1643-1649.

Nakagawa, T., and Hashi, K. (1994). The incidence and treatment of asymptomatic, unruptured cerebral aneurysms. J Neurosurg *80*, 217-223.

Nakao, K., Murata, H., Kanamaru, K., and Waga, S. (1996). Effects of nitroglycerin on vasospasm and cyclic nucleotides in a primate model of subarachnoid hemorrhage. Stroke *27*, 1882-1887; discussion 1887-1888.

Nakashima, S., Tabuchi, K., Shimokawa, S., Fukuyama, K., Mineta, T., and Abe, M. (1998). Combination therapy of fasudil hydrochloride and ozagrel sodium for cerebral vasospasm following aneurysmal subarachnoid hemorrhage. Neurol Med Chir (Tokyo) *38*, 805-810; discussion 810-801.

Naveri, L., Stromberg, C., and Saavedra, J.M. (1994). Angiotensin IV reverses the acute cerebral blood flow reduction after experimental subarachnoid hemorrhage in the rat. J Cereb Blood Flow Metab *14*, 1096-1099.

Neild, T.O., and Keef, K. (1985). Measurements of the membrane potential of arterial smooth muscle in anesthetized animals and its relationship to changes in artery diameter. Microvasc Res *30*, 19-28.

Nelson, M.T., Cheng, H., Rubart, M., Santana, L.F., Bonev, A.D., Knot, H.J., and Lederer, W.J. (1995). Relaxation of arterial smooth muscle by calcium sparks. Science *270*, 633-637.

Nelson, M.T., Conway, M.A., Knot, H.J., and Brayden, J.E. (1997). Chloride channel blockers inhibit myogenic tone in rat cerebral arteries. J Physiol *502 (Pt 2)*, 259-264.

Nelson, M.T., Patlak, J.B., Worley, J.F., and Standen, N.B. (1990). Calcium channels, potassium channels, and voltage dependence of arterial smooth muscle tone. Am J Physiol *259*, C3-18.

Nelson, M.T., and Quayle, J.M. (1995). Physiological roles and properties of potassium channels in arterial smooth muscle. Am J Physiol *268*, C799-822.

Nelson, M.T., Standen, N.B., Brayden, J.E., and Worley, J.F., 3rd (1988). Noradrenaline contracts arteries by activating voltage-dependent calcium channels. Nature *336*, 382-385.

Ngai, A.C., Ko, K.R., Morii, S., and Winn, H.R. (1988). Effect of sciatic nerve stimulation on pial arterioles in rats. Am J Physiol *254*, H133-139.

Nichols, C.G., and Lopatin, A.N. (1997). Inward rectifier potassium channels. Annu Rev Physiol *59*, 171-191.

Nikitina, E., Zhang, Z.D., Kawashima, A., Jahromi, B.S., Bouryi, V.A., Takahashi, M., Xie, A., and Macdonald, R.L. (2007). Voltage-dependent calcium channels of dog basilar artery. J Physiol *580*, 523-541.

Nishikawa, M., Shirakawa, S., and Adelstein, R.S. (1985). Phosphorylation of smooth muscle myosin light chain kinase by protein kinase C. Comparative study of the phosphorylated sites. J Biol Chem *260*, 8978-8983.

Nishimura, N., Schaffer, C.B., Friedman, B., Lyden, P.D., and Kleinfeld, D. (2007). Penetrating arterioles are a bottleneck in the perfusion of neocortex. Proc Natl Acad Sci U S A *104*, 365-370.

Nishizawa, S., and Laher, I. (2005). Signaling mechanisms in cerebral vasospasm. Trends Cardiovasc Med *15*, 24-34.

Nishizawa, S., Nezu, N., and Uemura, K. (1992). Direct evidence for a key role of protein kinase C in the development of vasospasm after subarachnoid hemorrhage. J Neurosurg *76*, 635-639.

Nishizawa, S., Obara, K., Nakayama, K., Koide, M., Yokoyama, T., Yokota, N., and Ohta, S. (2000). Protein kinase cdelta and alpha are involved in the development of vasospasm after subarachnoid hemorrhage. Eur J Pharmacol *398*, 113-119.

Nishizawa, S., Yamamoto, S., and Uemura, K. (1996). Interrelation between protein kinase C and nitric oxide in the development of vasospasm after subarachnoid hemorrhage. Neurol Res *18*, 89-95.

Nishizawa, S., Yamamoto, S., Yokoyama, T., Ryu, H., and Uemura, K. (1995). Chronological changes of arterial diameter, cGMP, and protein kinase C in the development of vasospasm. Stroke *26*, 1916-1920; discussion 1920-1911.

Nystoriak, M.A., Murakami, K., Penar, P.L., and Wellman, G.C. (2009). $Ca_v1.2$ splice variant with exon 9* is critical for regulation of cerebral artery diameter. Am J Physiol Heart Circ Physiol *297*, H1820-1828.

Ohkuma, H., Itoh, K., Shibata, S., and Suzuki, S. (1997). Morphological changes of intraparenchymal arterioles after experimental subarachnoid hemorrhage in dogs. Neurosurgery *41*, 230-235; discussion 235-236.

Ohkuma, H., Manabe, H., Tanaka, M., and Suzuki, S. (2000). Impact of cerebral microcirculatory changes on cerebral blood flow during cerebral vasospasm after aneurysmal subarachnoid hemorrhage. Stroke *31*, 1621-1627.

Ohkuma, H., and Suzuki, S. (1999). Histological dissociation between intra- and extraparenchymal portion of perforating small arteries after experimental subarachnoid hemorrhage in dogs. Acta Neuropathol *98*, 374-382.

Onoda, K., Ono, S., Ogihara, K., Shiota, T., Asari, S., Ohmoto, T., and Ninomiya, Y. (1996). Inhibition of vascular contraction by intracisternal administration of preproendothelin-1 mRNA antisense oligoDNA in a rat experimental vasospasm model. J Neurosurg *85*, 846-852.

Osol, G., Laher, I., and Cipolla, M. (1991). Protein kinase C modulates basal myogenic tone in resistance arteries from the cerebral circulation. Circ Res *68*, 359-367.

Ostrowski, R.P., Colohan, A.R., and Zhang, J.H. (2006). Molecular mechanisms of early brain injury after subarachnoid hemorrhage. Neurol Res *28*, 399-414.

Owsianik, G., Talavera, K., Voets, T., and Nilius, B. (2006). Permeation and selectivity of TRP channels. Annu Rev Physiol *68*, 685-717.

Park, K.W., Metais, C., Dai, H.B., Comunale, M.E., and Sellke, F.W. (2001). Microvascular endothelial dysfunction and its mechanism in a rat model of subarachnoid hemorrhage. Anesth Analg *92*, 990-996.

Parkington, H.C., Coleman, H.A., and Tare, M. (2004). Prostacyclin and endothelium-dependent hyperpolarization. Pharmacol Res *49*, 509-514.

Parsons, S.J., Sumner, M.J., and Garland, C.J. (1996). Phospholipase A2 and protein kinase C contribute to myofilament sensitization to 5-HT in the rabbit mesenteric artery. J Physiol *491 (Pt 2)*, 447-453.

Patel, T.R., Galbraith, S., Graham, D.I., Hallak, H., Doherty, A.M., and McCulloch, J. (1996). Endothelin receptor antagonist increases cerebral perfusion and reduces ischaemic damage in feline focal cerebral ischaemia. J Cereb Blood Flow Metab *16*, 950-958.

Paulson, O.B., and Newman, E.A. (1987). Does the release of potassium from astrocyte endfeet regulate cerebral blood flow? Science *237*, 896-898.

Perez, G.J., Bonev, A.D., and Nelson, M.T. (2001). Micromolar Ca^{2+} from sparks activates Ca^{2+}-sensitive K^+ channels in rat cerebral artery smooth muscle. Am J Physiol Cell Physiol *281*, C1769-1775.

Perez, G.J., Bonev, A.D., Patlak, J.B., and Nelson, M.T. (1999). Functional coupling of ryanodine receptors to K_{Ca} channels in smooth muscle cells from rat cerebral arteries. J Gen Physiol *113*, 229-238.

Peterson, E.W., and Leblanc, R. (1976). A theory of the mechanism of cerebral vasospasm and its reversal, the role of calcium and cyclic AMP. Can J Neurol Sci *3*, 223-226.

Petrov, T., and Rafols, J.A. (2001). Acute alterations of endothelin-1 and iNOS expression and control of the brain microcirculation after head trauma. Neurol Res *23*, 139-143.

Petruk, K.C., West, M., Mohr, G., Weir, B.K., Benoit, B.G., Gentili, F., Disney, L.B., Khan, M.I., Grace, M., Holness, R.O., *et al.* (1988). Nimodipine treatment in poor-grade aneurysm patients. Results of a multicenter double-blind placebo-controlled trial. J Neurosurg *68*, 505-517.

Pierre, L.N., and Davenport, A.P. (1999). Blockade and reversal of endothelin-induced constriction in pial arteries from human brain. Stroke *30*, 638-643.

Plane, F., Johnson, R., Kerr, P., Wiehler, W., Thorneloe, K., Ishii, K., Chen, T., and Cole, W. (2005). Heteromultimeric K_v1 channels contribute to myogenic control of arterial diameter. Circ Res *96*, 216-224.

Pluta, R.M., Afshar, J.K., Thompson, B.G., Boock, R.J., Harvey-White, J., and Oldfield, E.H. (2000). Increased cerebral blood flow but no reversal or prevention of vasospasm in response to L-arginine infusion after subarachnoid hemorrhage. J Neurosurg *92*, 121-126.

Pluta, R.M., Hansen-Schwartz, J., Dreier, J., Vajkoczy, P., Macdonald, R.L., Nishizawa, S., Kasuya, H., Wellman, G., Keller, E., Zauner, A., *et al.* (2009). Cerebral vasospasm

following subarachnoid hemorrhage: time for a new world of thought. Neurol Res *31*, 151-158.

Poloyac, S.M., Reynolds, R.B., Yonas, H., and Kerr, M.E. (2005). Identification and quantification of the hydroxyeicosatetraenoic acids, 20-HETE and 12-HETE, in the cerebrospinal fluid after subarachnoid hemorrhage. Journal of Neuroscience Methods *144*, 257-263.

Porter, V.A., Bonev, A.D., Knot, H.J., Heppner, T.J., Stevenson, A.S., Kleppisch, T., Lederer, W.J., and Nelson, M.T. (1998). Frequency modulation of Ca^{2+} sparks is involved in regulation of arterial diameter by cyclic nucleotides. Am J Physiol *274*, C1346-1355.

Pragnell, M., De Waard, M., Mori, Y., Tanabe, T., Snutch, T.P., and Campbell, K.P. (1994). Calcium channel beta-subunit binds to a conserved motif in the I-II cytoplasmic linker of the alpha 1-subunit. Nature *368*, 67-70.

Prunell, G.F., Svendgaard, N.A., Alkass, K., and Mathiesen, T. (2005). Inflammation in the brain after experimental subarachnoid hemorrhage. Neurosurgery *56*, 1082-1092; discussion 1082-1092.

Pucovsky, V., and Bolton, T.B. (2006). Localisation, function and composition of primary Ca^{2+} spark discharge region in isolated smooth muscle cells from guinea-pig mesenteric arteries. Cell Calcium *39*, 113-129.

Puri, T.S., Gerhardstein, B.L., Zhao, X.L., Ladner, M.B., and Hosey, M.M. (1997). Differential effects of subunit interactions on protein kinase A- and C-mediated phosphorylation of L-type calcium channels. Biochemistry *36*, 9605-9615.

Quan, L., and Sobey, C.G. (2000). Selective effects of subarachnoid hemorrhage on cerebral vascular responses to 4-aminopyridine in rats. Stroke *31*, 2460-2465.

Quayle, J.M., Bonev, A.D., Brayden, J.E., and Nelson, M.T. (1994). Calcitonin gene-related peptide activated ATP-sensitive K^+ currents in rabbit arterial smooth muscle via protein kinase A. J Physiol *475*, 9-13.

Quayle, J.M., Nelson, M.T., and Standen, N.B. (1997). ATP-sensitive and inwardly rectifying potassium channels in smooth muscle. Physiol Rev *77*, 1165-1232.

Reading, S.A., and Brayden, J.E. (2007). Central role of TRPM4 channels in cerebral blood flow regulation. Stroke *38*, 2322-2328.

Reading, S.A., Earley, S., Waldron, B.J., Welsh, D.G., and Brayden, J.E. (2005). TRPC3 mediates pyrimidine receptor-induced depolarization of cerebral arteries. Am J Physiol Heart Circ Physiol *288*, H2055-2061.

Reid, J.M., Davies, A.G., Ashcroft, F.M., and Paterson, D.J. (1995). Effect of L-NMMA, cromakalim, and glibenclamide on cerebral blood flow in hypercapnia and hypoxia. Am J Physiol *269*, H916-922.

Reuter, H. (1979). Properties of two inward membrane currents in the heart. Annu Rev Physiol *41*, 413-424.

Reuter, H. (1983). Calcium channel modulation by neurotransmitters, enzymes and drugs. Nature *301*, 569-574.

Rhee, S.W., Stimers, J.R., Wang, W., and Pang, L. (2009). Vascular smooth muscle-specific knockdown of the noncardiac form of the L-type calcium channel by microRNA-based short hairpin RNA as a potential antihypertensive therapy. J Pharmacol Exp Ther *329*, 775-782.

Robertson, B.E., and Nelson, M.T. (1994). Aminopyridine inhibition and voltage dependence of K^+ currents in smooth muscle cells from cerebral arteries. Am J Physiol *267*, C1589-1597.

Robertson, B.E., Schubert, R., Hescheler, J., and Nelson, M.T. (1993). cGMP-dependent protein kinase activates Ca-activated K channels in cerebral artery smooth muscle cells. Am J Physiol *265*, C299-303.

Roman, R.J., Renic, M., Dunn, K.M., Takeuchi, K., and Hacein-Bey, L. (2006). Evidence that 20-HETE contributes to the development of acute and delayed cerebral vasospasm. Neurol Res *28*, 738-749.

Roux, S., Loffler, B.M., Gray, G.A., Sprecher, U., Clozel, M., and Clozel, J.P. (1995). The role of endothelin in experimental cerebral vasospasm. Neurosurgery *37*, 78-85; discussion 85-76.

Rubart, M., Patlak, J.B., and Nelson, M.T. (1996). Ca^{2+} currents in cerebral artery smooth muscle cells of rat at physiological Ca^{2+} concentrations. J Gen Physiol *107*, 459-472.

Sagher, O., Jin, Y., Thai, Q.A., Fergus, A., Kassell, N.F., and Lee, K.S. (1994). Cerebral microvascular responses to endothelins: the role of ETA receptors. Brain Res *658*, 179-184.

Sakaki, S., Kuwabara, H., and Ohta, S. (1986). Biological defence mechanism in the pathogenesis of prolonged cerebral vasospasm in the patients with ruptured intracranial aneurysms. Stroke *17*, 196-202.

Sakurai, T., Yanagisawa, M., Takuwa, Y., Miyazaki, H., Kimura, S., Goto, K., and Masaki, T. (1990). Cloning of a cDNA encoding a non-isopeptide-selective subtype of the endothelin receptor. Nature *348*, 732-735.

Sanguinetti, M.C., and Kass, R.S. (1984). Voltage-dependent block of calcium channel current in the calf cardiac Purkinje fiber by dihydropyridine calcium channel antagonists. Circ Res *55*, 336-348.

Santana, L.F., Kranias, E.G., and Lederer, W.J. (1997). Calcium sparks and excitation-contraction coupling in phospholamban-deficient mouse ventricular myocytes. J Physiol *503 (Pt 1)*, 21-29.

Sato, M., Tani, E., Fujikawa, H., and Kaibuchi, K. (2000). Involvement of Rho-kinase-mediated phosphorylation of myosin light chain in enhancement of cerebral vasospasm. Circ Res *87*, 195-200.

Schaffer, C.B., Friedman, B., Nishimura, N., Schroeder, L.F., Tsai, P.S., Ebner, F.F., Lyden, P.D., and Kleinfeld, D. (2006). Two-photon imaging of cortical surface microvessels reveals a robust redistribution in blood flow after vascular occlusion. PLoS Biol *4*, e22.

Seisenberger, C., Specht, V., Welling, A., Platzer, J., Pfeifer, A., Kuhbandner, S., Striessnig, J., Klugbauer, N., Feil, R., and Hofmann, F. (2000). Functional embryonic cardiomyocytes after disruption of the L-type alpha1C ($Ca_v1.2$) calcium channel gene in the mouse. J Biol Chem *275*, 39193-39199.

Shiota, T., Bernanke, D.H., Parent, A.D., and Hasui, K. (1996). Protein kinase C has two different major roles in lattice compaction enhanced by cerebrospinal fluid from patients with subarachnoid hemorrhage. Stroke *27*, 1889-1895.

Shohami, E., Jacobs, T.P., Hallenbeck, J.M., and Feuerstein, G. (1987). Increased thromboxane A2 and 5-HETE production following spinal cord ischemia in the rabbit. Prostaglandins Leukot Med *28*, 169-181.

Sieber, F.E., Wilson, D.A., Hanley, D.F., and Traystman, R.J. (1993). Extracellular potassium activity and cerebral blood flow during moderate hypoglycemia in anesthetized dogs. Am J Physiol *264*, H1774-1780.

Silverthorn, D.U. (2004). Human Physiology, Third Edition.

Simeone, F.A., Ryan, K.G., and Cotter, J.R. (1968). Prolonged experimental cerebral vasospasm. J Neurosurg *29*, 357-366.

Siminiak, T., Flores, N.A., and Sheridan, D.J. (1995). Neutrophil interactions with endothelium and platelets: possible role in the development of cardiovascular injury. Eur Heart J *16*, 160-170.

Smith, W.L., Garavito, R.M., and DeWitt, D.L. (1996). Prostaglandin endoperoxide H synthases (cyclooxygenases)-1 and -2. J Biol Chem *271*, 33157-33160.

Sobey, C.G., and Faraci, F.M. (1998). Subarachnoid haemorrhage: what happens to the cerebral arteries? Clin Exp Pharmacol Physiol *25*, 867-876.

Sobey, C.G., and Faraci, F.M. (2000). Knockout blow for channel identity crisis : vasodilation to potassium is mediated via $K_{ir}2.1$. Circ Res *87*, 83-84.

Sobey, C.G., Heistad, D.D., and Faraci, F.M. (1997). Effect of subarachnoid hemorrhage on cerebral vasodilatation in response to activation of ATP-sensitive K^+ channels in chronically hypertensive rats. Stroke *28*, 392-396; discussion 396-397.

Soldatov, N.M. (1992). Molecular diversity of L-type Ca^{2+} channel transcripts in human fibroblasts. Proc Natl Acad Sci U S A *89*, 4628-4632.

Somjen, G.G. (1979). Extracellular potassium in the mammalian central nervous system. Annu Rev Physiol *41*, 159-177.

Sonkusare, S., Palade, P.T., Marsh, J.D., Telemaque, S., Pesic, A., and Rusch, N.J. (2006). Vascular calcium channels and high blood pressure: pathophysiology and therapeutic implications. Vascul Pharmacol *44*, 131-142.

Standen, N.B., Quayle, J.M., Davies, N.W., Brayden, J.E., Huang, Y., and Nelson, M.T. (1989). Hyperpolarizing vasodilators activate ATP-sensitive K^+ channels in arterial smooth muscle. Science *245*, 177-180.

Steinke, D.E., Weir, B.K., Findlay, J.M., Tanabe, T., Grace, M., and Krushelnycky, B.W. (1989). A trial of the 21-aminosteroid U74006F in a primate model of chronic cerebral vasospasm. Neurosurgery *24*, 179-186.

Straub, S.V., Girouard, H., Doetsch, P.E., Hannah, R.M., Wilkerson, M.K., and Nelson, M.T. (2009). Regulation of intracerebral arteriolar tone by K_v channels: effects of glucose and PKC. Am J Physiol Cell Physiol *297*, C788-796.

Strobaek, D., Teuber, L., Jorgensen, T.D., Ahring, P.K., Kjaer, K., Hansen, R.S., Olesen, S.P., Christophersen, P., and Skaaning-Jensen, B. (2004). Activation of human IK and

SK Ca^{2+} -activated K^{+} channels by NS309 (6,7-dichloro-1H-indole-2,3-dione 3-oxime). Biochim Biophys Acta *1665*, 1-5.

Strutz, F., Okada, H., Lo, C.W., Danoff, T., Carone, R.L., Tomaszewski, J.E., and Neilson, E.G. (1995). Identification and characterization of a fibroblast marker: FSP1. The Journal of cell biology *130*, 393-405.

Sugai, K., Yaganisawa, T., Motohashi, O., Suzuki, M., and Yoshimoto, T. (1999). Levcromakalim decreases cytoplasmic Ca^{2+} and vascular tone in basilar artery of SAH model dogs. J Cardiovasc Pharmacol *33*, 868-875.

Suzuki, S., Kimura, M., Souma, M., Ohkima, H., Shimizu, T., and Iwabuchi, T. (1990). Cerebral microthrombosis in symptomatic cerebral vasospasm--a quantitative histological study in autopsy cases. Neurol Med Chir (Tokyo) *30*, 309-316.

Svendgaard, N.A., Edvinsson, L., Owman, C., and Sahlin, C. (1977). Increased sensitivity of the basilar artery to norepinephrine and 5-hydroxytryptamine following experimental subarachnoid hemorrhage. Surg Neurol *8*, 191-195.

Szok, D., Hansen-Schwartz, J., and Edvinsson, L. (2001). In depth pharmacological characterization of endothelin B receptors in the rat middle cerebral artery. Neurosci Lett *314*, 69-72.

Tachibana, E., Harada, T., Shibuya, M., Saito, K., Takayasu, M., Suzuki, Y., and Yoshida, J. (1999). Intra-arterial infusion of fasudil hydrochloride for treating vasospasm following subarachnoid haemorrhage. Acta Neurochir (Wien) *141*, 13-19.

Takahashi, M., Seagar, M.J., Jones, J.F., Reber, B.F., and Catterall, W.A. (1987). Subunit structure of dihydropyridine-sensitive calcium channels from skeletal muscle. Proc Natl Acad Sci U S A *84*, 5478-5482.

Takeuchi, H., Handa, Y., Kobayashi, H., Kawano, H., and Hayashi, M. (1991). Impairment of cerebral autoregulation during the development of chronic cerebral vasospasm after subarachnoid hemorrhage in primates. Neurosurgery *28*, 41-48.

Takeuchi, K., Miyata, N., Renic, M., Harder, D.R., and Roman, R.J. (2006). Hemoglobin, NO, and 20-HETE interactions in mediating cerebral vasoconstriction following SAH. Am J Physiol Regul Integr Comp Physiol *290*, R84-89.

Takuwa, Y., Matsui, T., Abe, Y., Nagafuji, T., Yamashita, K., and Asano, T. (1993). Alterations in protein kinase C activity and membrane lipid metabolism in cerebral vasospasm after subarachnoid hemorrhage. J Cereb Blood Flow Metab *13*, 409-415.

Tanabe, T., Takeshima, H., Mikami, A., Flockerzi, V., Takahashi, H., Kangawa, K., Kojima, M., Matsuo, H., Hirose, T., and Numa, S. (1987). Primary structure of the receptor for calcium channel blockers from skeletal muscle. Nature *328*, 313-318.

Tanaka, Y., Meera, P., Song, M., Knaus, H.G., and Toro, L. (1997). Molecular constituents of maxi K_{Ca} channels in human coronary smooth muscle: predominant alpha + beta subunit complexes. J Physiol *502 (Pt 3)*, 545-557.

Tang, G., Kitten, T., Munro, C.L., Wellman, G.C., and Mintz, K.P. (2008a). EmaA, a potential virulence determinant of Aggregatibacter actinomycetemcomitans in infective endocarditis. Infect Immun *76*, 2316-2324.

Tang, Z.Z., Liang, M.C., Lu, S., Yu, D., Yu, C.Y., Yue, D.T., and Soong, T.W. (2004). Transcript scanning reveals novel and extensive splice variations in human l-type voltage-gated calcium channel, $Ca_v1.2$ alpha1 subunit. J Biol Chem *279*, 44335-44343.

Tang, Z.Z., Liao, P., Li, G., Jiang, F.L., Yu, D., Hong, X., Yong, T.F., Tan, G., Lu, S., Wang, J., *et al.* (2008b). Differential splicing patterns of L-type calcium channel $Ca_v1.2$ subunit in hearts of Spontaneously Hypertensive Rats and Wistar Kyoto Rats. Biochim Biophys Acta *1783*, 118-130.

Tanishima, T. (1980). Cerebral vasospasm: contractile activity of hemoglobin in isolated canine basilar arteries. J Neurosurg *53*, 787-793.

Teunissen, L.L., Rinkel, G.J., Algra, A., and van Gijn, J. (1996). Risk factors for subarachnoid hemorrhage: a systematic review. Stroke *27*, 544-549.

Thorin-Trescases, N., Bartolotta, T., Hyman, N., Penar, P.L., Walters, C.L., Bevan, R.D., and Bevan, J.A. (1997). Diameter dependence of myogenic tone of human pial arteries. Possible relation to distensibility. Stroke *28*, 2486-2492.

Tiwari, S., Zhang, Y., Heller, J., Abernethy, D.R., and Soldatov, N.M. (2006). Atherosclerosis-related molecular alteration of the human $Ca_V1.2$ calcium channel alpha1C subunit. Proc Natl Acad Sci U S A *103*, 17024-17029.

Tomas, M., Vazquez, E., Fernandez-Fernandez, J.M., Subirana, I., Plata, C., Heras, M., Vila, J., Marrugat, J., Valverde, M.A., and Senti, M. (2008). Genetic variation in the KCNMA1 potassium channel alpha subunit as risk factor for severe essential hypertension and myocardial infarction. J Hypertens *26*, 2147-2153.

Tomassoni, D., Lanari, A., Silvestrelli, G., Traini, E., and Amenta, F. (2008). Nimodipine and its use in cerebrovascular disease: evidence from recent preclinical and controlled clinical studies. Clin Exp Hypertens *30*, 744-766.

Treggiari-Venzi, M.M., Suter, P.M., and Romand, J.A. (2001). Review of medical prevention of vasospasm after aneurysmal subarachnoid hemorrhage: a problem of neurointensive care. Neurosurgery *48*, 249-261; discussion 261-242.

Triggle, D.J. (1991). Calcium-channel drugs: structure-function relationships and selectivity of action. J Cardiovasc Pharmacol *18 Suppl 10*, S1-6.

Turner, C.P., Bergeron, M., Matz, P., Zegna, A., Noble, L.J., Panter, S.S., and Sharp, F.R. (1998). Heme oxygenase-1 is induced in glia throughout brain by subarachnoid hemoglobin. J Cereb Blood Flow Metab *18*, 257-273.

Vane, J.R., Anggard, E.E., and Botting, R.M. (1990). Regulatory functions of the vascular endothelium. N Engl J Med *323*, 27-36.

Vanhoutte, P.M. (2004). Endothelium-dependent hyperpolarizations: the history. Pharmacol Res *49*, 503-508.

Varsos, V.G., Liszczak, T.M., Han, D.H., Kistler, J.P., Vielma, J., Black, P.M., Heros, R.C., and Zervas, N.T. (1983). Delayed cerebral vasospasm is not reversible by aminophylline, nifedipine, or papaverine in a "two-hemorrhage" canine model. J Neurosurg *58*, 11-17.

Vatter, H., Weidauer, S., Konczalla, J., Dettmann, E., Zimmermann, M., Raabe, A., Preibisch, C., Zanella, F.E., and Seifert, V. (2006). Time course in the development of cerebral vasospasm after experimental subarachnoid hemorrhage: clinical and neuroradiological assessment of the rat double hemorrhage model. Neurosurgery *58*, 1190-1197; discussion 1190-1197.

Vergouwen, M.D., Vermeulen, M., Coert, B.A., Stroes, E.S., and Roos, Y.B. (2008). Microthrombosis after aneurysmal subarachnoid hemorrhage: an additional explanation for delayed cerebral ischemia. J Cereb Blood Flow Metab *28*, 1761-1770.

Vollmer, D.G., Takayasu, M., and Dacey, R.G., Jr. (1992). An in vitro comparative study of conducting vessels and penetrating arterioles after experimental subarachnoid hemorrhage in the rabbit. J Neurosurg *77*, 113-119.

Walsh, M.P. (1981). Calmodulin-dependent myosin light chain kinases. Cell Calcium *2*, 333-352.

Waters, A., and Harder, D.R. (1985). Altered membrane properties of cerebral vascular smooth muscle following subarachnoid hemorrhage: an electrophysiological study. I. Changes in resting membrane potential (Em) and effect on the electrogenic pump potential contribution to Em. Stroke *16*, 990-997.

Weir, B. (1995). The pathophysiology of cerebral vasospasm. Br J Neurosurg *9*, 375-390.

Weir, B., Erasmo, R., Miller, J., McIntyre, J., Secord, D., and Mielke, B. (1970). Vasospasm in response to repeated subarachnoid hemorrhages in the monkey. J Neurosurg *33*, 395-406.

Welling, A., Ludwig, A., Zimmer, S., Klugbauer, N., Flockerzi, V., and Hofmann, F. (1997). Alternatively spliced IS6 segments of the alpha 1C gene determine the tissue-specific dihydropyridine sensitivity of cardiac and vascular smooth muscle L-type Ca^{2+} channels. Circ Res *81*, 526-532.

Wellman, G.C. (2006). Ion channels and calcium signaling in cerebral arteries following subarachnoid hemorrhage. Neurol Res *28*, 690-702.

Wellman, G.C., and Bevan, J.A. (1995). Barium inhibits the endothelium-dependent component of flow but not acetylcholine-induced relaxation in isolated rabbit cerebral arteries. J Pharmacol Exp Ther *274*, 47-53.

Wellman, G.C., Bonev, A.D., Nelson, M.T., and Brayden, J.E. (1996). Gender differences in coronary artery diameter involve estrogen, nitric oxide, and Ca^{2+}-dependent K^+ channels. Circ Res *79*, 1024-1030.

Wellman, G.C., Nathan, D.J., Saundry, C.M., Perez, G., Bonev, A.D., Penar, P.L., Tranmer, B.I., and Nelson, M.T. (2002). Ca^{2+} sparks and their function in human cerebral arteries. Stroke *33*, 802-808.

Wellman, G.C., and Nelson, M.T. (2003). Signaling between SR and plasmalemma in smooth muscle: sparks and the activation of Ca^{2+}-sensitive ion channels. Cell Calcium *34*, 211-229.

Wellman, G.C., Santana, L.F., Bonev, A.D., and Nelson, M.T. (2001). Role of phospholamban in the modulation of arterial Ca^{2+} sparks and Ca^{2+}-activated K^+ channels by cAMP. Am J Physiol Cell Physiol *281*, C1029-1037.

Wellum, G.R., Irvine, T.W., Jr., and Zervas, N.T. (1980). Dose responses of cerebral arteries of the dog, rabbit, and man to human hemoglobin in vitro. J Neurosurg *53*, 486-490.

Wellum, G.R., Irvine, T.W., Jr., and Zervas, N.T. (1982). Cerebral vasoactivity of heme proteins in vitro. Some mechanistic considerations. J Neurosurg *56*, 777-783.

Welsh, D.G., Morielli, A.D., Nelson, M.T., and Brayden, J.E. (2002). Transient receptor potential channels regulate myogenic tone of resistance arteries. Circ Res *90*, 248-250.

Welsh, D.G., Nelson, M.T., Eckman, D.M., and Brayden, J.E. (2000). Swelling-activated cation channels mediate depolarization of rat cerebrovascular smooth muscle by hyposmolarity and intravascular pressure. J Physiol *527 Pt 1*, 139-148.

Weyer, G.W., Jahromi, B.S., Aihara, Y., Agbaje-Williams, M., Nikitina, E., Zhang, Z.D., and Macdonald, R.L. (2006). Expression and function of inwardly rectifying potassium channels after experimental subarachnoid hemorrhage. J Cereb Blood Flow Metab *26*, 382-391.

Williams, L.T., and Tremble, P. (1982). Binding of a calcium antagonist, [3H]nitrendipine, to high affinity sites in bovine aortic smooth muscle and canine cardiac membranes. J Clin Invest *70*, 209-212.

Worley, J.F., Quayle, J.M., Standen, N.B., and Nelson, M.T. (1991). Regulation of single calcium channels in cerebral arteries by voltage, serotonin, and dihydropyridines. Am J Physiol *261*, H1951-1960.

Wu, B.N., Luykenaar, K.D., Brayden, J.E., Giles, W.R., Corteling, R.L., Wiehler, W.B., and Welsh, D.G. (2007). Hyposmotic challenge inhibits inward rectifying K^+ channels in cerebral arterial smooth muscle cells. American journal of physiology *292*, H1085-1094.

Xu, C., Lu, Y., Tang, G., and Wang, R. (1999). Expression of voltage-dependent K^+ channel genes in mesenteric artery smooth muscle cells. Am J Physiol *277*, G1055-1063.

Xu, H.L., Feinstein, D.L., Santizo, R.A., Koenig, H.M., and Pelligrino, D.A. (2002a). Agonist-specific differences in mechanisms mediating eNOS-dependent pial arteriolar dilation in rats. Am J Physiol Heart Circ Physiol *282*, H237-243.

Xu, H.L., Santizo, R.A., Baughman, V.L., and Pelligrino, D.A. (2002b). ADP-induced pial arteriolar dilation in ovariectomized rats involves gap junctional communication. Am J Physiol Heart Circ Physiol *283*, H1082-1091.

Xu, H.L., Santizo, R.A., Koenig, H.M., and Pelligrino, D.A. (2001). Chronic estrogen depletion alters adenosine diphosphate-induced pial arteriolar dilation in female rats. Am J Physiol Heart Circ Physiol *281*, H2105-2112.

Yamaguchi, H., Muth, J.N., Varadi, M., Schwartz, A., and Varadi, G. (1999). Critical role of conserved proline residues in the transmembrane segment 4 voltage sensor function and in the gating of L-type calcium channels. Proc Natl Acad Sci U S A *96*, 1357-1362.

Yanagisawa, M., Kurihara, H., Kimura, S., Tomobe, Y., Kobayashi, M., Mitsui, Y., Yazaki, Y., Goto, K., and Masaki, T. (1988). A novel potent vasoconstrictor peptide produced by vascular endothelial cells. Nature *332*, 411-415.

Yarotskyy, V., Gao, G., Peterson, B.Z., and Elmslie, K.S. (2009). The Timothy syndrome mutation of cardiac $Ca_V1.2$ (L-type) channels: multiple altered gating mechanisms and pharmacological restoration of inactivation. J Physiol *587*, 551-565.

Yergey, J.A., and Heyes, M.P. (1990). Brain eicosanoid formation following acute penetration injury as studied by in vivo microdialysis. J Cereb Blood Flow Metab *10*, 143-146.

You, J., Johnson, T.D., Childres, W.F., and Bryan, R.M., Jr. (1997). Endothelial-mediated dilations of rat middle cerebral arteries by ATP and ADP. Am J Physiol *273*, H1472-1477.

You, J., Johnson, T.D., Marrelli, S.P., and Bryan, R.M., Jr. (1999). Functional heterogeneity of endothelial P2 purinoceptors in the cerebrovascular tree of the rat. Am J Physiol *277*, H893-900.

Yundt, K.D., Grubb, R.L., Jr., Diringer, M.N., and Powers, W.J. (1998). Autoregulatory vasodilation of parenchymal vessels is impaired during cerebral vasospasm. J Cereb Blood Flow Metab *18*, 419-424.

Zalk, R., Lehnart, S.E., and Marks, A.R. (2007). Modulation of the ryanodine receptor and intracellular calcium. Annu Rev Biochem *76*, 367-385.

Zaritsky, J.J., Eckman, D.M., Wellman, G.C., Nelson, M.T., and Schwarz, T.L. (2000). Targeted disruption of $K_{ir}2.1$ and $K_{ir}2.2$ genes reveals the essential role of the inwardly rectifying K^+ current in K^+-mediated vasodilation. Circ Res *87*, 160-166.

Zhang, S., Wang, L., Liu, M., and Wu, B. (2010). Tirilazad for aneurysmal subarachnoid haemorrhage. Cochrane Database Syst Rev *2*, CD006778.

Zhao, G., Zhao, Y., Pan, B., Liu, J., Huang, X., Zhang, X., Cao, C., Hou, N., Wu, C., Zhao, K.S., *et al.* (2007). Hypersensitivity of BK_{Ca} to Ca^{2+} sparks underlies hyporeactivity of arterial smooth muscle in shock. Circ Res *101*, 493-502.

Zhou, Y., Dirksen, W.P., Zweier, J.L., and Periasamy, M. (2004). Endothelin-1-induced responses in isolated mouse vessels: the expression and function of receptor types. Am J Physiol Heart Circ Physiol *287*, H573-578.

ZhuGe, R., Tuft, R.A., Fogarty, K.E., Bellve, K., Fay, F.S., and Walsh, J.V., Jr. (1999). The influence of sarcoplasmic reticulum Ca^{2+} concentration on Ca^{2+} sparks and spontaneous transient outward currents in single smooth muscle cells. J Gen Physiol *113*, 215-228.

Zuber, M.X., Goodman, D.W., Karns, L.R., and Fishman, M.C. (1989). The neuronal growth-associated protein GAP-43 induces filopodia in non-neuronal cells. Science (New York, NY *244*, 1193-1195.

Zubkov, A., Miao, L., and Zhang, J. (2004). Signal transduction of ET-1 in contraction of cerebral arteries. J Cardiovasc Pharmacol *44 Suppl 1*, S24-26.

Zuccarello, M., Boccaletti, R., Tosun, M., and Rapoport, R.M. (1996a). Role of extracellular Ca^{2+} in subarachnoid hemorrhage-induced spasm of the rabbit basilar artery. Stroke *27*, 1896-1902.

Zuccarello, M., Bonasso, C.L., Lewis, A.I., Sperelakis, N., and Rapoport, R.M. (1996b). Relaxation of subarachnoid hemorrhage-induced spasm of rabbit basilar artery by the K^+ channel activator cromakalim. Stroke *27*, 311-316.

Zygmunt, P.M., and Hogestatt, E.D. (1996). Role of potassium channels in endothelium-dependent relaxation resistant to nitroarginine in the rat hepatic artery. Br J Pharmacol *117*, 1600-1606.

APPENDIX A: BOOK CHAPTER

Assessment of Intracellular Calcium in Cerebral Artery Myocytes.

Matthew A. Nystoriak[1], Masayo Koide[1], George C. Wellman[1,2]

Departments of Pharmacology[1] and Surgery, Division of Neurosurgery[2], University of Vermont, College of Medicine, Burlington, VT.

Contact Information: G. C. Wellman, Univ. of Vermont, Dept. of Pharmacology, Given Bldg., 89 Beaumont Ave., Burlington, VT 05405-0068 (e-mail: george.wellman@uvm.edu).

Abstract

Vascular tone and consequently, cerebral blood flow, are regulated by the concentration of global cytosolic Ca^{2+} (global $[Ca^{2+}]_i$) in vascular smooth muscle. Global $[Ca^{2+}]_i$ is, in part, regulated by discrete Ca^{2+} release events from the sarcoplasmic reticulum (Ca^{2+} sparks) which activate plasma membrane large conductance Ca^{2+}-activated K^+ channels to cause membrane potential hyperpolarization, decreased global $[Ca^{2+}]_i$, and vasodilation. We have previously observed decreased Ca^{2+} spark frequency and elevated global $[Ca^{2+}]_i$ in cerebral artery myocytes using a rabbit model of subarachnoid hemorrhage. Here, we describe and discuss laboratory methods and procedures using the fluorescent Ca^{2+} indicator dyes fura-2 and fluo-4 to assess global and local Ca^{2+} signaling in cerebral arteries and isolated vascular myocytes.

Keywords: Fura-2, Fluo-4, Ca^{2+} sparks, vascular smooth muscle, subarachnoid hemorrhage.

1. Introduction

The cerebral circulation delivers constant blood flow to the brain over a broad range of physiological blood pressures. To achieve this remarkable phenomenon, cerebral arteries must actively constrict to elevations in blood pressure and dilate when blood pressure drops. In cerebral resistance arteries and arterioles, the constriction (myogenic tone) response to graded increases in intravascular pressure is dependent on membrane potential depolarization, enhanced Ca^{2+} influx via L-type voltage-dependent Ca^{2+} channels (VDCCs) and elevated global cytosolic Ca^{2+} (global $[Ca^{2+}]_i$) [1-2]. Global $[Ca^{2+}]_i$ represents average Ca^{2+} levels throughout the cytoplasm and mediates contraction of smooth muscle via Ca^{2+}/calmodulin-dependent activation of myosin light chain kinase, myosin light chain phosphorylation and actin-myosin interaction [3]. Thus, global $[Ca^{2+}]_i$ directly regulates the contractile state of vascular smooth muscle and therefore dictates cerebral vascular tone and blood flow.

The discovery of spatially localized, transient calcium release events ("Ca^{2+} sparks") has altered the view that an elevation of global $[Ca^{2+}]_i$ is the only effective mode of calcium signaling in smooth muscle [4-6]. Calcium sparks result from the opening of a cluster of ryanodine receptors in the sarcoplasmic reticulum (SR) membrane, causing a highly restricted (1% of the cell volume) and large (μM) increase in local Ca^{2+} with little direct effect on global $[Ca^{2+}]_i$ [5, 7]. In vascular smooth muscle, Ca^{2+} sparks are functionally coupled to nearby large conductance Ca^{2+}-activated K^+ (BK) channels located on the plasma membrane [6, 8]. Elevation of intracellular Ca^{2+} causes a shift in the voltage-

dependence of BK channel activation to more negative membrane potentials effectively leading to increased channel open probability [9]. Increased Ca^{2+} spark activity therefore leads to enhanced BK channel activity, membrane potential hyperpolarization, decreased global $[Ca^{2+}]_i$, and smooth muscle relaxation. Ca^{2+} spark activity is increased by vasodilators such as nitric oxide and forskolin and by elevations in cytosolic and SR calcium [10-11]. Thus, Ca^{2+} sparks act as an important negative feedback mechanism to oppose vasoconstriction by promoting a reduction in VDCC activity and a decrease in global $[Ca^{2+}]_i$.

Considering the pivotal role that vascular smooth muscle Ca^{2+} plays in the regulation of cerebral blood flow, precise measurement of local and global Ca^{2+} signaling in these cells is essential for understanding pathologies characterized by abnormal vascular tone, such as aneurysmal subarachnoid hemorrhage (SAH). With respect to SAH-induced "classical" or "angiographic" vasospasm, observed in large diameter conduit arteries on the brain surface, the role of elevated global $[Ca^{2+}]_i$ is unclear and controversial [12]. However, recent evidence suggests that enhanced constriction of much smaller "resistance" arteries and arterioles (< 200 μm in diameter) following SAH is associated with increased global $[Ca^{2+}]_i$ and enhanced VDCC activity [13]. Further, Ca^{2+} spark activity is decreased in cerebral arteries by the blood component oxyhemoglobin [14] and Ca^{2+} spark frequency is reduced in cerebral artery myocytes isolated from SAH model animals [13, 15]. In this chapter, we discuss the properties of two fluorescent Ca^{2+} indicator dyes, fura-2 and fluo-4, that enable the measurement of global $[Ca^{2+}]_i$ and Ca^{2+}

sparks, respectively, in cerebral artery myocytes. Further, we provide details of specific protocols used in our laboratory to assess global and local signaling in the cerebral vasculature.

2.1 The use of fura-2 to measure global $[Ca^{2+}]_i$ in cerebral artery smooth muscle.

The most popular technique for quantifying intracellular free Ca^{2+} is by monitoring the fluorescence of Ca^{2+}-sensitive indicator dyes [16]. The dual-wavelength ratiometric indicator fura-2 is currently the most widely used indicator for measurement of global $[Ca^{2+}]_i$ in isolated cerebral artery myocytes and intact pressurized vessels. Fura-2 shows 1:1 Ca^{2+} binding stoichiometry and undergoes a significant shift in excitation spectra depending on whether or not Ca^{2+} is bound (λ_{bound} = 340 nm; λ_{free} = 380 nm) while emission spectra (510 nm) is independent of Ca^{2+} binding to the dye [17]. Changes in fluorescence ratios are therefore independent of intensity, eliminating potentially confounding factors such as differential dye loading, photobleaching or time-dependent explusion of the dye by the cell. As a result, fura-2 is preferred over single-wavelength intensity-modulating indicators for quantification of absolute intracellular Ca^{2+} concentrations. In this section, we describe techniques used for measuring global $[Ca^{2+}]_i$ in intact pressurized cerebral arteries using fura-2.

2.2 Materials and Instruments

- 5 ml myograph chamber (Fig. 1A) (Living Systems Instrumentation)
- Fine-tipped forceps (Fine Science Tools)
- Cell-permeant fura-2 AM (Invitrogen)
- Calcium and diameter recording system (e.g. IonOptix Inc.)
  - Hyperswitch light source
  - Xenon arc lamp
  - IonWizard-Core and Analysis Soft Edge software
  - Fluorescence system interface
  - Myocam-S digital CCD video camera
  - Photomultiplier tube (PMT) sub-system
  - Dichroic mirror
  - Photon-to-voltage converter
- Inverted fluorescence microscope
- 20X/0.50 NA objective lens
- Peristaltic pump (Ismatec Inc.)
- PS-200 pressure servo controller with peristaltic pump (Living Systems Instrumentation)
- Dark room/red light

2.3 Procedures

Tissue preparation and dye loading:

Cerebral arteries and arterioles (50-200 μm in diameter) are dissected from the brain and kept in ice cold artificial cerebral spinal fluid (aCSF) of the following composition (in mM): 125 NaCl, 3 KCl, 18 $NaHCO_3$, 1.25 NaH_2PO_4, 1 $MgCl_2$, 2 $CaCl_2$, 5 glucose aerated with 5% CO_2, 20% O_2, 75% N_2 (pH, 7.30-7.35). Freshly isolated cerebral artery segments are cannulated on glass micropipettes mounted in a 5 ml myograph chamber (Fig. 1) [18]. Following cannulation, blood vessels are incubated with previously aerated aCSF containing fura-2 AM (acetoxymethyl ester membrane-permeable form; 5 μM; Invitrogen, Carlsbad, CA) and pluronic acid (0.1%; Invitrogen, Carlsbad, CA) at room temperature (~22˚C) for 45 minutes in the dark. The myograph chamber is then mounted on an inverted fluorescence microscope and arteries are pressurized and continuously superfused with aCSF (37˚C, 30 min) to allow equilibration and deesterification of fura-2.

It has previously been demonstrated that Ca^{2+} can be selectively measured in vascular smooth muscle or endothelium by loading fura-2 from the extraluminal or luminal side of the vessel, respectively [19]. However, the specific loading time and dye concentration described above may need to be slightly adjusted based on the specific tissue studied to enable sufficient permeation of dye into smooth muscle while avoiding loading of the dye into the endothelium. To examine whether dye loading is smooth muscle-specific, studies can be performed on arteries in which the endothelium is physically removed by

luminal passage of an air bubble [2]. Endothelial removal can be confirmed by lack of response to endothelium-specific pharmacological agents (e.g. acetylcholine, bradykinin, NS309) [20-21].

Data acquisition and estimation of intracellular Ca^{2+}:

First, an aperture located adjacent to the dichroic mirror is adjusted so that the blood vessel completely fills the rectangular field of view in the data acquisition software. This minimizes the contribution of extraneous light to the fluorescence signal. The dichroic mirror reflects fluorescence emission to the photomultiplier tube (PMT) while the use of a red filter in the microscope condenser allows the vessel image to be transmitted to the CCD camera. Thus, the image collected by the CCD camera for diameter measurement represents the same field from which fluorescence is detected by the PMT.

Following equilibration, fluorescence ratio (F_{340}:F_{380}) is obtained from background-corrected 510 nm emission from arteries alternately excited at 340 and 380 nm (Fig. 2) using software developed by IonOptix (Milton, MA). Arterial wall [Ca^{2+}] is estimated using the following equation [17] $[Ca^{2+}] = K_d \times \beta \times (R - R_{min})/(R_{max} - R)$.

R_{min} and R_{max} values represent the ratios of emission signal under Ca^{2+}-free and Ca^{2+}-saturated conditions, respectively. To obtain these values, arteries are first loaded with fura-2 and equilibrated as described above. Arteries are then perfused (10 min, 37˚C) with a baseline solution containing the following (in mM): 5 NaCl, 140 KCl, 5 HEPES, 1 $MgCl_2$ (pH 7.4). Next, to obtain R_{min}, arteries are perfused (30 min) with baseline

solution that includes EGTA (5 mM), ionomycin (10 μM) and nigericin (5 μM). Recording at the end of this period allows determination of R_{min}. EGTA is then washed from the bath by perfusion of baseline solution for 15 min. To obtain R_{max}, arteries are then perfused (15 min) with baseline solution containing $CaCl_2$ (10 mM), ionomycin (10 μM) and nigericin (5 μM) for 10 min. The ratio of calcium-free over calcium-bound fluorescence intensities at F_{380} (β) is determined from these values. In our studies, we have used an apparent dissociation constant (K_d) of 282 nM of fura-2 for Ca^{2+} determined by Knot and Nelson using rat cerebral arteries [2].

Measurement of arterial diameter

Luminal diameter is simultaneously recorded throughout the entire experiment using a CCD camera and the length-calibrated video edge detection function of IonOptix software (Fig. 1D and 2). Constriction is analyzed as the decrease in arterial diameter relative to the passive diameter using the following equation [22]:

$$\%constriction = \frac{DP - DA}{DP} X 100$$

where DP is the passive (fully-dilated) diameter of the artery in Ca^{2+}-free aCSF containing a VDCC blocker (e.g. 100 μM diltiazem or 300 nM nifedipine) and a second vasodilator such as forskolin (1 μM) and DA is the active diameter of the artery in response to the stimulus in aCSF. Percent dilation can be obtained using the following formula [22]:

$$\%Dilation = \frac{DV - DA}{DP - DA} X 100$$

where DV is the arterial diameter in the presence of vasodilator, DA is the active arterial diameter before application of vasodilator, and DP is the passive arterial diameter.

Variations in measurement of global $[Ca^{2+}]_i$

Most investigators obtain ratiometric measurements of fura-2 in isolated arterial segments or dissociated cerebral artery myocytes by collecting emitted photons using a photomultiplier tube (PMT). Fluorescence detection may also be achieved using electron multiplying CCD or intensified CCD cameras along with quantitative ratio imaging software for analysis and estimation of intracellular Ca^{2+} [2]. However, high sensitivity cameras required for these measurements are expensive and do not offer significant spatial information when used with wide-field microscopy. In cases where an investigator wishes to measure fura-2 fluorescence in a specific layer of the vascular wall (smooth muscle or endothelium), fluorescent imaging over photometric methods may be advantageous.

3.1 The use of fluo-4 to measure Ca^{2+} sparks in cerebral artery myocytes.

Single-wavelength Ca^{2+} indicators such as fluo-4, or its analogue fluo-3, have become widely used for imaging of fast, small volume Ca^{2+} signaling events such as Ca^{2+} sparks [23]. One advantage of fluo-4 over ratiometric indicators (e.g. fura-2) in the measurement sub-cellular Ca^{2+} signaling events is superior signal-to-noise ratio. Fluo-4 is excited at 488 nm and exhibits increased fluorescence intensity (>100 fold) upon binding Ca^{2+} without a shift in absorption or emission spectra [24]. Moreover, fluo-4 has a lower affinity for Ca^{2+} than fura-2 ($K_d \approx 400$ nM compared with $K_d \approx 282$ nM for fura-2) and fast binding and unbinding kinetics, making it suitable for tracking rapid Ca^{2+} signaling events [24]. Ca^{2+} sparks can be measured using a number of imaging approaches including single photon and multiphoton confocal microscopy, total internal reflection fluorescence (TIRF) microscopy, and wide-field microscopy using low-noise CCD cameras [23].

Previously, the temporal resolution of laser-scanning confocal microscope systems sufficient to measure Ca^{2+} sparks could only be achieved using line-scan mode, as opposed to two-dimensional (2-D) x-y image scanning [5]. However, the interpretation of images obtained using line-scanning is complicated by uncertainties in the position of the scan line with regard to the center of the Ca^{2+} release event resulting in a loss of spatial information such as accurate determination of Ca^{2+} spark area. Another disadvantage of this method is the inability to measure the total number of active spark

sites within a cell. Currently, a number of laser-scanning confocal microscope systems with sufficient 2-D sampling frequency (>30 Hz) are available. The following section provides a detailed description of protocols that we have used to measure Ca^{2+} sparks in cerebral artery myocytes using fluo-4 and two-dimensional (2-D) laser-scanning confocal microscopy.

3.2 Materials and Instruments

- Cell chamber with glass coverslip bottom
- Cell-permeant fluo-4 AM (Invitrogen)
- Laser scanning confocal system (e.g. Oz, Noran Instruments)
- Inverted fluorescence microscope (Nikon Diaphot)
- 60X/1.2 NA water-immersion objective lens
- Krypton/argon laser (480 nm is used to excite fluo-4)
- Dark room

3.3 Procedures

Isolation of cerebral artery myocytes:

Cerebral arteries are enzymatically dissociated to obtain individual smooth muscle cells (Fig. 3) [25]. After dissection, cerebral arteries are incubated in a glutamate-containing isolation solution (GIS) of the following composition (in mM) : 55 NaCl, 5.6 KCl, 80 L-glutamic acid (mono-sodium salt), 2.0 $MgCl_2$, 2 $CaCl_2$, 10 HEPES, 10 glucose (pH 7.3;

37 °C; 30 min) using a 1 ml vial placed in a water bath. Arteries are then transferred to a Ca^{2+}-free GIS containing papein (0.3 mg/mL) and 1,4-dithioerythriol (0.7 mg/mL; 37°C; 17 min) using a fire-polished Pasteur pipette. Next, arteries are incubated in GIS containing collagenase type F (0.7 mg/mL), collagenase type H (0.3 mg/mL) and 100 μM $CaCl_2$ (37 °C; 20 min). Finally, arteries are incubated in GIS containing 2 mM $CaCl_2$ on ice (3x; 10 min) and gently triturated into individual cerebral artery myocytes using a small bore fire-polished Pasteur pipette. Cerebral artery myocytes can easily be identified by characteristic spindle-shaped morphology (Fig. 3). The cells are kept on ice and used within six hours of isolation.

Dye loading:

Isolated myocytes are loaded with fluo-4 by mixing equal volumes (e.g. 250 μl) of cell suspension and HEPES buffered physiological saline solution (HEPES-PSS) of the following composition (in mM): 134 NaCl, 6 KCl, 1 $MgCl_2$, 1.8 $CaCl_2$, 10 glucose, 10 HEPES (pH 7.4) containing fluo-4 AM (20 μM) and pluronic acid (0.072%). The cell suspension containing a final concentration of 10 μM fluo-4 and 0.036% pluronic acid is placed in the recording chamber to allow cells to attach to the glass coverslip on the bottom of the chamber during the 30 minute loading/deesterification period at room temperature. Cells are then washed three times with HEPES-PSS.

Ca^{2+} spark measurement:

Initially, cells are located using bright field illumination. Once a myocyte has been centered in the scan field, images of emitted light (wavelengths >500 nm) are acquired at a frequency of 58 Hz (every ~ 17 msec, 256 pixels x 256 pixels), and magnified (2X) by acquisition software (68 μm for 256 pixels). Images are usually acquired for a period of 10-20 seconds and saved for future analysis (Fig. 4). Laser exposure can lead to cell damage which typically causes the cells to become much brighter in appearance and abolish Ca^{2+} spark activity. Excessive laser exposure can also lead to photo-bleaching of the indicator dye. Thus, it is recommended to combine the lowest laser intensity that provides good cell visualization with relatively short (10-20 seconds) periods of laser exposure.

Measurement of Ca^{2+} sparks can also be performed in intact pressurized cerebral arteries (Fig. 5) [11, 14, 26]. After dissection, intact arteries are loaded with fluo-4 AM (10 μM at room temperature for 1 hr, with 0.036% pluronic acid) followed by brief washes with aCSF (see section 2.3). Arteries are then cannulated, pressurized (see section 2.3) and Ca^{2+} sparks imaged using 2-D laser-scanning confocal microscopy as described above for isolated myocytes. Measurement of Ca^{2+} sparks in the intact tissue provides the ability to simultaneously examine events in multiple cells under more physiological conditions (i.e. at physiological intravascular pressures). However, due to the presence of connective tissue and multiple cell layers, the signal-to-noise ratio is decreased in images

from intact tissue compared to isolated cells. Thus, imaging performed on isolated cells is preferred for detailed analysis of the spatio-temporal properties of Ca^{2+} sparks.

Analysis of Ca^{2+} sparks:

A variety of custom-written software packages provide the ability to detect and analyze Ca^{2+} sparks. Ca^{2+} sparks are typically assessed using 2.1 μm X 2.1 μm analysis areas (centered over the Ca^{2+} spark-induced peak in fluorescence intensity) and defined as fractional fluorescence changes (F/F_0) greater than 1.3 [5, 25]. Background fluorescence intensity (F_0) is determined within analysis areas by averaging the first 30 consecutive images without Ca^{2+} spark activity (for example, see Fig. 4B). Frequency is the most commonly used parameter to describe Ca^{2+} spark activity. In isolated myocytes, Ca^{2+} spark frequency, expressed in Hz, represents the total number of events occurring in a cell divided by the sampling period (in seconds). In cerebral artery myocytes, Ca^{2+} spark frequency is increased by vasodilators acting via increased cyclic AMP-dependent protein kinase, cyclic GMP-dependent protein kinase and/or increased levels of cytosolic or SR Ca^{2+} [6, 10-11]. Conversely, enhanced cerebral artery constriction following subarachnoid hemorrhage is associated with a reduction in Ca^{2+} spark frequency in cerebral artery myocytes [13, 15]. Ca^{2+} spark amplitude is frequently expressed as the maximum fractional fluorescence (F/F_0) increase (Fig 5C). Using Ca^{2+} spark-induced large conductance Ca^{2+}-activated K^+ (BK) channel activity as a biological Ca^{2+} indicator, Perez et al. have estimated that local increases in Ca^{2+} during a Ca^{2+} spark are in the range of 4-30 μM [7]. Although Ca^{2+} concentrations can be estimated using non-

ratiometric Ca^{2+} indicator dyes such as fluo-4, using the equation: $[Ca^{2+}] = Kd * F /(F_{max}-F)$ [23], given the Kd of fluo-4 is ≈ 0.4 μM, this approach may underestimate local Ca^{2+} concentrations attained during Ca^{2+} sparks. Other frequently reported spatio-temporal characteristics of Ca^{2+} sparks include spark size or area (defined as the area measured at 50% peak amplitude), rise time (measured from 10-90% rise in signal), decay time constants and half-time to decay [27].

4.1 Conclusions

In this chapter, we provide a description of procedures used to assess both global and local Ca^{2+} signaling in cerebral artery myocytes using the Ca^{2+}-sensitive fluorescent dyes fura-2 and fluo-4. The ratiometric Ca^{2+} sensitive dye fura-2 is considered the indicator of choice for measurement of global cytosolic Ca^{2+}, or averaged Ca^{2+} levels throughout the cytoplasm. On the other hand, transient Ca^{2+} release events from the SR (Ca^{2+} sparks) require the use of single-wavelength Ca^{2+} indicators such as fluo-4. A thorough knowledge of these Ca^{2+} signaling processes is imperative for understanding mechanisms contributing to cerebral vascular pathologies such as subarachnoid hemorrhage.

Acknowledgements

This work was supported by the Totman Medical Research Trust Fund, the Peter Martin Brain Aneurysm Endowment, the NIH (NIHLBI, R01 HL078983, HL078983-05S1 and NCRR, P20 RR16435) and the American Heart Association (0725837T, 0815736D). The authors wish to thank to Dr. Adrian Bonev for his helpful comments and suggestions. The authors would also like to acknowledge the University of Vermont Neuroscience COBRE imaging core facilities.

5. References

1. Harder DR (1984) Pressure-dependent membrane depolarization in cat middle cerebral artery. Circ Res 55:197-202
2. Knot HJ, Nelson MT (1998) Regulation of arterial diameter and wall [Ca^{2+}] in cerebral arteries of rat by membrane potential and intravascular pressure. J Physiol 508 (Pt 1):199-209
3. Hai CM, Murphy RA (1989) Ca^{2+}, crossbridge phosphorylation, and contraction. Annu Rev Physiol 51:285-298
4. Cheng H, Lederer WJ, Cannell MB (1993) Calcium sparks: elementary events underlying excitation-contraction coupling in heart muscle. Science 262:740-744
5. Nelson MT, Cheng H, Rubart M, Santana LF, Bonev AD, Knot HJ, Lederer WJ (1995) Relaxation of arterial smooth muscle by calcium sparks. Science 270:633-637
6. Wellman GC, Nelson MT (2003) Signaling between SR and plasmalemma in smooth muscle: sparks and the activation of Ca^{2+}-sensitive ion channels. Cell Calcium 34:211-229
7. Perez GJ, Bonev AD, Nelson MT (2001) Micromolar Ca^{2+} from sparks activates Ca^{2+}-sensitive K^{+} channels in rat cerebral artery smooth muscle. Am J Physiol Cell Physiol 281:C1769-1775
8. Gollasch M, Wellman GC, Knot HJ, Jaggar JH, Damon DH, Bonev AD, Nelson MT (1998) Ontogeny of local sarcoplasmic reticulum Ca^{2+} signals in cerebral arteries: Ca^{2+} sparks as elementary physiological events. Circ Res 83:1104-1114
9. Cox DH, Cui J, Aldrich RW (1997) Allosteric gating of a large conductance Ca-activated K^{+} channel. J Gen Physiol 110:257-281
10. Porter VA, Bonev AD, Knot HJ, Heppner TJ, Stevenson AS, Kleppisch T, Lederer WJ, Nelson MT (1998) Frequency modulation of Ca^{2+} sparks is involved in regulation of arterial diameter by cyclic nucleotides. Am J Physiol 274:C1346-1355
11. Wellman GC, Santana LF, Bonev AD, Nelson MT (2001) Role of phospholamban in the modulation of arterial Ca^{2+} sparks and Ca^{2+}-activated K^{+} channels by cAMP. Am J Physiol Cell Physiol 281:C1029-1037
12. Wellman GC (2006) Ion channels and calcium signaling in cerebral arteries following subarachnoid hemorrhage. Neurol Res 28:690-702
13. Koide M, Nystoriak, M.A., Wellman, G.C. (2010) Impact of subarachnoid hemorrhage on local and global calcium signaling in cerebral artery myocytes
Acta Neurochir Suppl.
14. Jewell RP, Saundry CM, Bonev AD, Tranmer BI, Wellman GC (2004) Inhibition of Ca^{++} sparks by oxyhemoglobin in rabbit cerebral arteries. J Neurosurg 100:295-302
15. Koide M, Krishnamoorthy, G., O'Connor, K.P., Nystoriak, M.A., Nelson, M.T., Wellman, G.C. (2009) Decreases of Ca^{2+} spark frequency and ryanodine receptor-2 expression in cerebral artery myocytes after subarachnoid hemorrhage. Biophys J 96:278a-279a
16. Kao JP (1994) Practical aspects of measuring [Ca^{2+}] with fluorescent indicators. Methods Cell Biol 40:155-181

17. Grynkiewicz G, Poenie M, Tsien RY (1985) A new generation of Ca^{2+} indicators with greatly improved fluorescence properties. J Biol Chem 260:3440-3450
18. Ishiguro M, Puryear CB, Bisson E, Saundry CM, Nathan DJ, Russell SR, Tranmer BI, Wellman GC (2002) Enhanced myogenic tone in cerebral arteries from a rabbit model of subarachnoid hemorrhage. Am J Physiol Heart Circ Physiol 283:H2217-2225
19. Marrelli SP (2000) Selective measurement of endothelial or smooth muscle $[Ca^{2+}]_i$ in pressurized/perfused cerebral arteries with fura-2. J Neurosci Methods 97:145-155
20. Kleppisch T, Nelson MT (1995) ATP-sensitive K^+ currents in cerebral arterial smooth muscle: pharmacological and hormonal modulation. Am J Physiol 269:H1634-1640
21. Dalsgaard T, Kroigaard C, Bek T, Simonsen U (2009) Role of calcium-activated potassium channels with small conductance in bradykinin-induced vasodilation of porcine retinal arterioles. Invest Ophthalmol Vis Sci 50:3819-3825
22. Zaritsky JJ, Eckman DM, Wellman GC, Nelson MT, Schwarz TL (2000) Targeted disruption of Kir2.1 and Kir2.2 genes reveals the essential role of the inwardly rectifying K^+ current in K^+-mediated vasodilation. Circ Res 87:160-166
23. Cheng H, Lederer WJ (2008) Calcium sparks. Physiol Rev 88:1491-1545
24. Gee KR, Brown KA, Chen WN, Bishop-Stewart J, Gray D, Johnson I (2000) Chemical and physiological characterization of fluo-4 Ca^{2+}-indicator dyes. Cell Calcium 27:97-106
25. Wellman GC, Nathan DJ, Saundry CM, Perez G, Bonev AD, Penar PL, Tranmer BI, Nelson MT (2002) Ca^{2+} sparks and their function in human cerebral arteries. Stroke 33:802-808
26. Mandala M, Heppner TJ, Bonev AD, Nelson MT (2007) Effect of endogenous and exogenous nitric oxide on calcium sparks as targets for vasodilation in rat cerebral artery. Nitric Oxide 16:104-109
27. Perez GJ, Bonev AD, Patlak JB, Nelson MT (1999) Functional coupling of ryanodine receptors to K_{Ca} channels in smooth muscle cells from rat cerebral arteries. J Gen Physiol 113:229-238
28. Nystoriak MA, Murakami K, Penar PL, Wellman GC (2009) $Ca_v1.2$ splice variant with exon 9* is critical for regulation of cerebral artery diameter. Am J Physiol Heart Circ Physiol 297:H1820-1828

Figure Legends

Figure 1: Arteriograph chamber for intact pressurized cerebral arteries. A. Overhead view of 5 mL arteriograph chamber used for cannulation of cerebral artery segments. B. Glass micropipettes are pulled from capillary tubes and mounted in an arteriograph chamber. C. Image of a rat posterior cerebral artery (~150 μm diameter) cannulated on glass micropipettes. Suture thread is used to tie each end of the artery segment onto the micropipettes. D. Image of rat parenchymal arteriole (~60 μm diameter). Video edge detection (black horizontal lines) is used for measurement of arterial diameter.

Figure 2: Simultaneous measurement of global $[Ca^{2+}]_i$ and diameter of an intact pressurized cerebral artery. Fluorescence intensity (photomultiplier tube counts) at 340 nm and 380 nm excitation (F340 and F380, respectively), F340/F380 ratio, calculated free $[Ca^{2+}]_i$ and arterial diameter from a pressurized rabbit cerebellar artery. Smooth muscle membrane potential depolarization induced by elevating extracellular K^+ from 3 mM to 60 mM caused an increased in F340/F380 ratio (i.e. increased free $[Ca^{2+}]_i$) and vasoconstriction. The response to 60 mM K^+ was reversed by application of the VDCC blocker nifedipine (1 μM).

Figure 3: Freshly isolated native cerebral artery myocytes. A. Cerebral arteries were enzymatically dissociated to obtain isolated vascular smooth muscle cells. Image shows

individual smooth muscle cells using differential interference contrast microscopy (40X). B. Vascular smooth muscle can be identified by spindle-shaped cell morphology as well as immunostaining of smooth muscle alpha actin and smooth muscle myosin heavy chain. Scale bars represent 10 μm. From Nystoriak et al., *Am. J. Physiol*., 2009 [28] with permission.

Figure 4: Ca^{2+} sparks in isolated cerebral artery myocytes. A. Original images of a Ca^{2+} spark recorded every 17 msec from an isolated cerebral artery myocyte. White scale bar represents 10 μm. Red arrow indicates a Ca^{2+} spark. B. F_0 image obtained by averaging 30 consecutive images without a Ca^{2+} spark. Trace represents time course of fractional fluorescence changes (F/F_0) during the Ca^{2+} spark shown in panel A using the analysis area (2.1 μm x 2.1 μm) depicted as a red square in the F_0 image. Gray bar represents time elapsed during the images shown in panel A. C. Pseudo-colored images of the same Ca^{2+} spark depicted in panels A and B. Each pixel is converted to pseudo-color shown in the color bar to the right of the images. White scale bar represents 10 μm.

Figure 5: Ca^{2+} sparks in intact pressurized cerebral arteries. Ca^{2+} sparks were recorded in 56 μm x 53 μm areas of intact pressurized mouse cerebral arteries in the absence (A) and presence (B) of forskolin (10 μM), an activator of adenylyl cyclase. During a 10 second recording period, a total of 13 Ca^{2+} sparks were observed in the image depicted in panel A, and a total of 38 Ca^{2+} sparks were observed in the image depicted in panel B. White boxes represent sites where Ca^{2+} sparks occurred. Three

representative F/F_0 records (a-c) corresponding to three Ca^{2+} sparks sites (a-c) from each artery are displayed below their corresponding artery image. Horizontal scale bars represent a time of 1 second, and vertical scale bars represent a fractional fluorescence (F/F_0) change of 0.5. From Wellman et al., *Am. J. Physiol. Cell Physiol*., 2001 [11] with permission.

Figures

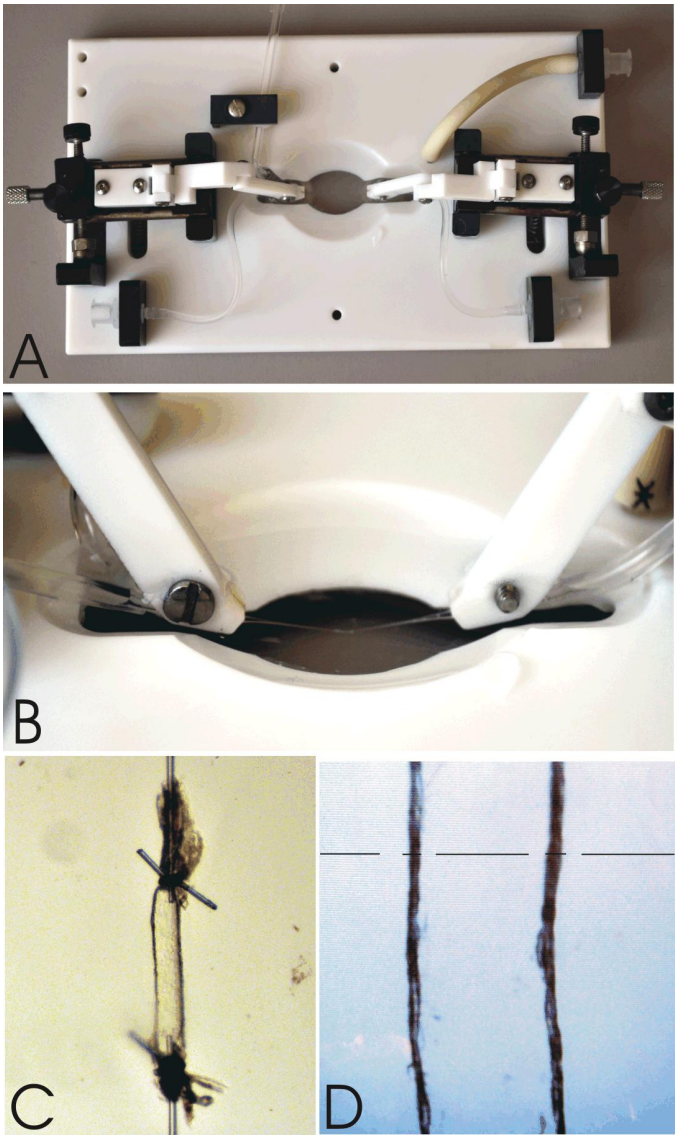

Figure 1: ***Arteriograph chamber for intact pressurized cerebral arteries.***

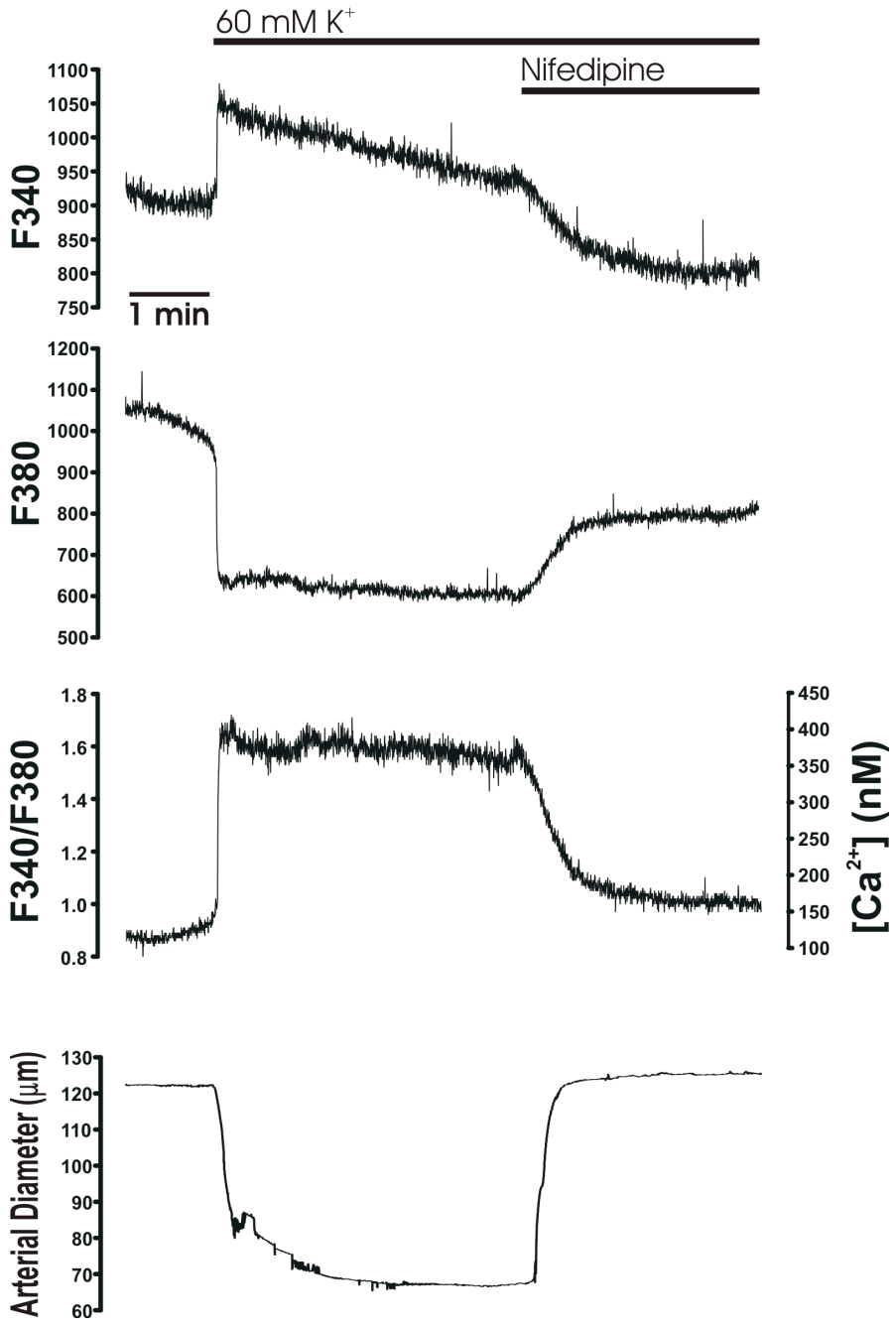

Figure 2: : *Simultaneous measurement of global $[Ca^{2+}]_i$ and diameter of an intact pressurized cerebral artery.*

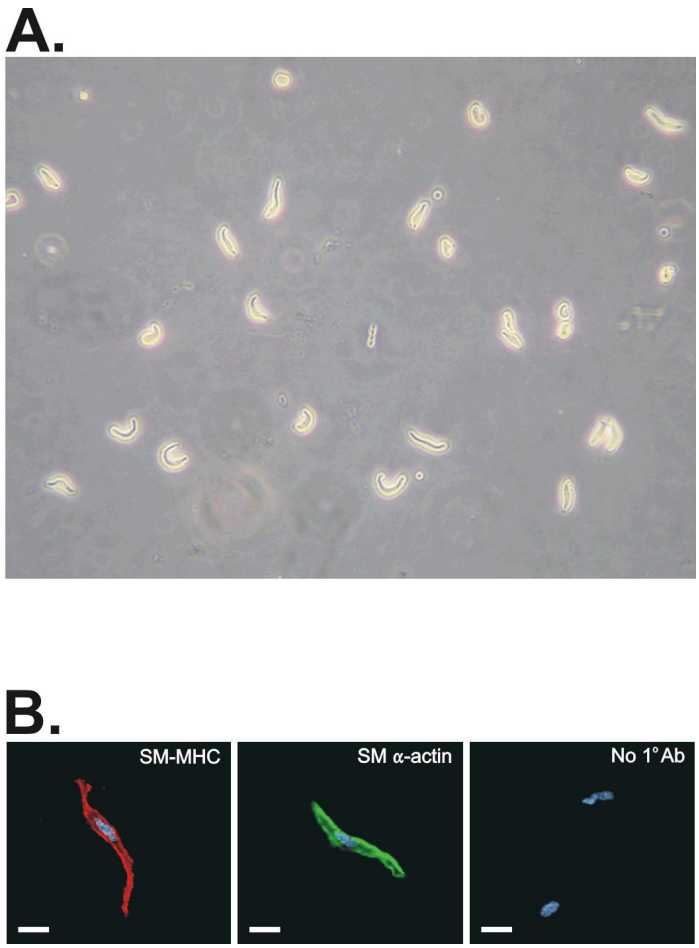

Figure 3: ***Freshly isolated native cerebral artery myocytes.***

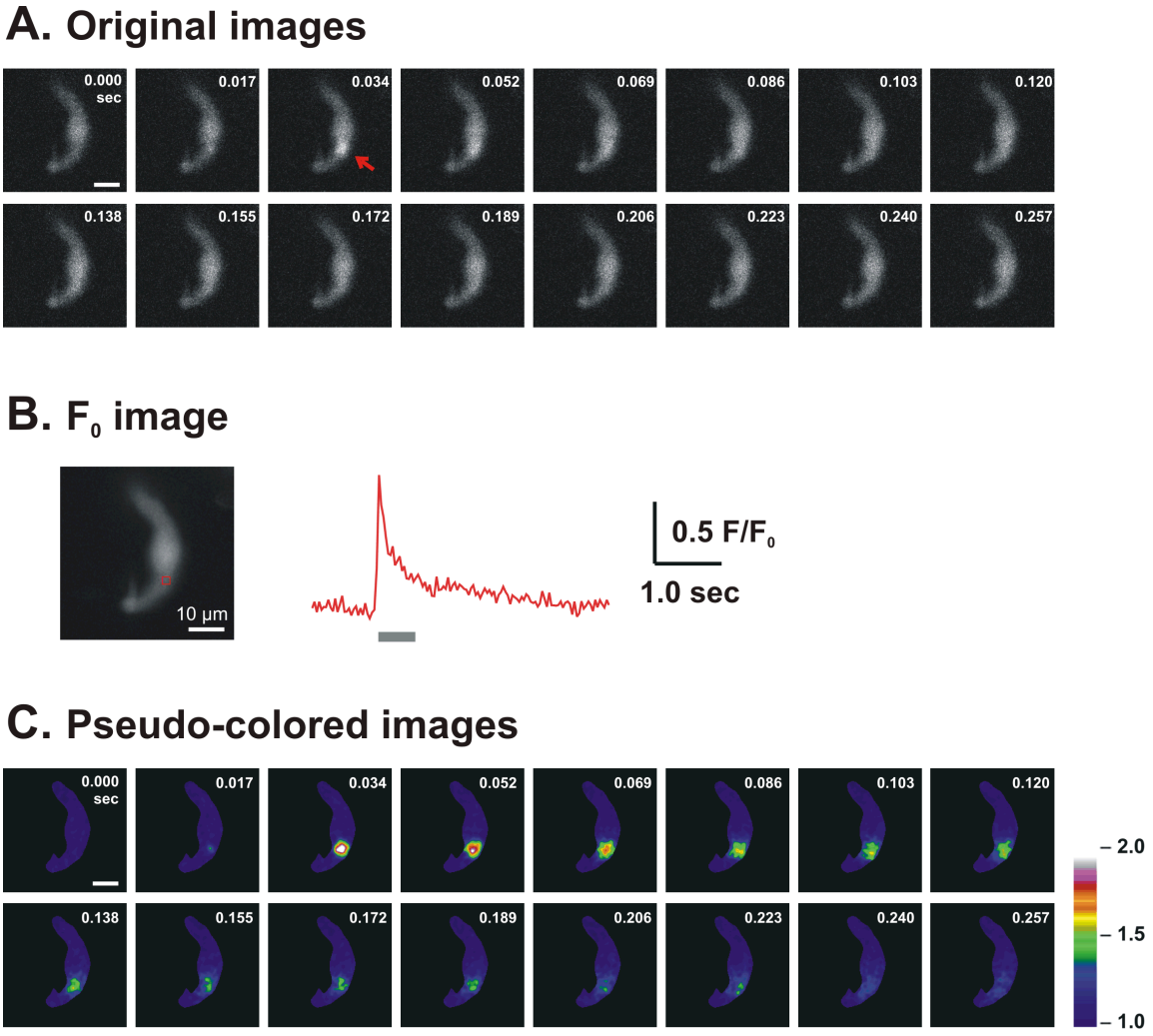

Figure 4: ***Ca^{2+} sparks in isolated cerebral artery myocytes.***

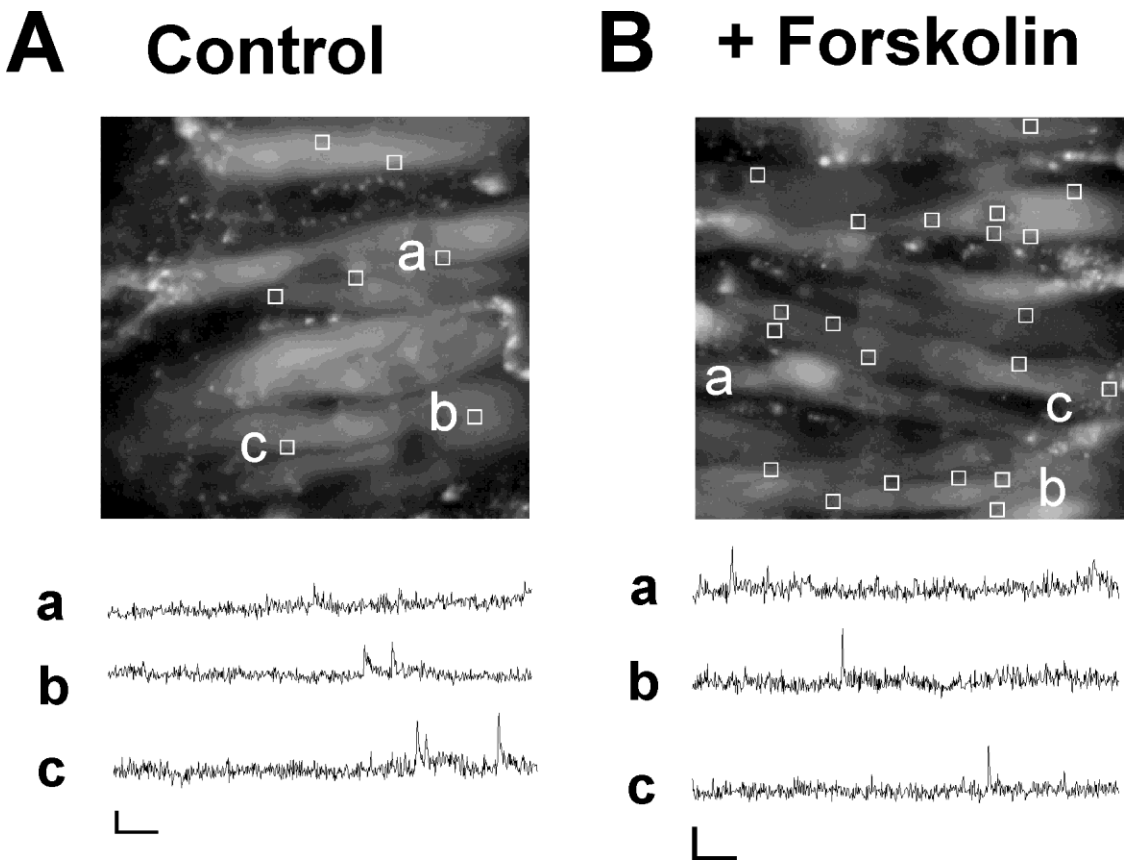

Figure 5: ***Ca^{2+} sparks in intact pressurized cerebral arteries.***

APPENDIX B: BOOK CHAPTER

Impact of subarachnoid hemorrhage on local and global calcium signaling in cerebral artery myocytes

Masayo Koide*, Matthew A. Nystoriak*, Joseph E. Brayden and George C. Wellman

Department of Pharmacology, University of Vermont College of Medicine, Burlington, Vermont, USA

Correspondence:

George C. Wellman, Ph.D.
University of Vermont
Department of Pharmacology
Given Building
89 Beaumont Avenue
Burlington, VT USA 05405-0068
george.wellman@uvm.edu
Tel: 802-656-3470
Fax: 802-656-4523

* M. Koide and M. Nystoriak contributed equally to this work.

Summary

Background: Ca^{2+} signaling mechanisms are crucial for proper regulation of vascular smooth muscle contractility and vessel diameter. In cerebral artery myocytes, a rise in global cytosolic Ca^{2+} concentration ($[Ca^{2+}]_i$) causes contraction while an increase in local Ca^{2+} release events from the sarcoplasmic reticulum (Ca^{2+} sparks) leads to increased activity of large-conductance Ca^{2+}-activated (BK) K^+ channels, hyperpolarization and relaxation. Here, we examined the impact of SAH on Ca^{2+} spark activity and $[Ca^{2+}]_i$ in cerebral artery myocytes following SAH.

Methods: A rabbit double injection SAH model was used in this study. Five days after the initial intracisternal injection of whole blood, small diameter cerebral arteries were dissected from the brain for study. For simultaneous measurement of arterial wall $[Ca^{2+}]_i$ and diameter, vessels were cannulated and loaded with the ratiometric Ca^{2+} indicator fura-2. For measurement of Ca^{2+} sparks, individual myocytes were enzymatically isolated from cerebral arteries and loaded with the Ca^{2+} indicator fluo-4. Sparks were visualized using laser scanning confocal microscopy.

Results: Arterial wall $[Ca^{2+}]_i$ was significantly elevated and greater levels of myogenic tone developed in arteries isolated from SAH animals compared with arteries isolated from healthy animals. The L-type voltage-dependent Ca^{2+} channel (VDCC) blocker nifedipine attenuated increases in $[Ca^{2+}]_i$ and tone in both groups suggesting increased VDCC activity following SAH. Membrane potential measurement using intracellular microelectrodes revealed significant depolarization of vascular smooth muscle following

SAH. Further, myocytes from SAH animals exhibited significantly reduced Ca^{2+} spark frequency (~50%).

Conclusions: Our findings suggest decreased Ca^{2+} spark frequency leads to reduced BK channel activity in cerebral artery myocytes following SAH. This results in membrane potential depolarization, increased VDCC activity, elevated $[Ca^{2+}]_i$ and decreased vessel diameter. We propose this mechanism of enhanced cerebral artery myocyte contractility may contribute to decreased cerebral blood flow and development of neurological deficits in SAH patients.

Key words: Ca^{2+} channels, K^+ channels, Ca^{2+} sparks, vascular smooth muscle, vasospasm

Introduction

Intracellular Ca^{2+} is a ubiquitous second messenger, playing critical roles in a wide array of physiological processes including muscle contraction (2). In the cerebral vasculature, average intracellular Ca^{2+} concentration or global cytosolic Ca^{2+} ($[Ca^{2+}]_i$) dictates smooth muscle contraction (and arterial diameter) via regulation of myosin light chain kinase activity (4). Thus, an elevation in global cytosolic Ca^{2+} leads to enhanced vasoconstriction and potentially a decrease in cerebral blood flow (12). Paradoxically, localized intracellular Ca^{2+} release events, termed Ca^{2+} sparks, promote a decrease in $[Ca^{2+}]_i$ and relaxation of cerebral artery myocytes (15, 27). Ca^{2+} sparks are generated by the coordinated opening of ryanodine receptors (RyRs) located on the sarcoplasmic reticulum of smooth muscle cells and activate plasmamemmal large conductance Ca^{2+}-activated K^+ (BK) channels leading to membrane potential hyperpolarization, decreased activity of voltage-dependent Ca^{2+} channels (VDCCs), decreased $[Ca^{2+}]_i$, and vasodilation. Currently, the impact of subarachnoid hemorrhage on local and/or global Ca^{2+} signals in myocytes from small diameter cerebral arteries is unclear (24).

Methods

SAH model:

A rabbit double-injection model of SAH was used in this study. Briefly, anesthetized New Zealand white rabbits (males, 3.0-3.5 kg) received an intracisternal injection of autologous arterial blood (2.5 ml) using a previously described surgical procedure (8, 9). Forty-eight hours after the initial injection, the procedure was repeated with animals

receiving a second injection of 2.5 ml of arterial blood. Five days after the initial surgery, rabbits were euthanized and posterior cerebral and cerebellar arteries (100-200 μm diameter) were dissected for in vitro studies. All protocols were conducted in accordance with the guidelines for the care and use of laboratory animals (NIH publication 85-23, 1985) and followed protocols approved by the Institutional Animal Use and Care Committee of the University of Vermont, USA.

Simultaneous measurement of global cytosolic Ca^{2+} and arterial diameter:

Intact cerebral arteries were cannulated on glass micropipettes mounted in a Living Systems Inc. (Burlington, VT) arteriograph chamber. Arteries were loaded, in the dark, with the ratiometric Ca^{2+} indicator fura-2-AM (5 μM) in a MOPS solution containing pluronic acid (0.05%) for 45 minutes at room temperature. The MOPS loading solution had the following composition (in mM): 145 NaCl, 5 KCl, 1 $MgSO_4$, 2.5 $CaCl_2$, 1 KH_2PO_4, 0.02 EDTA, 3 3-(N-morpholino)propanesulfonic acid (MOPS), 2 pyruvate, 5 glucose, 1% bovine serum albumin (pH 7.4). Arteries were then continuously superfused with aerated artificial cerebral spinal fluid (aCSF) at 37° C for the remainder of the experiment. The composition of the aCSF was (in mM): 125 NaCl, 3 KCl, 18 $NaHCO_3$, 1.25 NaH_2PO_4, 1 $MgCl_2$, 2 $CaCl_2$, 5 glucose aerated with 5% CO_2, 20% O_2, 75% N_2 (pH 7.35). Ratio images of the arterial wall were obtained from background corrected images of the 510 nm emission from arteries alternately excited at 340 and 380 nm using software developed by IonOptix Inc. (Milton, MA). Arterial wall $[Ca^{2+}]$ is calculated using the following equation (3): $[Ca^{2+}] = K_d \times \beta \times (R-R_{min})/(R_{max}-R)$. An apparent K_d of

282 nM of fura-2 for Ca^{2+} was used (12). Arterial constriction was expressed as a percent decrease from the maximal (fully dilated) diameter obtained at the end of each experiment in Ca^{2+}-free aCSF containing the vasodilators nifedipine (1 μM) and forskolin (1 μM). In some studies intracellular microelectrodes were used to measure smooth muscle membrane potential in intact pressurized arteries, as described previously (25).

Measurement of Ca^{2+} sparks in isolated cerebral artery myocytes:

Individual smooth muscle cells were enzymatically isolated from posterior cerebral and cerebellar artery segments (26). Isolated myocytes were then loaded with fluo-4-AM (10 μM) for 60 minutes (21˚ C) in a HEPES-buffered physiological saline solution (PSS) containing pluronic acid (0.05%). The HEPES-PSS had the following composition (in mM): 135 NaCl, 5.4 KCl, 1.8 $CaCl_2$, 1 $MgCl_2$, 10 HEPES, 10 glucose (pH 7.4 with NaOH). Myocyte images were acquired with a Noran Oz laser scanning confocal microscope (19). Fluo-4 was excited using the 488 nm line of a krypton/argon laser and the light emitted by this dye (520 nm) was separated from the excitation light and collected. Images were acquired at a frequency of ≈ 60 Hz for a period of 20 seconds. Ca^{2+} sparks are detected and analyzed using custom software (written by Dr. Adrian Bonev, University of Vermont, using IDL 5.0.2; Research Systems Inc., Boulder, CO). Baseline fluorescence (F_o) was determined by averaging 10 images without Ca^{2+} spark activity. Fractional fluorescence increases (F/F_o) are determined in areas (2.1 μm × 2.1 μm) where Ca^{2+} sparks were observed. Ca^{2+} sparks are defined as local fractional fluorescence increases greater than 1.3. All measurements were recorded at room temperature.

Results

Elevated global cytosolic Ca^{2+} and enhanced myogenic tone in small diameter cerebral arteries following SAH:

The relationship between intravascular pressure, arterial Ca^{2+} and myogenic tone was examined in small diameter (150-200 μm) cerebral arteries isolated from healthy control and SAH model rabbits. Arterial wall Ca^{2+} and constriction increased as intravascular pressure was elevated within the range (60-100 mmHg) typically experienced by these arteries in vivo. Arteries from SAH animals exhibited significant elevations in both arterial wall Ca^{2+} and constriction compared to similar arteries from control animals (Figure 1A). For example, at 100 mmHg, arterial wall Ca^{2+} was ~26% higher in arteries isolated from SAH animals (231 ± 17 nM, n = 4) compared with arteries isolated from healthy (184 ± 12 nM, n = 4). The level of constriction (myogenic tone) at 100 mmHg was ~1.5 fold higher in arteries isolated from SAH animals (39 ± 3 % decrease in diameter, n = 4) compared with arteries isolated from healthy animals (27 ± 2 % decrease in diameter, n = 4). In the presence of the L-type VDCC blocker nifedipine (1 μM), arterial Ca^{2+} was greatly reduced in arteries from both SAH (141 ± 15 nM) and control (118 ± 7 nM) rabbits. Nifedipine (1 μM) also reduced pressure-induced constrictions by 92 ± 1 % and 93 ± 1 % in arteries from SAH and control animals, respectively. These data suggest that increased VDCC activity underlies enhanced pressure-induced constriction observed in small diameter cerebral arteries from SAH.

Increased VDCC activity could reflect either increased L-type VDCC expression or enhanced VDCC activation due to smooth muscle membrane potential depolarization

following SAH. Quantitative real-time PCR was used to assess L-type VDCC expression encoded by the gene $Ca_V1.2$ (17). Using this approach, no significant difference in $Ca_V1.2$ mRNA levels was detected in cerebral artery homogenates from control and SAH animals (Figure 1B). Next, we used intracellular microelectrodes to directly measure vascular smooth muscle membrane potential from intact pressurized cerebral arteries. At 80 mmHg, smooth muscle membrane potential was significantly depolarized by approximately 8 mV in arteries isolated from SAH animals compared with arteries from control animals (Figure 1C). These findings suggest that membrane potential depolarization of vascular smooth muscle leads to increased VDCC activity, elevated global cytosolic Ca^{2+} and enhanced constriction of small diameter cerebral arteries following SAH.

Ca^{2+} spark frequency is decreased in cerebral artery myocytes from SAH animals:

A decrease in Ca^{2+} spark frequency and associated BK activity promotes membrane potential depolarization, elevated global cytosolic Ca^{2+}, and vasoconstriction (15, 27). To explore whether decreased Ca^{2+} spark frequency may contribute to enhanced cerebral artery constriction, Ca^{2+} sparks were measured in isolated cerebral artery myocytes using laser scanning confocal microscopy and the Ca^{2+} indicator dye fluo-4. As illustrated in figure 2, Ca^{2+} sparks were observed in cerebral artery myocytes obtained from both control and SAH animals. However, Ca^{2+} spark frequency was markedly decreased (by approximately 50%) in myocytes isolated from SAH animals. Consistent with the observed decrease in Ca^{2+} spark frequency, the frequency of transient BK currents

detected using patch clamp electrophysiology was also reduced by approximately 50 % in freshly isolated cerebral artery myocytes from SAH animals (Koide and Wellman, unpublished observations). These data suggest that a decrease in the frequency of Ca^{2+} sparks and their associated BK channel currents may contribute to enhanced constriction of small diameter cerebral arteries following SAH.

Discussion

Aneurysmal SAH is associated with high rates of morbidity and mortality (1). It has been a long-held belief that delayed and sustained large diameter (conduit) cerebral artery vasospasm ("angiographic vasospasm") is a major contributor to SAH-induced death and disability. However, there is a growing appreciation that a host of other factors are also likely involved in the pathological consequences associated with cerebral aneurysm rupture (5, 20). Here, we provide evidence that SAH enhances the dynamic constriction of small diameter pial arteries in response to physiological increases in intravascular pressure, an effect that could have a pronounced influence to decrease cerebral blood flow. Our findings indicate that this augmented constriction is associated with enhanced smooth muscle contraction due to membrane potential depolarization, enhanced voltage-dependent Ca^{2+} channel activity and elevated global cytosolic calcium. Further, our recent findings suggest a decrease in the frequency of Ca^{2+} sparks and associated BK channel activity may contribute to enhanced cerebral artery constriction and elevated global cytosolic Ca^{2+} (figure 3).

The cerebral circulation maintains a constant level of blood flow to the brain despite physiological fluctuations in cerebral perfusion pressure (14). To achieve stable cerebral blood flow in the face of changes in blood pressure, cerebral arteries must constrict in response to increased intravascular pressure and dilate when intravascular pressure is reduced. In pial arteries from healthy animals, physiological increases in intravascular pressure lead to smooth muscle membrane potential depolarization, an increase in the activity of L-type $Ca_V1.2$ channels (encoded by the gene CACNA1C), and increased global cytosolic Ca^{2+} (12, 17). The open-state probability of $Ca_V1.2$ is steeply voltage-dependent (16); thus, small changes in membrane potential can have a profound impact on smooth muscle Ca^{2+}. Our present results suggest membrane potential depolarization and enhanced L-type VDCC activity in small diameter arteries is likely to contribute to SAH-induced impairment in the autoregulation of cerebral blood flow reported by others (18, 23). Our evidence also suggests enhanced activity of L-type VDCCs play a large part in the SAH-induced elevation in global cytosolic Ca^{2+}. However, in the presence of the L-type VDCC blocker nifedipine, global Ca^{2+} remained elevated (by approximately 20%) in arteries from SAH animals. This nifedipine-resistant increase in global Ca^{2+} in cerebral arteries from SAH animals may reflect the emergence of R-type VDCC channels (9), or the possible upregulation of additional Ca^{2+} entry pathways.

Our present findings suggest decreased Ca^{2+} spark and associated BK channel activity contribute to SAH-induced membrane potential depolarization and enhanced VDCC activity in cerebral artery myocytes. Harder and colleagues (6) were the first to report that the membrane potential of cerebral artery myocytes is depolarized following SAH

and a number of subsequent studies have provided further evidence for decreased voltage-dependent K^+ (K_V) channel activity in pial arteries following SAH (7, 10, 11, 13, 21, 22, 24). Interestingly, BK channel activity and expression have been reported to be unchanged in basilar artery myocytes obtained from a canine SAH model (11). Our current work demonstrates that decreased BK channel activity following SAH results from a decrease in local Ca^{2+} signaling from the SR to the plasma membrane (i.e. decreased Ca^{2+} spark activity), rather than a direct effect on BK channel properties or expression.

Conclusions

In this study, we examined global and local Ca^{2+} signaling in cerebral artery myocytes following SAH. As for global Ca^{2+}, we observed a significant increase in averaged cytosolic Ca^{2+} and constriction in cerebral arteries from SAH animals at physiological intravascular pressures. Regarding local Ca^{2+} signaling, we report a decrease in the frequency of Ca^{2+} sparks and associated transient outward BK currents, which likely contribute to membrane potential depolarization, increased VDCC activity and enhanced cerebral constriction artery following SAH. These data suggest that increased global Ca^{2+} and impaired local Ca^{2+} signaling may contribute to decreased cerebral blood flow and the development of neurological deficits frequently observed following aneurysmal SAH.

Acknowledgements

This work was supported by the Totman Medical Research Trust Fund, the Peter Martin Brain Aneurysm Endowment, the NIH (NIHLBI, R01 HL078983 and NCRR, P20 RR16435) and the American Heart Association (0725837T, 0815736D). The authors wish to thank to Ms. Sheila Russell for her assistance with this study. The authors would also like to acknowledge the University of Vermont Neuroscience COBRE molecular biology and imaging core facilities.

References

1. Bederson JB, Connolly ES, Jr., Batjer HH, Dacey RG, Dion JE, Diringer MN, Duldner JE, Jr., Harbaugh RE, Patel AB, Rosenwasser RH (2009) Guidelines for the management of aneurysmal subarachnoid hemorrhage: a statement for healthcare professionals from a special writing group of the Stroke Council, American Heart Association. Stroke 40:994-1025

2. Clapham DE (2007) Calcium signaling. Cell 131:1047-1058

3. Grynkiewicz G, Poenie M, Tsien RY (1985) A new generation of Ca2+ indicators with greatly improved fluorescence properties. J Biol Chem 260:3440-3450

4. Hai CM, Murphy RA (1989) Ca2+, crossbridge phosphorylation, and contraction. Annu Rev Physiol 51:285-298

5. Hansen-Schwartz J, Vajkoczy P, Macdonald RL, Pluta RM, Zhang JH (2007) Cerebral vasospasm: looking beyond vasoconstriction. Trends Pharmacol Sci 28:252-256

6. Harder DR, Dernbach P, Waters A (1987) Possible cellular mechanism for cerebral vasospasm after experimental subarachnoid hemorrhage in the dog. J Clin Invest 80:875-880

7. Ishiguro M, Morielli AD, Zvarova K, Tranmer BI, Penar PL, Wellman GC (2006) Oxyhemoglobin-induced suppression of voltage-dependent K+ channels in cerebral arteries by enhanced tyrosine kinase activity. Circ Res 99:1252-1260

8. Ishiguro M, Puryear CB, Bisson E, Saundry CM, Nathan DJ, Russell SR, Tranmer BI, Wellman GC (2002) Enhanced myogenic tone in cerebral arteries from a

rabbit model of subarachnoid hemorrhage. Am J Physiol Heart Circ Physiol 283:H2217-2225

9. Ishiguro M, Wellman TL, Honda A, Russell SR, Tranmer BI, Wellman GC (2005) Emergence of a R-type Ca2+ channel (CaV 2.3) contributes to cerebral artery constriction after subarachnoid hemorrhage. Circ Res 96:419-426

10. Jahromi BS, Aihara Y, Ai J, Zhang ZD, Nikitina E, Macdonald RL (2008) Voltage-gated K+ channel dysfunction in myocytes from a dog model of subarachnoid hemorrhage. J Cereb Blood Flow Metab 28:797-811

11. Jahromi BS, Aihara Y, Ai J, Zhang ZD, Weyer G, Nikitina E, Yassari R, Houamed KM, Macdonald RL (2008) Preserved BK channel function in vasospastic myocytes from a dog model of subarachnoid hemorrhage. J Vasc Res 45:402-415

12. Knot HJ, Nelson MT (1998) Regulation of arterial diameter and wall [Ca2+] in cerebral arteries of rat by membrane potential and intravascular pressure. J Physiol 508 (Pt 1):199-209

13. Koide M, Penar PL, Tranmer BI, Wellman GC (2007) Heparin-binding EGF-like growth factor mediates oxyhemoglobin-induced suppression of voltage-dependent potassium channels in rabbit cerebral artery myocytes. Am J Physiol Heart Circ Physiol 293:H1750-1759

14. Lee KR, Hoff, J.T. (1996) Intracranial Pressure. Neurological Surgery W.B. Saunders Co., Philadelphia

15. Nelson MT, Cheng H, Rubart M, Santana LF, Bonev AD, Knot HJ, Lederer WJ (1995) Relaxation of arterial smooth muscle by calcium sparks. Science 270:633-637

16. Nelson MT, Patlak JB, Worley JF, Standen NB (1990) Calcium channels, potassium channels, and voltage dependence of arterial smooth muscle tone. Am J Physiol 259:C3-18

17. Nystoriak MA, Murakami K, Penar PL, Wellman GC (2009) Ca(v)1.2 splice variant with exon 9* is critical for regulation of cerebral artery diameter. Am J Physiol Heart Circ Physiol 297:H1820-1828

18. Ohkuma H, Ogane K, Tanaka M, Suzuki S (2001) Assessment of cerebral microcirculatory changes during cerebral vasospasm by analyzing cerebral circulation time on DSA images. Acta Neurochir Suppl 77:127-130

19. Perez GJ, Bonev AD, Patlak JB, Nelson MT (1999) Functional coupling of ryanodine receptors to KCa channels in smooth muscle cells from rat cerebral arteries. J Gen Physiol 113:229-238

20. Pluta RM, Hansen-Schwartz J, Dreier J, Vajkoczy P, Macdonald RL, Nishizawa S, Kasuya H, Wellman G, Keller E, Zauner A, Dorsch N, Clark J, Ono S, Kiris T, Leroux P, Zhang JH (2009) Cerebral vasospasm following subarachnoid hemorrhage: time for a new world of thought. Neurol Res 31:151-158

21. Quan L, Sobey CG (2000) Selective effects of subarachnoid hemorrhage on cerebral vascular responses to 4-aminopyridine in rats. Stroke 31:2460-2465

22. Sobey CG, Faraci FM (1998) Subarachnoid haemorrhage: what happens to the cerebral arteries? Clin Exp Pharmacol Physiol 25:867-876

23. Takeuchi H, Handa Y, Kobayashi H, Kawano H, Hayashi M (1991) Impairment of cerebral autoregulation during the development of chronic cerebral vasospasm after subarachnoid hemorrhage in primates. Neurosurgery 28:41-48

24. Wellman GC (2006) Ion channels and calcium signaling in cerebral arteries following subarachnoid hemorrhage. Neurol Res 28:690-702

25. Wellman GC, Bonev AD, Nelson MT, Brayden JE (1996) Gender differences in coronary artery diameter involve estrogen, nitric oxide, and Ca(2+)-dependent K+ channels. Circ Res 79:1024-1030

26. Wellman GC, Nathan DJ, Saundry CM, Perez G, Bonev AD, Penar PL, Tranmer BI, Nelson MT (2002) Ca2+ sparks and their function in human cerebral arteries. Stroke 33:802-808

27. Wellman GC, Nelson MT (2003) Signaling between SR and plasmalemma in smooth muscle: sparks and the activation of Ca2+-sensitive ion channels. Cell Calcium 34:211-2

Figure Legends:

Figure 1: Elevated global cytosolic Ca^{2+} following SAH: A. Summary data from simultaneous measurement of arterial wall Ca^{2+} (using fura-2) and diameter. Arterial wall Ca^{2+} and tone were significantly increased at intravascular pressures between 60 and 100 mmHg in arteries isolated from SAH animals compared with controls. **B.** Summary data using quantitative real-time PCR. Total RNA was collected from posterior cerebral arteries. $Ca_V1.2$ expression was not altered following SAH. NS: not statistically significant. **C.** Summary data from membrane potential measurement using intracellular microelectrodes. Vascular smooth muscle membrane potential in arteries from SAH animals was significantly depolarized following SAH. * $P<0.05$.

Figure 2: Decreased Ca^{2+} spark frequency in cerebral myocytes from SAH animals: Imaging of Ca^{2+} sparks in cerebral artery myocytes loaded with the fluorescent Ca^{2+} indicator fluo-4. Fluorescent images were detected using laser scanning confocal microscopy with Ca^{2+} sparks defined as a fractional fluorescent increase of greater than 30% within 2.1 μm by 2.1 μm analysis areas. Large size images represent an average of 30 images in gray scale without Ca^{2+} spark activity. White crosses depict where individual Ca^{2+} sparks occurred during the 20 sec recordings. Scale bars represent 10 μm. Smaller images illustrate the time course of Ca^{2+} sparks in control and SAH myocytes. Images were obtained every 19 msec.

Figure 3: Summary cartoon: In control cerebral artery myocytes, local Ca^{2+} release events from the sarcoplasmic reticulum (Ca^{2+} sparks) activate large conductance Ca^{2+} activated (BK) K^+ channels, causing membrane potential hyperpolarization, decreased voltage-dependent Ca^{2+} channel (VDCC) activity and decreased global cytosolic Ca^{2+}. Following SAH, the frequency of Ca^{2+} sparks and therefore BK channel activity is decreased, promoting membrane potential depolarization, increased VDCC activity and increased global cytosolic Ca^{2+} levels.

Figures

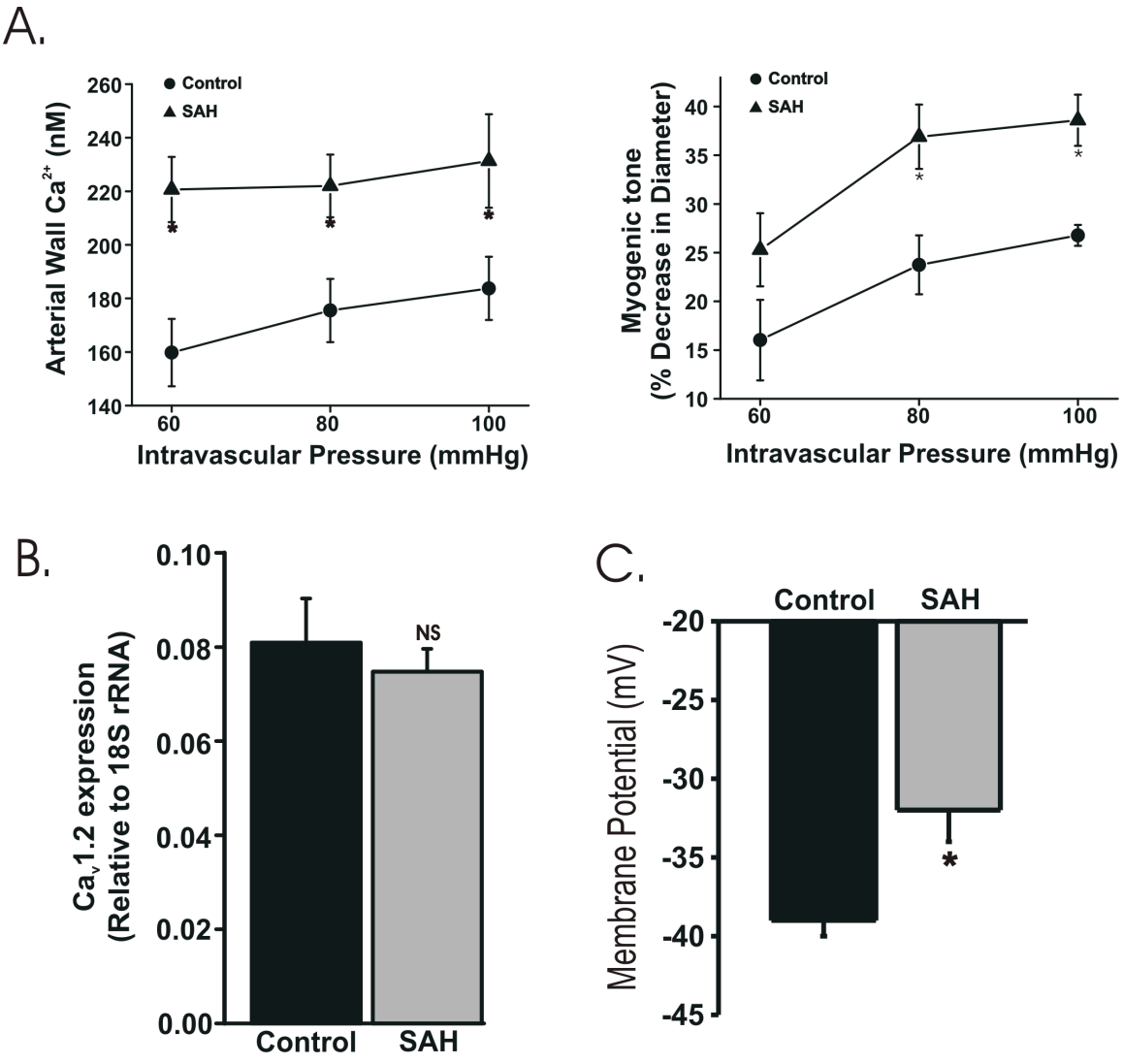

Figure 1: ***Elevated global cytosolic Ca^{2+} following SAH.***

Figure 2:

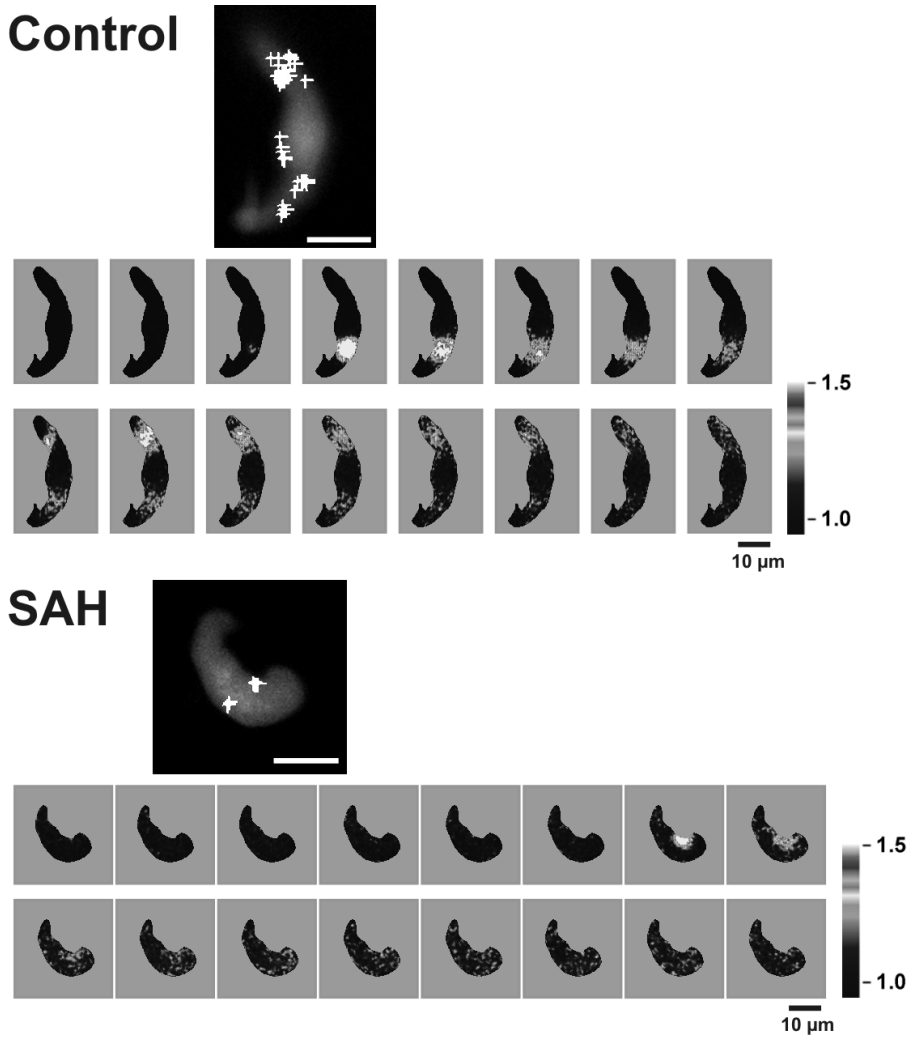

Decreased Ca^{2+} spark frequency in cerebral myocytes from SAH animals.

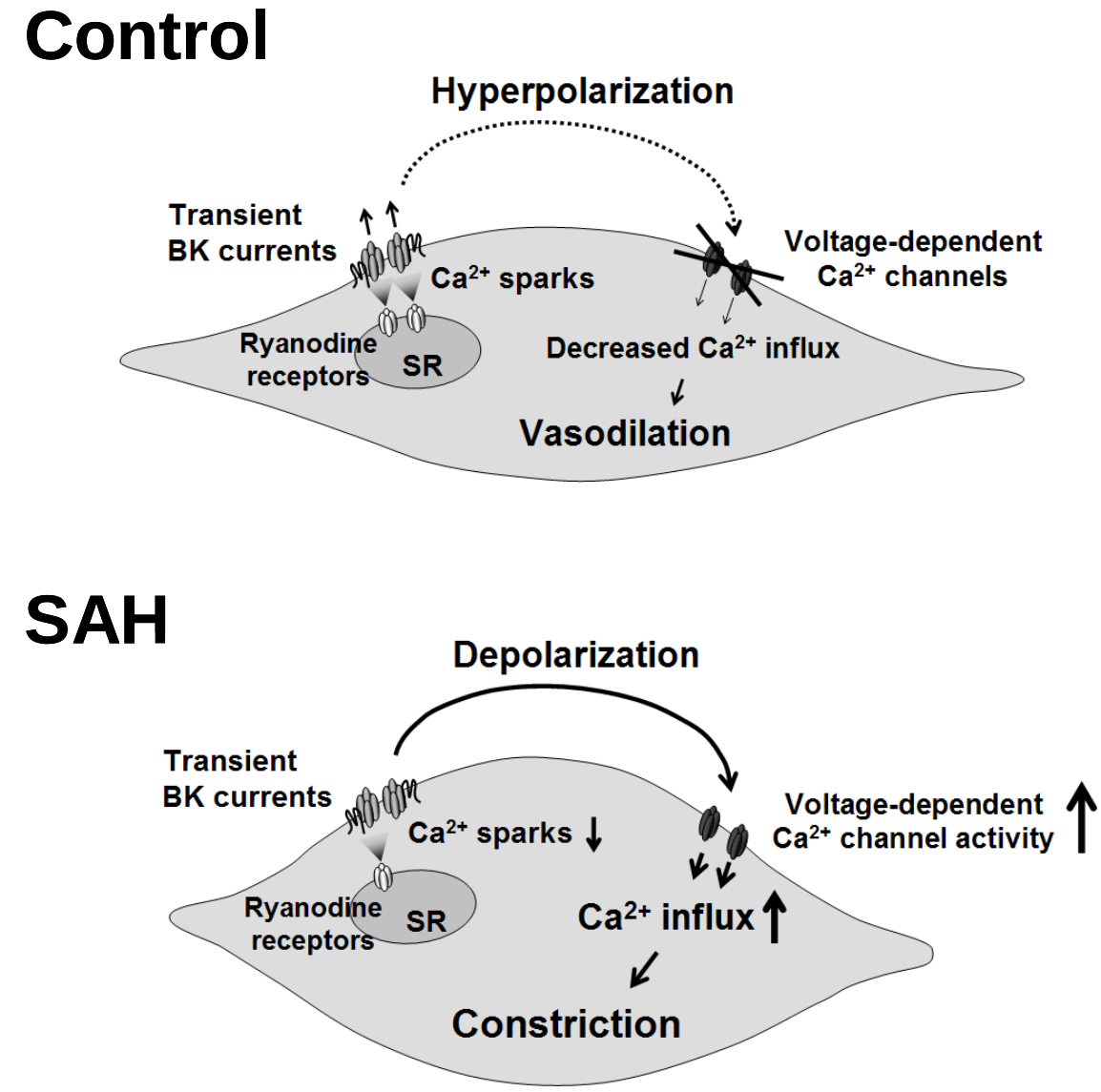

Figure 3: ***Summary cartoon.***

APPENDIX C: JOURNAL ARTICLE

My contribution to the following journal article comprises acquisition and analysis of arterial $[Ca^{2+}]_i$ data and caffeine-induced Ca^{2+}-transient data shown in figure 5.

Reduced Ca^{2+} spark activity following subarachnoid hemorrhage disables BK channel control of cerebral artery tone

Masayo Koide, Matthew A. Nystoriak, Gayathri Krishnamoorthy, Kevin P. O'Connor, Adrian D. Bonev, Mark T. Nelson, and George C. Wellman

Department of Pharmacology, University of Vermont College of Medicine, Burlington, Vermont, USA

Correspondence:
George C. Wellman, Ph.D.
University of Vermont
Department of Pharmacology
89 Beaumont Avenue
Burlington, VT USA 05405-0068
e-mail: george.wellman@uvm.edu
Tel: 802-656-3470
Fax: 802-656-4523

Running title: SAH decreases Ca^{2+} spark and BK channel activity

This work was supported by the Totman Medical Research Trust Fund, the Peter Martin Brain Aneurysm Endowment, the NIH (R01 HL078983, R01 HL078983-05S1, R01 HL44455, R37 DK053832, R01 DK065947, R01 HL098243, R01 HL44455, R01 HL077378, NCRR P20 RR16435 and P01 HL095488) and the American Heart Association (0725837T, 0725841T, 0815736D).

Abstract

Intracellular Ca^{2+} release events ("Ca^{2+} sparks") and transient activation of large-conductance Ca^{2+}-activated potassium (BK) channels represent an important vasodilator pathway in the cerebral vasculature. Considering the frequent occurrence of cerebral artery constriction following subarachnoid hemorrhage (SAH), our objective was to determine if Ca^{2+} spark and BK channel activity were reduced in cerebral artery myocytes from SAH model rabbits. Using laser scanning confocal microscopy, we observed ≈50 % reduction in Ca^{2+} spark activity, reflecting a decrease in the number of functional Ca^{2+} spark discharge sites. Patch clamp electrophysiology demonstrated a similar reduction in Ca^{2+} spark-induced transient BK currents, but no change in BK channel density or single channel properties. Consistent with a reduction in active Ca^{2+} spark sites, quantitative real-time PCR and western blotting revealed decreased expression of ryanodine receptor type 2 (RyR-2) and increased expression of the RyR-2 stabilizing protein, FKBP12.6, in cerebral arteries from SAH animals. Further, inhibitors of Ca^{2+} sparks (ryanodine) or BK channels (paxilline) constricted arteries from control, but not SAH animals. This work demonstrates that an SAH-induced decrease in sub-cellular Ca^{2+} signaling events disables BK channel activity leading to cerebral artery constriction. This phenomenon may contribute to decreased cerebral blood flow and the high rate of poor outcome following aneurysmal SAH. **Key Words: cerebral aneurysm, FKBP12.6, potassium channels, ryanodine receptors, vascular smooth muscle, vasospasm.**

Introduction

Cerebral aneurysm rupture and the ensuing subarachnoid hemorrhage (SAH) has an enormous impact on individuals and society, with 30-day mortality rates approaching 50 % and the majority of survivors left with moderate to severe disability (Hop *et al* 1997). For decades, "angiographically-defined" cerebral vasospasm of conduit arteries (> 1 mm in diameter) has been thought to be the major contributor to death and disability in SAH patients surviving the initial intracranial bleed. However, recent evidence indicates that factors other than large artery vasospasm contribute to SAH-induced pathologies (Macdonald *et al* 2007). Additional factors contributing to the deleterious consequences of aneurysmal SAH may include global transient ischemia, early brain injury, disruption of the blood-brain barrier, and activation of inflammatory pathways (Ostrowski *et al* 2006; Prunell *et al* 2005). It is now appreciated that SAH may also impact small diameter arteries and arterioles, i.e. those involved in the autoregulation of cerebral blood flow (Hattingen *et al* 2008; Ishiguro *et al* 2002; Ohkuma *et al* 2000).

In resistance arteries from healthy animals, vasoconstrictor stimuli such as physiological increases in intravascular pressure lead to smooth muscle membrane potential depolarization, increased voltage-dependent Ca^{2+} channel (VDCC) activity, and elevated global cytosolic calcium (Knot and Nelson 1998). Global cytosolic Ca^{2+} represents averaged Ca^{2+} levels throughout the cytoplasm and is a key regulator of smooth muscle contraction. One important dynamic negative feedback mechanism to limit vasoconstriction is the activation of large-conductance Ca^{2+}- and voltage-sensitive potassium (BK) channels by Ca^{2+} sparks. Ca^{2+} sparks are localized Ca^{2+} release events

occurring through ryanodine receptors (RyRs) in the sarcoplasmic reticulum (SR) abutting the plasma membrane. Ca^{2+} sparks oppose the contractile actions of global cytosolic Ca^{2+} by promoting smooth muscle relaxation via activation of plasmalemmal BK channels leading to membrane potential hyperpolarization and decreased Ca^{2+} influx through VDCCs (Nelson *et al* 1995; Wellman and Nelson 2003). In the vasculature, functional BK channels are composed of pore-forming α_1 subunits, encoded by the gene KCNMA1 and regulatory β_1 subunits, encoded by the gene KCNMB1 (Tanaka *et al* 1997). Loss-of and gain-of function polymorphisms of KCNMA1 and KCNMB1 have been linked to asthma and blood pressure regulation in humans (Kelley-Hedgepeth *et al* 2009; Tomas *et al* 2008). Further, decreased KCNMB1 expression causes reduced BK channel Ca^{2+} and voltage sensitivity, and is linked to enhanced vasoconstriction, hypertension and diabetes (Amberg and Santana 2003; Brenner *et al* 2000; Dong *et al* 2008). These vascular pathologies have all been associated with a decrease in BK channel activity in response to Ca^{2+} sparks, rather than a reduction in Ca^{2+} spark activity.

Decreased BK channel activity following SAH could lead to vasoconstriction and compromise cerebral autoregulation. However, BK channel properties and expression appear to be unaffected in basilar arteries obtained from a canine SAH model (Jahromi *et al* 2008b). In the present study, we demonstrate that decreased BK channel activity does contribute to enhanced pressure-dependent constriction of resistance-sized cerebral arteries from SAH model rabbits. However, rather than reduced BK channel activity resulting from decreased KCNMA1 or KCNMB1 expression, we provide evidence that impaired BK channel activity results from a decrease in sub-cellular Ca^{2+}

signaling from the SR to BK channels, i.e. reduced Ca^{2+} spark frequency. To our knowledge, these findings represent the first demonstration of a vascular pathology due to a decrease in Ca^{2+} spark activity. This SAH-induced reduction in Ca^{2+} spark frequency reflects a decrease in the number of functional Ca^{2+} spark discharge sites caused by a decrease in the expression of SR RyR-2 Ca^{2+}-release channels and an increase in the expression of the RyR-2 stabilizing protein, FKBP12.6. This novel pathway of decreased vascular BK channel activity may contribute to impaired autoregulation, reduced cerebral blood flow and the development of neurological deficits frequently observed in patients following aneurysmal SAH.

Materials and Methods

Rabbit SAH model

New Zealand White rabbits (males, 3.0-3.5 kg; Charles River Laboratories) were used for a double injection SAH model using surgical procedures described previously (Ishiguro *et al* 2002; Ishiguro *et al* 2005). Briefly, under isoflurane anesthesia, a small midline suboccipital incision was centered over the foramen magnum and neck muscles dissected until dura was visualized. Unheparinized autologous blood (2.5 ml) was then injected into the subarachnoid space via the cisterna magna. The animal was then positioned on an incline board at a 45 degree angle with the head down in neutral position for 30 minutes. To minimize increases in intracranial pressure, a similar volume of cerebral spinal fluid was removed prior to the injection of blood. Forty-eight hours later, the

above procedures were repeated. Buprenophine (0.01 mg/kg) was given every 12 hours for 36 hours after each surgery as an analgesic. Five days after the initial surgery, rabbits were euthanized by exsanguination under deep pentobarbital anesthesia (i.v.; 60 mg/kg), and posterior cerebral and cerebellar arteries (100-250 μm diameter) were dissected for *in vitro* studies in cold (4°C), oxygenated (20 % O_2 / 5 % CO_2 / 75 % N_2) physiological saline solution (PSS) of the following composition (in mmol/L): 118.5 NaCl, 4.7 KCl, 24 $NaHCO_3$, 1.18 KH_2PO_4, 2.5 $CaCl_2$, 1.2 $MgCl_2$, 0.023 EDTA, 11 glucose. Age-matched animals that did not undergo surgical procedures were used as controls. All protocols were conducted in accordance with *the guidelines for the care and use of laboratory animals* [National Institutes of Health (NIH) publication No. 85-23] and followed protocols approved by the Institutional Animal Care and Use Committee of the University of Vermont.

Electrophysiology

Transient BK currents: Arteries were enzymatically dissociated to obtain individual smooth muscle cells as described previously (Ishiguro *et al* 2005). Transient BK currents were measured using the perforated whole-cell patch-clamp technique at room temperature (Wellman *et al* 2002). The composition of the HEPES-PSS bath solution was (in mmol/L): 134 NaCl, 6 KCl, 1 $MgCl_2$, 1.8 $CaCl_2$, 10 glucose and 10 HEPES (pH 7.4). Patch pipettes (8-10 MΩ) were filled with an internal solution that contained (in mmol/L) 110 K^+ aspartate, 30 KCl, 10 NaCl, 1 $MgCl_2$, 10 HEPES, 0.05 EGTA and 0.2 amphotericin B (pH 7.2). Transient outward currents were recorded over a range of

holding potentials from -40 mV to 0 mV (~5 min at each membrane potential). Recordings were analyzed with the Mini Analysis 6.0.3 program (Synaptosoft Inc.), to determine transient BK current amplitude, frequency, rise time (30-70 %) and decay time (90-10 %). The threshold for current peak detection was set at two and half times the single channel amplitude of BK channel (e.g. 5.0 pA at -40 mV) (Perez *et al* 2001).

Single channel BK current recordings: BK single channel currents were recorded in excised inside-out membrane patches at room temperature (Perez *et al* 2001). The bath and pipette solution contained (in mmol/L): 140 KCl, 1 $MgCl_2$, 5 EGTA, 1.9 $CaCl_2$ and 10 HEPES (pH 7.2), with a calculated free Ca^{2+} concentration of 100 nmol/L (WinMax C software, http://www.stanford.edu/%7Ecpatton/maxc.html). When $CaCl_2$ was omitted from the bath solution ("zero" Ca^{2+}), free Ca^{2+} concentration was calculated to be < 1 nmol/L. The number of channels per patch was determined at +80 mV in 100 nmol/L free Ca^{2+}. Ca^{2+}- and voltage-sensitivity of BK channels were determined from Boltzman fit of data.

Whole-cell voltage-dependent K^+ current recordings: Whole cell K^+ currents were measured using the conventional whole cell configuration of the patch-clamp technique (Koide *et al* 2007). The composition of bath solution was the same as the 6 mmol/L K^+ HEPES-PSS described above. The internal solution contained (in mmol/L): 87 K^+ aspartate, 20 KCl, 1 $CaCl_2$, 1 $MgCl_2$, 10 HEPES, 10 EGTA and 25 KOH (pH 7.2). From a holding potential of -70 mV, outward K^+ currents were elicited by a series of 500 msec depolarizing voltage steps followed by a step to -40 mV for 300 msec. Voltage steps were made at 10 mV increments to +50 mV at intervals of 10 sec from a holding

potential of -70 mV. All electrophysiological studies were performed using Axopatch 200B, pCLAMP 9.2 and Clampfit 9.2 software (Axon Instruments Inc.).

Ca^{2+} spark measurements

Freshly isolated cerebral artery myocytes were incubated with the fluorescent Ca^{2+} indicator fluo-4 AM (10 μmol/L; Ex 488 nm, Em 520 nm; Invitrogen) and 0.036 % pluronic acid for 30 min at room temperature followed by a brief wash with HEPES-PSS. Ca^{2+} sparks were detected as previously described using a Noran Oz laser scanning confocal system coupled to an inverted Nikon TMD microscope equipped with a 60X water-immersion lens (N.A.1.2) (Perez *et al* 2001). Images were acquired at a frequency of 58.3 Hz (approximately every 17.2 msec) for 20 sec at room temperature. Fractional fluorescent changes (F/F_0) were analyzed in 2.1 μm x 2.1 μm analysis areas using custom software (SparkAn, written by Dr. Adrian Bonev), and F/F_0 changes > 1.3 defined as Ca^{2+} sparks. F_0 was obtained by averaging 30 images containing no Ca^{2+} events.

RNA isolation and quantitative real-time RT- PCR

Total RNA was extracted from posterior cerebral arteries (100-250 μm in diameter, ~1 mg wet weight) using RNA STAT-60 (Tel-Test Inc.) and cDNA was synthesized by SuperScript™ First-Strand Synthesis System (Invitrogen). The primer sets were designed using Primer-BLAST (NIH) for a unique region of targeted mRNA sequence and are detailed in the online supplementary information (Table 1). Expression of mRNA was quantified by real-time PCR using SYBR Green JumpStart Taq ReadyMix

and a real-time PCR system (Applied Biosystems). Quantification was performed using standard curves constructed by amplification of serially diluted plasmids containing target genes, and the threshold cycle value for each sample used to calculate the initial quantity of cDNA template. The results of quantitative real-time PCR were normalized to glyceraldehyde-3-phosphate dehydrogenase (GAPDH) expression.

Western blotting

Freshly isolated cerebral arteries were homogenized in buffer containing (in mmol/L): 100 NaCl, 20 Tris-HCl (pH 7.4), 1 EDTA, 1 EGTA, 5 dithiothreitol, 1 phenylmethylsulfonyl fluoride, 0.1 leupeptin and 1 % Triton-X using glass microgrinders. After sonication for 10 min on iced water, tissue debris was removed by centrifugation (8000 x *g*, 5 min). The protein concentration of lysate was measured by modified Bradford assay (Coomassie Plus; Pierce) using bovine serum albumin as a standard. The lysate (20 μg of protein) was mixed with 5X loading buffer (625 mmol/L Tris-HCl; pH 6.8), 20 % SDS and 25 % glycerol), and incubated at 37 °C for 15 min. Proteins were separated using 4-20 % acrylamide gradient gels, and electrophoretically transferred to a nitrocellulose membrane. After blocking the membrane with 5 % non-fat milk (1 hr at RT), the membrane was incubated with primary antibody at 4 °C over night. Following incubation with appropriate secondary antibody for 1 hr at RT, signals were detected by chemiluminescence for RYR-2 or by an Odyssey® infrared imaging system (LI-COR® Biosciences) for FKBP12.6 and α-smooth muscle actin. Bands depicting each protein were analyzed using Image J software (NIH). Antibodies were used as follows:

anti-RyR2 mouse monoclonal antibody (clone C3-33, 1:200; ABR), anti-FKBP12.6 goat polyclonal antibody (1:200, SantaCruz), anti-α smooth muscle actin mouse monoclonal antibody (1:100,000, Sigma), peroxydase conjugated sheep anti-mouse IgG (1:5,000, GE Healthcare), IRdye700® conjugated donkey anti-goat IgG and IRdye800® conjugated goat anti-mouse IgG (1:10,000, Rockland).

Diameter measurements in isolated arteries

Freshly isolated arteries from control and SAH rabbits were cannulated in a 5 ml myograph chamber (Living Systems Instrumentation, Inc.) and perfused with PSS (pH 7.4) aerated with 20 % O_2 / 5 % CO_2 / 75 % N_2 at 37˚C, as previously described (Ishiguro *et al* 2002). Arterial diameter was measured with video edge detection equipment and recorded using data acquisition software (Dataq Instruments Inc.). Arteries were discarded if an initial constriction representing less than a 50 % decrease in diameter was observed when arteries were exposed to elevated extracellular K^+ (60 mmol/L). Arterial constrictions to paxilline and ryanodine are expressed as a percent decrease in diameter from the basal level of pressure-induced myogenic tone at an intravascular pressure of 80 mmHg. Vasodilation to cumulative additions of acetylcholine (ACh) and sodium nitroprusside (SNP) are expressed as percent dilation of pressure-induced (myogenic) tone. Fully-dilated (passive) diameter was determined at the end of each experiment by exposing arteries to Ca^{2+}-free PSS containing diltiazem (100 μmol/L) and forskolin (1 μmol/L).

Measurement of cytosolic Ca^{2+} in pressurized cerebral arteries

Freshly isolated cerebral arteries were cannulated and loaded with the ratiometric Ca^{2+}-sensitive fluorescent dye, fura-2 AM (5 μmol/L; Invitrogen), with 0.1 % pluronic acid for 45 min at room temperature. To allow for equilibration and deesterification of fura-2 AM, arteries were superfused with PSS at 37°C for 30 min. Following the equilibration period, fluorescent ratio (R) was obtained from background corrected 510 nm emission from arterioles alternately excited at 340 and 380 nm using software developed by IonOptix Inc. Cytosolic Ca^{2+} concentration was estimated using the following equation (Grynkiewicz *et al* 1985): $[Ca^{2+}] = K_d \times ß \times (R-R_{min})/(R_{max}-R)$. Calibration values were not significantly different between arteries from control and SAH animals and were pooled. R_{min} (0.46 ± 0.02) and R_{max} (10.80 ± 0.66) represent the ratios of emission signal under Ca^{2+}-free and Ca^{2+}-saturated conditions, respectively and were obtained from separate sets of arteries in the presence of ionomycin (10 μmol/L) and nigericin (5 μmol/L). The ratio of Ca^{2+}-free over Ca^{2+}-bound fluorescence intensities at F_{380}, β (11.5 ± 0.70), was obtained from R_{min} and R_{max} measurements. An apparent dissociation constant (K_d) of 282 nM of fura-2 for Ca^{2+} was used (Knot and Nelson 1998).

Statistical Analysis

Data are expressed as mean ± SEM, and analyzed by Student's unpaired *t*-test or One-way ANOVA followed by Tukey multiple comparison test. Statistical significance was considered at the level of $p < 0.05$ (*) or $p < 0.01$ (**).

Results

Transient BK channel currents are decreased following SAH.

At physiological membrane potentials (e.g. -40 mV), micromolar increases in cytosolic Ca^{2+} are required to induce significant BK channel activation (Perez *et al* 2001). In cerebral artery myocytes, sub-cellular Ca^{2+} signaling events (Ca^{2+} sparks) lead to localized elevations of Ca^{2+} sufficient to cause the transient activation of nearby BK channels. Ca^{2+} spark-induced transient BK currents were recorded using the perforated patch whole-cell configuration of the patch clamp technique (Figure 1). At -40 mV, transient BK current frequency, but not amplitude, was decreased by approximately 60 % in cerebral artery myocytes freshly isolated from SAH model rabbits. Membrane potential depolarization increased the frequency and amplitude of transient BK currents to a similar extent in myocytes from both control and SAH animals, i.e. frequency was about 60 % lower at all voltages in cells from the SAH group. Temporal characteristics of these events (rise time and decay time) were similar between groups, as was cell size as indexed by cell capacitance (online supplementary information, Table 2). These data demonstrate a dramatic decrease in the frequency of Ca^{2+} spark-induced BK channel activity following experimental SAH.

Maintained expression and properties of BK channels in cerebral artery myocytes following SAH.

The apparent SAH-induced decrease in transient BK current frequency could conceivably reflect a fundamental change in the voltage or Ca^{2+} sensitivity, or expression of the BK

channel following SAH. To address this issue, single BK channel currents were measured in excised "inside-out" membrane patches. BK channel open-state probability (P_O) and voltage-dependence with 100 nmol/L intracellular free Ca^{2+} were not altered following SAH and a similar right-ward shift in voltage-dependent activation was observed in BK channels from both groups exposed to intracellular solution containing < 1 nmol/L free Ca^{2+} (Figure 2A, B). Single channel slope conductance was similar for channels from control (231.7 ± 3.6 pS, n = 9) and SAH (231.6 ± 3.5 pS, n = 9) animals, consistent with previous reports for BK channels (Perez *et al* 2001). Further, the density of functional BK channels detected in membrane patches was not different between groups (Figure 2C). To view the ensemble behavior of BK channels across the membrane of the entire cell, voltage-dependent K^+ currents were measured during depolarizing voltage steps using conventional whole-cell patch-clamp electrophysiology. Here, $[Ca^{2+}]_i$ was maintained below 25 nmol/L by cell dialysis with 10 mmol/L of the Ca^{2+} chelator, EGTA, included in the intracellular (pipette) solution. Ca^{2+} spark or RyR activation of BK currents does not occur using this approach and the amplitude of conventional whole-cell BK currents reflects plasma membrane BK channel density and their open-state probability at the applied voltage and $[Ca^{2+}]_i$. Steady-state outward currents sensitive to the BK channel blocker paxilline (1 μmol/L, 10 min) were similar in myocytes from control and SAH animals (Figure 2D). To confirm that expression of BK channel pore-forming α-subunits and regulatory β1-subunits are maintained in our SAH model, quantitative real-time PCR was performed on RNA extracted from intact cerebral arteries. BK channel α and β1 subunit mRNA, expressed as a ratio to glyceraldehyde 3-

phosphate dehydrogenase (GAPDH) mRNA, were not significantly different between control and SAH animals (Figure 2E, n = 6 for each group). These data suggest that the SAH-induced decrease in the frequency of transient BK currents is not due to a decrease in the number or functionality of BK channels.

Ca^{2+} spark frequency is decreased in SAH model animals.

BK channel properties and expression appear unaltered in smooth muscle cells from cerebral arteries of SAH animals. We therefore explored the possibility that the lower transient BK current frequency reflects a fundamental decrease in Ca^{2+} spark activity. Ca^{2+} sparks were optically measured in freshly isolated cerebral artery myocytes from control and SAH rabbits using laser scanning confocal microscopy and the fluorescent Ca^{2+} indicator, fluo-4. Ca^{2+} sparks were observed in cells from both control and SAH animals (Figure 3A, also see movies included within the online supplementary data). However, as with the frequency of transient BK currents, whole cell Ca^{2+} spark frequency was dramatically lower (≈50 %) in myocytes isolated from SAH animals (SAH: 0.38 ± 0.04 Hz; Control: 0.76 ± 0.05 Hz, Figure 3B). Although frequency was decreased, Ca^{2+} spark amplitude, expressed as a fractional change in fluorescence intensity (F/F_0), was similar in myocytes isolated from control and SAH animals (Figure 3C). Other spatio-temporal characteristics such as rise-time, duration, size, and decay were similar for Ca^{2+} sparks recorded from myocytes of control and SAH animals (online supplementary information, Table 2).

A reduction in functional Ca^{2+} spark sites underlies decreased Ca^{2+} spark frequency in SAH model animals.

In smooth muscle, Ca^{2+} sparks tend to occur repeatedly within a limited number of distinct areas, or spark sites (Janiak *et al* 2001; Pucovsky and Bolton 2006). The SAH-induced decrease in Ca^{2+} spark frequency could reflect either a reduction in the number of functional spark sites or a decrease in the frequency of events occurring at all spark sites throughout the cell. Spark sites were defined as regions where one or more Ca^{2+} sparks were observed during a 20 second imaging period (Figure 4A-C). Two or more Ca^{2+} sparks were considered to originate from the same spark site if these events exhibited greater than 50 % overlap of their spatial spread (determined at 50 % peak amplitude). In 45 cerebral artery myocytes from five control animals, a total of 1,082 Ca^{2+} sparks were observed with an average of 7.9 ± 0.6 spark sites per cell. However, in myocytes from SAH animals, the number of active spark sites was decreased by approximately 43 % to 4.5 ± 0.4 (n = 594 sparks in 48 cells from 6 animals, Figure 4D). Although the number of functional spark sites was decreased, Ca^{2+} spark frequency at individual sites was similar in cells isolated from control and SAH animals (Figure 4E). Further, the correlation between the number of functional spark sites and whole cell Ca^{2+} spark frequency was similar between groups (Figure 4F). These data suggest SAH-induced decreased Ca^{2+} spark frequency reflects a reduction in the number of functional spark sites.

RyR-2 expression is decreased and FKBP12.6 expression is increased in cerebral arteries from SAH animals.

It is conceivable that the SAH-induced decrease in functional spark sites could reflect either an increase in the activation threshold of RyRs or decreased SR Ca^{2+} load. To assess RyR activity, Ca^{2+} sparks were examined in the presence of a relatively low concentration (10 μmol/L) of the RyR activator, caffeine. Caffeine lowers the luminal Ca^{2+} threshold for RyR activation (Kong *et al* 2008) and at micromolar concentrations causes an increase in both Ca^{2+} spark frequency and the number of active spark sites in smooth muscle (Janiak *et al* 2001; Wellman *et al* 2001). In absolute terms, the number of active Ca^{2+} spark sites and whole-cell Ca^{2+} spark frequency in the presence of caffeine (10 μmol/L) remained decreased in myocytes isolated from SAH animals (Figure 5A-C; control n = 7 cells from 3 animals, SAH n = 14 cells from 3 animals). However, on a relative basis, i.e. when expressed as a percent of basal activity, treatment with caffeine (10 μmol/L) increased the number of active spark sites by approximately 50 % in cerebral artery myocytes from both control and SAH animals. Corresponding to the increase in the number of active spark sites, caffeine (10 μmol/L) also caused a similar percent increase in whole cell Ca^{2+} spark frequency in cerebral artery myocytes from both groups. SR Ca^{2+} content was also examined in cerebral arteries isolated from control and SAH animals using the ratiometric fluorescent Ca^{2+}-sensitive dye, fura-2. Decreased SR Ca^{2+} content has been reported to decrease whole cell Ca^{2+} spark frequency and reduce the amplitude of individual Ca^{2+} sparks (ZhuGe *et al* 1999). Rapid application of high concentrations (millimolar) of caffeine leads to a significant release of Ca^{2+} from the SR

through activation of RyRs. The relative amplitude of these caffeine-induced global Ca^{2+} transients has been used as an index of SR Ca^{2+} content (Santana *et al* 1997; Wellman *et al* 2001) . The amplitudes of caffeine-induced global Ca^{2+} transients were not significantly different in cerebral arteries from control and SAH model animals (Figure 5D). Further, quantitative real-time PCR demonstrated that mRNA levels of the SR Ca^{2+}-binding proteins calsequestrin-2 and calreticulin and the smooth muscle sarco/endoplasmic reticulum Ca^{2+}-ATPase, SERCA-2 were not significantly different in arteries from control and SAH animals (Figure 5E; n = 6 for each group). These data suggest RyR activation properties and SR Ca^{2+} load in myocytes from SAH animals are unaltered, and that increasing RyR activity does not restore the number of functional spark sites to control levels.

The RyR-2 subtype is the dominantly expressed RyR isoform in arterial smooth muscle, and is thought to underlie Ca^{2+} spark activity in these cells (Ji *et al* 2004). RyR-2 activity is modulated by the FK506-binding protein, FKBP12.6, that stabilizes RyR-2 channels in the closed state (Zalk *et al* 2007). Conditional overexpression of FKBP12.6 has been reported to decrease Ca^{2+} spark frequency in cardiac myocytes (Gellen *et al* 2008). Thus, decreased expression of RyR-2 or increased expression of FKBP12.6 may contribute to a reduction in Ca^{2+} spark activity following SAH. To examine whether RyR-2 expression was decreased following SAH, quantitative real-time RT-PCR was performed on RNA extracted from intact cerebral arteries (Figure 6A). When normalized to GAPDH, RyR-2 expression was decreased by approximately 65 % in cerebral arteries from SAH animals compared to controls (n = 6 for each group). Protein levels of RyR-2,

detected by western blot, were also decreased by approximately 50 % in cerebral artery homogenates from SAH rabbits (Figure 6B, C; n = 4 for each group). Interestingly, we also observed that FKBP12.6 mRNA expression was increased two-fold (n = 5) and protein levels were over four-fold greater (n = 4) in cerebral artery homogenate from SAH compared to control animals (Figure 6). These data are consistent with decreased RyR-2 expression and increased FKBP12.6 expression contributing to a reduction in functional spark sites and decreased Ca^{2+} spark frequency in myocytes from SAH animals.

Decreased RyR and BK channel activity contribute to enhanced cerebral artery constriction following SAH.

At physiological intravascular pressures (e.g. 80 mmHg), constriction was greater in cerebral arteries isolated from SAH (34.7 ± 2.7 % decrease in diameter, n = 9) compared to control (18.5 ± 2.6 % decrease in diameter, n = 9) animals. To examine whether SAH-induced decreased Ca^{2+} spark and transient BK current activity contribute to enhanced cerebral artery constriction, arterial diameter measurements were made in the presence and absence of paxilline, a blocker of BK channels and ryanodine, a blocker of RyRs (Figure 7A-C and online supplementary information, Table 3). At an intravascular pressure of 80 mmHg, paxilline (1 μmol/L) caused a robust constriction in arteries from control animals, decreasing diameter from 94.6 ± 10.2 μm to 78.4 ± 8.4 μm, or by 17.1 % (Figure 7B). Thus, with arteries from control animals, BK channel block mimicked SAH to enhance constriction. In contrast, paxilline did not significantly constrict arteries from

SAH animals (diameter prior to paxilline: 96.6 ± 8.1 μm; diameter in the presence of paxilline 95.5 ± 8.6 μm), consistent with SAH causing a decrease in Ca^{2+} spark-induced BK channel activity. In a similar manner, the inhibitor of Ca^{2+} sparks, ryanodine (10 μmol/L), caused a significantly greater constriction in arteries from control compared to SAH animals (Figure 7C). Also consistent with SAH-induced decreased BK channel activity and enhanced vasoconstriction, global cytosolic Ca^{2+}, measured using fura-2, was elevated in cerebral arteries from SAH animals (F_{340}/F_{380}: 1.18 ± 0.04; estimated Ca^{2+}: 222 ± 12 nM, n = 4) compared to control animals (F_{340}/F_{380}: 1.00 ± 0.07; estimated Ca^{2+}: 175 ± 12 nM, n = 4). In contrast to the SAH-induced disruption of the Ca^{2+} spark/BK channel dilator pathway, dilations to the endothelial-dependent agonist, acetylcholine, and the endothelial-independent dilator, sodium nitroprusside, were similar in arteries from control and SAH animals (Figure 7D, E). These data are consistent with decreased Ca^{2+} spark-induced BK channel activity contributing to enhanced constriction of cerebral arteries from SAH animals.

Discussion

Here, we provide evidence that a reduction in subcellular Ca^{2+} release events (i.e. Ca^{2+} sparks) underlies decreased BK channel activity and enhanced cerebral artery constriction following SAH. The following observations support this concept: 1) cell-wide Ca^{2+} spark frequency is decreased in cerebral artery myocytes from SAH animals, reflecting a decrease in active Ca^{2+} spark discharge sites; 2) mRNA and protein levels of RyR-2, the SR Ca^{2+} release channel responsible for Ca^{2+} sparks in smooth muscle, is reduced in

cerebral artery myocytes following SAH; 3) mRNA and protein levels of the RyR-2 stabilizing protein, FKBP12.6, is increased in cerebral arteries from SAH animals; 4) the frequency of Ca^{2+} spark-induced transient BK currents is decreased in cerebral artery myocytes from SAH animals, with no change in BK channel properties, whole-cell BK currents or BK subunit expression; 5) constriction caused by inhibitors of Ca^{2+} sparks (ryanodine) or BK channels (paxilline) is decreased in cerebral arteries from SAH animals. Together, these data suggest that SAH-induced decreased Ca^{2+} spark frequency and the resulting decrease in transient BK channel activity promotes membrane potential depolarization, enhanced Ca^{2+} influx via VDCCs and cerebral artery constriction.

To our knowledge, these findings represent the first demonstration of a vascular pathology due to a decrease in Ca^{2+} spark frequency. Although altered frequency of Ca^{2+} spark-induced transient BK currents has been reported in other cardiovascular diseases such as hypertension and hypovolemic shock, these phenomena have been attributed to altered BK channel function/expression. Enhanced constriction associated with hypertension and diabetes has been linked to decreased expression of the BK channel β_1 subunit (Amberg and Santana 2003; Brenner *et al* 2000; Dong *et al* 2008) while an acute upregulation of BK channel β_1 subunit contributes to vasodilation and the drop in peripheral resistance associated with hemorrhagic shock (Zhao *et al* 2007). In the above pathologies, Ca^{2+} spark activity was unaltered. In marked contrast, we observed a parallel decrease in the frequency of Ca^{2+} sparks and Ca^{2+} spark-induced transient BK currents following SAH. Notably, experimental SAH did not directly alter BK channel properties or expression. Our observed lack of direct effect of SAH on BK channels in

pial arteries obtained from SAH model rabbits is consistent with observations using basilar artery myocytes obtained from a dog SAH model (Jahromi *et al* 2008b).

We found that the overall decrease in Ca^{2+} spark frequency in myocytes from SAH animals reflected a decrease in the number of functional spark sites. Both the number of functional spark sites and whole cell Ca^{2+} spark frequency were reduced by approximately 50 % in myocytes following SAH. Although the RyR activator, caffeine (10 μmol/L), caused proportionately the same increase in the number of functional spark sites and Ca^{2+} spark frequency in myocytes from control and SAH animals, both parameters remained approximately 50 % lower in SAH animals. Spark sites within arterial myocytes are comprised of a variable number of RyRs, and functional spark sites require the activity of a critical number of RyRs for Ca^{2+}-induced Ca^{2+} release and Ca^{2+} sparks to occur (Janiak *et al* 2001; Pucovsky and Bolton 2006). Using quantitative real-time PCR and western blot, we observed a significant reduction in mRNA and protein levels of RyR-2 in cerebral arteries following SAH. A decrease in RyR-2 expression has been previously reported in cardiac myocytes following heart failure (Go *et al* 1995) and in vascular smooth muscle undergoing phenotypic changes during cell culture (Berra-Romani *et al* 2008). It is conceivable that the SAH-induced decreased RyR-2 expression caused some, but not all, spark sites to no longer have the threshold number of RyRs required for Ca^{2+} spark initiation.

In addition to decreased RyR-2 expression, increases in the relative expression of proteins that reduce RyR-2 activity may also contribute to the observed decrease in the number of functional Ca^{2+} spark sites. For example, we observed increased mRNA and

protein levels of the RyR-2 regulatory protein, FKBP12.6. Binding of FKBP12.6 stabilizes RyR-2 in the closed state (Zalk *et al* 2007). Ablation of the gene encoding FKBP12.6 has been reported to increase Ca^{2+} spark frequency in smooth muscle (Ji *et al* 2004) and conversely, conditional overexpression of FKBP12.6 has been linked to decreased Ca^{2+} spark frequency in cardiac myocytes (Gellen *et al* 2008). Our current data suggest that increased FKBP12.6 expression acting in concert with decreased RyR-2 expression underlie the decrease in active Ca^{2+} sparks in cerebral artery myocytes from SAH model animals. Based on the present study, the relative contribution of decreased RyR-2 expression versus increased FKBP12.6 expression to the observed SAH-induced reduction in Ca^{2+} spark activity is unclear.

Decreased SR Ca^{2+} content has also been linked to decreased Ca^{2+} spark frequency and amplitude in smooth muscle (ZhuGe *et al* 1999), thus, reduced SR Ca^{2+} could potentially contribute to decreased Ca^{2+} spark frequency following SAH. However, our data argue against this possibility. First, we observed no difference in the amplitude of global Ca^{2+} transients induced by rapid application of a high concentration (10 mmol/L) of caffeine following SAH. Secondly, we observed a reduction in the number of functional Ca^{2+} spark sites, rather than a uniform reduction in Ca^{2+} spark frequency, and Ca^{2+} spark amplitude was similar in myocytes from control and SAH animals. Further, mRNA levels of SR-Ca^{2+}-ATPase (SERCA-2) and the SR Ca^{2+} binding proteins, calsequestrin-2 and calreticulin, were similar in cerebral arteries from control and SAH animals. It is possible that additional factors such as RyR-2 phosphorylation

(Zalk *et al* 2007) could contribute to a reduction in functional Ca^{2+} spark sites in cerebral artery myocytes following SAH.

The present work may help to explain the impact of SAH leading to enhanced constriction of small diameter cerebral arteries and decreased cerebral blood flow. We have previously reported an increase in VDCC current density, in part due to the emergence of R-type VDCCs encoded by the gene $Ca_V2.3$, in cerebral artery myocytes from SAH model rabbits (Ishiguro *et al* 2005). Membrane potential depolarization caused by a decrease in Ca^{2+} spark-induced transient BK currents would be predicted to cause an increase in the open-state probability of VDCCs and combined with enhanced VDCC expression would increase global cytosolic Ca^{2+} leading to enhanced contraction of cerebral artery myocytes. Additional mechanisms such as decreased voltage-dependent potassium (K_V) channel expression (Jahromi *et al* 2008a) and activity (Ishiguro *et al* 2006; Koide *et al* 2007; Quan and Sobey 2000) and increased protein kinase C activity (Nishizawa *et al* 2000) are also likely to contribute to enhanced cerebral artery constriction following SAH.

In conclusion, we report that the frequency of Ca^{2+} sparks and associated transient BK currents were significantly decreased in cerebral artery myocytes following SAH, contributing to enhanced vasoconstriction. Our findings suggest this SAH-induced decrease in Ca^{2+} spark frequency results from a reduction in RyR-2 expression and increased FKBP12.6 expression leading to a decrease in the number of functional spark sites within these myocytes. This mechanism may contribute to a reduction in cerebral blood flow and the development of neurological deficits experienced by patients

following cerebral aneurysm rupture. Further, this mechanism of decreased vascular BK channel activity may also contribute to other types of brain pathologies, including traumatic brain injury.

Acknowledgements:

The authors wish to thank Ms. Sheila Russell for her assistance and acknowledge the University of Vermont Neuroscience COBRE molecular biology and imaging core facilities.

Disclosures/Conflict of Interest: The authors declare no conflict of interest.

Supplementary information is available at the *Journal of Cerebral Blood Flow and Metabolism* website.

References

Amberg GC, Santana LF (2003) Downregulation of the BK channel beta1 subunit in genetic hypertension. *Circ Res* 93:965-71

Berra-Romani R, Mazzocco-Spezzia A, Pulina MV, Golovina VA (2008) Ca^{2+} handling is altered when arterial myocytes progress from a contractile to a proliferative phenotype in culture. *Am J Physiol Cell Physiol* 295:C779-90

Brenner R, Perez GJ, Bonev AD, Eckman DM, Kosek JC, Wiler SW, Patterson AJ, Nelson MT, Aldrich RW (2000) Vasoregulation by the beta1 subunit of the calcium-activated potassium channel. *Nature* 407:870-6

Dong L, Zheng YM, Van Riper D, Rathore R, Liu QH, Singer HA, Wang YX (2008) Functional and molecular evidence for impairment of calcium-activated potassium channels in type-1 diabetic cerebral artery smooth muscle cells. *J Cereb Blood Flow Metab* 28:377-86

Gellen B, Fernandez-Velasco M, Briec F, Vinet L, LeQuang K, Rouet-Benzineb P, Benitah JP, Pezet M, Palais G, Pellegrin N, Zhang A, Perrier R, Escoubet B, Marniquet X, Richard S, Jaisser F, Gomez AM, Charpentier F, Mercadier JJ (2008) Conditional FKBP12.6 overexpression in mouse cardiac myocytes prevents triggered ventricular tachycardia through specific alterations in excitation-contraction coupling. *Circulation* 117:1778-86

Go LO, Moschella MC, Watras J, Handa KK, Fyfe BS, Marks AR (1995) Differential regulation of two types of intracellular calcium release channels during end-stage heart failure. *J Clin Invest* 95:888-94

Grynkiewicz G, Poenie M, Tsien RY (1985) A new generation of Ca^{2+} indicators with greatly improved fluorescence properties. *J Biol Chem* 260:3440-50

Hattingen E, Blasel S, Dettmann E, Vatter H, Pilatus U, Seifert V, Zanella FE, Weidauer S (2008) Perfusion-weighted MRI to evaluate cerebral autoregulation in aneurysmal subarachnoid haemorrhage. *Neuroradiology* 50:929-38

Hop JW, Rinkel GJ, Algra A, van Gijn J (1997) Case-fatality rates and functional outcome after subarachnoid hemorrhage: a systematic review. *Stroke* 28:660-4

Ishiguro M, Puryear CB, Bisson E, Saundry CM, Nathan DJ, Russell SR, Tranmer BI, Wellman GC (2002) Enhanced myogenic tone in cerebral arteries from a rabbit model of subarachnoid hemorrhage. *Am J Physiol Heart Circ Physiol* 283:H2217-25

Ishiguro M, Wellman TL, Honda A, Russell SR, Tranmer BI, Wellman GC (2005) Emergence of a R-type Ca^{2+} channel (Ca_V 2.3) contributes to cerebral artery constriction after subarachnoid hemorrhage. *Circ Res* 96:419-26

Ishiguro M, Morielli AD, Zvarova K, Tranmer BI, Penar PL, Wellman GC (2006) Oxyhemoglobin-induced suppression of voltage-dependent K^+ channels in cerebral arteries by enhanced tyrosine kinase activity. *Circ Res* 99:1252-60

Jahromi BS, Aihara Y, Ai J, Zhang ZD, Nikitina E, Macdonald RL (2008a) Voltage-gated K^+ channel dysfunction in myocytes from a dog model of subarachnoid hemorrhage. *J Cereb Blood Flow Metab* 28:797-811

Jahromi BS, Aihara Y, Ai J, Zhang ZD, Weyer G, Nikitina E, Yassari R, Houamed KM, Macdonald RL (2008b) Preserved BK channel function in vasospastic myocytes from a dog model of subarachnoid hemorrhage. *J Vasc Res* 45:402-15

Janiak R, Wilson SM, Montague S, Hume JR (2001) Heterogeneity of calcium stores and elementary release events in canine pulmonary arterial smooth muscle cells. *Am J Physiol Cell Physiol* 280:C22-33

Ji G, Feldman ME, Greene KS, Sorrentino V, Xin HB, Kotlikoff MI (2004) RYR2 proteins contribute to the formation of Ca^{2+} sparks in smooth muscle. *J Gen Physiol* 123:377-86

Kelley-Hedgepeth A, Peter I, Montefusco MC, Levy D, Benjamin EJ, Vasan RS, Mendelsohn ME, Housman D, Huggins GS, Mitchell GF (2009) The KCNMB1 E65K variant is associated with reduced central pulse pressure in the community-based Framingham Offspring Cohort. *J Hypertens* 27:55-60

Knot HJ, Nelson MT (1998) Regulation of arterial diameter and wall [Ca^{2+}] in cerebral arteries of rat by membrane potential and intravascular pressure. *J Physiol* 508 (Pt 1):199-209

Koide M, Penar PL, Tranmer BI, Wellman GC (2007) Heparin-binding EGF-like growth factor mediates oxyhemoglobin-induced suppression of voltage-dependent potassium channels in rabbit cerebral artery myocytes. *Am J Physiol Heart Circ Physiol* 293:H1750-9

Kong H, Jones PP, Koop A, Zhang L, Duff HJ, Chen SR (2008) Caffeine induces Ca^{2+} release by reducing the threshold for luminal Ca^{2+} activation of the ryanodine receptor. *Biochem J* 414:441-52

Macdonald RL, Pluta RM, Zhang JH (2007) Cerebral vasospasm after subarachnoid hemorrhage: the emerging revolution. *Nat Clin Pract Neurol* 3:256-63

Nelson MT, Cheng H, Rubart M, Santana LF, Bonev AD, Knot HJ, Lederer WJ (1995) Relaxation of arterial smooth muscle by calcium sparks. *Science* 270:633-7

Nishizawa S, Obara K, Nakayama K, Koide M, Yokoyama T, Yokota N, Ohta S (2000) Protein kinase cdelta and alpha are involved in the development of vasospasm after subarachnoid hemorrhage. *Eur J Pharmacol* 398:113-9

Ohkuma H, Manabe H, Tanaka M, Suzuki S (2000) Impact of cerebral microcirculatory changes on cerebral blood flow during cerebral vasospasm after aneurysmal subarachnoid hemorrhage. *Stroke* 31:1621-7

Ostrowski RP, Colohan AR, Zhang JH (2006) Molecular mechanisms of early brain injury after subarachnoid hemorrhage. *Neurol Res* 28:399-414

Perez GJ, Bonev AD, Nelson MT (2001) Micromolar Ca^{2+} from sparks activates Ca^{2+}-sensitive K^{+} channels in rat cerebral artery smooth muscle. *Am J Physiol Cell Physiol* 281:C1769-75

Prunell GF, Svendgaard NA, Alkass K, Mathiesen T (2005) Inflammation in the brain after experimental subarachnoid hemorrhage. *Neurosurgery* 56:1082-92; discussion -92

Pucovsky V, Bolton TB (2006) Localisation, function and composition of primary Ca^{2+} spark discharge region in isolated smooth muscle cells from guinea-pig mesenteric arteries. *Cell Calcium* 39:113-29

Quan L, Sobey CG (2000) Selective effects of subarachnoid hemorrhage on cerebral vascular responses to 4-aminopyridine in rats. *Stroke* 31:2460-5

Santana LF, Kranias EG, Lederer WJ (1997) Calcium sparks and excitation-contraction coupling in phospholamban-deficient mouse ventricular myocytes. *J Physiol* 503 (Pt 1):21-9

Tanaka Y, Meera P, Song M, Knaus HG, Toro L (1997) Molecular constituents of maxi K_{Ca} channels in human coronary smooth muscle: predominant alpha + beta subunit complexes. *J Physiol* 502 (Pt 3):545-57

Tomas M, Vazquez E, Fernandez-Fernandez JM, Subirana I, Plata C, Heras M, Vila J, Marrugat J, Valverde MA, Senti M (2008) Genetic variation in the KCNMA1 potassium channel alpha subunit as risk factor for severe essential hypertension and myocardial infarction. *J Hypertens* 26:2147-53

Wellman GC, Santana LF, Bonev AD, Nelson MT (2001) Role of phospholamban in the modulation of arterial Ca^{2+} sparks and Ca^{2+}-activated K^+ channels by cAMP. *Am J Physiol Cell Physiol* 281:C1029-37

Wellman GC, Nathan DJ, Saundry CM, Perez G, Bonev AD, Penar PL, Tranmer BI, Nelson MT (2002) Ca^{2+} sparks and their function in human cerebral arteries. *Stroke* 33:802-8

Wellman GC, Nelson MT (2003) Signaling between SR and plasmalemma in smooth muscle: sparks and the activation of Ca^{2+}-sensitive ion channels. *Cell Calcium* 34:211-29

Zalk R, Lehnart SE, Marks AR (2007) Modulation of the ryanodine receptor and intracellular calcium. *Annu Rev Biochem* 76:367-85

Zhao G, Zhao Y, Pan B, Liu J, Huang X, Zhang X, Cao C, Hou N, Wu C, Zhao KS, Cheng H (2007) Hypersensitivity of BK_{Ca} to Ca^{2+} sparks underlies hyporeactivity of arterial smooth muscle in shock. *Circ Res* 101:493-502

ZhuGe R, Tuft RA, Fogarty KE, Bellve K, Fay FS, Walsh JV, Jr. (1999) The influence of sarcoplasmic reticulum Ca^{2+} concentration on Ca^{2+} sparks and spontaneous transient outward currents in single smooth muscle cells. *J Gen Physiol* 113:215-28

Figure Legends

Figure 1: Decreased frequency of transient outward BK currents in cerebral artery myocytes from SAH model rabbits. (**A**) Representative traces of transient BK currents in cerebral artery myocytes from control and SAH rabbits. Holding potential was changed in 10 mV increments every ~5 min. (**B**) Expanded traces are from the region denoted by black bars in panel A. (**C**) Average traces were obtained from all events at -40 mV shown in panel A (control: 52 events, SAH: 18 events). (**D**, **E**) Summarized data of transient BK current frequency and amplitude, respectively. Control: n = 9 cells from 6 animals; SAH: n = 8 from 6 animals. * $p < 0.05$, ** $p < 0.01$

Figure 2: Maintained expression and properties of BK channels in cerebral artery myocytes following SAH. (**A**) Representative BK single channel recordings from inside-out membrane patches in the presence of 10^{-7} mol/L free Ca^{2+}. Closed state (C) and individual channel open states (O1-O5) are included in each record. (**B**) Ca^{2+}- and voltage-sensitivity of BK channels in control (n = 6-16 patches from 4 animals) and SAH myocytes (n = 12-19 patches from 4 animals). Free Ca^{2+} concentration calculated for the "Zero" Ca^{2+} solution was < 1 nmol/L. Open-state probability curves were obtained from Boltzman fit of data. (**C**) BK channel densities shown as channel number per patch at +80 mV in control (n = 25) and SAH cerebral myocytes (n = 27). NS: $p > 0.05$. (**D**) Current-voltage relationship of paxilline-sensitive currents in myocytes from control (open circles, n = 5) and SAH rabbits (closed circles, n = 6). (**E**) Summary of

quantitative real-time PCR for α and β_1 subunits of the BK channel, normalized to GAPDH.

Figure 3: Decreased Ca^{2+} spark frequency, but not amplitude, in cerebral artery myocytes from SAH animals. (**A**) Representative Ca^{2+} spark images and fractional fluorescent traces from cerebral artery myocytes isolated from control and SAH rabbits. Gray scale images are an average of 30 images without Ca^{2+} spark activity (F_0 image). Red crosses depict where individual Ca^{2+} sparks occurred during the 20 second recordings. Pseudo-color images illustrate Ca^{2+} sparks in control and SAH myocytes. Fractional fluorescent (F/F_0) records are from 2.1 μm x 2.1 μm analysis areas (white boxes in first enlarged images) centered over Ca^{2+} sparks. White bars represent 10 μm. (**B**, **C**) Summarized data of whole cell frequency and amplitude, respectively, of Ca^{2+} sparks in cerebral artery myocytes (control: n = 45 cells from 5 animals, SAH: n = 48 cells from 6 animals). ** $p < 0.01$

Figure 4: Decreased functional Ca^{2+} spark sites in cerebral artery myocytes from SAH animals. (**A**) Gray scale images are an average of 30 images without Ca^{2+} spark activity (F_0 image) with red crosses depicting the location of individual Ca^{2+} sparks during 20 sec recordings. White boxes on pseudo-color images depict distinct spark sites within each cell. (**B**) Numbered images depict individual spark sites within each cell. (**C**) Corresponding fractional fluorescent (F/F_0) traces from spark sites shown in panel B. Arrows indicate Ca^{2+} sparks accounted to each site. (**D**) Summarized data of the number

of spark sites observed in each cell. (**E**) Average Ca^{2+} spark frequency in individual spark sites. (**F**) Relationship between the number of spark sites in individual cells and whole cell Ca^{2+} spark frequency. Solid lines with symbol color (control: gray, SAH: black) represent linear regression analysis of data. Data was obtained from 1082 sparks from 355 spark sites in 45 cells from 5 control animals and 594 sparks from 217 spark sites in 48 cells from 6 SAH animals. ** $p < 0.01$

Figure 5: RyR activation properties and SR Ca^{2+} load in cerebral arteries from SAH animals. (**A**-**C**): The RyR activator, caffeine (10 μmol/L), did not restore the number of functional spark sites or whole cell Ca^{2+} spark frequency in cerebral artery myocytes from SAH animals to control levels. (**A**) Average of 30 consecutive images without Ca^{2+} spark activity, with white crosses depicting the location of Ca^{2+} sparks observed during 20 sec recordings in the absence and presence (+Caffeine) of caffeine. White bars represent 10 μm. (**B**, **C**) Summary of the effect of caffeine on the number of functional spark sites per cell (**B**) and whole cell Ca^{2+} spark frequency (**C**). Control: n = 7 cells from 3 animals, SAH: n = 14 cells from 3 animals. * $p<0.05$, ** $p<0.01$ control vs SAH. (**D**) Estimated Ca^{2+} content in sarcoplasmic reticulum (SR) of cerebral arteries from control and SAH animals. The amplitude of global cytosolic Ca^{2+} transients induced by rapid application of a high concentration of caffeine (10 mmol/L) was not significantly different between groups (control: n = 4, SAH: n = 3). (**E**) Summarized data of quantitative real-time PCR for smooth muscle sarco-endoplasmic reticulum Ca^{2+}-

ATPase (SERCA-2), calsequestrin-2, and calreticulin expressed as a ratio to GAPDH (n = 6 for each group). ** $p < 0.01$

Figure 6: Decreased expression of ryanodine receptor-2 (RyR-2) and increased expression of FKBP12.6 in cerebral arteries from SAH animals. (**A**) Summarized quantitative real-time PCR data for RyR-2 (n = 6) and FKBP12.6 (n = 5). ** $p < 0.01$ (**B**) Immunoreactive bands corresponding to RyR-2, FKBP12.6 and α-smooth muscle actin in cerebral arteries detected by western blot. (**C**) Summarized RyR-2 and FKBP12.6 protein levels expressed as a ratio to α-smooth muscle actin (n = 4 for each groups). * $p < 0.05$

Figure 7: Inhibitors of Ca^{2+} sparks and BK channels constrict cerebral arteries from control, but not SAH model animals. (**A**) Diameter recordings of pressurized (80 mmHg) cerebral arteries from control (left) and SAH (right) animals treated with the BK channel blocker paxilline (1 μmol/L). Maximum dilation was obtained using a combination of diltiazem (100 μM) and forskolin (1μM) in Ca^{2+}-free physiological saline solution. (**B, C**) Summarized data of constriction caused by paxilline (B, n = 5) or ryanodine (C, n = 4), expressed as a percent decrease in diameter, of pressurized arteries isolated from control and SAH animals. (**D**) Vasodilation to cumulative additions of acetylcholine (ACh) are expressed as percent dilation of pressure-induced (myogenic) tone. Data expressed as mean ± SEM; n = 7 control, n = 5 SAH. (**E**) Vasodilation to cumulative additions of sodium nitroprusside (SNP) are expressed as percent dilation of

pressure-induced (myogenic) tone. Data are expressed as mean ± SEM; n = 4 control, n = 4 SAH.

Figures

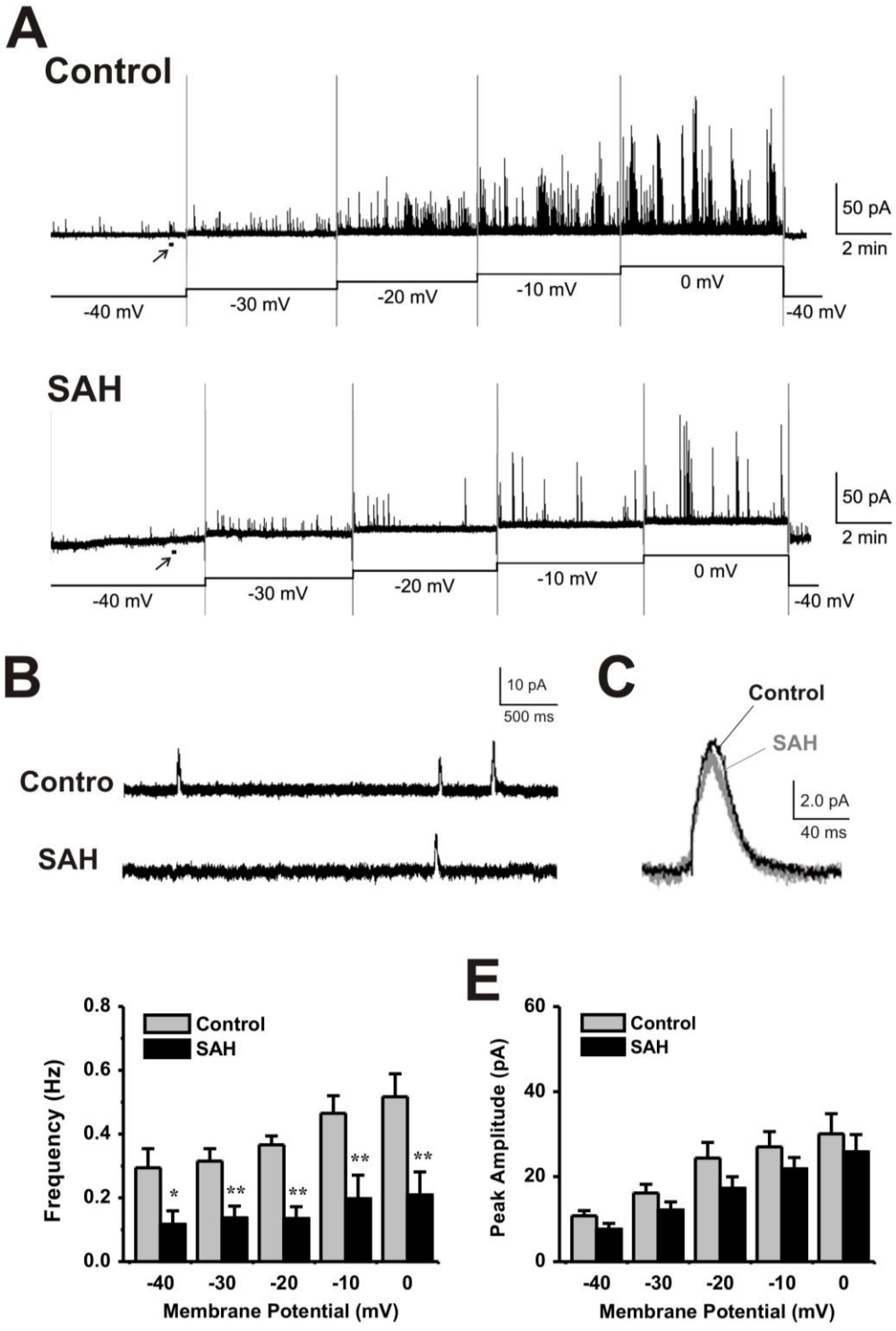

Figure 1: ***Decreased frequency of transient outward BK currents in cerebral artery myocytes from SAH model rabbits.***

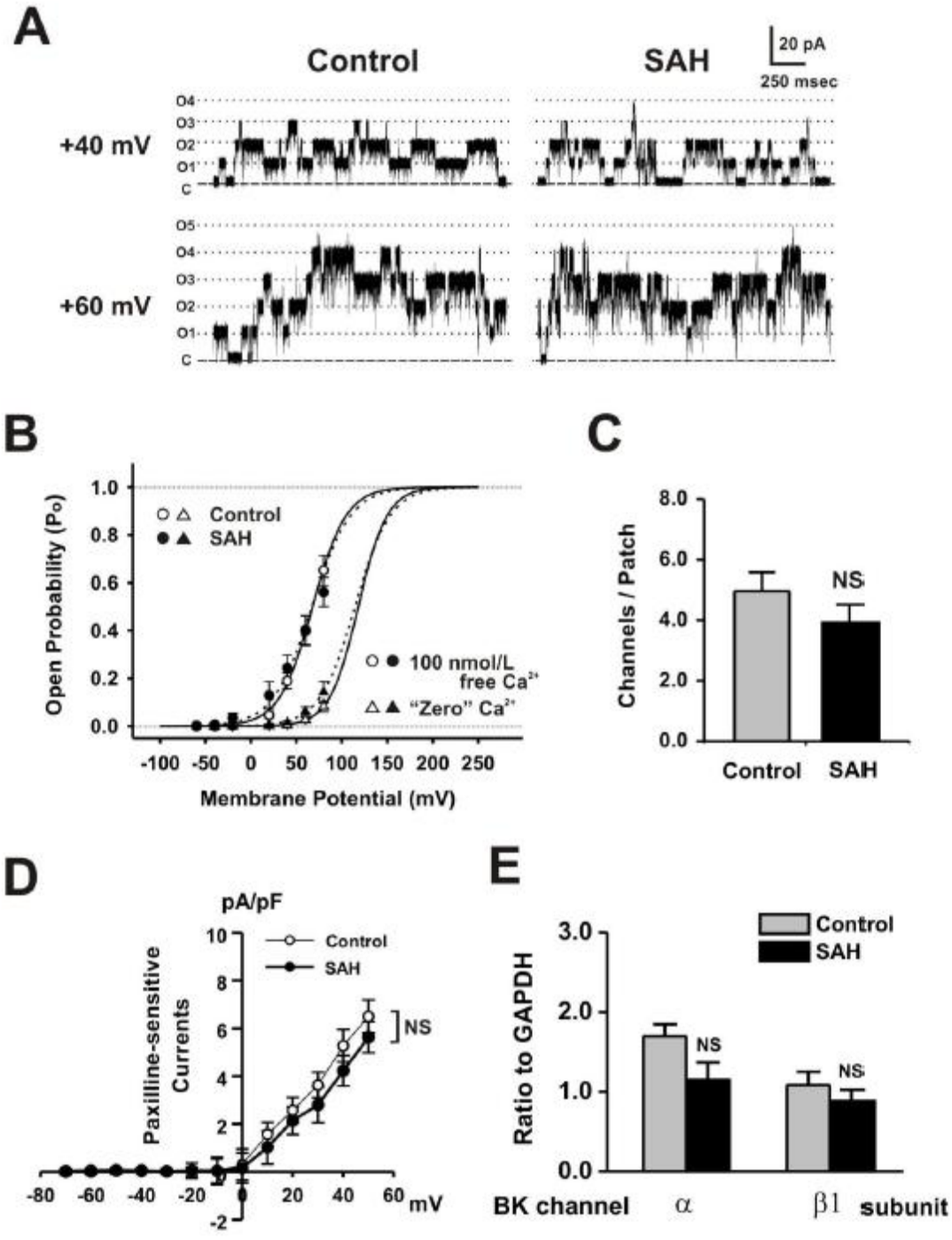

Figure 2: ***Maintained expression and properties of BK channels in cerebral artery myocytes following SAH.***

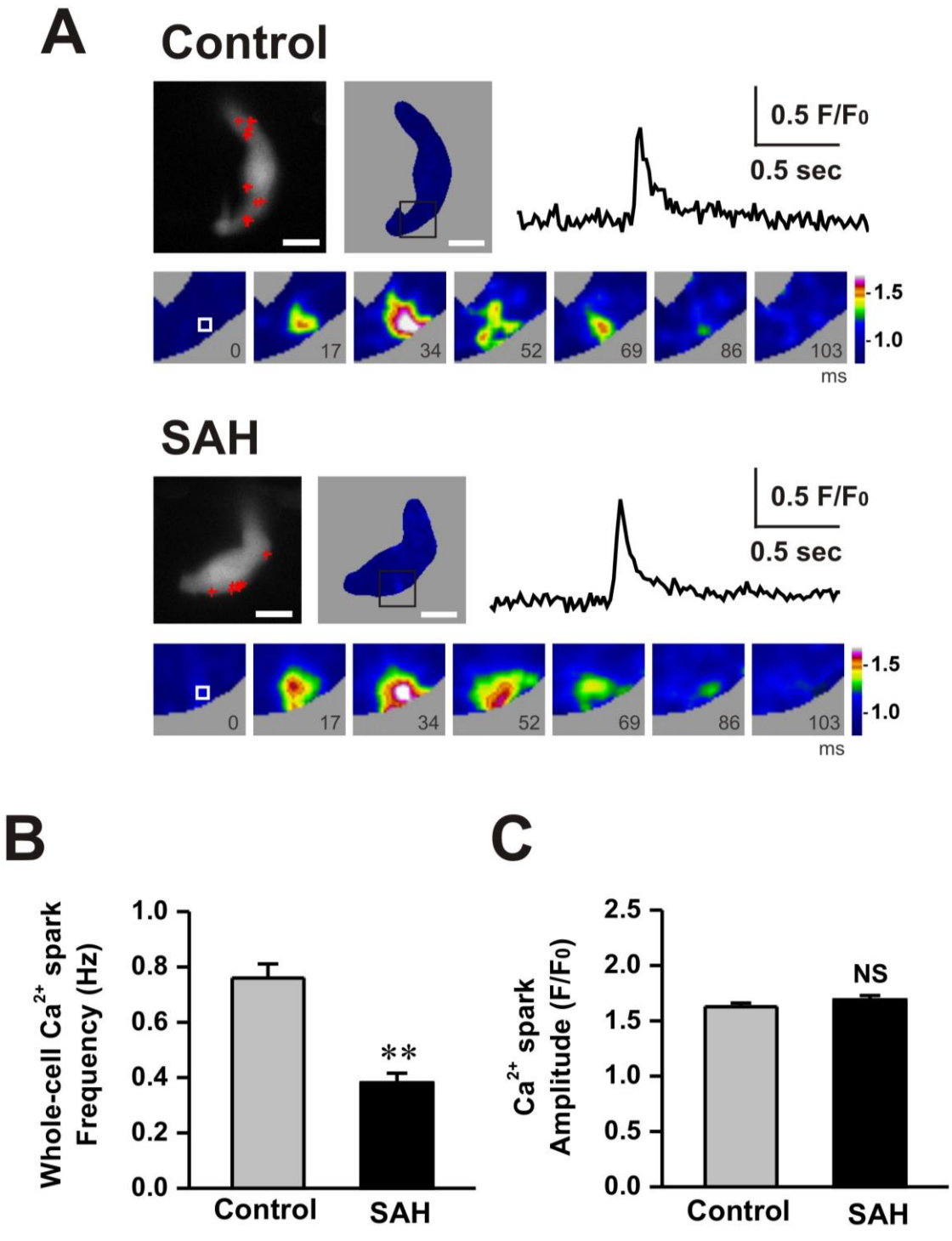

Figure 3: ***Decreased Ca^{2+} spark frequency, but not amplitude, in cerebral artery myocytes from SAH animals.***

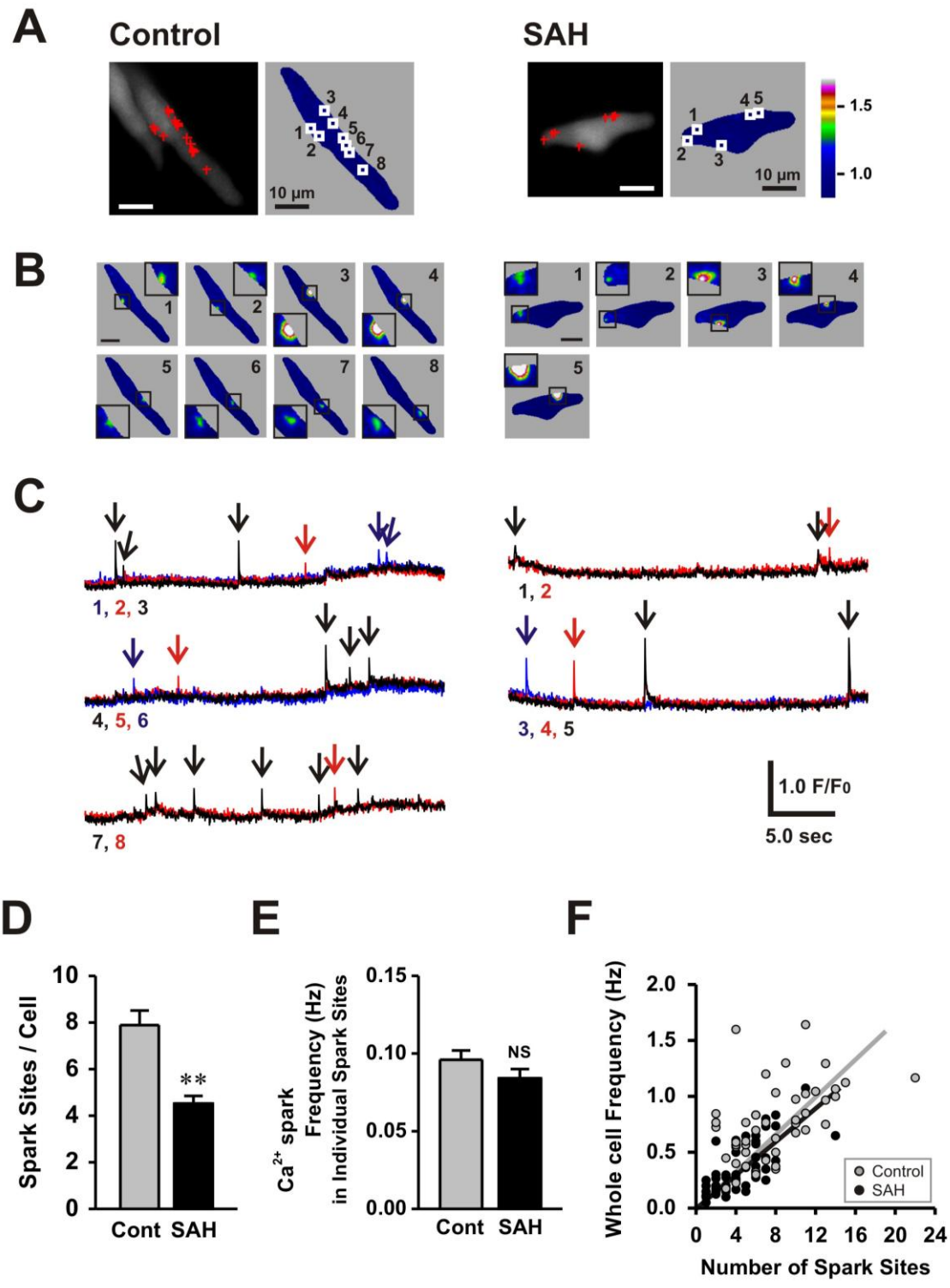

Figure 4*: Decreased functional Ca^{2+} spark sites in cerebral artery myocytes from SAH animals*.

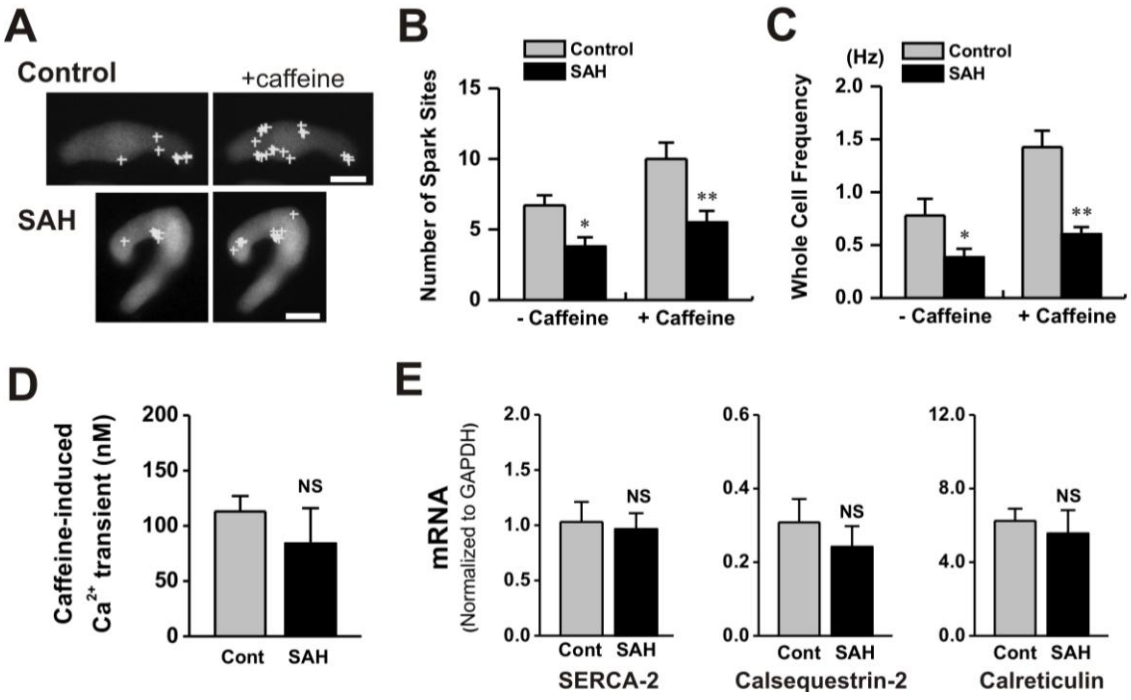

Figure 5: ***RyR activation properties and SR Ca^{2+} load in cerebral arteries from SAH animals.***

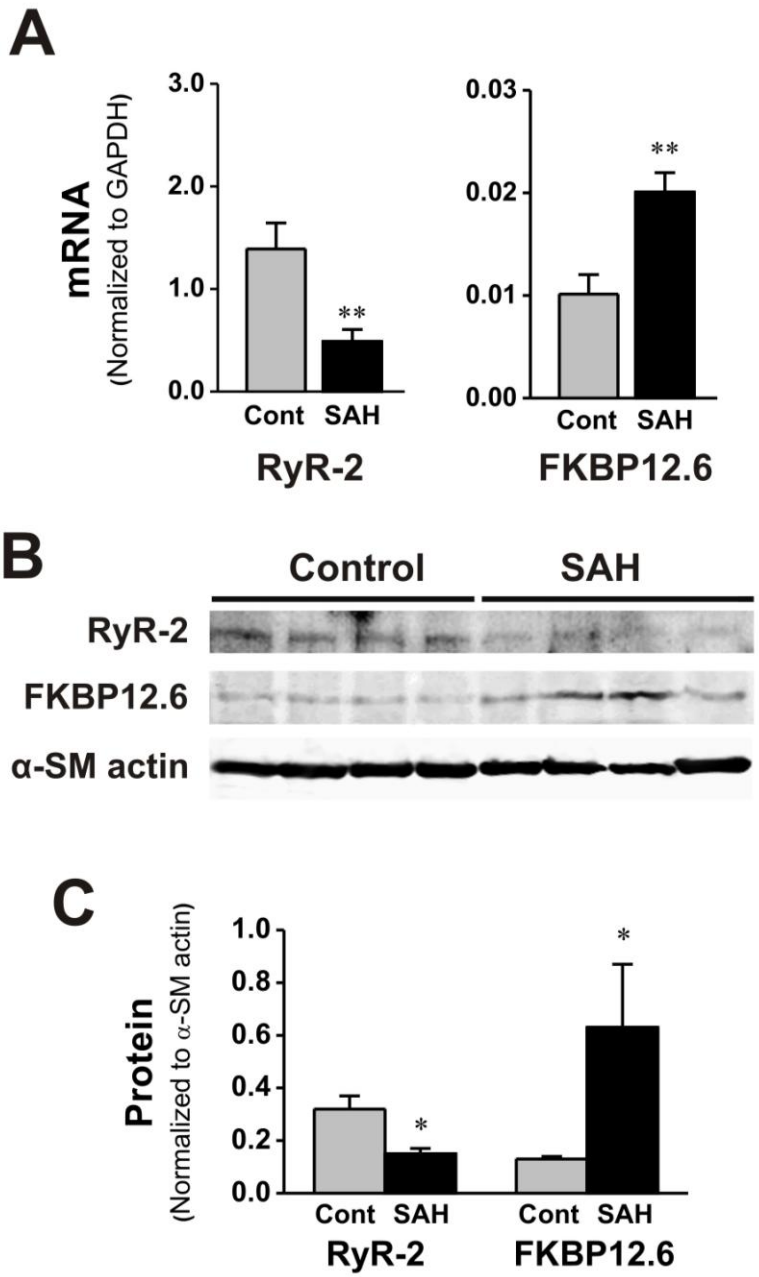

Figure 6: ***Decreased expression of ryanodine receptor-2 (RyR-2) and increased expression of FKBP12.6 in cerebral arteries from SAH animals.***

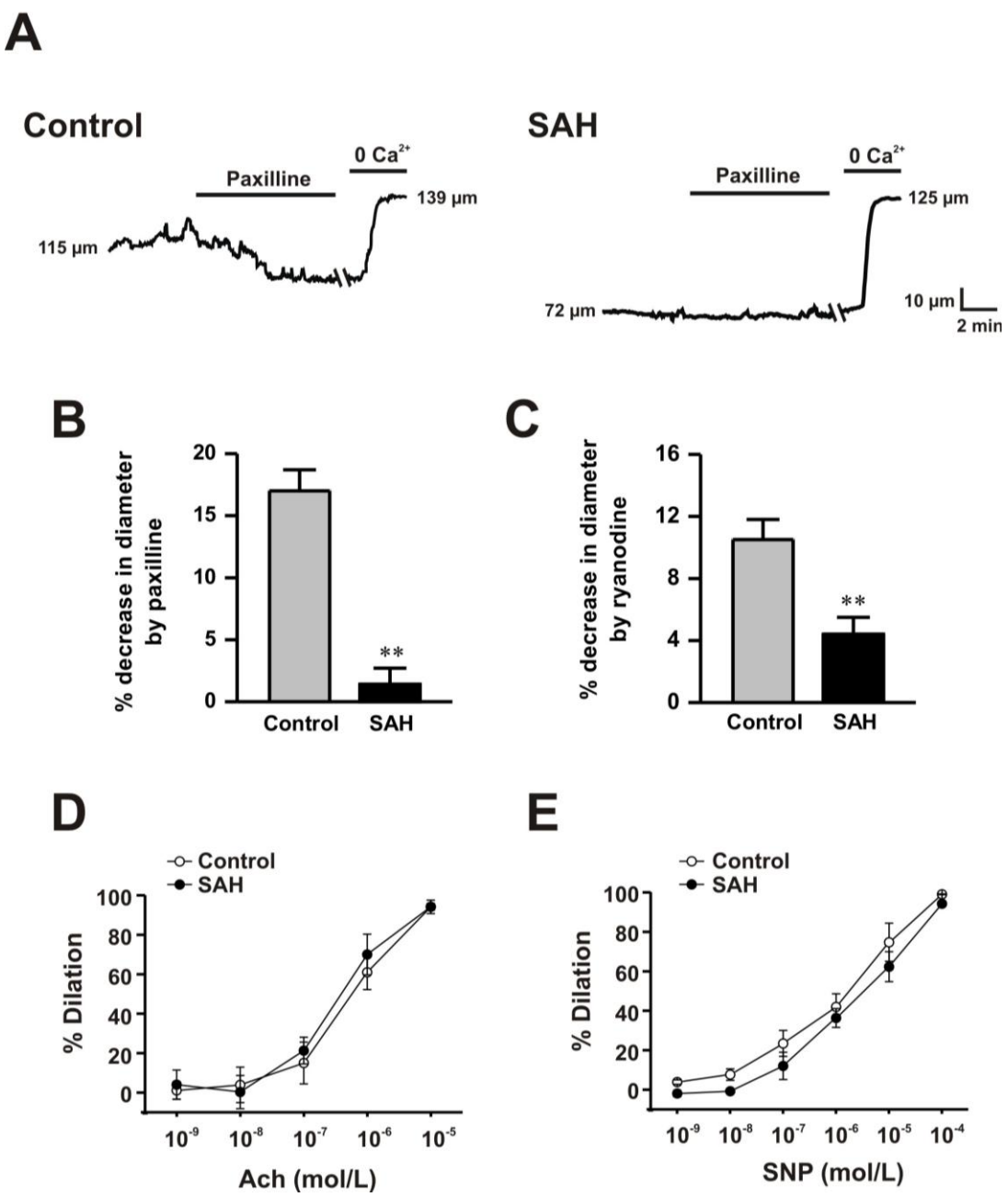

Figure 7: ***Inhibitors of Ca^{2+} sparks and BK channels constrict cerebral arteries from control, but not SAH model animals.***

Table 1: Primers for quantitative real time PCR

Target (rabbit)	Forward primer (5' → 3')	Reverse primer (5' → 3')	GeneBank accession number	Amplification region
RyR-2	CCCAAGAATGATCTGGAGGA	GCAGAATGGCTTGTGCTGTA	NM001082757	4301-4521
FKBP12.6	GGAGACGGGAGGACGTTT	CTCCGTATGCCACATCAGG	NM001082145	31-253
Calsequestrin-2	TTGCTAACTCACAAGCGTGG	AAATTAACCTCCCACCCCAG	NM001101691	1704-2022
Calreticulin	AGTACTCGCCCGACGCTAAC	CACGTCTCGTTGCCAAACTC	NM001082235	953-1100
SERCA-2	ACACTGACCCTGTCCCAGAC	CTTTGGAAAGCTGTTCTCCG	NM001089320	1084-1302
BK channel α subunit	CAAGAAGAGTTCCTCCGTGC	CATATCAAAGCCGCTCTTCC	NM001082070	3520-3635
BK channel ß1 subunit	CTTGTGTCGGCTGATTGAGA	GCTCTGACCTTCTCCACGTC	NM001082225	600-821
GAPDH	AGTATGATTCCACCCACGGC	TGGATTCCACCACGTACTCG	NM001082253	211-363

Table 2: Transient BK current and Ca^{2+} spark characteristics

	Control	SAH
Transient BK currents		
At -40 mV	*9 cells (6 animals)*	*8 cells (6 animals)*
Frequency (Hz)	0.29 ± 0.06	0.12 ± 0.04 *
Amplitude (pA)	10.8 ± 1.2	7.6 ± 1.4
Rise time (msec)	16.1 ± 0.9	21.1 ± 5.5
Decay time (msec)	31.2 ± 3.1	34.6 ± 10.0
Cell capacitance (pF)	10.8 ± 0.7	10.0 ± 0.7
Series resistance (MΩ)	30.6 ± 4.6	34.2 ± 3.5
Ca^{2+} sparks		
Whole cell	*45 cells (5 animals)*	*48 cells (6 animals)*
Frequency (Hz)	0.76 ± 0.05	0.38 ± 0.03 **
Amplitude (pA)	1.63 ± 0.03	1.69 ± 0.04
Rise time (msec)	30.3 ± 0.9	29.1 ± 0.8
Decay time (msec)	39.3 ± 2.3	41.8 ± 2.3
Duration (msec)	56.5 ± 2.6	61.0 ± 2.5
Spacial area (µm²)	14.6 ± 0.7	13.0 ± 0.7
Number of spark sites	7.9 ± 0.6	4.5 ± 0.4 **
Individual spark sites	*355 sites in 45 cells (5 animals)*	*217 sites in 48 cells (6 animals)*
Frequency (Hz)	0.095 ± 0.006	0.084 ± 0.006
Ca^{2+} sparks - Caffeine (10 µmol/L) treatment -		
Before treatment		
Whole cell	*7 cells (3 animals)*	*14 cells (3 animals)*
Frequency (Hz)	0.78 ± 0.16	0.38 ± 0.08 *
Amplitude (pA)	1.71 ± 0.09	1.77 ± 0.06
Rise time (msec)	35.4 ± 2.6	30.7 ± 1.4
Decay time (msec)	36.0 ± 4.9	36.8 ± 3.4
Duration (msec)	54.1 ± 6.9	53.2 ± 3.3
Spacial area (µm²)	9.4 ± 0.7	11.0 ± 0.9
Number of spark sites	6.7 ± 0.7	3.8 ± 0.7 *
Individual spark sites	*47 sites in 7 cells (3 animals)*	*53 sites in 14 cells (3 animals)*
Frequency (Hz)	0.11 ± 0.02	0.10 ± 0.02
After caffeine-treatment		
Whole cell	*7 cells (3 animals)*	*14 cells (3 animals)*
Frequency (Hz)	1.43 ± 0.16	0.60 ± 0.07 **
Amplitude (pA)	1.59 ± 0.08	1.53 ± 0.06
Rise time (msec)	34.5 ± 1.6	36.5 ± 1.8
Decay time (msec)	34.2 ± 1.9	35.1 ± 2.5
Duration (msec)	54.0 ± 5.6	55.0 ± 3.5
Spacial area (µm²)	10.0 ± 0.7	10.6 ± 1.0
Number of spark sites	10.0 ± 1.2	5.5 ± 0.8 **
Individual spark site	*70 sites in 7 cells (3 animals)*	*77 sites in 14 cells (3 animals)*
Frequency (Hz)	0.14 ± 0.02	0.11 ± 0.01

* $P < 0.05$, ** $P < 0.01$ *vs* control

Table 3: Arterial diameter measurements

	Control		SAH	
Paxilline treatment (at 80 mm Hg)	*n* = 5		*n* = 5	
Before paxilline	94.6 ± 10.2 µm	**	96.6 ± 8.1 µm	NS
In the presence of paxilline	78.4 ± 8.4 µm		95.5 ± 8.6 µm	
Decrease in diameter by paxilline	16.2 ± 2.3 µm		1.2 ± 1.1 µm	
Passive diameter	114.0 ± 12.1 µm		163.3 ± 12.7 µm	
Ryanodine treatment (at 80 mm Hg)	*n* = 4		*n* = 4	
Before ryanodine	139.5 ± 7.8 µm	**	158.8 ± 14.6 µm	NS
In the presence of ryanodine	125.0 ± 8.4 µm		152.3 ± 15.6 µm	
Decrease in diameter by ryanodine	14.5 ± 1.5 µm		6.5 ± 1.2 µm	
Passive diameter	177.0 ± 11.6 µm		216.5 ± 15.3 µm	
60 mM K^+ (at 20 mmHg)	*n* = 9		*n* = 9	
% decrease in diameter	62.2 ± 3.7	NS: SAH vs Control	64.7 ± 4.7	
Acetylcholine-induced vasodilation	*n* = 7		*n* = 5	
EC_{50}	5.3 x 10^{-7} M		3.5 x 10^{-7} M	
SNP-induced vasodilation	*n* = 4		*n* = 4	
EC_{50}	1.3 x 10^{-6} M		3.1 x 10^{-6} M	

** P < 0.01, NS: not significant.